

Department of Mechanical Engineering and Industrial Management

Faculty of Engineering, University of Porto

Department of Aeronautics

Imperial College London

Micromechanics of kink-band formation

Soraia Pimenta

March 2008

Abstract

Kink band formation is the most common failure mode found in fibre reinforced composites under axial compression. In this project, the phenomenon is studied at the microscale with the objective to develop an analytical model able to describe the process and band's final configuration.

An experimental program is carried out: a methodology for observation of loaded kink bands at the micro level is developed and applied; several kink bands are observed and discussed, and relevant conclusions are compiled.

2D numerical simulations using the FE method for kink band initiation and propagation are run and analysed in detail; models make use of initial imperfections, independent matrix and fibre representations and yielding and softening constitutive laws for both constituents. Useful information to understand how and why kink bands are formed is obtained from the analyses and their discussion; shear stresses and matrix yielding are found to play a major role on kink band formation. In addition to the basic process, several other experimental features are reproduced as well.

With the inputs from experiments and numerical analysis an analytical model is developed; this model is based in the equilibrium of a single fibre, considering the effect of compression and bending induced by the external load and also of shear stresses transferred by the matrix. Besides the explanation and justification of kink band formation, the model is able to predict the composite's axial compressive strength and the band's width.

The analytical model is validated qualitatively against experimental and numerical results, and quantitatively against numerical ones; a good agreement is observed.

Contents

Abstract	i
Table of Contents	vii
List of Figures	xii
Acknowledgements	xiii
Notation	xv
1 Introduction	1
2 Literature review	3
2.1 Experimental	4
2.2 Numerical	7
2.3 Analytical	9
2.4 Discussion and Conclusions	13
3 Experimental work	15
3.1 Objective	15
3.2 Strategy	15
3.3 Manufacturing	17
3.3.1 Lay-up	18
3.3.2 Curing	19
3.3.3 Machining	20
3.3.4 Polishing	21
3.3.5 Manufacture control	21
3.4 Set-ups and specimens description	22

3.4.1	UD test	22
	3.4.1.1 Specimen	22
	3.4.1.2 Test set-up	23
3.4.2	CC test	24
	3.4.2.1 Specimen	24
	3.4.2.2 Test set-up	25
3.4.3	r-UD test	26
	3.4.3.1 Specimen	26
	3.4.3.2 Test set-up	26
3.4.4	Evaluation and comparison of test set-ups	27
3.5	Results	29
3.5.1	Macroscopic kink band without broken fibres (specimen r-UD_0d1)	32
3.5.2	Kink band formation - overview (specimen r-UD_2d2)	34
3.5.3	Kink band formation and propagation (specimen r-UD_aux)	34
3.5.4	Kink band propagation - overview (specimen CC_6d)	38
3.5.5	Other results	38
3.6	Discussion	43
3.6.1	Macroscopic kink band without fibre failure (specimen r-UD_0d1)	43
	3.6.1.1 Fibre failure in kink band formation	43
	3.6.1.2 Kink band's width	43
	3.6.1.3 Splitting	44
	3.6.1.4 Different kink bands within the specimen	44
3.6.2	Kink band formation - overview (specimen r-UD_2d2)	45
	3.6.2.1 Sequence of events	45
	3.6.2.2 Fibre fracture surfaces	46
	3.6.2.3 Splitting	46
3.6.3	Kink band formation and propagation (specimen r-UD_aux)	47
	3.6.3.1 Propagation with single fibre failure	47
	3.6.3.2 Features at the fibre-scale	47
3.6.4	Kink band propagation - overview (specimen CC_6d)	48
	3.6.4.1 Parallel bands propagating	48
	3.6.4.2 Macroscopic splittings	49
	3.6.4.3 Out-of-plane component	50
3.7	Conclusions	50

4	Numerical analysis	55
4.1	Objective	55
4.2	Modelling strategy	55
4.2.1	2D equivalent model	55
4.2.2	Critical features	56
4.2.3	Overall description of the models	57
4.3	Results	59
4.3.1	Generic results	59
4.3.2	Response curves for models on kink band initiation	61
4.3.3	Model with failing interface for kink band initiation (<i>cohesive</i>)	62
4.3.4	Model with elastic-plastic matrix (<i>matrix</i>)	75
4.3.5	Extended model with elastic-plastic matrix and failing fibres (<i>CDM_extended</i>)	75
4.3.6	Results from model with kink band propagation (<i>propagation</i>)	80
4.3.7	Results from model with complementary kink band (<i>CDM_complementary</i>)	85
4.4	Discussion	89
4.4.1	Model representativeness	89
4.4.2	Load versus displacement curves for kink band initiation	91
4.4.3	Numerical features	91
4.4.4	Role of the matrix in kink band initiation	92
4.4.5	Shear stresses and deformation in the matrix	93
4.4.6	Role of fibres in kink band initiation	93
4.4.7	Response after first fibre failure	94
4.4.8	Transverse stresses in the matrix	95
4.4.9	Bands formed in kinking	96
4.4.10	Sequence of events for kink band initiation	96
4.4.11	Kink band propagation	97
4.4.12	Splittings in kink band formation and propagation	98
4.4.13	Formation of a complementary kink band	99
4.5	Conclusions	99

5	Analytical model	103
5.1	Strategy	103
5.1.1	Inputs from experimental and numerical work	103
5.1.2	Model outline	104
5.1.3	Assumptions and applicability	104
5.2	Development of the model	106
5.2.1	2D equivalent model	107
5.2.2	Equilibrium of the fibre	107
5.2.3	Loads applied to the fibre	108
5.2.4	Governing differential equations	110
5.2.5	Continuity and Boundary Conditions	110
5.2.5.1	Deformed shape before matrix yielding	110
5.2.5.2	Deformed shape after matrix yielding	111
5.2.6	Definition of composite's compressive strength	112
5.2.7	First fibre failure	112
5.3	Results	113
5.3.1	Response in the <i>elastic domain</i>	114
5.3.2	Response in the <i>softening domain</i>	117
5.4	Discussion	121
5.4.1	Load versus displacement response	121
5.4.2	Stress and displacement fields	122
5.4.3	First fibre failure	122
5.4.4	Terms in the slope equations	123
5.4.5	Attempt of a simplified model	125
5.4.6	Model outputs	126
6	Conclusions	129
6.1	Experimental	129
6.2	Numerical	129
6.3	Analytical	130
7	Future work	135
7.1	Experiments	135
7.2	Numerical	136
7.3	Analytical	138

List of Figures

2.1	Kink band in a real composite [2].	3
2.2	Kink band geometry.	3
2.3	Kink band broadening and fibre failure (unloaded) [7].	6
2.4	Kink band initiated by compression and shear, without fibre failure [8].	7
2.5	Kink band propagating [8].	7
2.6	Numerical models developed by Kyriakides [5].	8
2.7	Typical maximum axial stress in fibres versus shortening during kink band formation [5].	8
2.8	Equilibrium of a fibre as studied by Hahn and Williams. [15].	11
2.9	Morais and Marques model for matrix shear deformation [17].	12
3.1	Misalignment between fibres and load direction and resultant stress components.	16
3.2	Specimens used in the experimental program.	18
3.3	Micrographs of <i>cross – ply plate 1</i>	19
3.4	Specimen UD: definition drawings.	23
3.5	UD test set-up.	24
3.6	CC specimen: definition drawing.	25
3.7	CC test set-up.	25
3.8	r-UD specimen: definition drawing.	26
3.9	Shear induced in r-UD specimens.	26
3.10	r-UD test set-up.	27
3.11	Failure modes for UD specimens.	28
3.12	Images recorded by the DSP plugged on the hand microscope.	28
3.13	Specimen r-UD_0d1 (picture): macroscopic kink band.	32
3.14	Specimen r-UD_0d1 (SEM, unloaded): overview.	32
3.15	Specimen r-UD_0d1: zoom-in from figure 3.14.	33

3.16 Specimen r-UD_2d2 (optical microscope): overview (load step 2).	34
3.17 Zoom-in at kink band's tip (optical microscope, specimen r-UD_2d2 loaded).	35
3.18 Specimen r-UD_2d2 seen at the SEM (unloaded).	36
3.19 Specimen r-UD_aux seen at the SEM (loaded).	37
3.20 Specimen CC_6d: optical micrographs (unloaded, after outer layers removal, unpolished).	39
3.21 Kink band propagation - sequence of images (1).	40
3.22 Kink band propagation - sequence of images (2).	41
3.23 Other kink bands from the experiments.	42
3.24 Kink band width: under compression and under shear.	44
3.25 Schematics of single failure in unsupported fibres.	47
3.26 Schematics of the asymmetry in a kink band with out-of-plane component.	47
3.27 Schematics of kink band's out-of-plane component in specimen CC_d6.	49
3.28 Schematics of in-plane transverse tension and compression during propagation.	49
4.1 Hexagonal fibre arrangement and 2D equivalent model.	56
4.2 Numerical model: geometry, mesh and boundary conditions.	58
4.3 Constitutive laws used for the matrix in numerical models.	59
4.4 Types of imperfection with successful kink band formation.	60
4.5 Load (P) versus shortening ($u(L)$) curves for the four models on kink band initiation.	62
4.6 Maximum deflection ($v(L)$) versus shortening ($u(L)$) curves for the four models on kink band initiation.	63
4.7 Load (P) and maximum deflection ($v(L)$) versus shortening ($u(L)$) curves for the <i>cohesive</i> model.	64
4.8 Load (P) versus maximum deflection ($v(L)$) curve for the model with failing interface, highlighting seven particular points.	64
4.9 Axial stresses in the fibres (σ_{11}^f) in the <i>elastic</i> domain (<i>cohesive</i>).	66
4.10 Axial stresses in the bottom of the central fibre (σ_{11}^f) in the <i>elastic</i> domain (<i>cohesive</i>).	67
4.11 Axial stresses in the fibres (σ_{11}^f) in the <i>softening</i> domain (<i>cohesive</i>).	68
4.12 Axial stresses in the bottom of the central fibre (σ_{11}^f) in the <i>softening</i> domain (<i>cohesive</i>).	69
4.13 Axial stresses in the central fibre (σ_{11}^f), at its top and bottom boundaries, at $P = 3.5\text{N/mm}$ (<i>cohesive</i>).	69
4.14 Shear stresses in the matrix (τ_{12}^m) in the <i>elastic</i> domain (<i>cohesive</i>).	70
4.15 Shear stresses in the central layer of matrix (τ_{12}^m) in the <i>elastic</i> domain (<i>cohesive</i>).	71
4.16 Shear stresses in the matrix (τ_{12}^m) in the <i>softening</i> domain (<i>cohesive</i>).	72

4.17	Shear stresses in the central layer of matrix (τ_{12}^m) in the <i>softening</i> domain (<i>cohesive</i>).	73
4.18	Deflection (v , global referential) in the <i>elastic</i> domain (<i>cohesive</i>).	74
4.19	Deflection of the central fibre (v , global referential) in the <i>elastic</i> domain (<i>cohesive</i>).	75
4.20	Deflection (v , global referential) in the <i>softening</i> domain (<i>cohesive</i>).	76
4.21	Deflection of the central fibre (v , global referential) in the <i>softening</i> domain (<i>cohesive</i>).	77
4.22	Transverse stresses in the matrix (σ_{22}^m , local referential) (<i>cohesive</i>).	77
4.23	Split group of fibres, at the end of <i>cohesive</i> simulation.	78
4.24	Load (P) versus deflection ($v(L)$) curves for the numerical variations of the <i>cohesive</i> model.	78
4.25	Stress fields for the model with no stabilization (<i>softening</i> domain, $P = 3.5\text{N/mm}$).	78
4.26	Shear stresses in the matrix for the model with <i>cohesive_20fibres</i> (at first matrix yielding).	79
4.27	Axial stresses in fibres (σ_{11}^f) for the <i>matrix</i> model, in the <i>softening</i> domain, with overstressed areas highlighted.	79
4.28	<i>CDM_extended</i> model: configuration during fibre failure process.	80
4.29	<i>CDM_extended</i> model: geometry, axial stresses and comparison with <i>matrix</i> and <i>CDM</i> deformed shapes.	81
4.30	Model for kink band <i>propagation</i>	82
4.31	Kink band <i>propagation</i> (full model): sequence of events.	84
4.32	Kink band <i>propagation</i> in straight fibres.	85
4.33	Transverse stresses in the matrix (σ_{22}^m) during kink band <i>propagation</i> , in initially perfect fibres.	86
4.34	<i>Propagation</i> with transverse failure: splittings.	87
4.35	<i>Propagation</i> with top fibre constrained.	88
4.36	Complementary kink band in the <i>CDM_complementary</i> model.	89
4.37	Formation of a complementary kink band (<i>CDM_complementary</i>).	90
4.38	Shear stresses in the matrix (τ_{12}^f) in model with complementary kink band, after first band formation (<i>CDM_complementary</i>).	90
4.39	Detail of deformed shape (over initial shape) in <i>cohesive</i> model (<i>softening</i> domain): two fibres (blue) and one layer of matrix (red).	93
4.40	Comparison between final deflection in <i>cohesive</i> and <i>matrix</i> models (other model's deflection in dashed line).	94
4.41	Bands formed during kinking (<i>softening</i> domain, $P = 3.5\text{N/mm}$).	96
4.42	Kink band propagation: comparison between experimental and numerical results (same scale).	98
4.43	Formation of a complementary kink band.	100
5.1	Schematics of the fibre considered in the model: geometry and loads.	107

5.2	Equilibrium of an infinitesimal part of the fibre.	108
5.3	Matrix in-phase deformation.	109
5.4	Continuity and boundary conditions.	111
5.5	Fibre's deflection in the <i>elastic domain</i>	114
5.6	Load versus maximum displacement curve for the <i>elastic domain</i> and peak load.	115
5.7	Shear stresses along x in the <i>elastic domain</i>	115
5.8	Axial stresses on the top of the fibre, along x and in the <i>elastic domain</i>	116
5.9	Peak load and maximum deflection for different interface's strength.	116
5.10	Fibre's deflection in the <i>softening domain</i>	118
5.11	Shear stresses along x in the <i>softening domain</i>	119
5.12	Axial stresses at the top of the fibre, along x and in the <i>softening domain</i>	119
5.13	Load versus maximum displacement global curve.	120
5.14	Boundaries of the <i>yield band</i> and location of maximum bending moments.	121
5.15	Slope components, in the <i>softening domain</i>	124
5.16	Fibre failure load versus failure position, in a simplified model.	126

Acknowledgments

To Dr. Silvestre Pinho, supervisor of this project, for his expertise, for his contribution, for his guidance, interest and availability, for his rigour and demand, for the encouragement, patience and motivation.

To Renaud Gutkin, co-author of a great part of the work here reported, for his cooperation and contribution, for his advice, guidance and share of knowledge, and for his patience and fellowship.

To Dr. Paul Robinson, co-supervisor of this project, for his interest, advice and availability.

To Dr. Pedro Camanho, for all the background received prior to this project, for the support given on applying to an exchange study period in Imperial College London and for the interest on the work there developed.

To Mr. Gary Senior, for the help on manufacturing, machining and testing the specimens, and to Mr. Joseph Meggyesi, for the help on testing.

To William Francis, for the help on obtaining SEM micrographs.

To the University of Porto and to the Portuguese Foundation for Science and Technology, for making the Erasmus Program available and also for their funding and support.

To everyone who was somehow there.

Notation

Configuration parameters

u	axial displacement, shortening
v	transverse displacement, deflection
x	position along the axial direction
y	deformed shape (transverse direction)
θ	fibre rotation
ω	deflection's slope

Geometric parameters

e	distance to neutral axis
t_m	matrix thickness
y_0	fibre initial imperfection
$\overline{y_0}$	imperfection's half amplitude
A	cross section's area
I	cross section's second order moment of inertia
L	imperfection's length, model's length, half wavelength
ϕ_f	fibre diameter
φ	induced misalignment

Kink band parameters

w	kink band width
α	fibre angle (in a kink band)
β	kink band angle

Material properties

E	Young's modulus
G	shear modulus
S	shear strength
X	axial strength
Y	transverse strength
V_f	composite's fibre volume fraction
\mathcal{G}_C	critical energy release rate / fracture toughness

Fracture mechanics

a_0	initial crack length
b_0	initial crack width
f	normalized energy release rate
k	stress concentration factor

Stresses, strains and loads

p	confining pressure
P	compressive load
M	bending moment
γ_{12}	shear strain
μ	frictional coefficient
σ_{11}	axial stresses
σ_{22}	transverse stresses
τ_{12}	shear stresses
τ_μ	friction

Indexes

Constituents

f	fibre
m	matrix
C	composite
lam	laminated

Event / Time

0	initial
$yield$	at first yielding
f	final
ff	fibre failure
$post$	after matrix yielding / with matrix in the plastic domain
pre	before matrix yielding / with matrix in the elastic domain

Mode

I	mode I (toughness)
II	mode II (toughness)
C	compression
T	tension

Misc.

r	reduced (area)
L	load

Chapter 1

Introduction

Composite materials are nowadays widely used in advanced structures with high performance and low weight requirements. Among all, unidirectional fibre-reinforced polymers (FRP) are one of the most common choice. However, and notwithstanding their high strength- and stiffness-to-density ratios (which make them very attractive to transport and defense applications), FRPs suffer from a severe drawback: the lack of consistent and expedite design criteria.

Despite the recent developments in this field and due to the inherent complexity of this type of materials (composites), the mechanical behaviour of FRPs is not totally understood yet, especially when it comes to the physics and mechanisms involved in some failure and damage modes; this hinders the composite's mechanical capability to be fully used and makes the design and validation of structures an arduous job. Actually, due to the lack of confidence and/or difficult application of analytical models predicting the composite's response, much in the development of composite structures relies on experimental testing, which represents a great part of the project's cost; besides, in some industrial applications the strength of composite materials is still computed by unsuitable criteria (e.g. the von Mises criterion), which implies the use of high safety factors and leads therefore to an unnecessary overdimensioning of the components. For these reasons, it is easy to understand why the research on composite's failure is a so active field nowadays.

Contrarily to what happens in other materials, it is well known that the longitudinal compressive strength of FRPs is only a fraction of their tensile one; nevertheless, many structures in which composites are the desirable option do work under compressive loads, which increases the interest in this specific failure mode. However, under axial compression the FRPs present one of the most complex failures that can be found in composites: the formation of kink bands.

Both the initiation and propagation of kink bands in composites have been widely studied, but the physics and mechanics of the processes are not fully understood yet. Although it is generally accepted that this failure mode is related to misaligned fibres and matrix shear behaviour, there is still much work to be done before the composite's axial compressive strength and the final kink band's geometry can be predicted.

For this reason, the aim of the work presented in this report is the development of an analytical model on the physical and mechanical process of kink band formation, capable of predicting the composite's response (both in terms of load capability and deformation mode) under axial compressive loads. The final objective is to have a closed formulation model with the material's properties and load conditions as inputs, giving as outputs the composite's axial compressive strength and the geometry of the kink band formed.

A physically-based model requires the development of a theory on the features and events leading to failure; for that reason, an analytical model can not be developed without observing the phenomenon at a scale small enough for the important features to be captured. Therefore, the analytical work already identified as the final aim of this project was preceded and accompanied by experimental and numerical programs, both to provide information and to check hypothesis on kink band formation.

Considering this, and notwithstanding the fact that they are intimately related and carried out in parallel, this report is organized in three different - experimental, numerical and analytical - parts. The experimental work, focused on kink band observation, is presented in Chapter 3, through a discussion with main emphasis on the strategy followed and the quality of results obtained. In Chapter 4, the numerical (finite elements, FE) simulations are described and the results presented and discussed, as they proved to be the major source of information for the achievement of the project's goal. Finally, an analytical model for kink band formation is developed in Chapter 5, which includes a discussion on the main assumptions and their applicability, a detailed explanation of the governing equations and the analysis of results obtained.

Preceding these main chapters, a literature review on the subject is done in Chapter 2. This report is then closed by Chapters 6 and 7, with (respectively) the main conclusions and suggestion for further developments.

Chapter 2

Literature review

Structures made of fibre-reinforced composites, when submitted to compressive loads applied along the fibre direction, usually collapse due to material failure at the constituents level [1], being afterwards the damage propagated to the whole structure. Generally, four different failure modes for this case can be found: micro-buckling (instability at the micro-level, characterized by in-phase fibre waviness, dependent on initial defects and common in composites with strong matrix and fibres), fibre failure (simple failure of the fibres due to pure compression, dependent on fibre's properties and common in composites with weak fibres e.g. kevlar), longitudinal cracking or splitting (debonding between matrix and fibres or separation within the matrix, common in composites with weak interface) and, finally, fibre kinking (figure 2.1).

The formation of kink bands is the most common failure mode in high-performance FRP systems such as carbon fibres and epoxy polymer. When compressed, the material locally deforms within a band: inside this band, oriented at an angle β with respect to the transverse (normal to the load) direction and with a width w , the fibres are rotated from an angle α to the global longitudinal direction (figure 2.2).

Among the four mentioned failure modes, fibre failure and longitudinal cracking are the easiest ones to identify and understand, as they involve the failure of just one constituent (fibre, matrix or interface) and are therefore affected by fewer parameters. On the opposite way, micro-buckling and fibre kinking have been widely studied during the last 50 years, but despite all the efforts there is so far no full understanding about the physics and

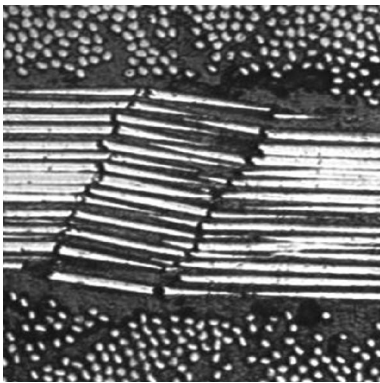


Figure 2.1: Kink band in a real composite [2].

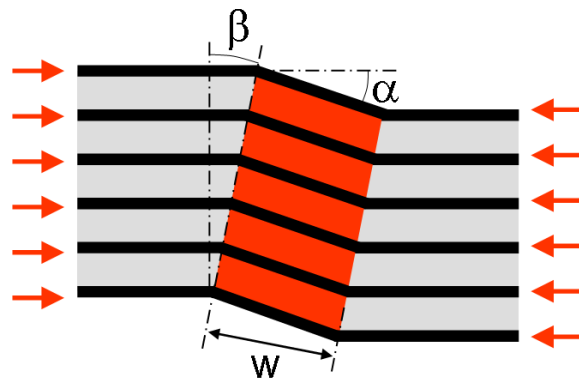


Figure 2.2: Kink band geometry.

mechanics taking part in those phenomena; moreover, there is no agreement yet between researchers on what differentiates them, as some authors consider kinking as a final result of micro-buckling while others argue that they are two independent failure modes.

Schultheisz and Waas present, in their review on the compressive failure of composites [1], a comparison between kinking and micro-buckling. The latter can be seen, as its name suggests, as a structural instability at the micro-level, leading the fibres to bend over the typical buckling mode as a critical (instability) compressive load is reached; according to some authors, this instability would lead to fibre breakage under bending and, ultimately, to the formation of kink bands. On the other hand, kinking (as an independent failure mode) would be the result of misaligned fibres under compression within a highly sheared matrix, being the process controlled not by an instability or a critical load but by initial imperfections and matrix shear behaviour.

Being partially done in parallel with the experimental, numerical and analytical work, this review contemplates for that reason a few generic papers on this topic and some more specific ones that were considered to raise interesting ideas or relevant suggestions to this project. Following the overall organization of this report, this literature review is organized in three parts - experimental, numerical and analytical -, being afterwards concluded by a discussion and summary of all the ideas gathered.

2.1 Experimental

Either found within the lamina's plane [1, 4, 5, 6, 7, 8] or through-the-thickness [1, 2, 3, 4], in UD laminates [1, 4, 5, 6, 7, 8] or in more complex stacking sequences [1, 3, 2, 4], developed spontaneously [1, 2, 3, 4] or somehow induced [1, 4, 6, 7], kink bands are reported in the results found in several experiments with composites under compression. Generally [1], a kink band can be described as a localized band found in the plies under axial compression, sharply defined by an abrupt change in fibre direction from $\theta = 0^\circ$ outside the band to $\alpha \approx 30^\circ$ to 45° inside it, usually with fibre failure at its boundaries; the inclination of the band is found to be $\beta \approx 0^\circ$ to 45° , and its width (measured in the fibre direction) varies within the range $w \approx 70\mu\text{m}$ to $1200\mu\text{m}$, for generic FRP materials [1]; for CFRP, typical values are reported as $\beta \approx 20^\circ$ and $w \approx 70\mu\text{m} = 10 \cdot \phi_f$ to $w \approx 200\mu\text{m} = 30 \cdot \phi_f$.

The formation and evolution of a kink band can be divided in three phases [6, 7, 8]: initiation - in which a few fibres begin to kink within a band -, propagation - in which the band grows transversely, increasing its length along the direction defined by β - and broadening - in which the band grows axially, increasing its width w along the direction defined by α . Besides, the formation of a kink band can also be followed by the development of a complementary kink band [1], formed to release the stresses generated by the global transverse displacement in confined specimens.

In **Waas and Schultheisz's** review [4], a summary of the most important parameters affecting kink band geometry is provided. The compressive strength of a composite was found to generally increase with the fibre diameter (improvement on bending stiffness), fibre volume fraction (higher fibre's stiffness and strength than matrix's) and fibre's stiffness (improvement on bending stiffness as well); however, for too high diameters and fibre volume fraction, the composite's response starts to degrade as failure is dominated by flaws. When the role of the matrix's properties is questioned the results are consistent, as both its strength and stiffness have a significant influence on the overall composite's response. The importance of the interface between matrix and

fibres is also stressed, as a weak interface leads usually to failure by splitting, while composites with a strong interface fail by fibre kinking.

In [5], **Kyriakides et al.** present their experimental work with a AS4/PEEK composite, using two different set-ups, both with confinement of the specimens. The first one, testing a cylindrical rod specimen only unsupported in the central section, resulted in sudden and unstable fibre kinking failure; due to stress concentrations, damage was initiated near the boundaries of the non-confined length; the deformation was reduced because of the confining pressure, and several kink bands formed in each specimen (inside the specimen and at its surface, single and complementary ones), with angles $12^\circ \leq \beta \leq 16^\circ$ and widths $75\mu\text{m} \leq w \leq 225\mu\text{m}$. The authors also verified that the propagation load was lower than the initiation one, and for that reason the similarities between kink band formation and structural instabilities were pointed out.

The specimen used in the second set-up was a thin composite ring. The experimental set-up consisted in three rings (polymer, loading and specimen) arranged in an ingenious way: one polymer ring, externally confined by a stiff retainer, was compressed axially by a loading ring; due to Poisson's effect, the polymer ring expanded radially inwards, compressing the specimen ring that was tightly adjusted to its inner surface, in the radial direction. These specimens presented a sudden and catastrophic failure due to fibre kinking for larger strains than the ones verified for the previous specimens (as no free-edge effect was possible along the load direction).

In addition, these researchers also quantified the fibre imperfections found in the composite, as their connection to fibre kinking was stressed. Bands of highly misaligned material were distinguished within the material and justified by manufacturing defects at the pre-preg level; the imperfections, developed in a three-dimensional way, were found to have half wavelength of $150\phi_f \leq L \leq 400\phi_f$ and an amplitude of $3\phi_f \leq \bar{y}_0 \leq 10\phi_f$, with no correlation between them.

In [6], **Moran** presents and interpretes the results of his experimental work done with thick (6mm) rectangular IM7/PEEK specimens, previously notched with a 4mm indentation and loaded in compression. According to his interpretation and after an initially linear behaviour, the matrix starts yielding around the notch (phenomenon named as "incipient kinking" by the author), just before the peak load is reached and a kink band is suddenly propagated from the notch across the entire specimen's width (10mm). The kink band, at this initial state, is characterized by $w = 10 \cdot \phi_f$ and $\beta = 10^\circ$ to 15° , and the rotation of the fibres increases slowly to $\alpha = 15^\circ$ to 20° as the compression progresses. At this point, fibre rotation becomes unstable and it suddenly changes to $\alpha = 40^\circ$ to 45° , followed by an increase at the band's angle ($\beta = 20^\circ$ to 25°), until the fibres are locked-up by the shear response of the matrix (stiffer in the large-strain domain). After this "transient band broadening" phase, corresponding to the increase of both α and β under a decreasing compressive load, the band starts to broaden at a steady state (broadening) load; in this phase, the width of the kink band increases progressively, as the fibres at the outside border of the band are bent until they fail and align themselves with the previously locked-up fibres. After the tests the specimens were observed unloaded, and it was found that the elastic recovering was small (a reduction on the fibre rotation of $\Delta\alpha = -5^\circ$), leading the author to conclude that the matrix was deformed mainly in the plastic domain.

Vogler and Kyriakides' experimental work (1999 and 2001) on the propagation and broadening of kink bands in AS4/PEEK composites is presented in two different papers. In the first one [7], the broadening of kink bands is analysed. Using thick (7.6mm) specimens with a semi-circular 2.4mm indentation under axial compression, these researchers were able to initiate and fully propagate a kink band across the specimen's width in an unstable

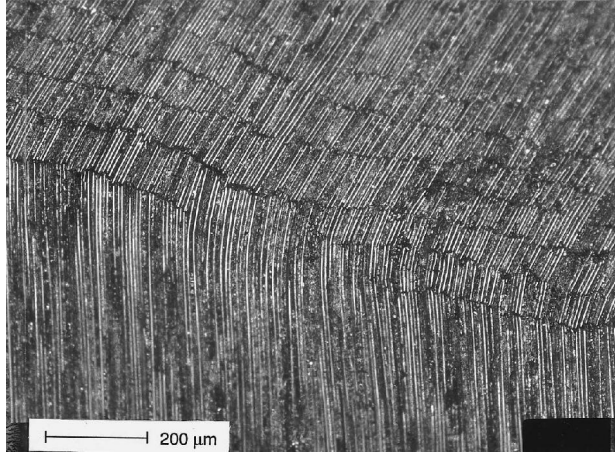


Figure 2.3: Kink band broadening and fibre failure (unloaded) [7].

way; afterwards, by reloading the pre-kinked specimen, the kink band broadened in a steady way (at a constant load around 50% of the initiation load value). In this experiments, the out-of-plane kink band's component was reduced by clamping the specimen between two rigid plates.

During the broadening, the kink band width was increased as the fibres were broken at segments around $10 \cdot \phi_f$ long, as it can be seen in figure 2.3. Also from this (unloaded) micrograph, it is possible to conclude that broadening is dominated by fibre failure due to bending, followed by further rotation of broken segments; in addition, as these broken segments are straight but there are unbroken fibres with high curvature, one can conclude that the fibres are kept in the elastic regime but the matrix does go into the plastic domain.

Within the band and during broadening, the fibre angle was kept around $\alpha = 41^\circ$ and the kink band angle at $\beta = 16^\circ$; as the authors pointed out, this does not follow the usual relation $\alpha = 2 \cdot \beta$.

These authors did a successful work on the propagation of kink bands [8] as well. By loading UD composites (AS4/PEEK) in axial compression combined with in-plane shear, these researchers managed to create and propagate stable kink bands. The test, using square specimens 3.18mm thick, consisted in five quasi-static steps: axial compression to a given load at first, followed by shear displacement (at constant compressive load) until the initiation of the kink band (identified by a reduction in the shear load), after which the specimens were completely unloaded; then, a new step of axial compression was performed, so that by finally applying shear the propagation of the kink band could be observed. During this final step, several pictures were taken, allowing the phenomenon to be followed; it was found that the inclination and width of the kink band remained constant through propagation at $\beta = 12^\circ$ and $w = 25 \cdot \phi_f$, while the angle of the fibres (for a given location) was increasing progressively with the propagation of the kink band to $\alpha = 26^\circ$.

Following the total propagation of the kink band through the width of the specimen, the band started broadening, increasing its width but keeping both angles constant. After the test, the kink band was observed unloaded under the microscope, and it was found that almost no fibre failure had occurred (figure 2.4); this, according to the authors, was due to the (comparatively) small fibre angle within the kink band (not requiring a curvature as high as usually observed). Taking this into account, one can conclude that the shear stresses are crucial to the formation of the kink band, being the failure of the fibres an eventual consequence.

An important remark from this work is the fact that, despite the effort to produce totally in-plane kink bands (the out-of-plane movement was restrained by two anti-buckling plates), it is evident from the shadow shown in

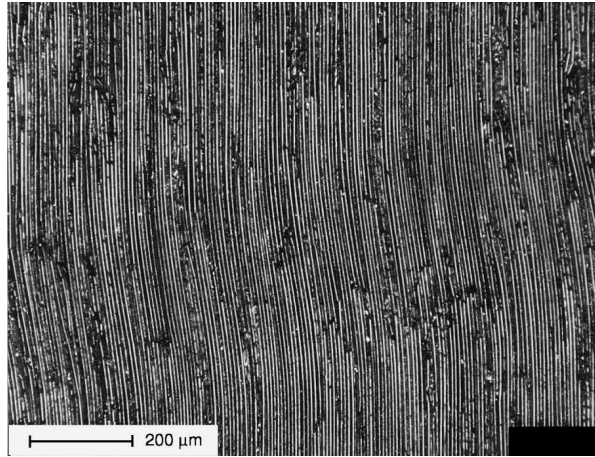


Figure 2.4: Kink band initiated by compression and shear, without fibre failure [8].

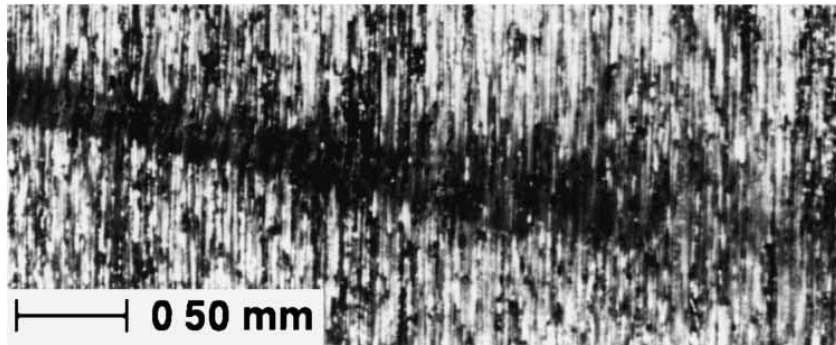


Figure 2.5: Kink band propagating [8].

figure 2.5 that there is an out-of-plane component when the kink band is loaded.

2.2 Numerical

The development of numerical (FE) models able to simulate the composite's behaviour during the formation of kink bands is also reported in the literature, although not at the same extent as for the experimental work. Several researchers developed numerical models to predict composite's strength assuming fibre micro-buckling (e.g., instability), while others modelled kinking using matrix yielding and initial imperfections.

Kyriakides is a researcher with a very detailed numerical study on kink bands. In his paper from 1995 [5], an extended study about the influence of several physical and modelling parameters on the composite's response and kink band's geometry is presented. The modelling strategy used a 2D layered approximation, assuming a periodic array of a finite number of fibres interposed with layers of matrix (figure 2.6 a); the constitutive law for the matrix considered a standard elastic-plastic (with initial hardening) isotropic behaviour, and the fibres were assumed to be isotropic and either with linear or non linear response. All models assumed a sinusoidal initial imperfection (figure 2.6 a) and were solved using the Riks modified method. The typical composite's global response (figure 2.7) is, initially, almost linear (points 0 to 2) , until a peak load (point 2) is reached; after that, due to both geometric and matrix non-linearity, the model evolves through a softening domain with

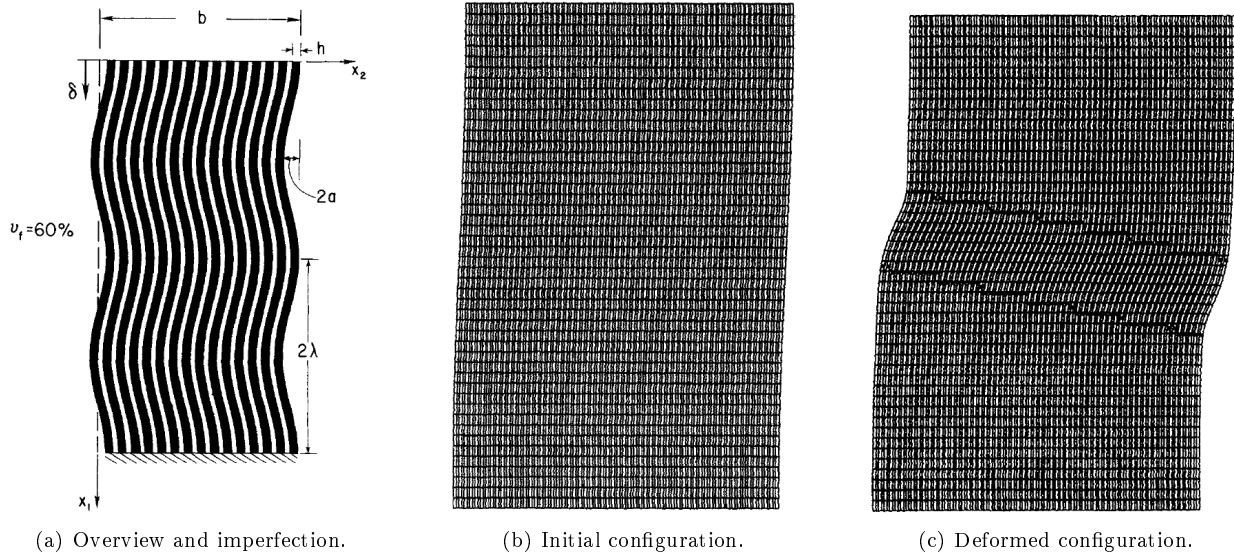


Figure 2.6: Numerical models developed by Kyriakides [5].

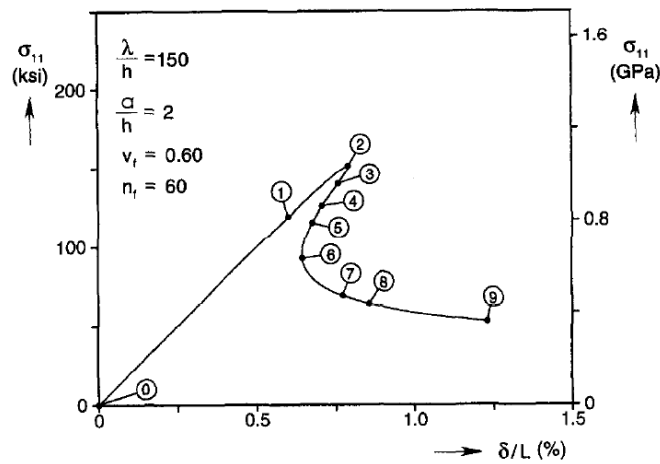


Figure 2.7: Typical maximum axial stress in fibres versus shortening during kink band formation [5].

a sudden reduction on the compressive load and a recover on the shortening (points 3 to 6), followed by further compression and load stabilisation (points 7 to 9). During this softening domain, the model develops a kink band with its boundaries defined by the points with maximum bending stresses in each fibre (figure 2.6 c), increasing its width w and angles α and β as the compression progresses. Considering this overall response, a parametric study was performed. It was found that the addition of more fibres in the model would affect - increasing - the peak remote stress (σ_{11}^{∞}); besides, the longer models (along the axial direction) presented a higher instability after the peak load, due to the greater amount of strain energy available; fibre material non-linearity was found to have reduced influence, both on the initial domain (increasing its non-linearity but without affecting the peak load) and final strain.

In addition, a deep study on the effect of the imperfection parameters was carried out as well; it was confirmed that increasing the imperfection's amplitude (and therefore its angle as well) would decrease the composite's stiffness and strength, while the length itself had a smaller effect. Moreover, the role of the location and spatial evolution of imperfections was also analysed, with kink bands formed in models with non-uniform imperfections

as well.

Morais [9] used a “basic-cell” approach in a micro-buckling analysis both for two or three dimensions, assuming a sinusoidal imperfection for the fibres and isotropic materials, being the matrix elastic-plastic and the fibres linear elastic. His results show that micro-buckling is sensitive to the imperfection’s misalignment angle (decreasing composite’s strength), to the matrix yield stress (increasing composite’s strength) and to both fibre and matrix Young’s modulus (increasing slightly composite’s strength). In addition, in his 3D models, this author found that, if a hexagonal arrangement for the fibres is assumed, the micro-buckling would be isotropic.

In an attempt to simulate numerically their experimental work on kink band propagation, **Vogler et al.** [10] developed 2D and 3D FE models of composites under compression and shear. The fibres were modelled with global (constant) and local (for kink band initiation) imperfections; besides this fact and the addition of direct shear, the models (both 2D and 3D, being the last just one slice of material) followed an approach very similar to the one used by Kyriakides et al. in [5]. Two constitutive laws were chosen for the matrix’s plastic domain: the J_2 type solid with isotropic hardening and the Drucker and Prager plasticity model (modified by Hsu). In the overall, the models were capable of reproducing the propagation of a kink band through the fibres, both using the combined action of direct shear and compression as only by pure compression (being the response with shear much more stable than the one obtained with simple compression); no major difference between the 2D and 3D responses were found.

A parametric analysis was also performed in this study. It was found that increasing fibre volume fraction improves the composite’s strength and leads to wider kink bands with a smaller fibre angle α , as well as did increasing the fibre diameter. Matrix’s yield stress affected material’s strength and the kink band geometry (a stronger matrix gave a wider band with fibres more inclined). On the shape of the initial imperfection, it was found that the most relevant parameter was the amplitude of the global imperfection, with a severe impact on the composite’s strength. Finally, it was found that the number of fibres included in the model had an effect on the kink band’s geometry, as for the models with less fibres both the band’s and fibres’ inclination (β , α) increased.

In addition, the impact of some features was analysed as well. It was confirmed that, in the 2D models, the type of planar stress state imposed (plane strain or plane stress) had not a significant repercussion on the composite’s strength or kink band’s geometry. On the other hand, matrix dilatancy proved to affect kink band’s angle, confirming that this parameter is controlled by volumetric constrains.

2.3 Analytical

The first researcher proposing a model for the failure of composites under axial compression was **Rosen** (1965) [11]. By considering a 2D (layered) infinite model with perfectly straight fibres evenly spaced by a linear elastic matrix, Rosen assumed that the failure would take place at the buckling load in shear mode (characterized by in-phase deformation of the layers). His models considers the bending of the fibres and the deformation of the matrix to, by minimizing the total potential energy, calculate the critical remote stress (composite’s compressive strength) as

$$X_C^C = \frac{G_m}{1 - V_f}, \quad (2.1)$$

where G_m is the matrix shear modulus and V_f the fibre volume fraction of the composite. This approach, which gives a similar result to consider simple shear of the matrix (without fibre bending), overpredicts composite's strength obtained through experimental data by a factor (for CFRP) between 2 and 3 [1]. In an attempt to solve this problem, several researchers proposed models based on Rosen's with additional modifications [1], trying to take into account several factors as the plasticity and non-linearity of the matrix, combined buckling of matrix and fibres, residual thermal stresses, interface between fibre and matrix and free edge effects, always with no significant improvements on the correlation between analytical and experimental results [1].

It was only when initial imperfections (waviness or misalignment) on the fibre's initial geometry were considered that the results began to improve [1]. However, these models assume failure by micro-buckling, and experimental data from composites under compression show that the most common type of failure on CFRP composites is the formation of kink bands. Pure micro-buckling could result into the formation of a band similar to a kink band, but it would be expected to lie aligned with the load (as a group of in-phase buckling segments), with $\beta = 0^\circ$; this is not the common kink band angle ($\beta \approx 20^\circ$ to 30°), which reveals the different nature of the two processes, as pointed by Schultheisz and Waas [1].

Argon [12] proposed the first model for failure due to kinking as an independent mode; this researcher considered an initial misalignment on fibres as the trigger for the formation of kink bands, as it would promote shear stresses on the material that, by inducing moments, would force the fibres to rotate more, in a positive feedback process. His 2D model for the initiation of kink bands considered the work done by shearing the matrix within the band and by bending fibres in its boundaries, giving as a result

$$X_C^C = \frac{S_m^{yield}}{\theta_i}, \quad (2.2)$$

where S_m^{yield} is the matrix yielding stress in shear and θ_i is the initial misalignment angle. This expression defines the composite's compressive strength as the remote stress that leads to the shear failure of the matrix in the misaligned referential; after this initiation, Argon suggests that the propagation of the kink band would occur at $\beta = 45^\circ$, emphasizing the relevance of shear in the process excessively, as this is not the common kink band angle. Many other micromechanical models were developed to explain the formation of kink bands, as it is well presented in Schutheisz and Waas' review [1].

A consistent relation between α and β was studied by **Chaplin** [13]: considering simply the geometry of an inclined band in an incompressible material, this author concluded that $\alpha = 2 \cdot \beta$.

Budiansky found, in his analysis [14], that the plasticity of the matrix and an initial misalignment could be included in Rosen's model with an effect on the predicted compressive strength, which was now given by

$$X_C^C = \frac{G_m}{1 - V_f} \cdot \frac{\gamma_m^{yield}}{\gamma_m^{yield} + \theta_i}, \quad (2.3)$$

where γ_m^{yield} is the matrix shear strain at yielding. Despite the improvement given in the strength (better agreement with experimental results), this model did still predict the kink band's angle to be $\beta = 0^\circ$; Budiansky suggested another model to predict a different angle (based on the wavelengths of the imperfections), and also pointed that the width of the kink band (w) should be defined by fibre failure under combined bending and compression.

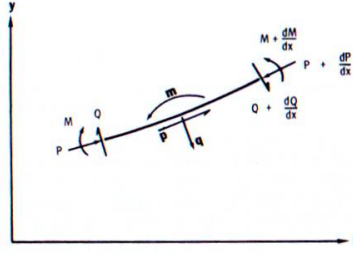


Figure 2.8: Equilibrium of a fibre as studied by Hahn and Williams. [15].

An approach equating the equilibrium of one fibre under buckling was followed by **Hahn and Williams**. [15]. Assuming small deflections, these researchers proposed several models for different cases: infinite matrix (equivalent to low fibre content), perfect fibre under buckling (similar to Rosen's model), and a nonlinear model including both the effects of initial imperfections and matrix non-linearity. This last one considered an initially imperfect (sinusoidal) fibre, loaded through internal loads P , Q and M and stresses induced by the matrix q and m (figure 2.8).

The equilibrium equation was defined as balance of moments; the composite's strength was then given by the buckling (instability) stress, in a closed formulation, as:

$$X_C^C = V_f \left(G_C + \sqrt{\frac{4 \frac{E_m}{t_m} E_f}{\pi}} \right) \frac{\gamma_{critical}}{\gamma_{critical} + \frac{\pi \cdot \bar{y}_0}{L}}, \quad (2.4)$$

where $G_C = G_m / (1 - V_f)$ is the composite shear modulus, E_m and E_f are (respectively) the Young's modulus of matrix and fibres, $\gamma_{critical}$ is the composite average shear strain at the critical stress, and \bar{y}_0 and L are (respectively) the initial imperfection's amplitude and length. As pointed out by the author, this approach differs from the previous buckling analysis by considering the equilibrium of only the fibre (and not a fibre and matrix), which leads to the inclusion of the fibre volume content and therefore decreases the strength that would, otherwise, be overestimated. The correlation between this analytical model and the experimental data is good, especially for composites with stiff matrix.

Reference [16] presents an analysis for fibre bending taking into account the external work done by the compressive load and the internal energy due to bending of the fibres and shearing of the matrix; key features for kink band formation are the fibre failure due to micro-buckling and the deformation of the material within the band, by this order. **Steif's** model considers an imperfect (sinusoidal) fibre under bending, with finite deflections and large fibre rotations (θ); the equation governing the problem is deduced from the equilibrium of moments, considering the action of the compressive load, the bending moments and the shear stresses transferred by the matrix. Although it assumes an in-phase shear deformation during kink band formation, one of the novelties found in this model is the way the shear stresses τ_m are computed as one continuous function of the fibre rotation, providing an almost linear response for small θ and a nearly perfect plastic (strength S_m) response for large θ :

$$\tau_m = S_m \cdot \tanh \frac{G_m \cdot \theta}{S_m} \quad (2.5)$$

Fibre failure is considered to occur when the tensile strain (considering both axial strains due to bending and compression) reaches the fracture tensile strain for fibres; the results are very sensitive to the initial imperfection (kink band's width corresponds to half of its wavelength $w = L/2$) considered, but seem to cope with the range

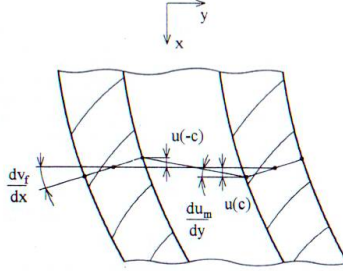


Figure 2.9: Morais and Marques model for matrix shear deformation [17].

of the experimental results.

Morais and Marques [17] developed a model similar to the previous one, including second-order terms for the matrix shear strain, using curved (not straight) beam theory, imposing a sinusoidal shape both for initial and deformed configurations of the fibre and assuming a constitutive law for the matrix that incorporates both non-linearity and yielding; besides, it calculates the deformation of the matrix considering its deformed geometry at in-phase mode (as show in figure 2.9). The governing equation is then solved numerically through incrementation of stress on fibres, until the system reaches a critical state, which is considered to correspond to the composite's strength. The correlation between the results from this model and the ones from FE analysis is considered excellent, being the compressive strength predicted with an accuracy up to 99%.

In the same paper, Morais and Marques present also an extension of the previous 2D model to 3D, by computing a 3D equivalent of the matrix shear modulus given as

$$G_m^{3D} = (1 + V_f) \cdot G_m^{2D} \quad (2.6)$$

Also in this case, the agreement with FE results was very good. When it comes to experimental results, the analytical model developed shows differences that can reach 34%, being the 3D version more accurate than the 2D one.

More recently, **Dávila et al.** [18] propose, in their LaRC03 criteria, a prediction for damage initiation under axial compression based on the assumption of initially misaligned fibres and a shear dominated failure. These authors were able to compute the fibre misalignment for any given (2D) load combination, and that angle would then be used to calculate the stress components in the material's principal directions; having σ_{22} and τ_{12} for the matrix in the misaligned material, these could be used as inputs for matrix failure criteria. By assuming that once the matrix fails the fibres loose their support and break as a consequence, this model separates completely the formation of kink bands from micro-buckling or fibre failure.

In this model, the initial fibre misalignment (θ_0) is not a required parameter: it is deduced from failure by pure compression, leaving θ_0 as the unknown and imposing $\sigma_{11}^{failure} = X_C^C$.

In their review on the theories developed to explain compressive axial failure of composites [1], **Schultheisz and Waas** emphasize the importance of taking into account fibre misalignments, matrix non-linear behaviour and tridimensional stress states in further models on fibre kinking.

2.4 Discussion and Conclusions

Taking into account the goal of this project - development of an analytical model predicting failure load and kink band's geometry, supported by experimental and numerical results -, a discussion and summary of the previously presented review is going to conclude this chapter.

Despite the several different models that are already developed on fibre kinking, the physics of the process are not fully understood yet. Some authors still consider kink bands as the result of an instability occurring in the material, and for that reason the micromechanics are explained by buckling analysis; however, more recently the idea of a separate failure mode - explained by a localized deformation due to non-linearities instead of an instability - began to be more accepted among the researchers.

Most of the models consider, during kink band formation, a fibre under bending and (eventually) surrounded by a continuum matrix with shear response. It seems reasonable to consider, for the fibres, only the axial stresses, while for the matrix both compression and shear should be taken into account.

Several models predicting the formation of kink bands under compressive loading, bending moments and interfacial shear stresses have already been developed; differences between them are related to the complexity of the mathematics used to formulate the problem, as the mechanics (equilibrium of moments) are considered to be the same; in addition, differences are also found in the point when a kink band is defined, as the researchers finish their analysis either when instability, matrix yielding or fibre failure occur. Among the models with bending analysis that do not end with a buckling solution, it should be noticed that none of them frees the deformed shape for the fibres, always assuming it to be sinusoidal.

Considering the great diversity of theories developed on fibre kinking, the need for a proper understanding of its physics and mechanics before the development of another analytical model comes as evident; both numerical simulations and experimental tests proved to be able to clarify some of the issues that fibre kinking raises. From the overall results, it can be concluded that fibre axial stresses, matrix yielding and shear stresses do play an important role in kink band formation; the typical response of a material when creating a kink band is initially linear, presenting a drop in the load after the peak is reached and slowly tending to a steady state response.

Numerical models for kink bands initiation and propagation are usually 2D (or semi-3D) models, representing layers of fibres and matrix. The fibres are well modelled as linear elastic and isotropic, while the matrix is usually considered to be isotropic and following a linear elastic - plastic with hardening - perfect plastic constitutive law. The effect of several parameters in the composite's strength and kink band's geometry was studied by several authors with consistent results. There is, however, a lack of a qualitative information from numerical models in the literature, namely when it comes to stress and strain fields; these would make the several load versus displacements curves more understandable from the physical point of view.

When kink bands are to be studied experimentally, the best approach is considered to be the development of stable and in-plane kink bands; this type of formation and propagation can be reached (in an approximate way) if thick composites are used and if a shear component is added to the load. Although much information obtained from experimental results is already available, there is barely no information that allow the material's response at the micro-level to be understood, as kink bands are often observed in post-mortem specimens or with a low resolution, not revealing much about the behaviour of each constituent during the development of the band.

Finally, it should be noticed that even the definition of kink band is not perfectly clear: the fibre failure at band's boundaries, one of the main characteristics of a typical kink band, is not mandatory, as perfectly well defined

kink bands were found even without broken fibres at the edges; in addition, although the band's inclination ($\beta \neq 0^\circ$) is one of the main reasons for considering fibre kinking independent from fibre micro-buckling, a great part of the analytical models developed considers the kink band as an in-phase ($\beta = 0^\circ$) deformation of fibres. This reveals somehow the long way to be crossed before fibre kinking can be considered a completely understood failure mode.

Chapter 3

Experimental work

3.1 Objective

The development of a phenomenological analytical model for kink band formation requires the physics and mechanics of the process to be fully understood. Despite the considerable amount of data that can be found in the literature on kink band's geometry and loading curves, there is a lack of qualitative information that is needed to identify all the phenomena occurring and to establish the correct sequence of events leading to kink band initiation.

The aim of the experiments done in the scope of this project was therefore to obtain detailed information on how and why a kink band is formed; instead of quantitative results, the main goal was to study kink bands during initiation and propagation in order to track exactly what happens in this failure mode; this requires the composite to be observed at the micro-scale (so fibres, matrix and interface are distinguished) and fully loaded (so both the elastic and plastic deformations are accounted for).

3.2 Strategy

Considering the previously defined objectives for the experimental work, it comes evident that the simple initiation and propagation of a random kink band is not sufficient. In fact, the most common type of kink band observed in composite's research is found to initiate in an unstable way and through-the-thickness, leaving no time or room for a smooth propagation; additionally, the easiest way to look at a kink band under the microscope is in post-mortem specimens, which allows the material in the kink band and its neighbourhood to partially recover deformation. Therefore a different strategy, fully oriented to the obtainment of high amplification and high definition micrographs of loaded kink bands, was planned as described.

Material

The material used in the experiments is an industrial high-performance carbon-epoxy composite (T800/924), provided by Renault F1 as unidirectional pre-preg CFRP with nominal ply thickness of 0.125mm and a fibre volume fraction of 63%; as only a qualitative analysis was carried out, its characterization is not required in the scope of this program. The material was manufactured using the standard methods for pre-preg laminates.

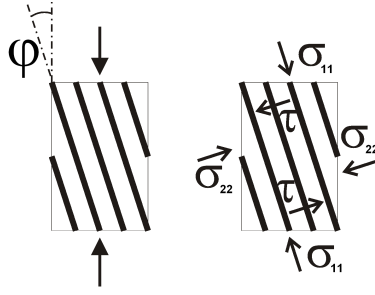


Figure 3.1: Misalignment between fibres and load direction and resultant stress components.

Thick specimens

One of the main goals for the experiments is to look at kink bands propagating, which requires them to be in-plane; in the literature (references [6, 7]), it is found that the specimens (or sub-laminates) developing in-plane kink bands are usually thicker than the ones presenting through-the-thickness kink bands. Following this suggestion (and with the additional advantage of hindering macro-buckling), thick specimens were intended to be used.

Considering the range of thicknesses that had already resulted in in-plane kink bands (3.18 to 7.6mm) and the ply thickness of the material used in this project (0.125mm), a thickness of 6.0mm was chosen for the plates, as it is within the referred values and gives a reasonable number of plies (48) for manual lay-up.

Combined direct compression and induced shear

For any observation to be feasible, the propagation of kink bands needs to be stable. This was also previously achieved by the combined action of both compressive and shear loads [8], applied independently to the specimens; however, such a loading scheme requires linear bearings able to sustain a high compressive load and a loading cell to control the shear displacement, being this equipment not available. Therefore, an alternative was searched, and the solution proposed was the use off-axis specimens (figure 3.1): by applying the unidirectional compression in a direction with a misalignment φ with respect to fibre direction, a combined compressive plus shear stress state is induced in the material's principal axes, being the relation between compression and shear defined by the off-axis angle as $\tau_{12} = \tan(\varphi) \cdot \sigma_{11}$.

In order to achieve the same shear to compression ratio used by [8], a misalignment angle of $\varphi = 8^\circ$ is needed; variations of $\pm 34\%$ in this ratio are produced when angles of $\varphi = 12^\circ$ or $\varphi = 6^\circ$ (respectively) are used.

This misalignment angle was introduced when manufacturing the specimens, by cutting them at angle with respect to fibre direction.

Stress concentrations

It was stated previously that kink bands are usually triggered by defects in the material or structure, either at the micro or macroscopic level; for this reason, their location is dependent on the randomness if no significant stress concentrations are introduced at one point, so notches or pre-cracks were manufactured in the specimens to define the position of kink band formation.

Monitoring

The study of this phenomenon using micrographs is much more efficient if the kink band is captured on early stages and before other failure mechanisms (e.g. material crushing) can take place; as a consequence, it is important to identify accurately the moment when a kink band is initiated and starts propagating in the specimen, so a clean image can be obtained. Besides, being a compressive and usually unstable failure mechanism, the formation of kink bands can easily damage the material in a catastrophic fashion, leading to fibre crushing and out-of-plane movements. A proper monitoring, capable of identifying kink band formation, is then strongly advisable, so both a load versus displacement recorder and acoustic emission equipment were used whenever possible, to track the macro (peak load) and microscopic (fibre failure) responses.

Types of experiments

Notwithstanding these strategic guidelines, a complete test plan could not be defined completely a priori: the main goal of this experimental program was to develop a method resulting into kink bands observable at the microscopic level and loaded, and therefore iterations to the specimens and test procedures were likely to be necessary (and actually took place). In the overall, three different types of specimens were used, each one in a different kind of experiment.

UD test the unidirectional specimens have a tall and narrow rectangular geometry, weakened at one edge with a semi-circular notch or short pre-crack, compressed in a load machine by edge displacement (figure 3.2 a);

CC test the compact compression specimens are nearly square specimens, with a cross ply lay-up and a long pre-crack, compressed in a load machine by point displacement applied at the holes (figure 3.2 b);

r-UD test the reduced unidirectional specimens are a shorter version of the UD specimens, to be compressed under the microscope using a clamp or especially-conceived rig (figure 3.2 c).

Among these three experiments, the first two (UD and CC) were planned a priori, despite some details (dimensions and loading scheme) that were adjusted after the first set of tests. However, the r-UD specimen and set-up was fully developed afterwards, due to the lack of quality of the results provided by the two predefined methods.

3.3 Manufacturing

The manufacturing of the specimens followed the common procedures for pre-preg CFRP and is shortly summarized hereafter; only those issues directly related to how the manufacturing was performed are approached in this section, as the general design justifications were already given in the previous section and the specific one will be provided separately for each specimen afterwards.

In addition, some problems occurred while the specimens were being produced; although not hindering the testing plan already sketched, this had some implications on the manufacturing process and also in the specimens themselves, so a discussion will be given as well.

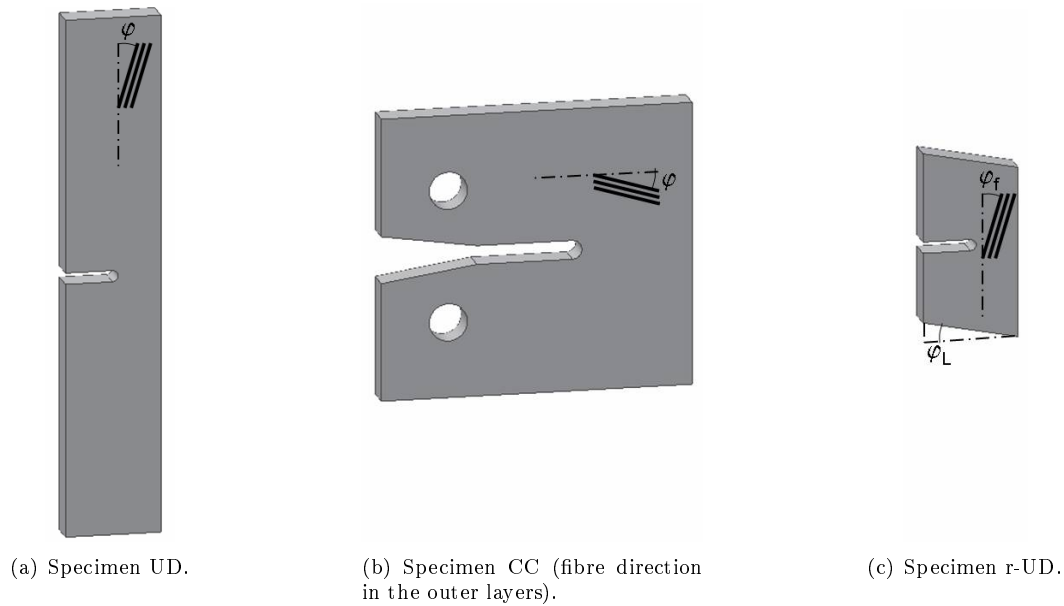


Figure 3.2: Specimens used in the experimental program.

3.3.1 Lay-up

The material used in this work was provided in a continuous roll, so in order to lay-up the composites it was necessary to cut a specific number of plies with the proper dimensions and to stack them with the right orientation in plates. As it was already mentioned, two different stacking sequences were needed for experimental program: a unidirectional one - for UD/r-UD specimens - and a cross-ply one - for CC specimens; for this reason, two plates were laid-up:

UD plate with a stacking sequence $[0_{48}^{\circ}]$;

Cross-ply plate with a stacking sequence $[90_6^{\circ}/0_6^{\circ}]_{2S}$.

The dimensions of the plates - $300\text{mm} \times 300\text{mm}$ for both of them - were defined in order to optimize the use of material, as the manufacturing of misaligned shapes would already result into a significant amount of scrap.

After being cut, the plies were laid up manually in the previous stacking sequences, caring to keep the fibre direction properly oriented; during the lay-up, a vacuum table was used in every set of 3 or 4 plies to improve the bonding and remove the air kept enclosed between them.

Due to the adoption of an inappropriate laying-up strategy, the stacking sequence of the first cross-ply plate (*cross - ply plate 1*) was not reliable; for this reason, a second plate was laid-up (*cross - ply plate 2*), this time following a proper approach so with a reliable stacking sequence.

After curing, the three lay-ups were observed under the optical microscope; the stacking sequence seemed to be correct for all of them, although it was not possible to be totally sure about that for the cross-ply laminates, due to high fibre movement during curing.

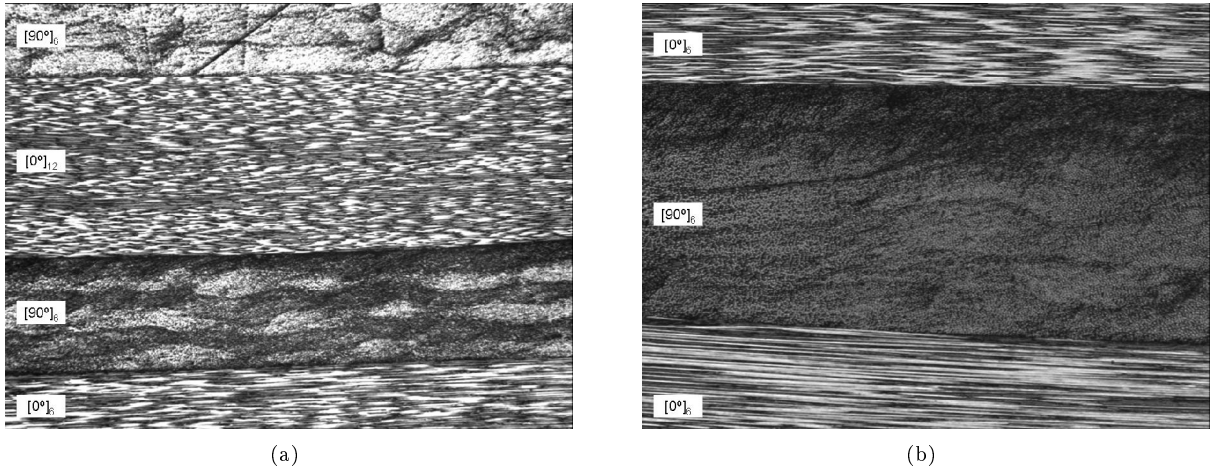


Figure 3.3: Micrographs of *cross – ply plate 1*.

3.3.2 Curing

After the lay-up, the plates went into the autoclave to be cured by the combined action of temperature and pressure, in a standard cycle for the material and dimensions in use; unfortunately, all the three plates (cured in the same run) came out of the autoclave considerably bent (figure 3.3 a).

Although it is not possible to be sure about any justification, the most likely reason for this is to have happened is a problem during the curing cycle: the material had been used before without any problems, and as the UD (confirmed by micrographs) plate was bent as well then the hypothesis of any asymmetry through the thickness was discarded.

Two details can reveal what went wrong during the autoclave run: at first, the panels were constrained by a lateral frame before going into the autoclave (to avoid a high flow of resin near panels' edges), which could have hindered the panels' thermal expansion and induced bending. On the other hand, some of the thermocouple monitoring the temperature during the curing cycle showed an odd response, which suggests that the temperature inside the autoclave was either not uniform or not the correct one; if it was the case, then it is possible that the thermal residual stresses were high enough to induce bending.

The panels' sections were checked by optical microscopy; micrographs (figure 3.3) show a large waviness of the fibres and blunt boundaries between layers (subfigure a), which implies an unusual fibre movement and matrix flow through the thickness. In addition, a significant variation in the thickness was found in the panels (subfigure b), but the micrographs do not evidence any variation in the fibre volume fraction through the thickness, which excludes the possibility of a massive matrix flow in that direction.

Concluding, the most likely cause for the bent laminates is an internal problem with the autoclave on the control of temperature or pressure during the curing cycle; besides the hints previously discussed, other plates (laid-up by different people, with different material and stacking sequences) also went through similar problems, which supports the lack of reliability in the autoclave runs.

Notwithstanding the fact that the bent shape implies large residual stresses, being therefore no significant quantitative results obtainable, the experimental program was carried on, as the physics and mechanics involved in the formation of kink bands should not be affected in a severe way. Moreover, the high waviness detected on the fibres plays the role of fibre imperfection, and the curved shape of the plates implies their concave side to

be under compression, being both aspects benefic for kink band formation.

However, being the plates bent, it was likely that, under compression, they would fail by macro-buckling instead of fibre kinking; for this reason, it was decided that all the specimens should be flattened by grinding (machining); this caused their thickness to decrease (especially for the taller specimens), which could have an impact on the type of kink band obtained (increase of the out-of-plane component).

Additionally, after polishing the specimens' surface, the initial waviness and curvature of the fibres would make it impossible to follow one fibre along a long path.

3.3.3 Machining

After the cure, the specimens were machined. As it was mentioned before, the experimental program was flexible enough to accommodate changes in the shape of the specimens, so a detailed description and justification of the specimens' shape will be provided in a further section; nevertheless, the processes and tools used to cut the specimens are sequentially summarized hereafter.

UD specimens:

1. The reference edges were aligned using a guide protractor and cut with a dry saw with diamond blade;
2. The secondary edges were cut with a wet saw;
3. The specimens were flattened by grinding (machining);
4. A notch or crack was opened using a band saw;
5. For some specimens, the top and bottom edges were cut in an angle, using the procedure 1.

CC specimens:

1. The reference edges were aligned using a guide protractor and cut with a dry saw with diamond blade;
2. The secondary edges were cut with a wet saw;
3. The specimens were flattened by grinding (machining);
4. A crack was opened using the dry saw and a wooden guide block;
5. A V-shape was opened using a band saw;
6. Two holes were drilled between two pieces of scrap material with a high speed steel drill;
7. After testing, the specimens were grinding (machining) until the outer plies oriented at the transverse direction were removed and a ply with longitudinal orientation was exposed.

r-UD specimens:

1. The four edges were sketched on the plate's surface and cut using a band saw;
2. A pre-crack and V-shaped opening were sketched on the specimen and cut with a band saw;
3. The pre-crack was sharpened with a modelling blade;
4. Both main surfaces were flattened by grinding (#220) on a polishing machine;
5. Specimen's top and bottom surfaces were flattened and parallelized using polishing paper;
6. Specimen's edges and corners were smoothed using polishing paper;
7. The front surface of the specimen was polished with a diamond suspension.

3.3.4 Polishing

Being the qualitative observation the main goal of this experimental program, the quality of specimens' surface was of the highest relevance. As it will be confirmed in further sections, a proper observation of kink bands had to be done using high magnifications, requiring a very fine polishing so matrix and fibres could be distinguished.

Additional difficulties were raised when polishing the specimens. The standard procedure is to cut a small specimen sample and to immerse it in resin, being the block polished automatically on a polishing disk using a rotative head afterwards; however, as in this project the kink bands were to be observed while loaded, it was not reasonable to destroy the specimens by cutting small samples. Two problems raised at this point: first, the surface to polish was much larger than usually, so any misalignment between the specimen's surface and the polishing disk would imply a huge amount of material to be removed; second, polishing could not be done automatically, as the specimens were too large to be fixed directly to the rotative head.

Taking this all into account, it is understandable that polishing had become an issue in the experiments. Among all the strategies tried, the most successful one consisted in stopping the rotative head and fixing the specimen to it through a small resin cylinder bonded to its surface; to avoid the effect of misalignments, all the steps - from grinding at #220 to polishing with a $3\mu\text{m}$ diamond suspension - were done with the specimen oriented in the very same way (being the polishing direction aligned with the fibres). Nevertheless, 20min was the minimum duration of the last polishing step.

3.3.5 Manufacture control

As no quantitative results were expected from the experiments, the manufacture of the specimens was monitored at the minimum extension.

C-scan

Some specimens from each plate were checked by C-scan after manufacturing, which confirmed that no major defects were present.

As it was assumed that small defects would not hinder the development of kink band, and as the existence of large delamination areas or ineffectiveness of curing were already discarded (by micrographs of the plates'

section), the majority of the specimens were tested without being scanned; none of the specimens was monitored after testing. Although this is not a severe fault (for the reasons already mentioned), the C-scan could have been useful to identify failure modes found in some specimens.

Micrographs

As it was previously referred, microscopic observation was used to confirm the stacking sequence of the laminates and to check the quality of the curing process. In addition, the quality of the pre-crack tip in the r-UD specimens (sharpened with a modelling saw) was checked by optical microscopy.

3.4 Set-ups and specimens description

3.4.1 UD test

3.4.1.1 Specimen

Initial design

The initially planned UD specimen, cut from the UD plate at a misalignment φ , was based on several rectangular and notched specimens already tested by other researchers [6, 8] in successful initiation, propagation and broadening of in-plane kink bands, being the off-axis orientation the principal innovation.

Specimen's width and thickness were defined a priori, keeping the specimen as wider as the one used in [6] and sufficiently thick to promote an in-plane kink band; its length was adjusted in order to allow an already manufactured anti-buckling plate with an window (figure 3.5 a) to be used.

Stress concentrations were induced in the specimen using a semi-circular notch in one edge with a radius of 1.2mm, as used in [8]. From this geometry, the expected failure load was predicted by:

$$P^{max} = k_{notch} \cdot X_C^C \cdot A_r, \text{ with } \begin{cases} X_C^C = 1300\text{MPa as the composite's axial compressive strength} \\ A_r = 112.8\text{mm}^2 \text{ as the specimen's reduced cross section} \\ k_{notch} = 60\% \text{ as the notch's stress concentration factor [7]} \end{cases} \quad (3.1)$$

$P^{max} = 88\text{kN}$ was the load predicted, which is within the load cell's range (100kN) planned to be used.

Before testing, the compressed face of the specimens was polished.

Iterative design

Having the baseline design previously described, some modifications had to be introduced due to manufacturing problems (curing) and to test results with undesirable failure modes (first specimens failed either by unstable collapse or by fibre splitting, figure 3.11).

As the UD plate came out of the autoclave bent along fibre direction, the UD specimens had to be ground (by machining) until their surfaces were flat; the specimens were considerably long along the curved direction, so a

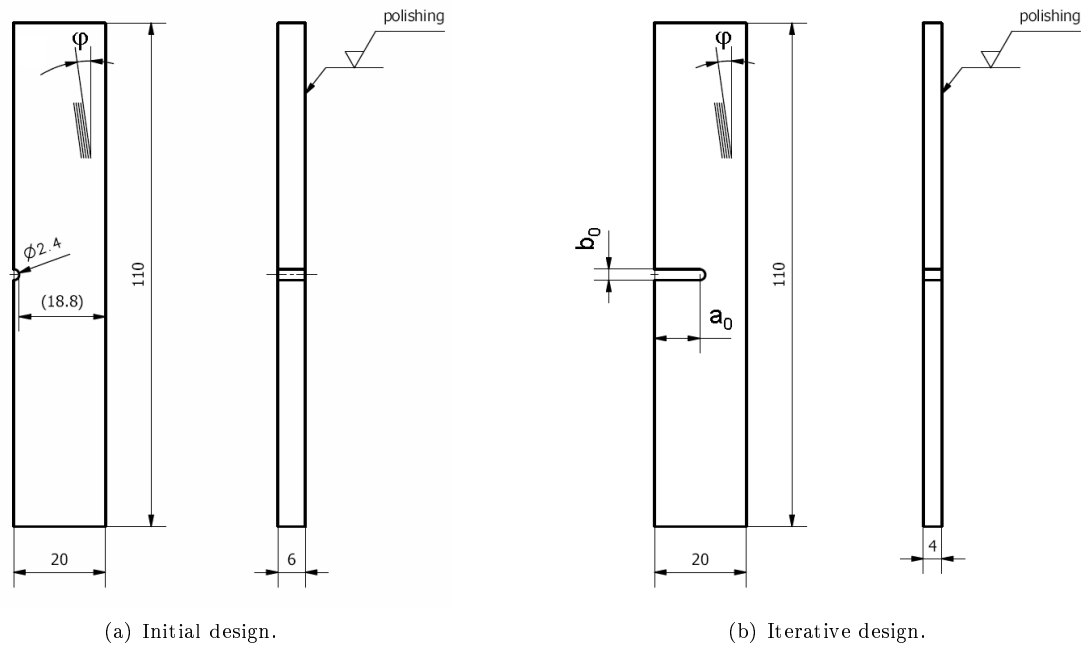


Figure 3.4: Specimen UD: definition drawings.

great amount of material had to be removed. Therefore, specimens' final thickness was reduced to 4mm, with the implications already discussed.

After the first set of tests carried out, it was found that the range of misalignment angles previously calculated was not suitable for this geometry, as it led to failure by splitting instead of kink band formation (figure 3.11 b); for that reason, smaller misalignment angles (from $\varphi = 0^\circ$ to $\varphi = 4^\circ$) were used in further experiments. However, as some specimens were already cut with too large angles, the solution was to cut the top and bottom surfaces at a given angle, in order to reduce the misalignment between load and fibre direction; this had the consequence of adding an in-plane moment to the loading scheme.

In addition, it was also noticed that, using the semi-circular 1.2mm indentation, the failure was unstable (figure 3.11 a). For that reason, a J-integral FE analysis of a crack under tension was performed, predicting a stable crack propagation for a minimum pre-crack length around 15mm; as, in the experimental case, the specimen was under compression and kink bands could be formed, it was expected that a stable failure would develop for smaller pre-cracks; for that reason, the initial small notch was extended to a pre-crack (3mm thick) 10 to 15mm long.

Before testing, the specimen's face under compression was ground (#220) in the polishing disk, to improve the quality of the images obtained.

3.4.1.2 Test set-up

The UD specimens were tested in a universal Zwick testing machine, using a 100kN load cell.

The aim of this test was to record the kink band that would be formed during compression with a DSP camera plugged in a hand microscope; this required the kink band to be formed at the specimen's free surface, which should not be obstructed. However, as it was foreseen that, without the proper support near the test rig, the specimen would fail by macro-instability, an anti-buckling plate with a central window was used (figure 3.5 a).

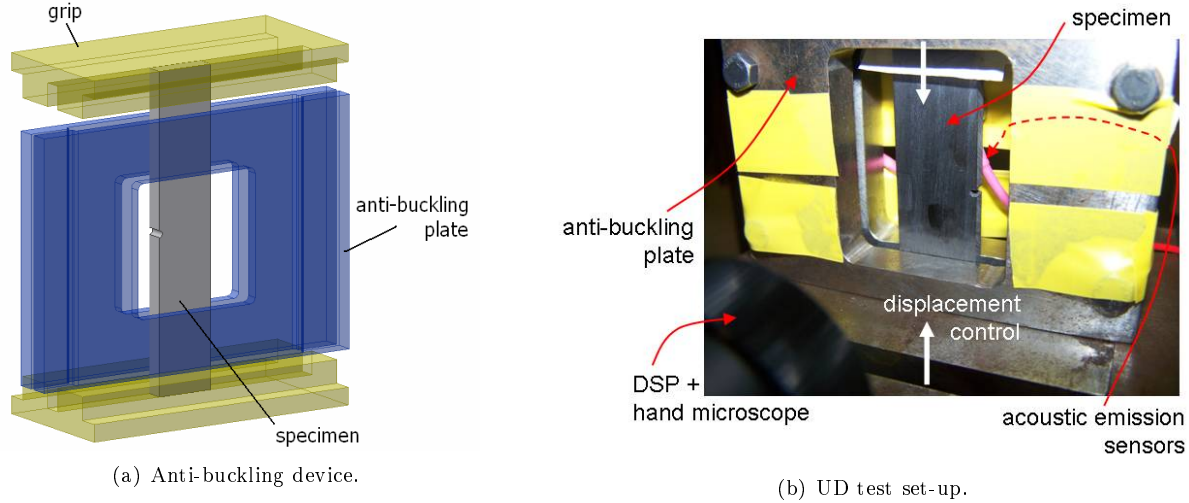


Figure 3.5: UD test set-up.

To avoid friction between the anti-buckling device and the specimen (which would induce undesirable constraints to the kink band formation), the surfaces in contact were covered by a Teflon film.

Two acoustic emission sensors were fixed at the back of specimen with tape; a proper calibration of the system was performed before every test. The outputs from the acoustic emission were used to monitor the damage in the specimen at the micro-scale, as fibre failure would be easily distinguished from the other failure modes and damage localization was possible to be estimated using this method. In addition, the test machine's load versus displacement curve would allow the peak load to be detected.

The image recording system was mounted in front of the specimen, carefully aligned and configured to optimized the quality of the images, with additional lightening. During the test and as the specimen was moving, the DSP and light were frequently adjusted in order to optimize its position and orientation.

The tests were performed at displacement control, with a testing velocity between 0.5mm/min and 2mm/min.

3.4.2 CC test

3.4.2.1 Specimen

The CC specimen, cut from the *cross – ply plate 1* at a misalignment φ in relation to the 0° layers, was based on the CC specimen used for fracture toughness measurements [2], as they were effective in compressive testing and generating (through-the-thickness) kink bands. Besides the off-axis orientation (from $\varphi = 0^\circ$ to $\varphi = 12^\circ$), the CC specimens used in this experimental program had a thicker inner layer (1.5mm, oriented at an angle φ with respect to the load), which would hopefully be enough to generate an in-plane kink band.

Specimen's main geometry was defined as in the CC standard specimens; the crack length a_0 was estimated

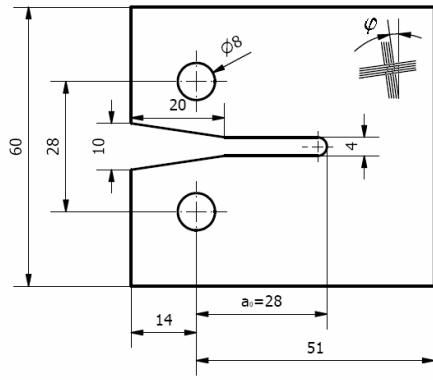


Figure 3.6: CC specimen: definition drawing.

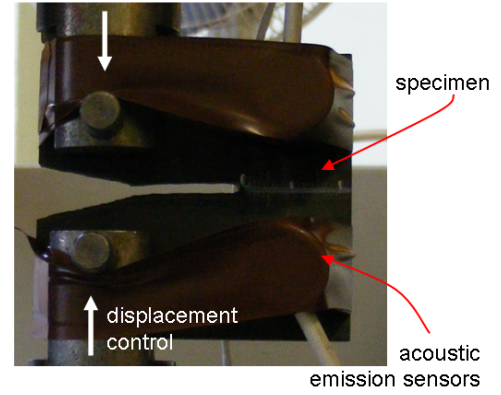


Figure 3.7: CC test set-up.

using the expression (as in [3]):

$$\mathcal{G}_{IC}^{lam} = f(a_0) \cdot \left(\frac{P}{t}\right)^2, \text{ being } \begin{cases} P = 5\text{kN} \text{ the desirable load for propagation} \\ t = 6\text{mm} \text{ the specimen's thickness} \\ f(a_0) \text{ the normalized energy release rate for the } a_0 \text{ crack length} \\ \mathcal{G}_{IC}^{lam} \approx \mathcal{G}_{IC}^{(90,0)ss} = 50\text{kJ} \cdot \text{m}^{-2} \text{ the laminate's fracture toughness at mode I} \end{cases} \quad (3.2)$$

From that calculation, $f(a_0) = 7.20 \times 10^{-5} \text{m}^2/\text{kJ}$, which gives an estimation for the initial crack length of $a_0 = 28\text{mm}$.

Due to the loading scheme - displacement directly imposed to the specimen's holes -, this geometry required a cross-ply stacking sequence, as otherwise there would be significant damage and possibly even failure near the holes; this and the fact that, under axial compression, buckling delamination was likely to occur, turned the presence of transversely oriented outer plies unavoidable for the stage of kink band initiation. However, and as the propagation load is much lower than the initiation one, after first testing the outer transverse layers of some specimens were removed by grinding (machining) so to expose the kink bands previously initiated; this made it possible to re-test and observe the kink band propagating while loaded, using the same apparatus (DPS and hand microscope) that was already described for the UD specimens.

Due to the bending also found in the cross-ply plates, these specimens were ground (by machining) to a thickness of 4mm as well.

3.4.2.2 Test set-up

The CC specimens were tested in a universal Instron testing machine, using a 10kN load cell.

The specimens were fixed to the testing rig through the holes and then compressed in displacement control at a rate between 0.5mm/min and 2mm/min. Following the same strategy that was already described for the UD test set-up, an acoustic emission system and the load versus displacement curve were used to monitor the test.

When re-testing after outer layers removal, the central thick (1.5mm) longitudinal (with a misalignment φ) layer was visually accessible, so the previously described DSP plus hand microscope set-up was used to record kink band propagation.

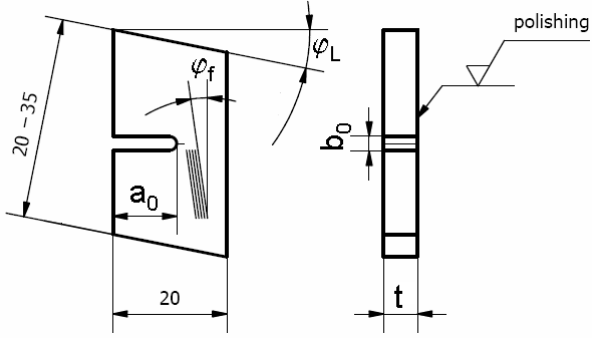


Figure 3.8: r-UD specimen: definition drawing.

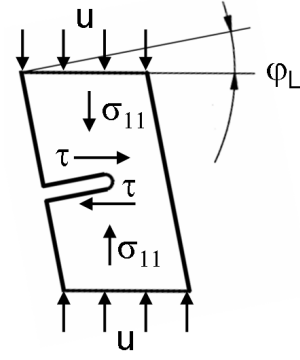


Figure 3.9: Shear induced in r-UD specimens.

3.4.3 r-UD test

As it was discussed before, none of the two initially planned testing set-ups was successful in achieving the goals of this experimental program, as it was not possible to observe a kink band with a sufficient magnification using the hand microscope plugged on the DSP (figure 3.12); by this stage, it became evident that it was necessary to compress the kink band in a test rig that could be placed directly for observation under a proper optical microscope. For this reason, a reduced version of the UD specimen, for manual compression in a small clamp, was designed.

3.4.3.1 Specimen

The r-UD specimen kept the same width as the UD specimens, being its length reduced to a value from 20mm to 35mm. As the specimens were bent over a shorter length, the amount of material to remove by grinding was much smaller, so thicker specimens were obtainable; however, some r-UD specimens were cut directly from UD ones, so the thickness of the samples varied between 4mm and 6mm.

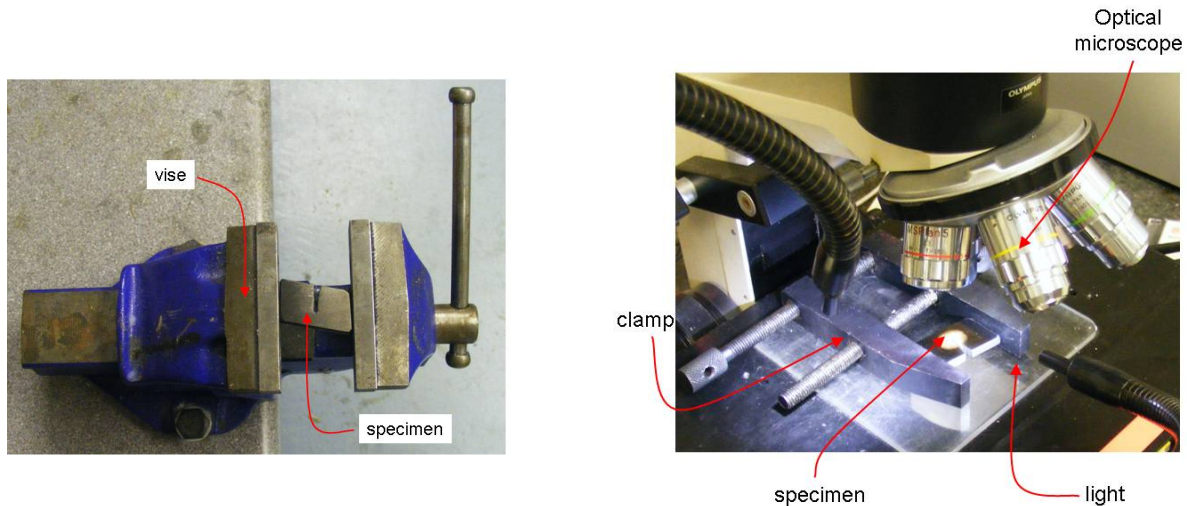
As the compression of these specimens would be manual (although making use of clamping tools), the initiation of the kink band should not require high loads. For this reason, a long pre-crack ($a_0 = 10$ to 15mm and $b_0 \approx 3$ mm, sharpened with a modelling blade in almost all specimens) was cut in the r-UD specimens, leaving a reduced cross section 5mm long.

A shear component was added to the compressive load by cutting the specimens at a small misalignment φ_f with the load direction and / or by cutting them in a parallelogram-like shape (at an angle φ_L , which offsets the two load vectors and induces an in-plane moment, figure 3.9).

As a microscopic observation was planned, one surface of each specimens was polished (before or after kink band initiation). In addition, it came out from the first tests that a proper alignment between the two loading surfaces and the absence of stress concentrations near the specimen's edges were needed (to promote the desired failure mode), so the following specimens had their top and bottom surfaces, edges and corners smoothed by polishing.

3.4.3.2 Test set-up

At a first stage, a kink band was initiated by compression in a vise (figure 3.10 a): the specimen was carefully placed between the two arms of the tool, so to properly align it in the out-of-plane direction (to avoid inducing



(a) Set-up for kink band initiation.

(b) Set-up for kink band observation.

Figure 3.10: r-UD test set-up.

bending moments) and to guarantee a smooth contact between the vise's and specimen's surfaces (to reduce stress concentrations). The vise was then closed manually, using an extension arm for better control of the displacement, until a kink band was formed.

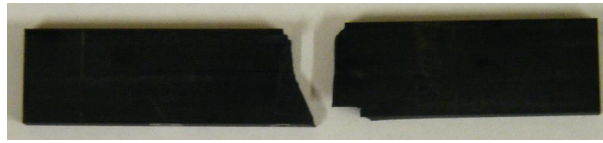
After kink band initiation (confirmed by microscopic observation), the propagation load would decrease, so the specimen was further compressed in a small clamp (figure 3.10 b); as the test progressed, the clamped specimen was repeatedly placed under the optical microscope for micrographs to be taken. As it was noticed that out of plane movement occurred both near the tip as in the fully-developed kink band, an additional lightening system was used to improve the visualization of the inclined areas.

3.4.4 Evaluation and comparison of test set-ups

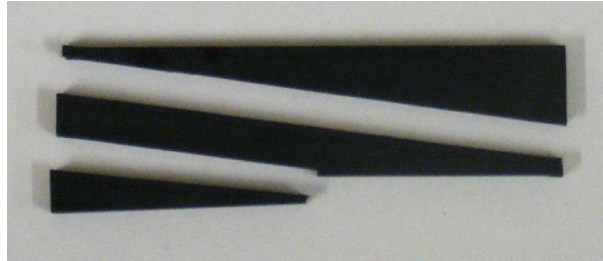
UD

The UD set-up was conceived to guarantee visual access to the kink band's path, so initiation and propagation could be followed and recorded; however, the images obtained using the hand microscope plugged in the DSP were far away from the required quality to make useful observations (figure 3.12 a). In addition, this set-up proved to be very sensitive to specimen's design, as undesirable failure modes (splitting and unstable cracking) were observed (figure 3.11); also, it is inefficient from the material point of view, as the area of interest is very small when compared to the specimen's size.

Besides the low magnification attainable by the hand microscope and DPS, this set-up proved not to be very suitable for observation at the micro-level and under load, as the noise generated by the test machine was significant and the need for constant focus discouraging. It became obvious, at this point, that a testing rig especially conceived for microscopic observation was needed.

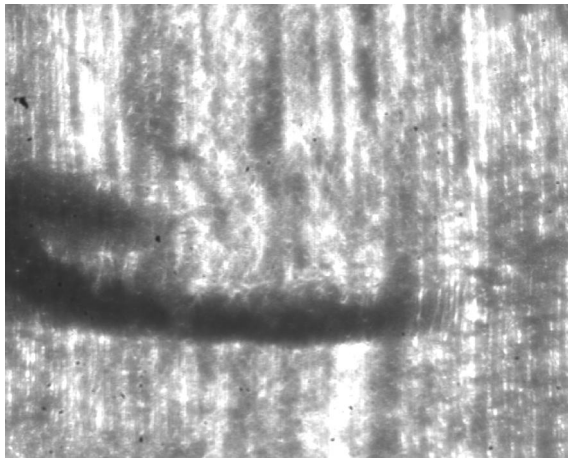


(a) Unstable failure.

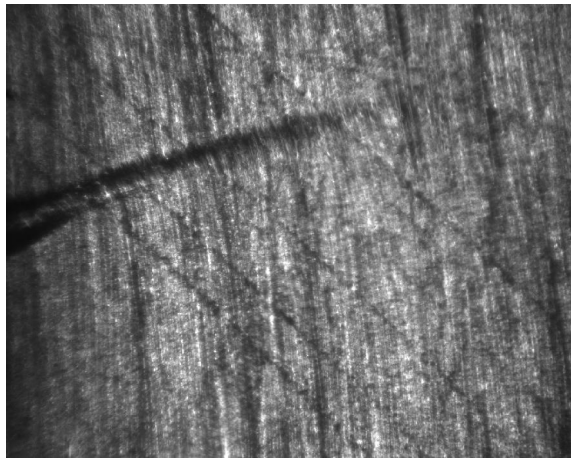


(b) Splitting.

Figure 3.11: Failure modes for UD specimens.



(a) With extension tube (magnification 2 \times).



(b) Without the extension tube.

Figure 3.12: Images recorded by the DSP plugged on the hand microscope.

CC

The CC test was chosen as an alternative to the UD one, providing a different loading scheme (point load instead of uniformly distributed load) and a different lay-up; however, one great disadvantage of the CC specimens was obvious from the beginning, as they do not allow direct access to the in-plane kink band expected to develop in the central layer. Despite that, and comparatively to the UD specimen, the CC test proved to be more efficient in generating kink bands (almost all the specimens failed by fibre kinking) and propagating them in a stable way, even after removing the outer layers.

However, the main problem mentioned for the UD specimens was not solved with this different configuration: the combined use of the hand microscope and DSP camera did not provide images with sufficient quality for the desired type of analysis (figure 3.12 b). Nevertheless, the CC specimens provided a larger path for the kink band to propagate, so a somehow good overview of the phenomenon was obtainable with this set-up.

r-UD

Being conceived specifically to surpass the main limitations found in the other testing set-ups (lack of microscopic observation of loaded kink bands), the r-UD specimen was able to improve significantly the amount and quality of information obtainable from a test: as it was possible to observe the specimen under the optical microscope while compressed, pictures of loaded kink bands with high magnification and high resolution were attainable.

However, three significant problems were found with this approach too: at first, as the kink bands were not totally in-plane, it was not possible to focus properly the image, turning the interpretation of the micrographs into a much less straight forward task that it would be without the interference of shadows and out-of-plane movement. Secondly, as the compression was done using regular clamping tools, no proper support or alignment was given to the specimen, which resulted sometimes in other failure modes than fibre kinking (helped also by non-flat loading surfaces). Finally, the fact that initiation could only be triggered using the vise made it impossible to follow the development of the kink band from the beginning and under the same load scheme.

Nevertheless, the r-UD set-up was the one that produced the most promising results, encouraging the development of a proper test rig specifically conceived for kink band observation.

3.5 Results

A summary on the results is provided in tables 3.1 and 3.2.

Specimen Type_ID	Configuration			Results		
	Cross section	Off-axis	Pre-crack	Failure mode	Outputs	Highlights / Comments
UD_0d1	$t = 4\text{mm}$	0	$\phi = 1.2\text{mm}$	UC	0	
UD_6d	$t = 4\text{mm}$	$\varphi_f = 6^\circ$	$\phi = 1.2\text{mm}$	S	0	
UD_8d	$t = 4\text{mm}$	$\varphi_f = 8^\circ$	$\phi = 1.2\text{mm}$	S	0	
UD_0d10	$t = 4\text{mm}$	0	$a_0 = 10\text{mm}$ $b_0 = 3\text{mm}$	KB - p	HM - L	
CC_0d1	$[90^*/0^\circ/90^\circ/0_2^\circ/90^\circ/0^\circ/90^*]$	0	$a_0 = 28\text{mm}$ $b_0 = 3\text{mm}$	KB - p	OM - uL	
CC_0d2	$[90^*/0^\circ/90^\circ/0_2^\circ/90^\circ/0^\circ/90^*]$	0	$a_0 = 28\text{mm}$ $b_0 = 3\text{mm}$	KB - p	OM - uL	In- and out-of-plane components.
CC_0d3	$[90^*/0_2^\circ/90^\circ]$	0	$a_0 = 28\text{mm}$ $b_0 = 3\text{mm}$	MB+D	0	
CC_2d	$[90^*/0^\circ/90^\circ/0_2^\circ/90^\circ/0^\circ/90^*]$	$\varphi_f = 2^\circ$	$a_0 = 28\text{mm}$ $b_0 = 3\text{mm}$	UKB	OM - uL	Interaction between kink bands.
CC_4d1	$[90^*/0_2^\circ/90^\circ/0^\circ]$	$\varphi_f = 4^\circ$	$a_0 = 28\text{mm}$ $b_0 = 3\text{mm}$	KB - i	0	
CC_4d2	$[0^*/90^\circ/0_2^\circ/90^\circ/0^\circ]$	$\varphi_f = 4^\circ$	$a_0 = 28\text{mm}$ $b_0 = 3\text{mm}$	KB - i	0	
CC_6d (1 st test)	$[90^*/0^\circ/90^\circ/0_2^\circ/90^\circ/0^\circ/90^*]$	$\varphi_f = 6^\circ$	$a_0 = 28\text{mm}$ $b_0 = 3\text{mm}$	KB - i	OM - uL	Uneven broadening.
CC_6d* (re-tested)	$[0^\circ/90^\circ/0_2^\circ]$	$\varphi_f = 6^\circ$	$a_0 = 28\text{mm}$ $b_0 = 3\text{mm}$	KB - i	HM - L	Kink band propagating.
CC_8d	$[0^*/90^\circ/0_2^\circ/90^\circ/0^\circ]$	$\varphi_f = 8^\circ$	$a_0 = 28\text{mm}$ $b_0 = 3\text{mm}$	KB - i	0	
CC_12d	$[90^*/0^\circ/90^\circ/0_2^\circ/90^\circ/0^\circ/90^*]$	$\varphi_f = 12^\circ$	$a_0 = 28\text{mm}$ $b_0 = 3\text{mm}$	KB - i	OM - uL	Ending in splitting.

Key :

Failure modes - UC: unstable crack; S: splitting; KB - i: kink band initiation; KB - p: kink band propagation; UKB: several kink bands.

Outputs - 0: none; HM: micrographs from the hand microscope plugged on the DSP; OM: micrographs from the optical microscope; SEM: micrographs from the SEM; L: outputs obtained under load; uL: outputs obtained after unloading; X*: specimen re-tested.

Cross section - $[\Phi^*]$: layer partially removed by grinding.

Table 3.1: Results (UD and CC specimens).

Specimen Type_ID	Configuration			Results		
	Cross section	Off-axis	Pre-crack	Failure mode	Outputs	Highlights / Comments
r-UD_0d0	$t = 4\text{mm}$	φ_L	$a_0 = 15\text{mm}$ $b_0 = 2\text{mm}$	KB - i	OM - L	sine-shape; out-of-plane movement
r-UD_0d1	$t = 4\text{mm}$	φ_L	$a_0 = 15\text{mm}^+$ $b_0 = 0.2\text{mm}$	KB - p	SEM - uL	macro kink band; no fibre failure; small 2nd kink bands; fibres break in groups
r-UD_0d2	$t = 4\text{mm}$ S	φ_L	$a_0 = 15\text{mm}^+$ $b_0 = 0.2\text{mm}$	KB - i	OM - L	Specimen polished after kink band formation; Edges defined unevenly.
r-UD_0d3	$t = 6\text{mm}$	0	$a_0 = 15\text{mm}$ $b_0 = 2\text{mm}$	KB - i	OM - L	$\beta = 0^\circ$; Jump in one edge.
r-UD_0d4	$t = 4\text{mm}$	φ_L	$a_0 = 15\text{mm}^+$ $b_0 = 0.2\text{mm}$	KB - p	0	
r-UD_0d5	$t = 4\text{mm}$	φ_L	$a_0 = 15\text{mm}^+$ $b_0 = 0.2\text{mm}$	S	0	
r-UD_0d6	$t = 4\text{mm}$	φ_L	$a_0 = 15\text{mm}^+$ $b_0 = 0.2\text{mm}$	S	0	
r-UD_0d7	$t = 6\text{mm}$	φ_L	$a_0 = 15\text{mm}^+$ $b_0 = 0.2\text{mm}$	S + C	0	
r-UD_0d8	$t = 6\text{mm}$ S	φ_L	$a_0 = 15\text{mm}^+$ $b_0 = 0.2\text{mm}$	-	0	
r-UD_0d9	$t = 6\text{mm}$ S	φ_L	$a_0 = 15\text{mm}^+$ $b_0 = 0.2\text{mm}$	KB - i	0	
r-UD_2d1	$t = 4\text{mm}$	φ_L φ_f	$a_0 = 10\text{mm}^+$ $b_0 = 0.2\text{mm}$	KB + S	0	Twisted deformed shape
r-UD_2d2	$t = 6\text{mm}$	φ_f	$a_0 = 15\text{mm}^+$ $b_0 = 0.2\text{mm}$	KB + S	OM - L SEM - uL	
r-UD_2d3	$t = 4\text{mm}$	φ_L φ_f	$a_0 = 15\text{mm}^+$ $b_0 = 0.2\text{mm}$	S	0	
r-UD_***	$t = 5\text{mm}$				SEM - L	Propagation length

Key :

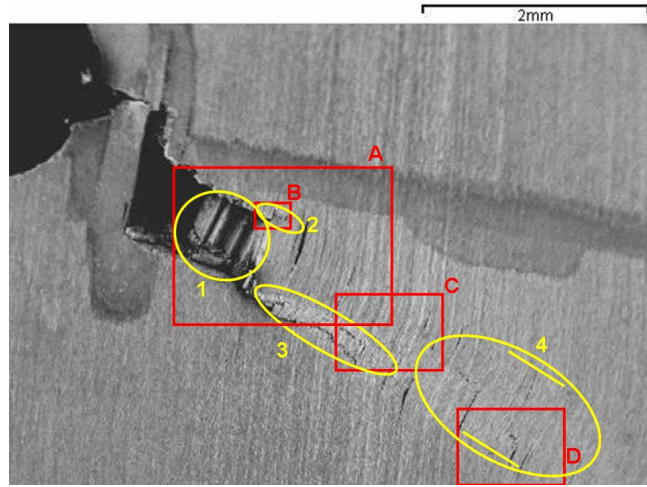
Failure mode - UC: unstable crack; S: splitting; KB - i: kink band initiation; KB - p: kink band propagation; UKB: several kink bands.
Outputs - 0: none; HM: micrographs from the hand microscope plugged on the DSP; OM: micrographs from the optical microscope; SEM: micrographs from the SEM; L: outputs obtained under load; uL: outputs obtained after unloading; X*: specimen re-tested.

Pre-crack - $a_0 = \bar{a}_0^+$: pre-crack extended with the modelling saw; *Cross section* - S: specimen smoothed with polishing paper.

Table 3.2: Results (r-UD specimens).



Figure 3.13: Specimen r-UD_0d1 (picture): macroscopic kink band.



1: macro-kink band with broken fibres;
 2: micro-kink band at the top edge;
 3: micro-kink band at the bottom edge;
 4: macro-kink band without broken fibres.

Figure 3.14: Specimen r-UD_0d1 (SEM, unloaded): overview.

3.5.1 Macroscopic kink band without broken fibres (specimen r-UD_0d1)

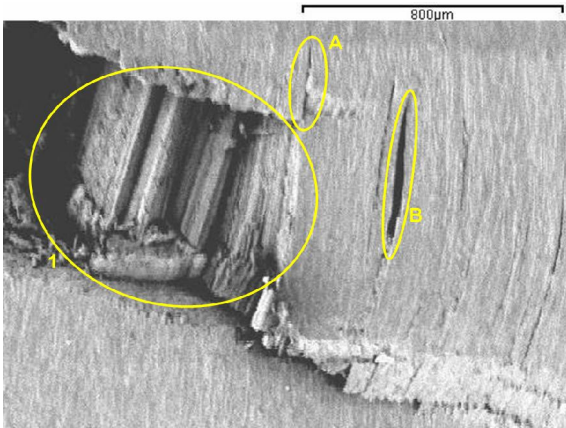
The kink band formation in the specimen r-UD_0d1 was sudden, with full propagation across the specimen's width. As it can be seen in figure 3.13, this kink band can be easily identified by unaided eye, presenting a width $w \approx 800\mu\text{m}$ and perfectly defined boundaries.

Analysing the micrographs obtained in the SEM¹, it can be noticed that, at the microscopic level, four kink bands were formed, all with a similar band orientation $\beta \approx 24^\circ$. In figure 3.14, these are identified by numbers from 1 to 4:

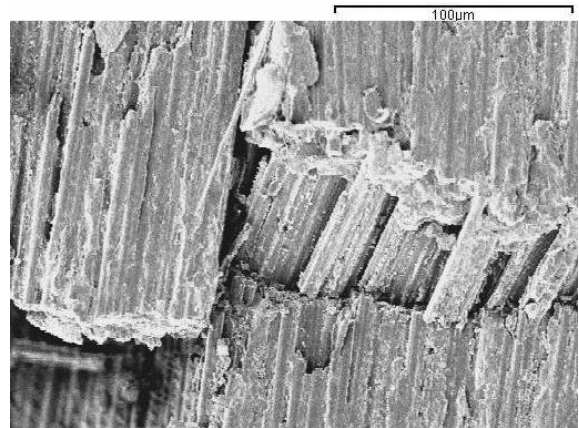
1. A large kink band, with broken fibres, is formed near the notch, with $w \approx 700\mu\text{m}$ (feature 1 and figure 3.15 a);
2. A microscopic (very narrow, $w \approx 50\mu\text{m}$) kink band is formed at the top edge of the macro-kink band, where the first kink band ends (feature 2 and figure 3.15 b);
3. Another microscopic kink band ($w \approx 150\mu\text{m}$), at the bottom edge of the macro-kink band, where the first kink band ends (feature 3);
4. A large ($w \approx 800\mu\text{m}$) kink band (as a continuation of the first one), without broken fibres (feature 4 and figures 3.15 c and d), crosses the specimen until reaching its edge.

All micrographs show, at the unloaded configuration, several splittings along fibre direction (figure 3.15 a), both inside (B) the band and at its boundaries (A); the spacing between splittings is irregular. For the kink bands with broken fibres, it is suggested by figures 3.15 a and b that kinking occurs by blocks of few fibres, with splittings between each block.

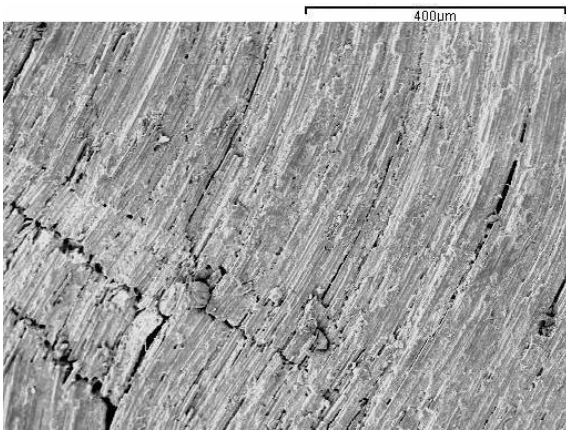
¹Acknowledgments to Renaud Gutkin and William Francis for these micrographs.



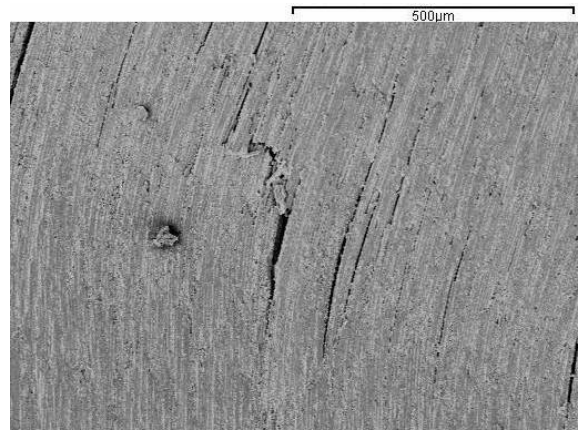
(a) A: macro-kink band 1 (with fibre failure and splittings).



(b) B: micro-kink band 2 defined at the macro-kink band's top boundary.



(c) C: micro-kink band 3 at the macro-kink band's bottom boundary and fibre curvature in the macro-kink band 4.



(d) D: Bottom boundary of the macro-kink band 4, without fibre failure.

Figure 3.15: Specimen r-UD_0d1: zoom-in from figure 3.14.

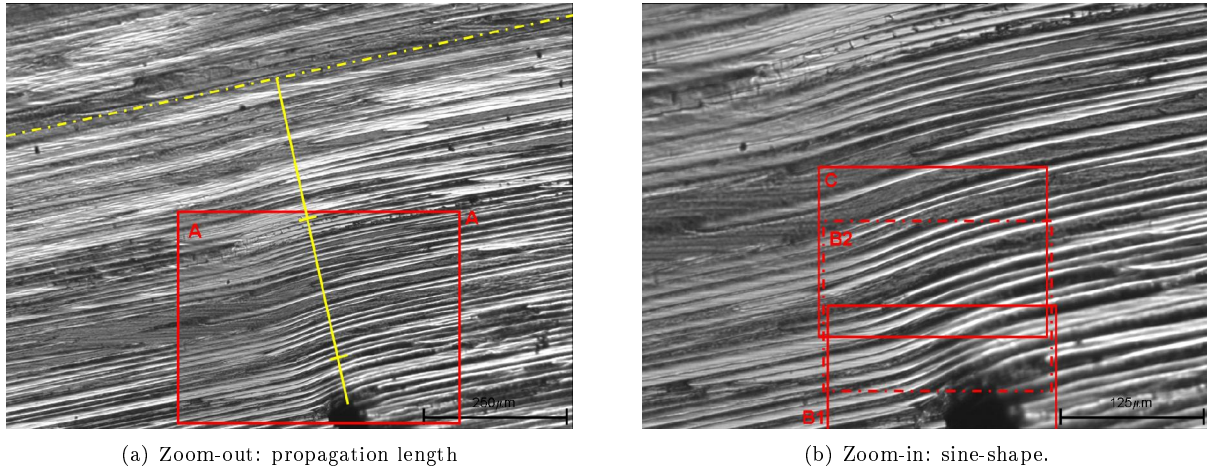


Figure 3.16: Specimen r-UD_2d2 (optical microscope): overview (load step 2).

3.5.2 Kink band formation - overview (specimen r-UD_2d2)

Specimen r-UD_2d2 presents a narrow kink band ($w \approx 40\mu\text{m}$) developed during 4 load steps (the first one done in the vise, and the other three in the small clamp). Micrographs obtained both in the optical (specimen loaded, figures 3.16 and 3.17) and scanning electron (specimen unloaded, figure 3.18²) microscopes are shown.

From figure 3.16 a, it is possible to estimate the propagation length (from the tip of the fully-formed kink band to nearly straight fibres) as $L_{prop} \approx 600\mu\text{m}$. A zoom-in from this micrograph (3.16 b) highlights the fibres' deformed shape as the kink band develops, a sine-shape with both in- and out-of-plane components that are progressively reduced with the distance to the kink band's tip.

Figure 3.17 focuses on the three areas (B1 and B2 at the third load step, C at the fourth load step) represented in figure 3.16 b: subfigure a shows the transition between the kink band with completely broken and discontinuous fibres (feature 1) and the kink band with broken fibres but without sharp edges (feature 2); subfigures b and c show a region further away in the tip, also with fibre failure (features 2) but with smooth and reduced fibre rotation. The kink band's out-of-plane component is evident in the three pictures.

Figures 3.17 and 3.18 show several broken fibres; among all, three different types of fracture can be found: features 2a point fibre failure normal the fibre's axis, features 2b show fibre failure oriented at an angle in relation to fibre's axis, and feature 2c combines the two previous cases. In addition, splittings at the fibre to matrix interface are undoubtedly found in the unloaded specimen (feature 3 in figure 3.18 c), but the optical micrographs (features 3 in figures 3.17 b and c) are not conclusive in this issue.

3.5.3 Kink band formation and propagation (specimen r-UD_aux)

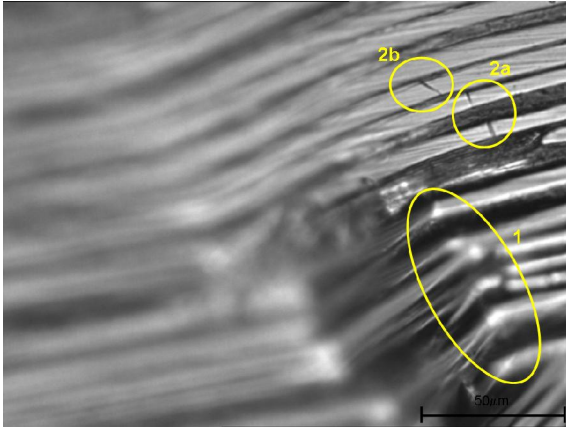
The specimen r-UD_aux³ was loaded in a compression rig especially conceived⁴ to keep the specimen loaded during microscopic observation; the SEM micrographs are shown in figure 3.19.

In this specimen, a kink band $w \approx 120\mu\text{m}$ wide was formed at the notch (figure 3.19 a), but quickly developed into a narrower ($w \approx 40\mu\text{m}$) one propagating across the specimen (propagation length $L_{prop} \approx 550\mu\text{m}$, micrograph

²Acknowledgments to Renaud Gutkin and William Francis for these micrographs.

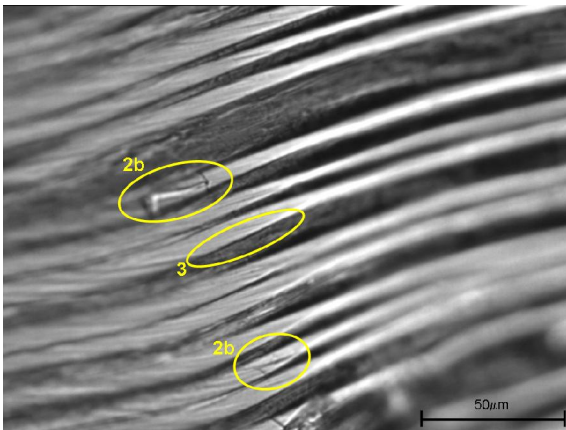
³Acknowledgments to William Francis for manufacturing this specimen.

⁴Acknowledgments to Renaud Gutkin for designing this rig.

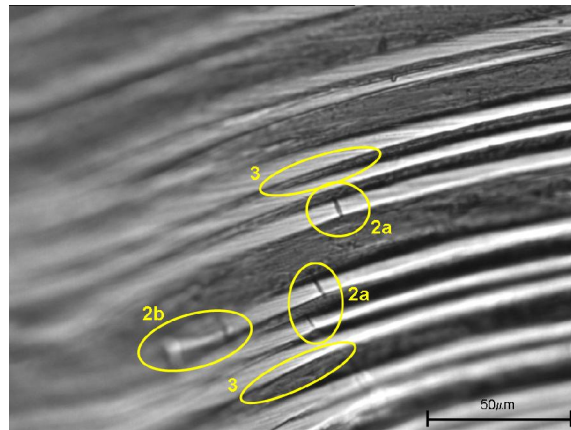


(a) Zone B1: fully-formed kink band (load step 3).

- 1: Kink band's edge, defined by broken fibres;
- 2a: Fibre failure with fracture surface normal to the axis;
- 2b: Fibre failure with fracture surface defined at an angle;
- 3: Possible matrix-to-fibre splitting.

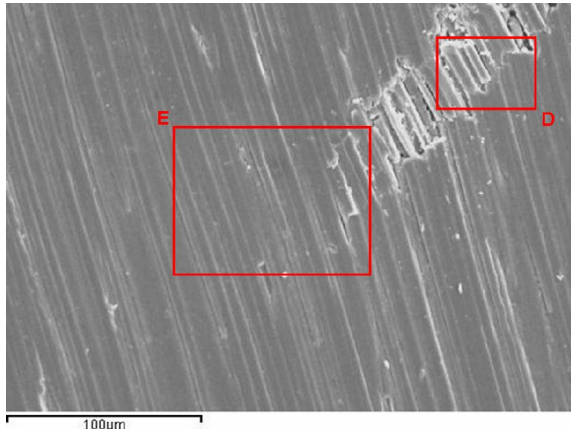


(b) Zone B2: kink band's tip (load step 3).



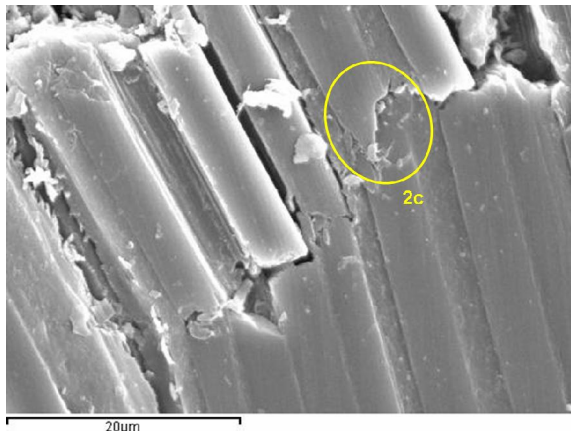
(c) Zone C: kink band's tip (load step 4).

Figure 3.17: Zoom-in at kink band's tip (optical microscope, specimen r-UD_2d2 loaded).

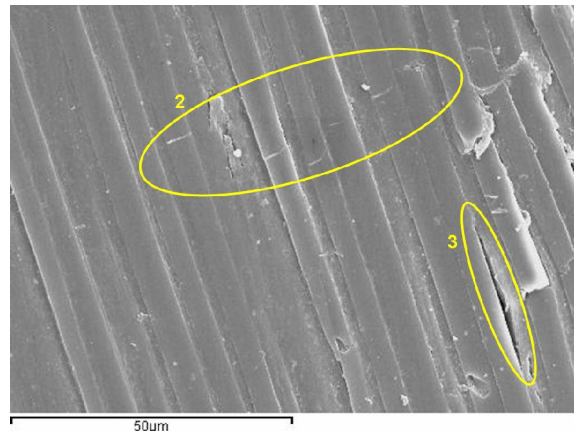


(a) Kink band's tip (overview).

- 2: Several broken fibres;
- 2c: Fibre failure surface: normal (right) and inclined (left) in relation to the axis;
- 3: Open crack at fibre-matrix interface.

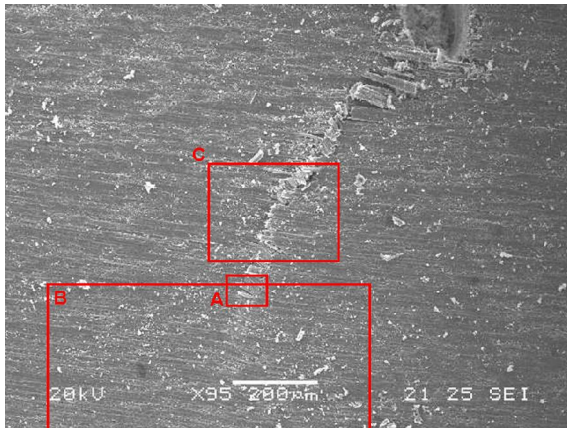


(b) Zoom-in in area D.

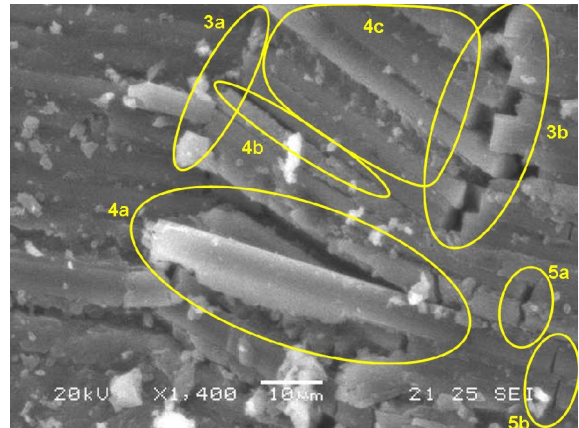


(c) Zoom-in in area E.

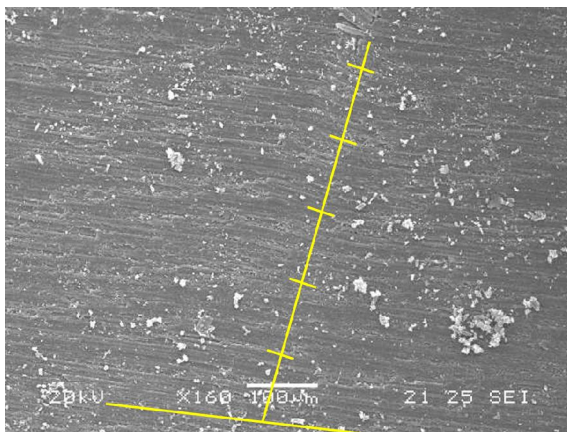
Figure 3.18: Specimen r-UD_2d2 seen at the SEM (unloaded).



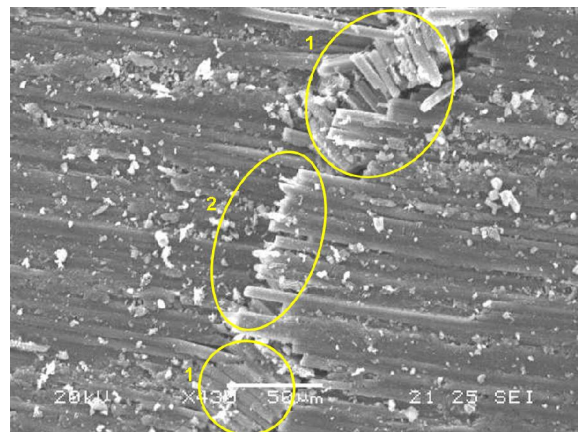
(a) Overview.



(b) Zoom-in A.



(c) Zoom-in B.



(d) Zoom-in C.

Key:

- 1: Common kink bands, with double fibre failure;
- 2: Band with single (unilateral) fibre failure;
- 3a: Broken fibres (aligned, fracture closed);
- 3b: Broken fibres (misaligned, fracture open);

- 4a: Split fibre;
- 4b: Splitting;
- 4c: Group of fibres rotated together;
- 5a: Misaligned fibre failure (open);
- 5b: Misaligned fibre failure (closed).

Figure 3.19: Specimen r-UD_aux seen at the SEM (loaded).

3.19 c).

This kink band propagated partially in the common way (with double fibre failure, features *1* in figure 3.19 d), but alternating in some areas with an unusual propagation with single fibre failure (feature *2* in figure 3.19 d). Looking closer near the tip (figure 3.19 b), one can see the kink band's edges defined by broken fibres (a straight edge with closed fibre fracture on the left (feature *3a*) and an irregular edge with open fibre failure on the right (feature *3b*)), several splittings (of one single fibre (feature *4a*), partially open (feature *4b*)), a group of fibres rotated together (feature *4c*), and a jump in the right edge (features *5a* - complete failure - and *5b* - initial failure).

3.5.4 Kink band propagation - overview (specimen CC_6d)

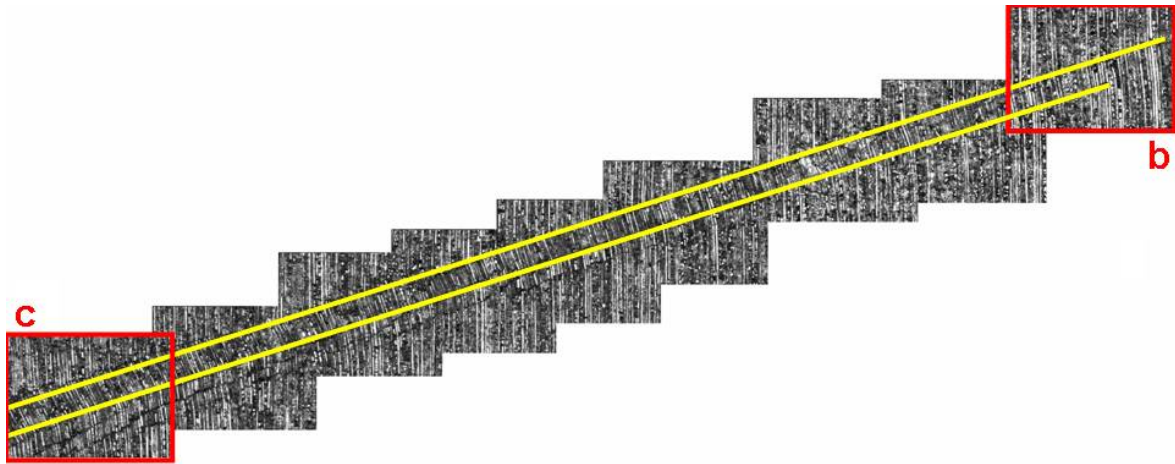
Specimen CC_6d was compressed at first with its outer layers (at $\varphi = 90 + 6^\circ$), and a kink band in the central layer (1.5mm thick, at $\varphi = 6^\circ$) initiated and started propagating; afterwards, the outer layers were removed and that kink band observed under the optical microscope (figure 3.20). There, one saw an in-plane kink band propagated along a considerable length (subfigure a), with the lower edge (feature *2*) delayed in relation to the top one (subfigures a and b) and with uneven broadening in the full developed region (subfigure c).

Having now the kink band in the central layer visually accessible, the specimen was re-compressed in the test machine and propagation recorded with the hand microscope plugged on the DSP; a sequence of images is shown in figures 3.21 and 3.22. There, the previously initiated kink band (dark band on the left, *1*) propagated along the specimen followed by the formation of a second band (*3*); splittings were opening (*2*) and closing (*4*) outside the bands as propagation developed.

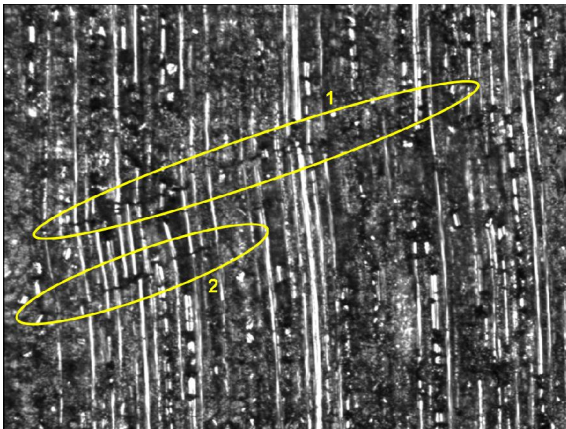
3.5.5 Other results

Other kink bands besides the already presented ones were observed in other specimens; figure 3.23 shows some of those that, although not being further discussed, are also interesting:

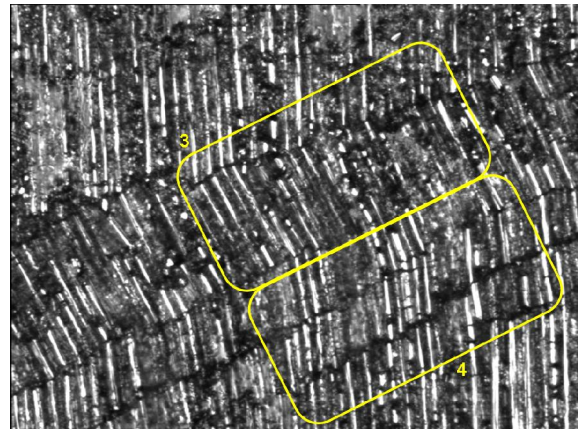
- a** shows a $\varphi = 0^\circ$ CC specimen in which the kink band, after unloading, is completely in-plane in the central band but out-of-plane in its boundaries;
- b** presents a $\varphi = 2^\circ$ CC specimen with several kink bands (different widths (w) and angles (β), in- and out-of-plane) interacting in the same central layer;
- c** shows a highly misaligned ($\varphi = 12^\circ$) CC specimen, with the kink band ending in a splitting;
- d** highlights the agreement between the deformed fibres and a sine-shape in the r-UD_0d0 specimen;
- e** shows the out-of-plane remaining (plastic deformation) component of a kink band formed at specimen's r-UD_0d2 post polished surface;
- f** presents a jump in a kink band's edge, preceded by a change in the fibre fracture surface.



(a) Overview.



(b) Kink band's tip.



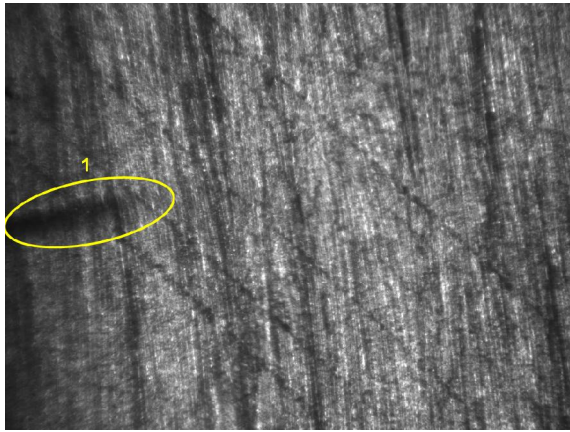
(c) Kink band broadening.

Key:

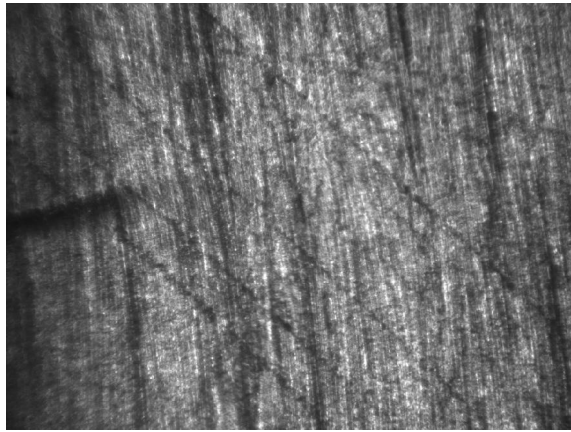
- 1: Upper kink band edge
- 2: Lower kink band edge;

- 3: Rotated segments;
- 4: Aligned segments.

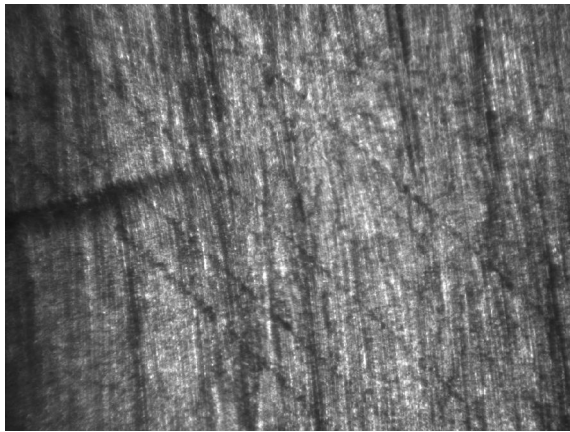
Figure 3.20: Specimen CC_6d: optical micrographs (unloaded, after outer layers removal, unpolished).



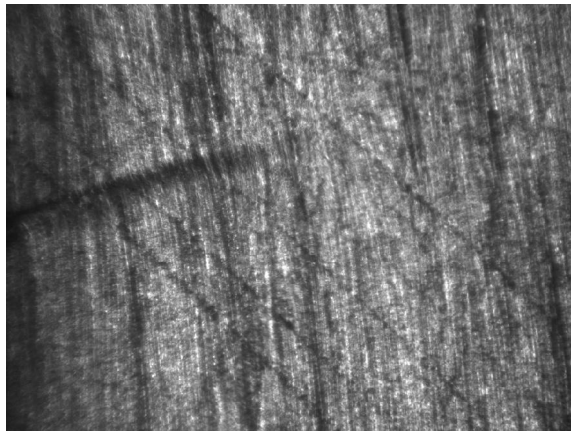
(a)



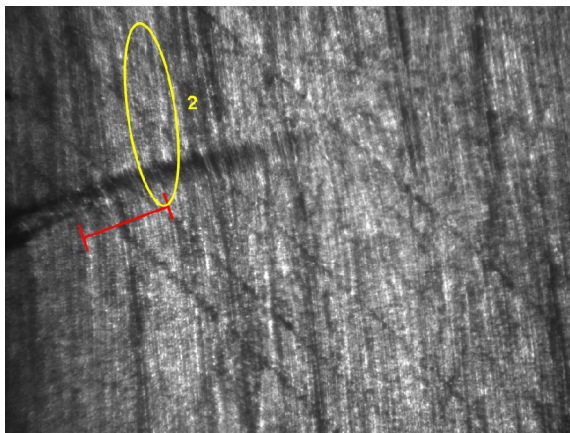
(b)



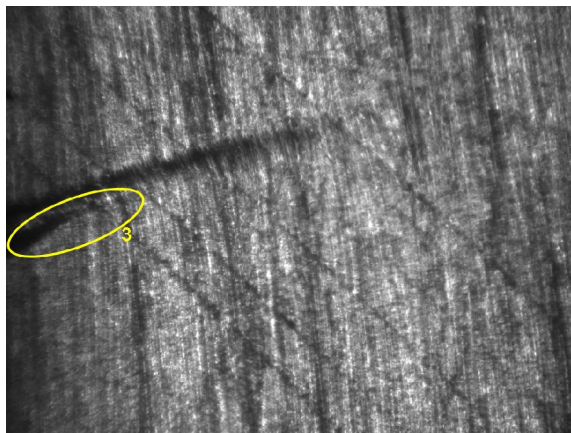
(c)



(d)



(e)



(f)

Key:

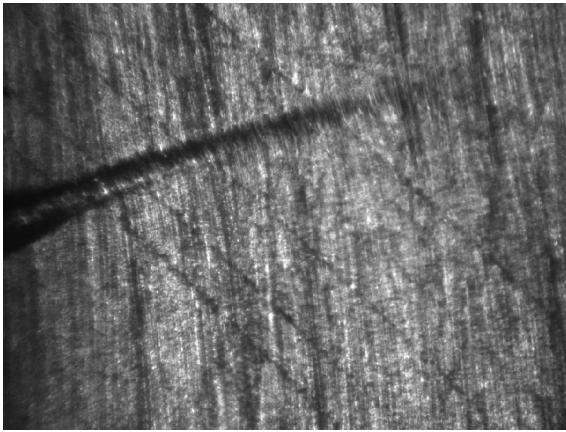
1: Kink band previously initiated;

3: Second kink band developing or uneven broadening;

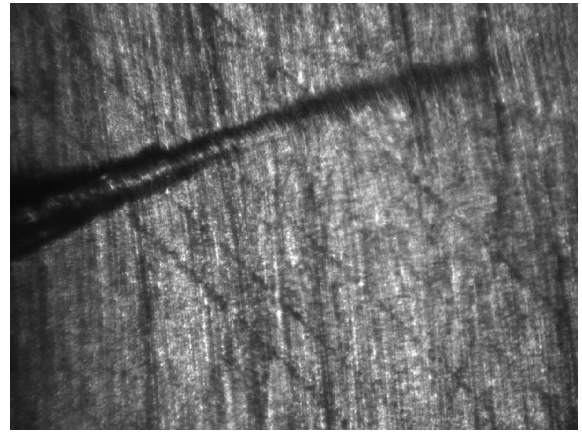
2: Splitting opening;

4: Splitting closing.

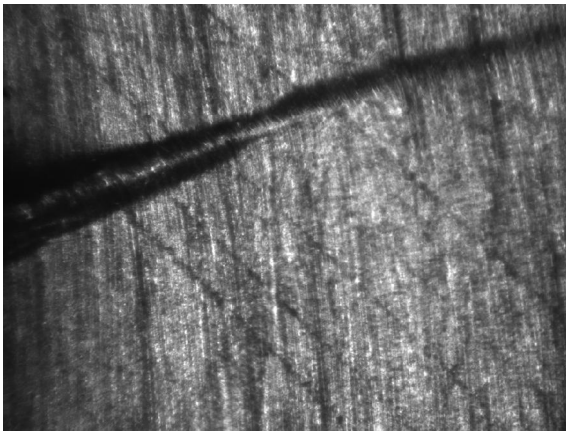
Figure 3.21: Kink band propagation - sequence of images (1).



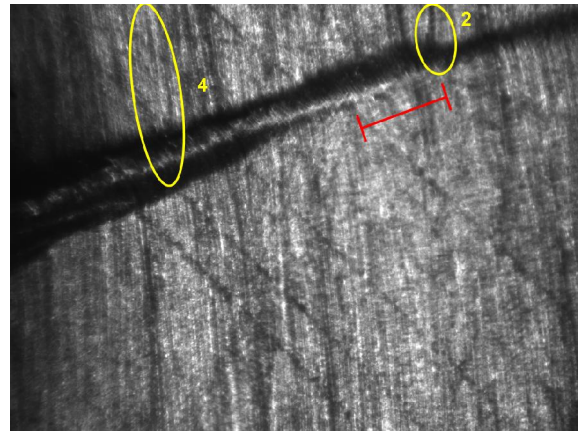
(a)



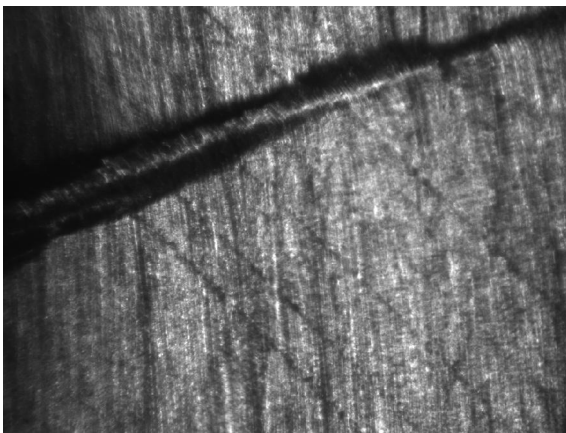
(b)



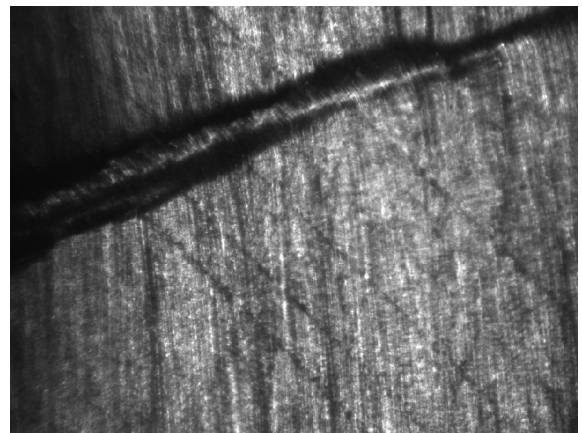
(c)



(d)



(e)



(f)

Key:

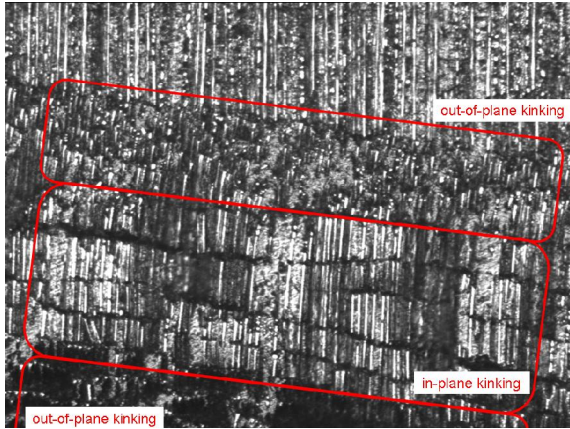
1: Kink band previously initiated;

3: Second kink band developing or uneven broadening;

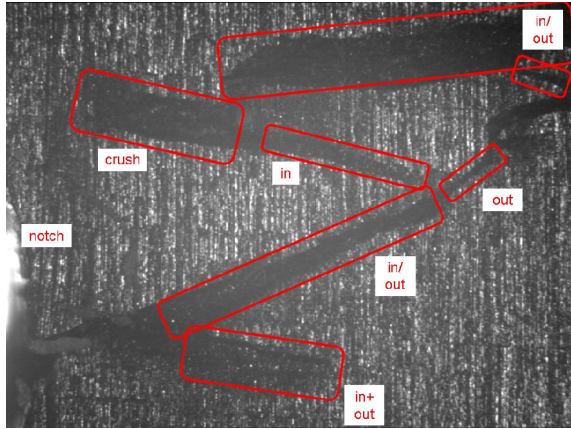
2: Splitting opening;

4: Splitting closing.

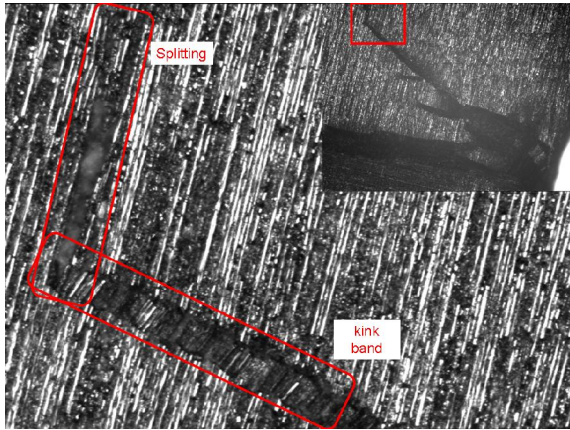
Figure 3.22: Kink band propagation - sequence of images (2).



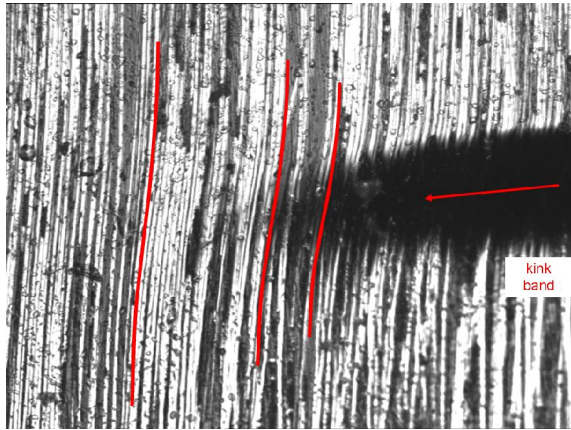
(a) Specimen CC_0d2: in- and out-of-plane components (central layer, unloaded, ground).



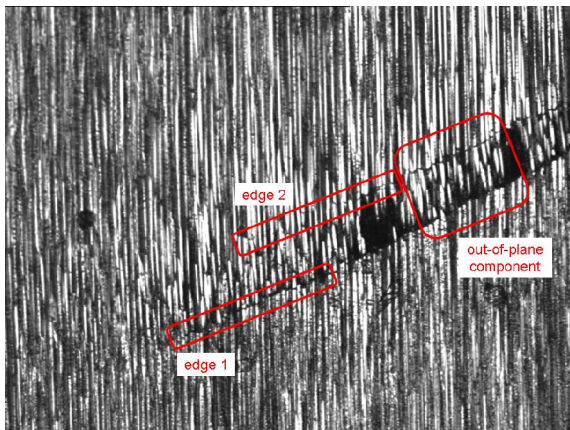
(b) Specimen CC_d2: several kink bands: in-plane, out-of-plane, with crushed material (central layer, unloaded, ground).



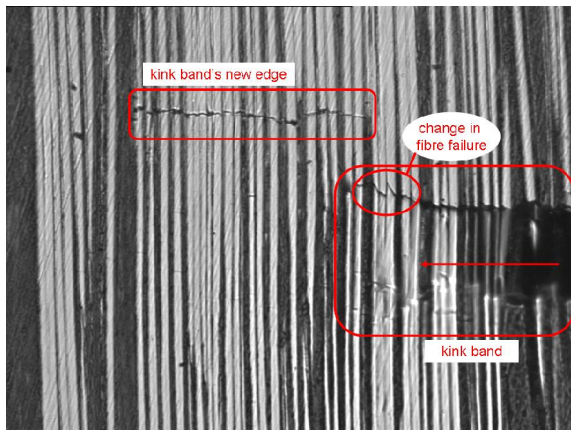
(c) Specimen CC_12d: kink band ending in a splitting (central layer, unloaded, ground).



(d) Specimen r-UD_0d0: kink band and sine-shapes (loaded).



(e) Specimen r-UD_0d2: kink band in a specimen polished after kink band initiation (unloaded).



(f) Specimen r-UD_0d3: kink band's edge changing position, after change in fibre failure mode.

Figure 3.23: Other kink bands from the experiments.

3.6 Discussion

3.6.1 Macroscopic kink band without fibre failure (specimen r-UD_0d1)

3.6.1.1 Fibre failure in kink band formation

As it was presented in section 3.5.1, it is undeniable that the specimen r-UD_0d1 failed by kink band formation; however, when observed at the micro-scale, it is also evident that kinking occurred partially without fibre failure (kink band 4, figure 3.15 d).

This phenomenon - kink band formation without fibre failure - was already reported in [8]; there, it was considered to be due to a smaller fibre rotation (α) and stabler propagation, formerly related by the authors to the loading scheme with direct shear.

In the r-UD_0d1 specimen, the load was applied also with a shear (from specimen's shape, $\varphi_L \neq 0$) component, but fibre rotation in the unloaded configuration is not so smaller that it can justify the absence of fibre failure (figure 3.15 d). However, one feature distinguishes noticeably this kink band from the classic ones: its width is much higher ($w = 800\mu\text{m}$) than usually ($w \approx 200\mu\text{m}$). In addition, the same specimen shows narrower kink bands with broken fibres, which reveals that fibre failure is affected by other parameters than material properties and loading scheme.

Considering all this, it is suggested that fibre failure is affected by the kink band's width w at an extent that is partially independently of fibre rotation α . To attempt an explanation for this fact, let one assume (as it was widely found in the literature) that, during kink band formation, the fibre deforms in a sinusoidal shape $y(x)$ with half wavelength w ,

$$y(x) = \bar{y}_0 \cdot \sin\left(\frac{\pi}{w} \cdot x\right),$$

and that matrix shear stresses are related to its slope, and fibre axial stresses to its curvature⁵:

$$\begin{cases} \text{matrix shear stresses: } \tau_m \propto y'(x) = \frac{\pi}{w} \cdot \bar{y}_0 \cdot \cos\left(\frac{\pi}{w}x\right) \\ \text{fibre axial stresses: } \sigma_f \propto y''(x) = \frac{\pi^2}{w^2} \cdot \bar{y}_0 \cdot \sin\left(\frac{\pi}{w}x\right) \end{cases}. \quad (3.3)$$

Assuming this, and for the same rotation ($\alpha \approx \frac{\pi}{w} \cdot \bar{y}_0$) and deflection \bar{y}_0 , shear stresses in the matrix are independent of kink band's width ($\tau_m^{max} \propto \alpha$), so if matrix yielding occurs due to shear it does not depend on this parameter; however, the axial stresses in the fibres would vary with the width ($\sigma_f^{max} \propto \alpha \cdot \pi/w$), increasing for small widths and decreasing for larger ones.

Accepting the previous analysis, matrix yielding would occur no matter the kink band's width, but fibre failure (if controlled by axial stresses) would rather take place in narrower kink bands than in wider ones; this is precisely what happened actually in this specimen.

3.6.1.2 Kink band's width

Considering the preliminary model (equations 3.3), and assuming that matrix shear yielding ($\tau_m = S_m$, with $\tau_m \propto \alpha$) controls the initiation of a kink band⁶, one can conclude that its width w would be proportional to the transverse displacement \bar{y}_0 .

⁵A justification for this is given in Chapter 5.

⁶This is supported by the results in Chapter 4.

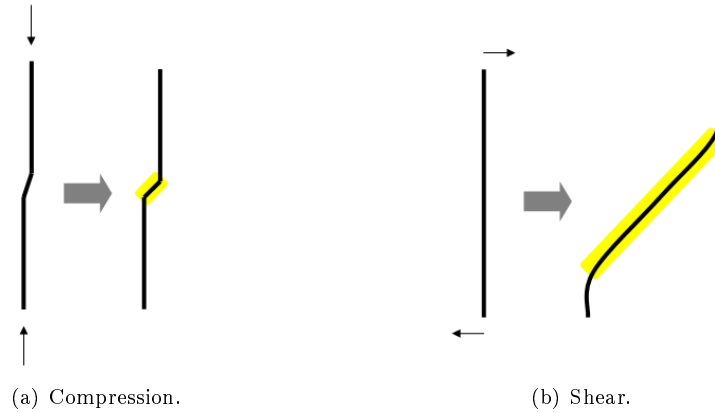


Figure 3.24: Kink band width: under compression and under shear.

Usually (in research), kink bands are developed under pure compression, so fibre rotation is triggered only by initial misalignments and the resultant in-plane moments (in a positive feedback process); the misalignments affect a small length (in the axial direction), so the matrix starts yielding in a very narrow band (figure 3.24 a). If the specimen is loaded in shear, however, the opposite happens: the fibre is moved (transversely) within a macroscopic (axial direction) length, so the band formed is much wider (figure 3.24 b).

Summarizing, and according to this theory, the kink band's width would be related to the length, within the fibre, in which shear is applied (directly or not), and not so much to the amount of fibre rotation.

3.6.1.3 Splitting

A splitting corresponds to a crack formed in the material, either through matrix or interface (between matrix and fibres) failure in shear or tension, to release the strain energy in the material detached.

Figures 3.15 a and b evidence groups of few fibres broken and rotated together, suggesting that splitting (between groups) had occurred prior to fibre failure and further rotation; observing 3.15 a, one can confirm that the fibres in the central band between splittings *A* and *B* are much straighter than the ones at their right. The number of fibres within a split group depends on the deformed configuration and matrix / interface toughness, in a relation that could not be deduced from the micrographs.

Figure 3.14 also shows several splittings along the kink band's path, mainly near the boundaries (where the curvature is higher). From the micrographs of this specimen (r-UD_0d1), it is not possible to know if failure occurred in the matrix or in the interface, neither if it was due to shear only or also to tension (as the open cracks can be closed when loaded, due to further fibre rotation and Poisson's effect). Nevertheless, it is undeniable that either the matrix or the interface suffered ultimate failure during kink band formation.

In addition, in figure 3.14 it is also possible to see that the kink band was initiated not directly from the notch, but from a split that seems to have been formed in shear; this suggests shear in the matrix or interface to play an important role in kink band formation.

3.6.1.4 Different kink bands within the specimen

Another peculiar feature in this specimen is the several kink bands superposed, all with the same orientation (β).

At first, two kink bands - kink band *1* with broken fibres and kink band *4* without - are shown in figure 3.15 a; however, given these bands' similar location and width, it is sensible to conclude that they are the same entity, only in a different state. If so, fibre failure in the neighbourhood of the notch can be easily explained either due to stress concentrations (so fibre failure in this region is simply a local effect) and/or to over-compression (and fibre failure would also occur in kink band *4* if the compression progressed).

The presence of the micro-kink bands (kink band *2* and kink band *3*) found in the boundaries of the macro one is less straight forward to discuss. Figures 3.17 a and b show that these narrow kink bands were both formed at major splittings (figure 3.17 a, features *A* and *B* respectively) in the transition between kink band *1* and kink band *4*; this implies that a significant change in the stress state had occurred and triggered the process. Kink band *2* is indubitably independent from the macro-kink band (figure 3.17b); however, figure 3.17c suggests that kink band *3* can be simply the broadening of kink band *4*, although the fact that the latter has no broken fibres in its top edge at this region makes it a non-conventional broadening.

3.6.2 Kink band formation - overview (specimen r-UD_2d2)

3.6.2.1 Sequence of events

The optical micrographs shown in figures 3.16 and 3.17 provide the information required to sketch the sequence of events leading to kink band formation.

In figure 3.16 b, the dark region (in the bottom, with constant width) corresponds to a large out-of-plane movement inside the kink band, and ends suddenly; on the other hand, the slight out-of-focus found away from that band's tip reveals a much smaller displacement that is smoothly reduced in the transverse direction. Considering this, the conclusion is that the initiation starts progressively with fibre rotation until a certain angle, after which the movement is much more abrupt.

Besides, in micrograph 3.17 a, the in-plane component is not so discontinuous as the out-of-plane component is (as one goes away from feature *1*, the out-of-focus amount decreases significantly, but the 2D (in the micrograph's plane) fibre rotation does not), suggesting that this sudden movement has a stronger out-of-plane component than initially; for this reason, the kink band would start developing almost in-plane, going more out-of-plane in a latter stage.

Looking closer on figure 3.17 a, one can confirm that fibre failure is responsible for that abrupt increase in the out-of-plane displacement, being the kink band's edges sharply defined by broken fibres (feature *1*). However, first fibre failure is not sufficient for full rotation to occur, as there are broken fibres with smoother curvature (features *2a* and *2b*). This implies that either the matrix has to fail completely after fibre failure to allow the movement, or that the fibres are not completely broken in two sections (in figure 3.17 a, those fibres might be broken only on the right side and not on the left one) and resist to rotation for that reason, or even that the overall stiffness in the neighbourhood is enough to prevent a sudden rotation as soon as fibres break. As the matrix is weaker than the fibres, the latter two hypothesis appear to be more likely; besides, and taking into account that the fibres at specimen's surface are unsupported on the exposed side (so under stress concentrations), it is probable that, even when apparently complete fibre failure is seen on a micrograph (2D), the fibre is not fully broken across its entire section (3D).

The propagation length, from fully broken and rotated fibres to straight ones, cannot be determined with a high accuracy because, as it was just mentioned, the deformed shape starts being defined in a very smooth way; for

that reason, the length estimated for this kink band - $L_{prop} \approx 600\mu\text{m}$ - copes with an uncertainty of at least $\pm 100\mu\text{m}$.

3.6.2.2 Fibre fracture surfaces

Micrographs 3.17 show several occurrences of fibre failure. The fracture surface of broken fibres identified with $2a$ is normal to the fibre's axis; typically, this occurs when failure happens in tension. Fibres marked with $2b$ have a fracture surface inclined in relation to fibre's axis, which would correspond to failure in compression or shear. A relation between the two types of failure (compression and tension) with the two types of fracture (inclined and normal) can be seen from these micrographs, as (considering the out-of-plane movement from a lower level on the left to higher level on the right) the features $2b$ appear to be predominant at the left (concave deformed shape, in compression) and the features $2a$ appear to be predominant at the right (convex deformed shape, in tension).

The unloaded micrograph 3.18 b from the SEM shows the typical fibre fracture in bending: on the right side the fibre would be in tension, with a fracture surface normal to the axis, and at the left side the fibre would be in compression, with a fracture surface at an angle to the axis.

Figure 3.18 c shows the kink band tip, with fibre failure at the upper boundary (feature 2); in this region, the concavity formed by fibre deformed shape is open to the right. Looking onto the fibre fracture lines, it is possible to conclude that they were formed in bending: for each broken fibre, the fracture surface is open and normal to the axis on the left side - so failure occurred in tension -, and inclined and closed on the right one - where failure occurred in compression.

3.6.2.3 Splitting

As happened with the previously one (r-UD_0d1), a discussion on splitting in this specimen cannot be conclusive, as the micrographs from the optical microscope are distorted by the out-of-plane component and the SEM one are unloaded.

Nevertheless, the SEM figure 3.18 c shows clearly an open crack at the fibre-to-matrix interface (feature 3). In addition, loaded micrographs 3.17 b and c also show dark and sharp lines in some interfaces (feature 3), which can be interpreted either as shadows or splittings; however, one of these lines is present in both figures (at the bottom in figure 3.18 c and at the centre in figure 3.18 b), taken with different focus, which suggests that interface failure did actually occur during kink band formation.

On the contrary to what was reported from specimen r-UD_0d1 in the previous section, in this kink band the fibres do not appear to be rotated as large groups but fibre by fibre (figures 3.18 a and b), so splittings would have occurred between each fibre (or pair of fibres). It is not possible, however, to find whether these interface (fibre to matrix) splittings were open during kink band formation or during unloading.

Finally, it must be noted that no matrix splitting is found in the micrographs.

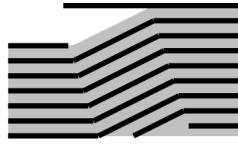


Figure 3.25: Schematics of single failure in unsupported fibres.

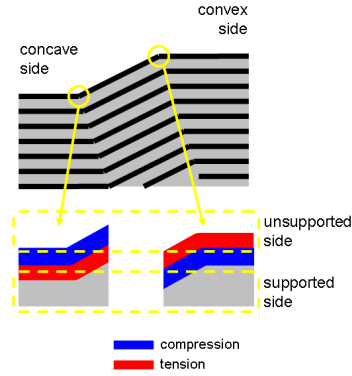


Figure 3.26: Schematics of the asymmetry in a kink band with out-of-plane component.

3.6.3 Kink band formation and propagation (specimen r-UD_ aux)

3.6.3.1 Propagation with single fibre failure

The kink band propagated in the specimen r-UD_ aux in a unusual way; feature 2 in 3.19 d shows fibre failure aligned with the kink band's (features 1) left edge, but instead of fibre failure along the right edge the material moved noticeably out-of-plane. The most logical explanation for this is a stronger out-of-plane component in this region, and due to the lack of material in the that direction the fibres were able to, after failure at the left side, release the sinusoidal deformation as shown in figure 3.25. One of the reasons for this to happen specifically in this region is a weaker cohesion along the out-of-plane direction, as for instance due to local delamination.

The region where single fibre failure (feature 2) can be observed is surrounded by two kinked regions with the typical double fibre failure (features 1); this means that fibre kinking is actually the most favourable state for the material under compression, as it returns to that failure mode even after failing in an apparently less complex way.

As previously discussed for specimen r-UD_ 2d2, the estimation of the propagation length ($L_{prop} \approx 550\mu\text{m}$) is not accurate (tolerance around $\pm 50\mu\text{m}$).

3.6.3.2 Features at the fibre-scale

Figure 3.19 b shows the kink band's tip (in terms of fibre failure) with high magnification, which allows some features at the scale of a fibre diameter to be discussed.

One of the most notable features in this kink band is the lack of symmetry in its edges; in fact, the left edge is not only much more even than the right one, as it appears to have been formed at first (further fibres completely failed). Besides, the fracture surfaces suggest an out-of-plane movement upwards from the left to the right, as they are closed on the left side (compression on the concave side) and open on the right one (tension on the convex side).

Theoretically, and disregarding any material randomness, a kink band would be anti-symmetrical in its propagation plane; however, in this experimental program several kink bands were found to be unsymmetrical, both when it comes to formation and broadening. When a kink band is found at the specimen's surface and with an out-of-plane component, the material is not evenly supported on both band's sides: the fibres on the concave

one (on the left in figure 3.19 b) are unsupported in the compressed part, while the fibres on the convex side (on the right) are unsupported under tension (as sketched in figure 3.26). This could be the reason for the unsymmetrical behaviour in kink band formation: if (as it is usually reported) the fibre's compressive strength is lower than the tensile one, the effect of stress concentrations at the unsupported side would lead to first failure in the concave side of the kink band, which agrees with micrograph 3.19 b.

Another interesting fact in this micrograph is the absence of splitting between the fibres in the top (*4c*) together with a completely split fibre in the centre (*4a*) and a small intermediate split (*4b*); these splits appear precisely where the kink band's right edge is moved outwards in relation to its original alignment (features *5*). Actually, this new failure location might have caused the splitting: the last broken fibres could not follow the rotation of the former without either crushing them or breaking at the former edge location. Feature *5a* shows fibre failure under tension in bending with an out-of plane component; on the contrary, failure in features *5b* appears to have only an in-plane bending component. Looking onto fibre *4a*, one can see its out-of-plane movement, which is likely to have caused the closure shown in *5b*. It is not possible to know, however, what led to these different behaviours; it can be suggested that different imperfections in adjacent fibres would change the wavelength and orientation of the deformed shape; nevertheless, it seems that the relation between in-plane and out-of-plane components is more complex and less deterministic than it could be supposed.

3.6.4 Kink band propagation - overview (specimen CC_6d)

3.6.4.1 Parallel bands propagating

The most interesting feature found in this specimen is the appearance of a second dark band (figures 3.21 e to 3.22 f) parallel to the first kink band, propagating through the specimen with a delay in relation to the first one.

As it can be seen on the unloaded (after outer layer removal) micrograph 3.20 b, the kink band's tip prior to propagation presented broken fibres further in the band's upper edge than in the lower one, which could suggest that each dark band in figures 3.21 and 3.22 was one kink band's edge; however, the scale is not identical in both figures (3.20 and 3.21/3.22), so the two features - dark bands in the pictures from the DSP and kink band's edges with broken fibres - cannot be the same.

Considering now micrographs 3.20 a and c, it is possible to see two different bands in the area where the kink band is fully developed and broadened: sub-band *3* has highly deformed broken fibres (α is considerable, even in the unloaded configuration), along a path nearly constant all across the propagation length, but sub-band *4* shows broken fibres almost aligned with the global axis (so the deformation would be mainly elastic) and becomes narrower as one moves towards the tip. Taking these two features and their scale into account, it is sensible to assume that they are in the origin of the two parallel bands propagating in figures 3.21 and 3.22. However, the dark regions in the image are related to a local change in the specimen's surface orientation and to out-of-plane movement, which is not present in the micrographs of figure 3.16; nevertheless, these reproduce a kink band in a central layer of a laminate and in the unloaded configuration, so it is perfectly possible that, after removing the support given by the outer layers and compressing the specimen further more, an out-of-plane component had developed.

The presence of a bright band between the two dark ones, with fibre rotation (micrographs in figure 3.22), suggests that region to be an in-plane kink band (*band 2* in figure 3.27). Now the two dark bands can be either in the configuration a - with the third band developing to release the deformation in the fibres outside the kinked

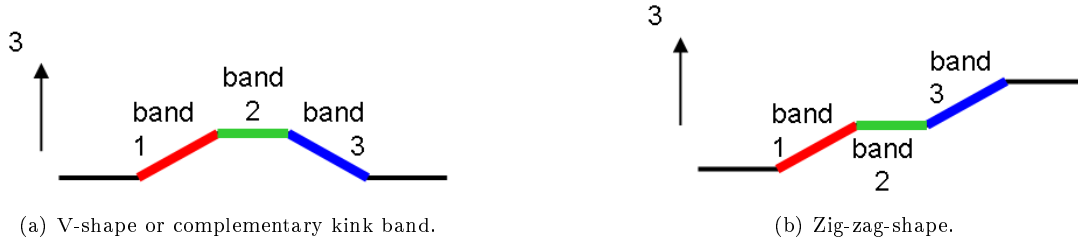


Figure 3.27: Schematics of kink band's out-of-plane component in specimen CC_d6.

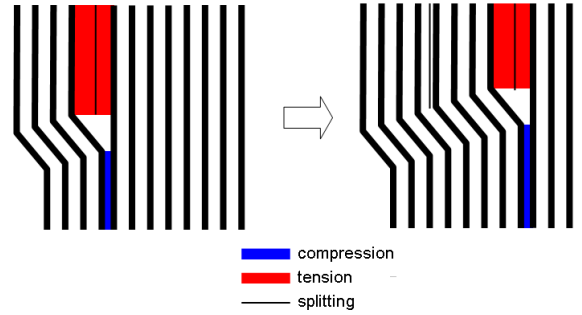


Figure 3.28: Schematics of in-plane transverse tension and compression during propagation.

region - or in the configuration b - with the third band increasing the amount of out-of-plane movement. The first option would be preferred as it restores the overall equilibrium of the specimen, but the second one would agree better with a relation between the development of the second band and the macro-splittings (as explained in the next section).

After re-testing the specimen, it was confirmed by microscopic observation that the two kink bands shown in figures 3.21 and 3.22 were formed with considerable out-of-plane movement that remained in the specimen after unloading; unfortunately, this fact together with the lack of polishing resulted into micrographs with barely no useful information, so the actual kink band configuration is still open to discussion between hypothesis a and b in figure 3.27.

3.6.4.2 Macroscopic splittings

Two macroscopic splittings along the fibre direction are open (features 2) in figures 3.21 e and 3.22 d, in the upper part of the specimen; an explanation is provided as it follows.

The sequence of images captured by the DSP shows that fibre rotation within the kink band leads the upper part of the specimen to move to the left and the lower part to the right; as those movements are partially constrained by the fibres ahead of the kink band tip, the material is under transverse tension above the kink band, and under transverse compression below it (as sketched in figure 3.28); for this reason, cracks open at the tensile side to release the transverse stresses in the matrix, allowing the split material to move significantly. As the kink band propagates, more splittings develop due to the same principle, being the last one closed (feature 4 in figure 3.22 d) as soon as a new is formed (feature 2 in figure 3.22 d). The macroscopic splittings found in this specimen are therefore caused not by transverse tension within the kink band or shear, but simply by the propagation process and the global displacement that a kink band tends to create.

An interesting fact about these macroscopic splittings is highlighted in figures 3.21 e and 3.22 d: the two

splittings did open at the same distance from the second band's tip. If not a coincidence, this would mean that the development of this second band enlarged significantly the deformation in the regions away from the band; recalling the discussion on the orientation of band's out-of-plane component (as represented in figure 3.27), hypothesis b would agree better with this fact, as a complementary kink band (hypothesis a) usually forms to release the stresses in the unkinked material, avoiding the formation of a splitting. Nevertheless, this analysis is not conclusive, as the splitting could have released mainly the in-plane component and would not, for that reason, hinder the formation of a V-shape to release the out-of-plane one.

3.6.4.3 Out-of-plane component

The specimen CC_6d was initially compressed with the central ($\varphi = 6^\circ$) layer supported by the surrounding ($\varphi = 90^\circ + 6^\circ$) ones; the kink band formed here was observed under the optical microscope, unloaded and after the outer layers were removed, with no evidence of any out-of-plane component (figure 3.20). The same specimen, now with the central layer exposed and unsupported on one side, was then re-compressed and the kink band propagated; while loaded, the out-of-plane movement was identified by the shadows in the images recorded, and even after unloading the plastic deformation had actually a considerable out-of-plane component that was seen in the optical microscope.

A similar behaviour was found in several other specimens: the ones with a kink band developed at a free surface (specimens UD and r-UD) shown a strong out-of-plane component in the deformed shape, both during and after loading, while some of the CC ones (with the kink band formed in the central layer) present micrographs with a totally in-plane appearance. In relation to these latter ones, it is not possible to know whether fibre kinking had developed actually in-plane when loaded, or if an out-of-plane movement had occurred and was released when the specimen was unloaded; nevertheless, the difference between the out-of-plane component in kink bands from CC and from UD / r-UD specimens is notorious anyway.

This change in the out-of-plane behaviour can be only justified by the support from the other layers that is given in the CC specimens and lacks in the other (UD / r-UD) ones. It is not likely that this effect is related to the orientation of those adjacent layers as, in the CC specimens, they are oriented at a $90^\circ + \varphi$ angle (easier to deform out-of-plane). In addition, the previously formed kink band in the specimen CC_d6* developed an out-of-plane component when re-tested (figure 3.21 a), so this tendency is not avoidable by initiating the kink band and removing the outer layers afterwards, as as soon as that is done and the specimen is compressed again, the out-of-plane component appears.

One of the derived objectives of this experimental program was the development of fully in-plane kink bands; considering all this discussion, this appears to be much more difficult to achieve than it could be expected.

3.7 Conclusions

Kink band's geometry

The kink bands found in the specimens (all of the same material) are within a wide range of geometries: widths were found from $w \approx 7 \cdot \phi_f$ to $w \approx 115 \cdot \phi_f$, and band's angle varied from $\beta = 0^\circ$ to $\beta \approx 30^\circ$.

The propagation length in the loaded configuration was estimated as $L_{prop} \approx 500\mu\text{m}$ to $700\mu\text{m} \approx 12 \cdot w$ to $17 \cdot w \approx 71 \cdot \phi_f$ to $100\phi_f$.

Sequence of events

The overall observation of the micrographs allows the sketching of the following sequence of events for typical kink band kink formation: at first, the fibres deform in a sine-shaped wave, in a smooth way along each fibre and along the kink band's propagation path; as compression progresses, the fibres rotate further more and start failing by bending (eventually first in the compressive side), keeping a smooth deformed shape; finally, fibre by fibre, the failure is complete across its both critical cross sections, and the fibre rotates suddenly more (eventually only after failure of adjacent fibres), assuming a sharp kinked shape.

During these three fibre-dominated steps, matrix yielding must occur; it is not possible, however, to precise when, as there is no visible sign of matrix yielding (not even when the specimen is unloaded, as if fibres were not broken then their elastic recovering would surpass the effect of any matrix yielding). From the specimen that kinked partially without fibre failure (r-UD_0d1) it is suggested that, generally, matrix yielding occurs prior to fibre failure, but that sequence might not be the same for all kink band's geometries. Nevertheless, although being present in the common process of kink band formation, fibre failure is not mandatory.

Definition of kink band formation

Kink band formation is usually defined by fibre failure in the literature; however, it was proved that it is possible to obtain a kink band in a CFRP composite with no fibre failure occurring (specimen r-UD_0d1). Taking this into account, the formation of a kink band must be defined by matrix yielding, matrix failure or interface failure, being fibre failure simply a consequence (not the cause) of kinking.

The micrographs obtained in the SEM show interface failure (debonding between fibres and matrix) in the unloaded configurations; however, and despite some micrographs with features that might be splittings at the interface (specimen r-UD_2d2), there is no evidence of matrix or interface final failure in a kink band's tip under development (loaded). For these reasons, matrix yielding is the best candidate to the primary failure mode in the process of kink band formation.

Fibre failure in bending

Although a proper conclusion about fibre failure mode would require a much deeper study than the one done in the scope of this project, the type of failure surface found in the fibres broken by kinking does suggest a failure due to bending, with one part of the fibre failing under compression and the other under tension, in a consistent way.

Unsymmetric edge definition

Almost all the kink bands with fibre failure observed in this experimental program presented edges defined unevenly, with fibre breakage further developed in one edge than in the other.

The lack of symmetry is too consistent to be justified by material randomness; therefore, it has to be so by some unsymmetry in the stress state found when the the kink band is being formed, at the fibre level. One possible explanation to this fact is the different effect of stress concentrations due to the free surface (or change in layer's orientation, for CC specimens) in tensile and compressive failures (figure 3.26); however, this was not a conclusive analysis and the issue is still open to discussion.

Deformed shape

It was confirmed that the sinusoid is a reasonable approximation for fibre's deformed shape during kink band formation; the curve's amplitude decreases as one moves away from the kink band's tip, and the wavelength follows the opposite tendency.

In all loaded micrographs, the deformed shape presented both in-plane and out-of-plane components; while the former is reduced in a smooth way across propagation's length, the latter disappears first and in a more sudden fashion, around the area where fibre failure stops.

Besides, fibre failure (when actually occurring) was confirmed to have a strong effect in the deformed shape, defining the kink band's edges sharply; however, the kink band's final configuration is not completely defined by initiation of fibre failure, being so by final fibre failure instead.

Out-of-plane tendency

All the kink bands observed under compression showed an out-of-plane component that cannot be neglected. So far, it was proved that this movement is favored by the lack of support at the specimen's free surface, but it is still open to discussion whether the kink band formed in the middle of the cross-section is totally in-plane or not.

The presence of an out-of-plane deformation component reveals that out-of-plane stresses exist as well; for this reason, and even if individual fibre kinking is a 2D phenomenon, it is necessary to consider the overall 3D stress state in the composite, if an accurate analytical model is to be developed.

Loaded and unloaded configurations

By comparison between the micrographs of specimens under compression and unloading, one can conclude that both elastic and plastic deformation occur during kink band formation, and that none of them can be neglected; therefore, if the objective is to understand how a kink band is formed, then it is mandatory to observe it while loaded.

Splittings within the kink band

Several open splittings were found in the specimens; this is an important issue for the development of analytical models, as if they are actually found at the kink band's tip it means that fibres are unsupported while kinking occurs and the effect of the matrix can be neglected in some extent. However, not every splitting does imply a material discontinuity between fibres and matrix in the region of interest: it can also be found outside the kink band (specimen CC_6d*), in unloaded configurations (specimen r-UD_0d1) or due the propagation process or imperfections (specimens CC_6d* and r-UD_aux), which decreases its relevance for the referred purpose.

The splittings identified in the specimen r-UD_2d2 can be representative of the stress state found during normal kink band formation; the fibre is unsupported in some segments, but not in its whole kinked extension, at this phase. Considering now the fully-formed kink bands in specimens r-UD_0d1 and r-UD_2d2, it is evident that splitting occurred between groups of fibres, although it is not possible to know whether it took place during the compression or after unloading.

This subject is left, for the reasons presented, open to discussion by the experimental results; nevertheless, it is suggested that the support that each fibre receives from the matrix is not even, neither in terms of a single fibre's extension nor among a group of fibres.

Role of shear

Tables 3.1 and 3.2 evidence that splitting was a very common failure mode, taking place together with fibre kinking or alone. As it was previously discussed, splitting can occur in tension as a consequence of kink band propagation; however, when happening without kink band formation, splitting is usually attributed to an in-plane shear stress state instead. Considering that very similar specimens failed randomly by kinking and by splitting, one can conclude that some similarities between the stress states found in the two cases must exist; for this reason, in-plane shear stresses cannot be neglected in the analysis of kink band formation and propagation.

Complex features in kink band formation

The formation and propagation of a kink band proved to be a very complex process: the micrographs report the development of double kink bands (either in V or zig-zag shape), uneven fibre failure and failure surface, jumps in the kink band's path, initiation at a splitting instead of at the notch, unilateral broadening and sudden changes in the out-of-plane component.

Material randomness might be an explanation for these features, but the subject is left open to further research and discussion.

Set-ups

Three different set-ups were used in this experimental program; among them, only the r-UD one was effective regarding the goals previously defined.

It was found to be impossible to obtain micrographs with high magnification with a specimen under compression in an universal test machine (UD and CC specimens) as, even if a portable microscope could be used, the focus would be very difficult to achieve; besides, it was proved that a reduced specimen can be compressed and kink bands formed using simple tools, so there is no benefit on using such complex apparatus for this type of observation.

Compressing the specimen in a device which allows the observation under the microscope⁷ was achieved (r-UD specimens and set-up). Optical microscopy gives a better distinction between fibres and matrix, but the reduced depth of field limits the information obtainable; the SEM surpasses this problem and has higher magnification capabilities, being for that reason the most promising method for kink band observation.

Although it was one of the derived objectives for the experiments, a set-up producing a totally in-plane kink band was not achieved.

⁷The rig used for SEM observation of loaded specimens was developed by Renaud Gutkin, out of the scope of this project.

Chapter 4

Numerical analysis

4.1 Objective

An analytical model, able to explain and reproduce the formation of kink bands, requires the perfect understanding of the mechanics involved in the process, at the micro scale. As it is supported by the previous chapter, it is very difficult to get such knowledge from experimental data, so the numerical simulation presents itself as the best tool to provide useful inputs for the development of analytical models, as it allows the free manipulation of every parameter and avoids the randomness that is always present in experimental results.

The main goal of performing a full numerical analysis (finite elements (FE) method) on the formation of kink bands was therefore to get the picture of the components at the micro level, in order to identify the important features and to establish the sequence of events leading to kink band formation in real composites. Furthermore, the numerical simulations were used to validate the analytical model for kink band initiation developed in Chapter 5.

4.2 Modelling strategy

One of the main problems on using numerical simulations as an auxiliary tool to the development of analytical theories is that the phenomenon to be modelled is not well understood a priori; for this reason, the modelling strategy in this case must be discussed.

4.2.1 2D equivalent model

To be able to study the micromechanics of kink bands requires a high level of detail when modelling the composite, so bending and shear behaviour of its constituents can be properly captured; this means that fibre and matrix have to be modelled separately with a fine mesh. Considering this and the fact that there is experimental evidence that kinking can be planar (when it is constrained in one direction), it seems sensible to use a 2D equivalent model of the real 3D composite; however, to define a 2D model of a real 3D arrangement of fibres within the matrix requires several levels of idealisation. At first, the actual disposition of the components within the composite is not perfect, and needs therefore to be approximate by a reasonable 3D pattern; afterwards, this 3D idealisation has to be adapted to a 2D shape.

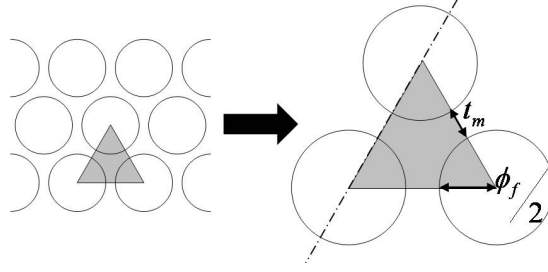


Figure 4.1: Hexagonal fibre arrangement and 2D equivalent model.

Let one assume a 3D hexagonal arrangement of perfectly cylindrical fibres (diameter ϕ_f) within a composite with volume fraction V_f . From figure 4.1, it is possible to deduce the distance between fibres (t_m) as:

$$V_f = \frac{\frac{1}{2}\pi \cdot \frac{\phi_f^2}{4}}{(t_m + \phi_f)^2 \cdot \frac{\sqrt{3}}{4}} \text{ and therefore } t_m = \phi_f \left(\sqrt{\frac{\pi}{2 \cdot \sqrt{3} \cdot V_f}} - 1 \right) \quad (4.1)$$

So, if one considers that the kink band is developed along one of the unit cell's symmetry planes (represented as a dash-dot line in figure 4.1), then a 2D equivalent can be a layered material with the fibres represented by layers ϕ_f thick interposed with matrix layers t_m thick (figure 4.2).

4.2.2 Critical features

It is well known that the formation of a kink band is a complex phenomenon affected by defects on the shape and arrangement of the fibres within the composite and geometric and material non-linearities; due to these aspects, it is obvious that a numerical model actually producing a kink band may be not trivial to find. In fact, several models tried at the beginning of this numerical work did not result into kink bands due to the misuse of at least one of the features that proved to be critical; these can be grouped into three categories: related to initial defects, related to the interface between fibres, and related to numerical issues.

Defects

The introduction of an initial defect is fundamental for the initiation of a kink band; without it, the model tends simply to pure compression or pure buckling. Different types of defect (fibre misalignment or waviness, matrix rich zone, weak elements, micro-notches, material misorientation, load misalignment) were tried, being fibre waviness the most effective one. The extension of the defect also proved to play a role, as all the small local defects (with an extension of the same order of magnitude as ϕ_f) led to failure by micro-buckling instead of kinking.

Interface between fibres

As it was already expected, the interface between the fibres has a major influence on the formation of kink bands. From the several modelling approaches carried out, it was shown that a bounded strength for the interface is mandatory, being all the other interface's parameters somehow irrelevant for the qualitative response. Kink bands were obtained both considering material (matrix) and discontinuous (frictional) interfaces; when a material interface was used, yielding and failing constitutive laws proved to work as well.

Numerical features

Besides the modelling issues directly related to the physics of the process, also some numerical features were found to be critical for the formation of kink bands in the models as well. The most important one is the geometric non-linearity, which proved to be mandatory; without it (assuming a geometrically linear problem), the initial waviness of the fibre was simply magnified proportionally during the compression. Another sensitive aspect was the use of numerical damping to stabilize the model: although it improved significantly the convergence to a correct solution when a proper value was used, too high damping led to failure by crushing instead of kinking.

4.2.3 Overall description of the models

Although several different models were analysed in this work, the modelling strategy was quite similar for all of them. Generally, the standard model for kink band formation is a geometrically non-linear model ran in a static analysis in ABAQUS Standard; besides the use of (low) numerical damping and some adjustments to the convergence control parameters, no other especial analysis features were used.

A general overview of the standard model used in the numerical simulations is provided next. For the variations to this model, a short description will be given when the results are to be presented (section 4.3).

Geometry and initial imperfection

A sine-shaped waviness was adopted as non stressed initial imperfection (equation 4.2); this is not totally realistic, as this waviness is usually induced by the manufacturing process and results therefore in residual stresses applied to the fibre, which is neglected here. However, the alternative would be to model the fibres as geometrically perfect and then produce a stressed imperfection by loading them transversely; this would shear significantly the matrix before the real load step, which is not realistic at all as, during the curing, the matrix flows and a significant amount of strain is released.

$$y_0(x) = \bar{y}_0 \cdot \left(1 - \cos\left(\frac{x}{L} \cdot \pi\right)\right) \quad (4.2)$$

The model (figure 4.2 a) is (along the global x-axis) $L = 0.750\text{mm}$ (imperfection's half wavelength) long; its peak-to-peak amplitude is $2 \cdot \bar{y}_0 = 30\mu\text{m}$, giving a maximum misalignment of $\theta_0^{max} = 3.6^\circ$; these values are slightly over the real misalignments found in the literature, but proved to be much more efficient when it comes to convergence issues. In its transverse direction, $n_f = 100$ fibres were modelled and a constant width was kept along the global y-direction, being therefore the thickness slightly reduced for the central region (where the slope is higher, figures 4.2 b and c).

As it was previously explained in section 4.2.1, the fibres are represented by layers with a thickness equal to their nominal diameter $\phi_f = 7\mu\text{m}$; the fibre volume fraction for the composite is $V_f = 60\%$, giving a layer of matrix $t_m = 1.6\mu\text{m}$ thick.

Constitutive laws

The constituents' mechanical properties follows those of a standard carbon fibre (IM7) + epoxy system (8551-7):

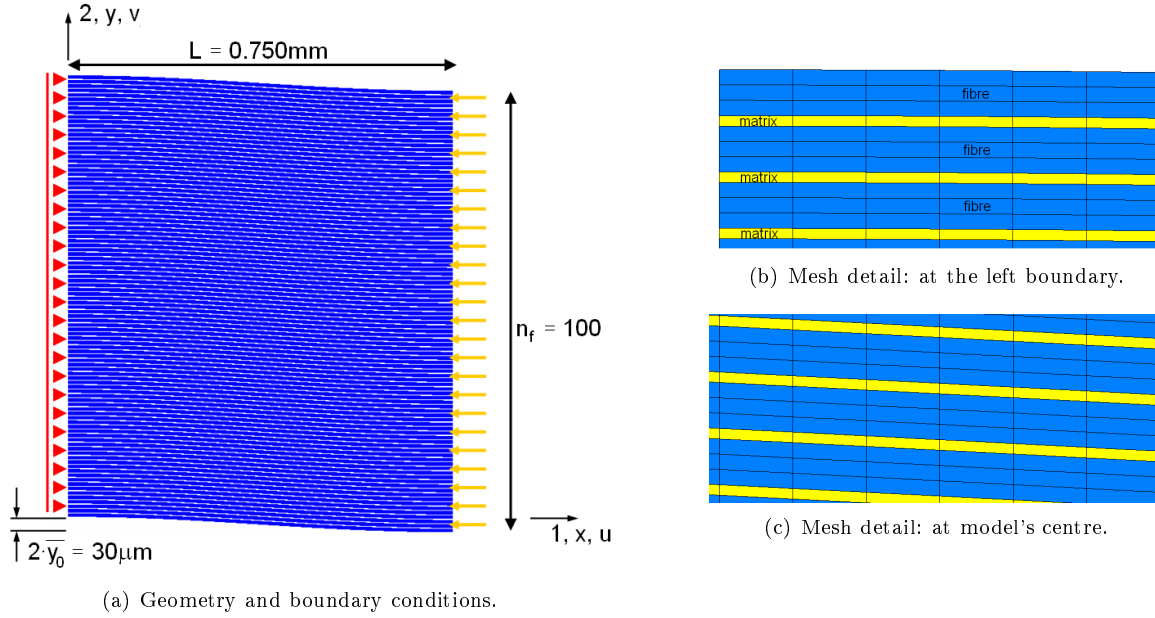


Figure 4.2: Numerical model: geometry, mesh and boundary conditions.

Fibres are considered to be isotropic and linear elastic, with $E_f = 276\text{GPa}$ and $\nu_f = 0.20$. In some models, a continuous damage formulation was used to predict the post-failure behaviour both under compression and tension, with given strengths of $X_C^f = 3200\text{MPa}$ and $X_T^f = 5180\text{MPa}$, and fracture toughnesses of $\mathcal{G}_C^f = 100\text{kJ/m}^2$ and $\mathcal{G}_T^f = 100\text{kJ/m}^2$, for (respectively) compression and tension.

Matrix was modelled either by elastic-plastic formulated elements or by interface / decohesive elements. Although the experimental results from compressive, tensile and shear tests do present significant differences, the matrix is always considered to be isotropic; because shearing is expected to be the main load component and also as it is the most complete test (includes pure shear, pure compression and pure tension), the constitutive law is deduced from the von Mises equivalent of experimental data (shear stresses versus shear strain) provided by a shear test, using the following expressions:

$$\begin{cases} \sigma_{Mises} = \sqrt{3} \cdot \tau \\ \varepsilon_{Mises} = \frac{\sqrt{3}}{2(1+\nu)} \cdot \gamma \end{cases} \quad (4.3)$$

The linear elastic properties (from the tangent to response at $\varepsilon = 0$) are given as $E_m = 4.050\text{GPa}$, $\nu_m = 0.38$ and $G_m = 1.478\text{GPa}$. For the non-linear domain, two different constitutive laws can be defined, according to the type of material formulation:

Elastic-plastic formulation (figure 4.3 a) considered the (transformed) experimental data and assumed a perfect plastic ($X^m = 98\text{MPa}$) behaviour for larger deformations;

Decohesive formulation (figure 4.3 b) assumed an initial linear-elastic response until the strength is reached (by a quadratic criterion with $X^m = 98\text{MPa}$ and $S^m = 56\text{MPa}^1$), following then a linear degradation process

¹Experimental data for the matrix. An alternative would be to consider, for the cohesive elements, a strength equal to the lowest value within matrix strength and composite strength

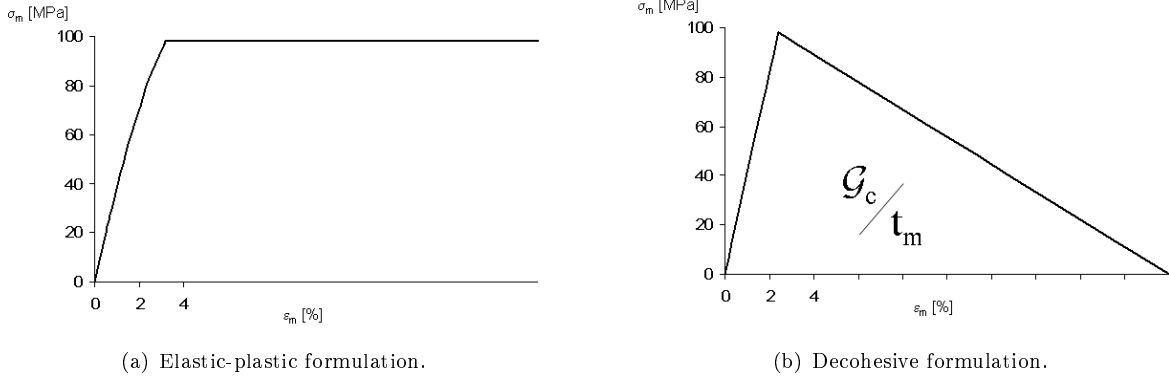


Figure 4.3: Constitutive laws used for the matrix in numerical models.

(with $\mathcal{G}_{Ic}^m = 0.21\text{kJ/m}^2$ and $\mathcal{G}_{IIc}^m = 0.80\text{kJ/m}^2$ as mode I and mode II toughnesses), and a mixed mode behaviour governed by the Benzeggagh-Kenane fracture criterion with exponent $\eta = 1.5$.

Mesh and boundary conditions

A fine mesh of 4-noded reduced integration elements with a general aspect ratio of 1:2 was used (figures 4.2 b and c); the elements in the initial configuration were distorted (and not rotated) so to define the correct slope, with the impact on the constituents' thickness already mentioned. The fibres were modelled with three elements through their thickness (giving the minimum number of integration points to capture bending properly) and the matrix (thinner and considered to respond mainly in shear) just with one (so each matrix element was under constant stresses).

During the analysis, the model was compressed under displacement control applied to the right edge's nodes, being the left edge fixed in the horizontal direction (figure 4.2 a); no boundary conditions were applied along the vertical direction, as it was found that fixing one node to avoid rigid body movements could result in stress concentrations (mainly due to the use of stabilization and its inertial-like effect).

4.3 Results

4.3.1 Generic results

Although a deep study on the effect of all the parameters and features involved in the numerical modelling of kink bands is out of the scope of this project, it is helpful for the development of the analytical model to have a general overview on the impact induced by simplifications and different features on the global response. The most relevant results are summarized next.

Properties of the fibres

Models with isotropic and orthotropic fibres were analysed; it was shown that fibre anisotropy is not a relevant feature for the formation of kink bands, as the behaviour of these two models was very similar (both when it comes to kink band's geometry and to load versus displacement curves).

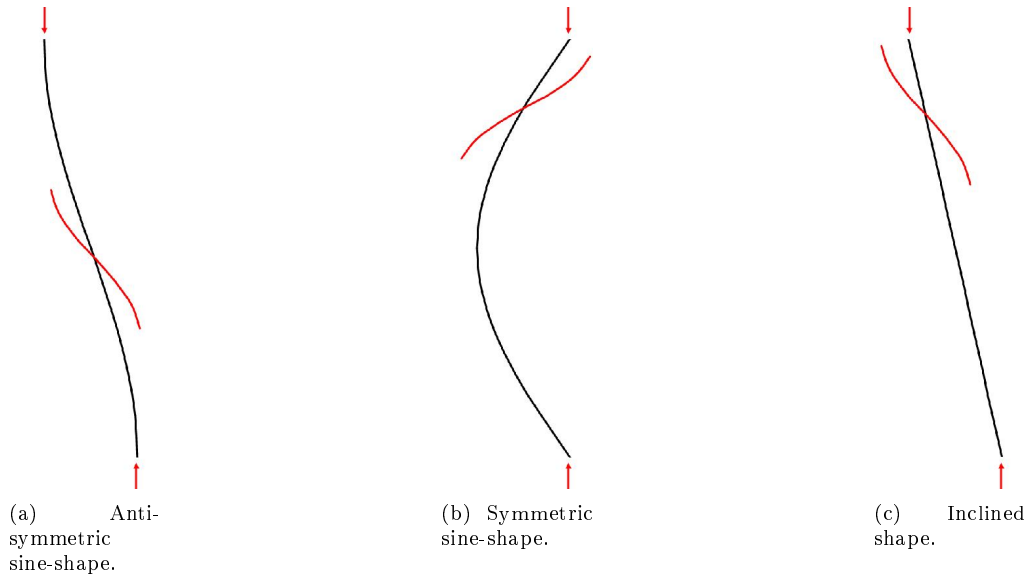


Figure 4.4: Types of imperfection with successful kink band formation.

Fibres were also modelled with different constitutive laws after a common linear elastic domain (limited by the fibre's strength X^f): one model was fully linear-elastic, other perfect-plastic and another used linear softening. The results show that fibre failure is not critical for the formation of kink bands, having no influence on the composite's strength; it has, however, a small impact on kink band's parameters α , β and w , and on the sharpness of its edges (which increases as one goes from the elastic law to the perfect plastic one and, even more evidently, to the softened behaviour).

Type of imperfection

Besides the anti-symmetric sine-shape, other two global imperfections - symmetric sine-shape and inclined shape with respect to load direction - also led to kink band formation.

The standard (anti-symmetric sine-shape, figure 4.4 a) imperfection resulted consistently in a kink band in the centre of the model, where the shear stresses in the matrix and the slope of the deformed fibres are higher. The symmetric sine shape (figure 4.4 b), without an inflection point within the model (inflections are located exactly at the boundaries), kinked not in the centre by any instability, but at one of the edges of the model where shear and slope are maxima as well. On the other hand, the model with straight inclined shape (figure 4.4 c, with no inflection point at all) failed by kinking at the edge, where stress concentrations due to the boundary conditions appear.

Models with no imperfection failed to produce kink bands and resulted in global buckling² instead. In these cases, the maxima bending stresses in fibres were always found at the boundaries, and the deformation went to the higher order buckling modes in latter compression stages.

Consistently, the imperfections resulting in kink bands had induced shear in the constituents, being the band initiated where these stresses on the matrix were higher; pure elastic instability proved to be a different failure mode from kink band formation.

²First order buckling and kinking differ in the location of maxima bending stresses on the fibres: in pure buckling, they are exactly at the boundaries and define an angle of $\beta = 0^\circ$ with the loading direction, while in kinking they are moved inwards and oriented at $\beta > 0^\circ$.

Type of interface between fibres

Three different interfaces between the fibres (with bounded shear strength) were numerically tested: yielding interface, failing interface and frictional interface.

The first two - yielding (elastic-plastic constitutive law) interface and failing (decohesive constitutive law) interface - are part of the models that will be analysed in detail and represent a material (matrix) interface between fibres; the mechanical behaviour obtained with both is very similar.

The other type of interface - frictional - is formally different from the previous ones. In the simulations using this feature³, the fibres were modelled as usually, but no material interface was defined between them; instead, the analysis was run with a contact interaction for each pair of fibres. The contact between fibres, apart from avoiding interpenetration, also induces frictional stresses τ_μ at their contacting surfaces, which act in a similar way to the shear stresses induced by the matrix in the other models. The frictional stress is assumed to vary linearly with the relative shear displacement between the two fibres (using a penalty factor to keep the relative displacements small) until a limit point is reached, above which the frictional stress remains constant (directly proportional to the contact pressure, $\tau_\mu^{max} = \mu \cdot p$). From this behaviour, the condition of having the shear stresses between fibres bounded by a finite value is also fulfilled; considering all the similarities between these two types of interface, it is not surprising that the simple interaction between fibre layers by contact with friction resulted into kink bands as well. However, this only happened when a sufficient overburden pressure was applied transversely to the fibres; was it not the case, and the fibres separated in the central region of the model (where the kink band was likely to form), and due to the lack of contact no friction arose and a kink band was not initiated.

4.3.2 Response curves for models on kink band initiation

The formation of kink bands was simulated by several FE models, being each one a variation of the standard one described in section 4.2.3. Among all, four models were deeper studied to understand the phenomenon:

- *cohesive* model with failing interface, implemented through a decohesive constitutive law for the matrix;
- *matrix* model with yielding interface, implemented through a elastic-plastic constitutive law for the matrix;
- *CDM* model with failing fibres (short configuration), using a bi-linear constitutive law for the fibres (both in compression and tension) implemented through a CDM (Continuous Damage Mechanics) model;
- *CDM_extended* model with failing fibres and extended (twice as long) configuration, with straight ends added to the initial imperfection (with standard wavelength and amplitude).

The response curves for the previously referred four models are provided in the next graphics (figures 4.5 and 4.6). These curves report, for the *cohesive* and *matrix* models, the composite's overall response from the initial configuration till first failure had occurred in model's central fibre ($0 \leq u(L) \leq 100\mu\text{m}$); for the *CDM* and *CDM_extended* models, the analyses were run further ($0 \leq u(L) \leq 250\mu\text{m}$).

The load versus shortening curve (figure 4.5) shows the expected behaviour for fibre kinking: the response is stiff and nearly linear at the beginning (here named as the *elastic* domain), with a sudden reduction in the stiffness

³Acknowledgments to Renaud Gutkin for the models with frictional interface.

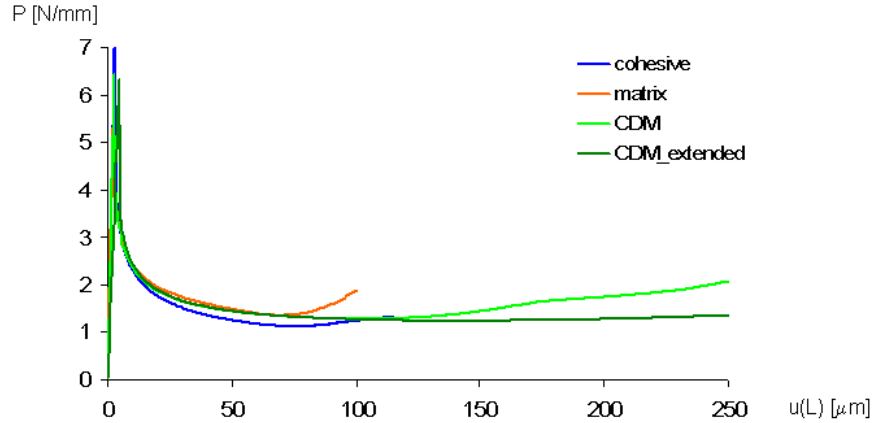


Figure 4.5: Load (P) versus shortening ($u(L)$) curves for the four models on kink band initiation.

after the peak load is reached; afterwards, the material continues to be compressed under a progressively reducing load (here named as *softening* domain).

The initial stiffness is approximately the same in the four models; the major difference is found in the *CDM_extended* model, slightly softer than the other three. The peak load is also similar in all of them, being slightly higher in the model with failing interface (*cohesive*).

Right after the peak load, all the models converge to the same solution; as compression continues, the model with failing interface (*cohesive*) shows a slightly more severe softening than the other three. Near central fibre failure, both models without failing fibres (*cohesive* and *matrix*) do stiffen, so the load increases for further compression; that behaviour is delayed in the short model with failing interface (*CDM*), and visibly reduced in the extended configuration (*CDM_extended*).

The transverse displacement (averaged from the model's right edge, $v(L)$) also agrees with the typical response found for kink band initiation (figure 4.6).

Initially, the deflection is small and very similar in all models, being the only difference found in the extended one with failing fibres (*CDM_extended*, with lower $v(u)$ slope). This domain ends with an instability (being the tangent to the graphic almost vertical), which is quickly surpassed as the slope decreases progressively, with the four models showing coincident curves.

Afterwards, the models without failing fibres (*cohesive* and *matrix*) continue to exhibit the same stiffening (v tends to stabilize) behaviour; the model with failing fibres (*cohesive*) is compressed at slightly smaller deflections. The models with failing interface (*CDM* and *CDM_extended*) are further compressed at an approximately constant deflection stiffness (constant slope); the short version (*CDM*) becomes slightly stiffer at latter compression stages, but shows a convergent tendency to the extended version at the end.

4.3.3 Model with failing interface for kink band initiation (*cohesive*)

In this simulation, the interface between fibres was modelled with cohesive elements, assuming a bi-linear constitutive law for the matrix. The main results, from the beginning of compression to the moment when all the

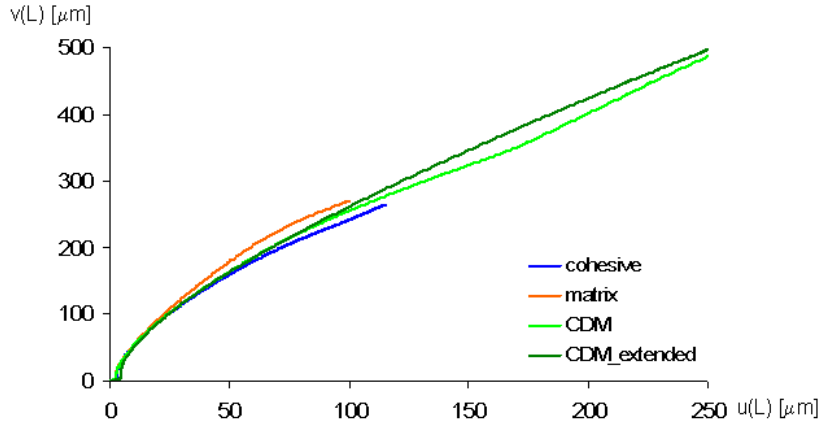


Figure 4.6: Maximum deflection ($v(L)$) versus shortening ($u(L)$) curves for the four models on kink band initiation.

fibres are overloaded, are presented next.

Load versus displacement curves

The load and deflection curves were already presented in the previous section for global analysis; here, the goal is to look at both together to identify corresponding features, and also to specify moments in the compression at which detailed information on stress and displacement fields will be given.

Having the $P(u)$ and $v(u)$ curves plotted together (figure 4.7), one can see that the peak load and the instability in the deflection effectively match; for this reason, not only the load response changes from the *elastic* to the *softening* domain, but also does the deflection shape.

Figure 4.8 shows the load versus deflection curve; its shape is similar to the $P(u)$ curve, being the main difference found for the less sharp stiffness reduction after the peak load. In addition, it can be seen that matrix yielding takes place just before the peak load is reached, and that both first and central fibre failure occur in the softening domain; besides, there is a considerable gap between the moment when the first fibre (at the boundaries) in the model starts failing (*first fibre failure*) and the one when all the fibres are partially overloaded (*central fibre failure*).

The main stress and displacement fields will be shown and analysed in detail for the seven points highlighted in the previous graphic. These main stress fields were chosen by comparing the von Mises stress to the several stress components in fibres and matrix; it was concluded that, for fibres, the axial stress σ_{11}^f was the main stress component, while for matrix the dominant stress was the in-plane shear one (τ_{12}^m).

Axial stresses in fibres

The axial stresses in the fibres present two different (qualitatively) configurations: one in the *elastic* domain, and another in the *softening* one.

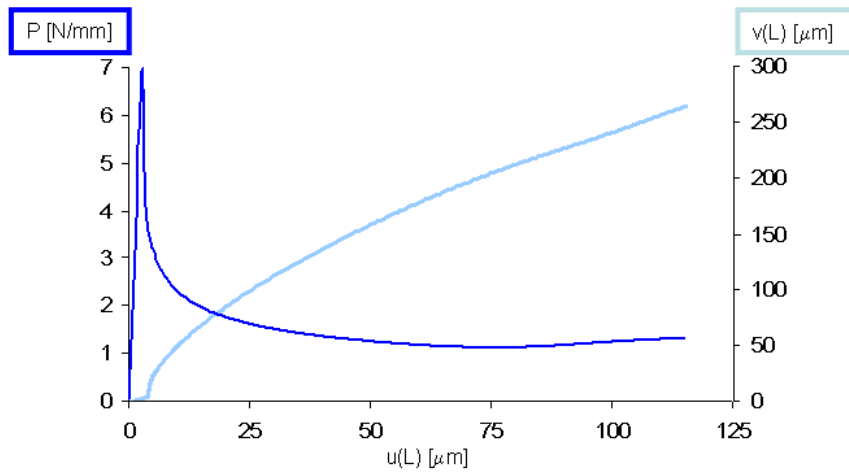


Figure 4.7: Load (P) and maximum deflection ($v(L)$) versus shortening ($u(L)$) curves for the *cohesive* model.

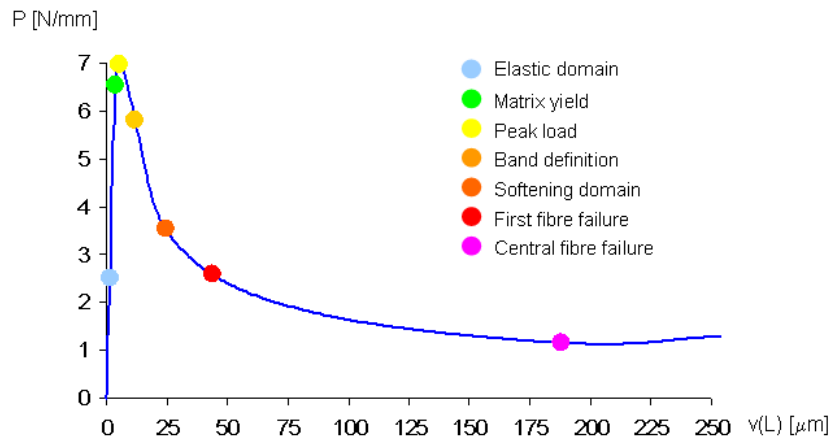


Figure 4.8: Load (P) versus maximum deflection ($v(L)$) curve for the model with failing interface, highlighting seven particular points.

Figures 4.9 and 4.10 show σ_{11}^f in the *elastic* domain and at peak load; as it can be seen, the stress field initially corresponds to the almost constant compression along fibre's length, with a low-amplitude sinusoidal component superposed; at the longitudinal (top and bottom) boundaries, the free-edge effect induces considerable stress concentrations.

At matrix yielding, the overall field is qualitatively similar (quantitatively, σ_{11}^f has increased); however, a careful look at the central fibres show already the development of a different response within a short fibre length (here called as *yield band*).

When the peak load is reached, two parallel bands (here called as *maximum bending bands*) with high σ_{11}^f stresses start being defined at the centre; these bands, oriented at a small angle with the transverse direction, do not cross the entire model's section yet, and the model's critical points are still found at corners. Nevertheless, the previously mentioned feature (in the *yield band*) in the $\sigma_{11}^f(x)$ curve for the central fibre is now more defined, with a central shape similar to a sinusoid and almost flat ends. At this stage, all the stresses are compressive yet.

After the peak load is reached and in the *softening* domain, the axial stresses follow the evolution shown in figure 4.11 and 4.12. The definition of *maximum bending bands* improves, and the critical (maximum σ_{11}^f) points move from the corners inwards to the bands, along the fibres at the transverse boundaries; at the same time, tensile stresses start appearing. The overall compressive stresses, away from the two bands, start decreasing, and the sine-like shape for the axial stresses in the central fibre (in the *yield band*) is magnified.

As the compression proceeds, these two *maximum bending bands* move apart from each other and become more inclined (but still straight and parallel); the stresses outside the central *yield band* continue to decrease, but the compression and tension components in the central sine-shape increase furthermore. For a single fibre, these sine-shaped stresses are symmetrical when one considers the points at the top and bottom of the fibre (figure 4.13).

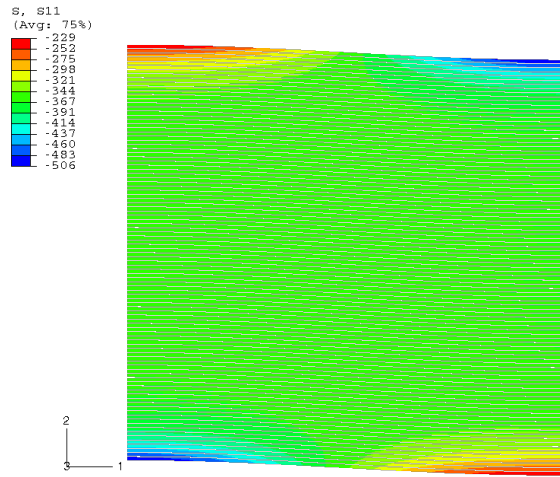
At a given point, the compressive stress at the two boundary (top and bottom) fibres reaches the compressive strength in the bands; at this moment, the model stops being representative, as fibres (in the simulation) continue to follow a linear elastic law. Nevertheless, would the compression continue and all the fibres in the model would be overloaded, with the two bands considerably inclined and almost reaching the transverse model's edges; the maximum compressive stress in the central fibre would be equal to the fibre's strength under compression, and the tensile one would almost present the symmetrical value, being the regions outside the central band nearly unloaded.

Shear stresses in the matrix

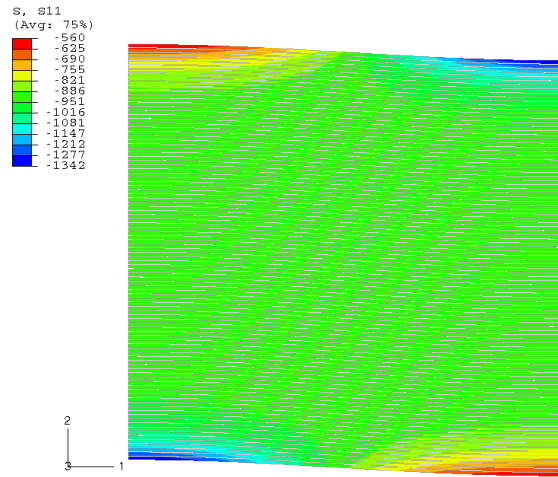
The shear stresses in the matrix in the *elastic* domain are shown in figures 4.14 and 4.15.

At the beginning, the shear stresses in the central fibres follow an approximately cosinusoidal law, being the maximum found exactly in the centre of the model; the free longitudinal edges affect this distribution by decreasing the shear stress progressively to zero along the last 10 fibres on each side, but the remaining fibres show a very similar and in-phase stress distribution.

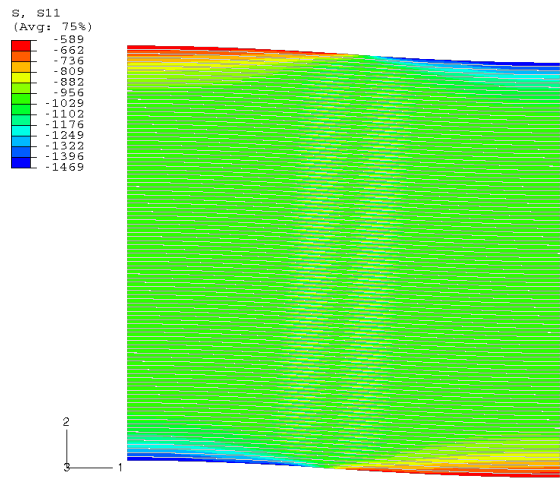
As compression proceeds, the shear stress in matrix layers continues increasing, and at a given point it actually reaches the matrix's shear strength; at that moment, the stresses are bounded and a *yield band* - with constant shear stresses - is formed in the centre of the model.



(a) Elastic domain ($P = 2.5\text{N/mm}$).



(b) First matrix yield.



(c) Peak load.

Figure 4.9: Axial stresses in the fibres (σ_{11}^f) in the *elastic* domain (*cohesive*).

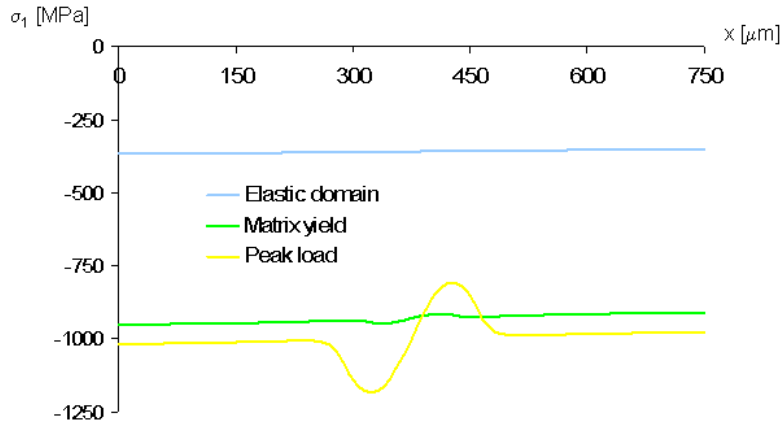


Figure 4.10: Axial stresses in the bottom of the central fibre (σ_{11}^f) in the *elastic* domain (*cohesive*).

After matrix first yielding, the *yield band* expands both in the axial (along each fibre) and transverse direction; at the peak load, all the matrix layers are yielded in a small segment, with maximum width ($w^{yield} \approx 200\mu\text{m}$) at the centre of the model. Outside this band, the shear stresses are quickly reduced near the band's boundaries, decreasing then smoothly to zero towards the model's transverse boundaries.

After the peak load (figures 4.16 and 4.17), the *yield band* quickly crosses the entire model with a nearly constant width; this band is inclined in relation to the transverse boundaries, but outside the band the shear stresses appear to be in-phase. Within the central matrix layer (figure 4.17) one can see that, inside the *yield band*, the shear stresses are slightly reduced from its boundaries to the centre; outside, there is an abrupt reduction in the shear stresses near band's boundaries, followed by a smooth reduction to zero at the model's transverse edges.

As the compression proceeds, the *yield band* grows along the axial direction and becomes more inclined; within the band, the reduction in the shear stresses from band's boundaries to its centre gets slightly more pronounced, and the stresses decrease even more suddenly at the outer neighbourhood of band's boundaries.

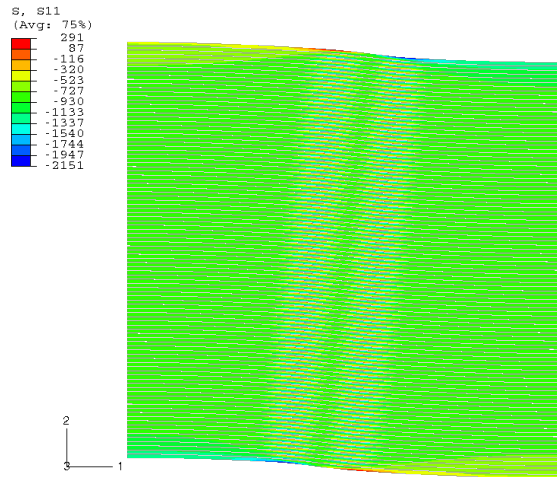
When all the fibres are overloaded, the *yield band* has already reached the model's transverse boundaries at the upper right and lower left corners; at this moment, the shear stress reduction within the band is more drastic, and outside the band the tendency of releasing the stresses is inverted.

Transverse displacements

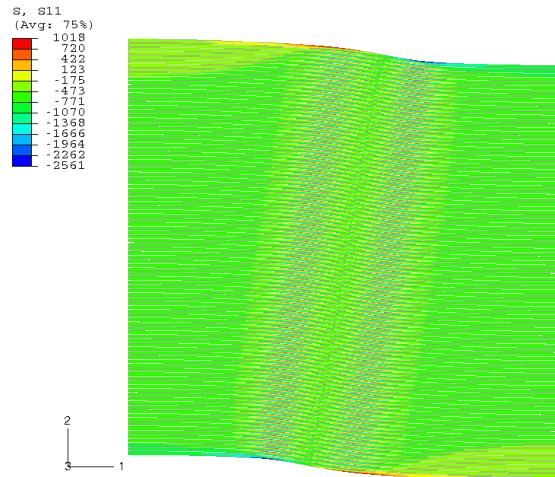
The transverse displacement measures the deflection that fibres undergo during kink band formation; different fields are found in the *elastic* and *softening* domains.

In the *elastic* domain, the displacement field is smooth (figure 4.18), with the left part of the model moving upwards and the right one downwards. A closer look at the deflection of the central fibre (modified so the left section is fixed, figure 4.19) shows a sinusoidal deformed shape until matrix yielding occurs; at the peak load, however, the presence of a kinked (highly deflected) region in the centre can be already noticed.

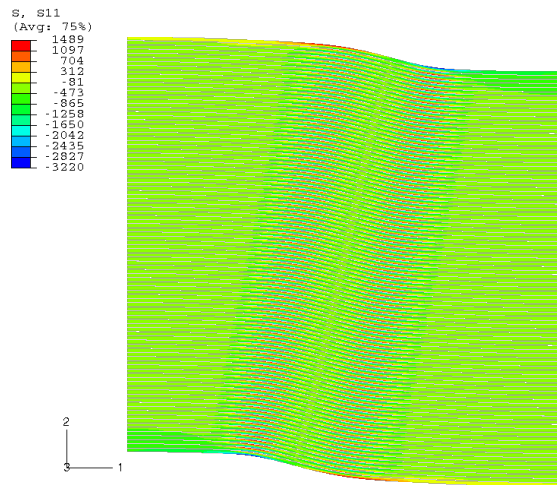
It must be noticed that, contrarily to what was suggested by the stress fields, the fibres do not deform entirely in-phase even in the *elastic* domain.



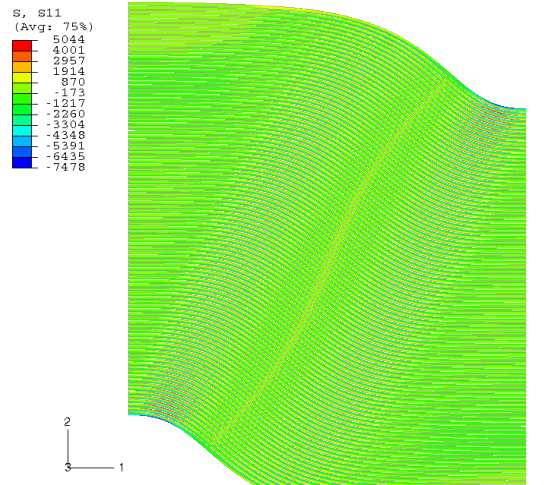
(a) Band formation ($P = 5.5\text{N/mm}$).



(b) Softening domain ($P = 3.5\text{N/mm}$).



(c) First fibre failure (edges).



(d) Central fibre failure.

Figure 4.11: Axial stresses in the fibres (σ_{11}^f) in the *softening* domain (*cohesive*).

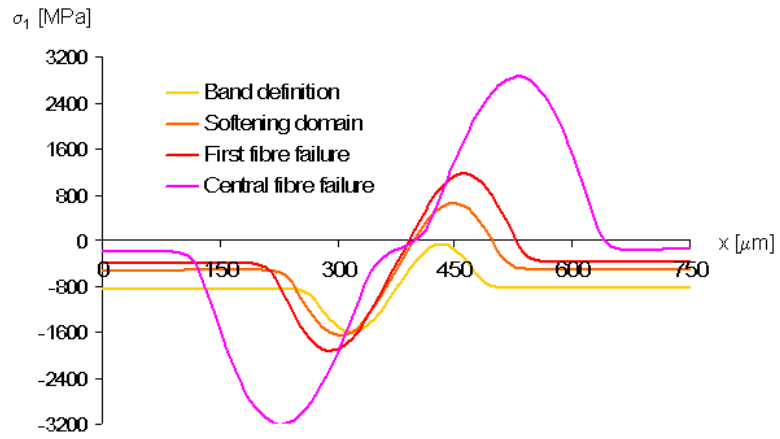


Figure 4.12: Axial stresses in the bottom of the central fibre (σ_{11}^f) in the *softening* domain (*cohesive*).

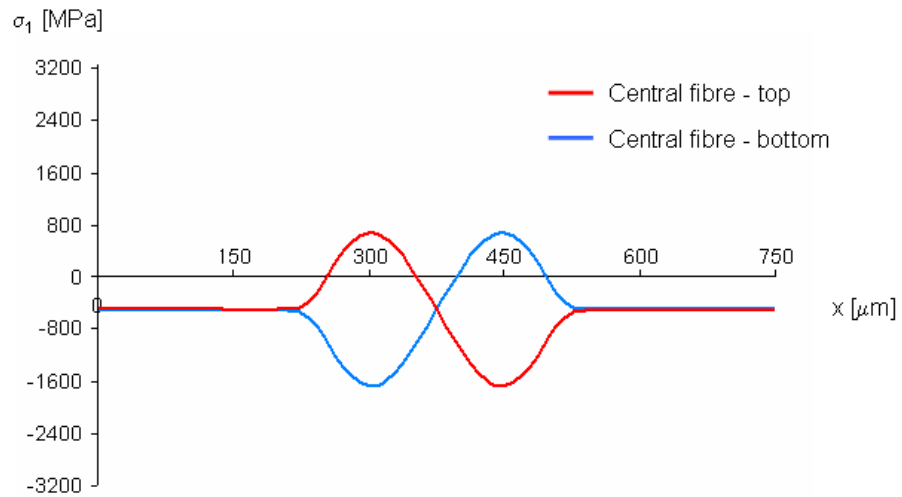
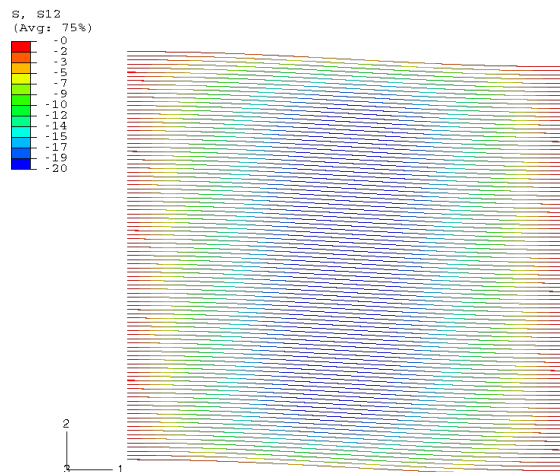
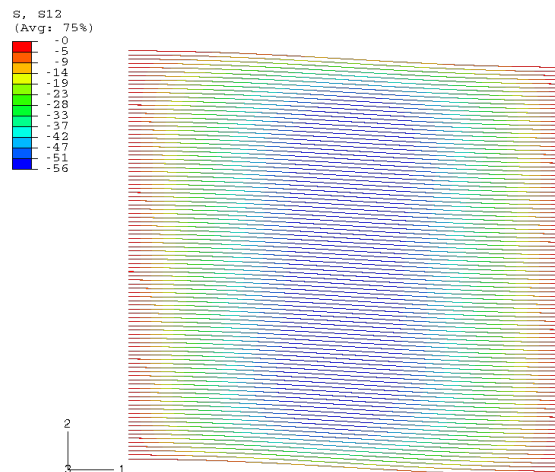


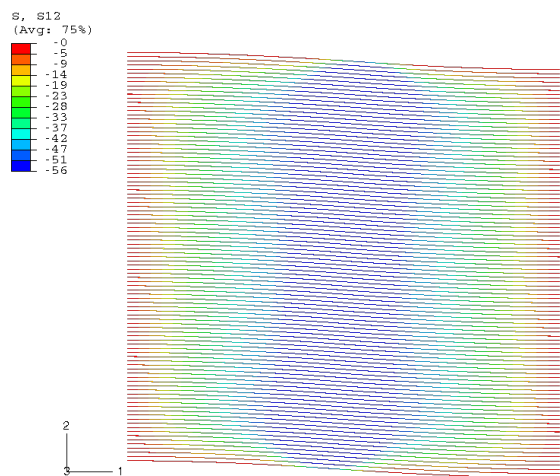
Figure 4.13: Axial stresses in the central fibre (σ_{11}^f), at its top and bottom boundaries, at $P = 3.5\text{N/mm}$ (*cohesive*).



(a) Elastic domain ($P = 2.5 \text{ N/mm}$).



(b) First matrix yield.



(c) Peak load.

Figure 4.14: Shear stresses in the matrix (τ_{12}^m) in the *elastic* domain (*cohesive*).

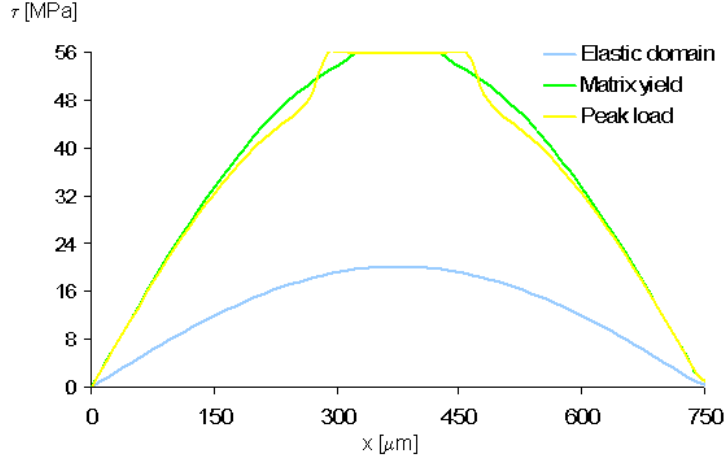


Figure 4.15: Shear stresses in the central layer of matrix (τ_{12}^m) in the *elastic* domain (*cohesive*).

After the peak load, the displacement field changes drastically: a perfectly defined band crosses the entire model from the lower to the upper boundary, at an angle with the global transverse direction (figure 4.20); inside this band the displacements change quickly from positive (left) to negative (right), but in the outside regions the deflection is near zero.

The deformed shape loses then completely its sinusoidal appearance (figure 4.21); two almost flat regions surround the central kinked area, which is itself straight in the centre. As the composite is compressed furthermore, the kinked band is rotated further more and extended towards model's edges; within each fibre, the three regions already identified as almost flat (left region outside the band, central region within the kinked band, right region outside the band) become flatter, and the segments linking them become more curved.

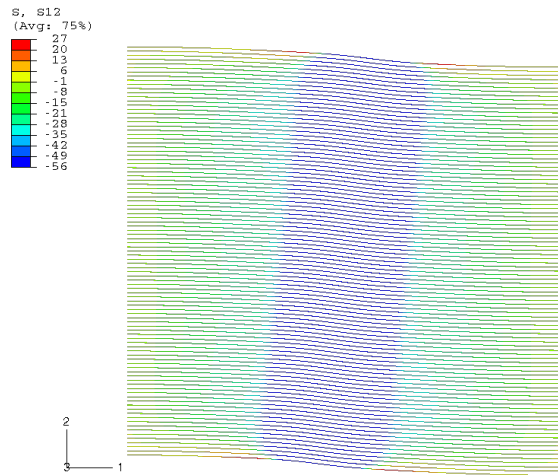
At the final stage of the simulation (at central fibre first failure), a boundary effect appears and the kinked band becomes curved near the top and bottom free edges.

Transverse stresses in the matrix

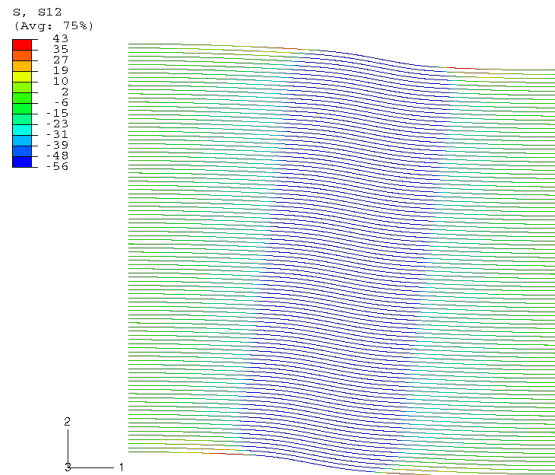
Although not as relevant as the shear stresses, the transverse stresses in the matrix can also play an important role in fibre kinking. Figure 4.22 shows the transverse stresses (local coordinates) in the matrix, at the moment of first matrix yielding (just before the peak load) and at first fibre failure (in the *softening* domain).

As it can be seen, as soon as the matrix starts yielding a thin band under transverse compression is formed; four other areas under high transverse stresses (compression and tension) are shown near the horizontal boundaries, outside the central compressed band.

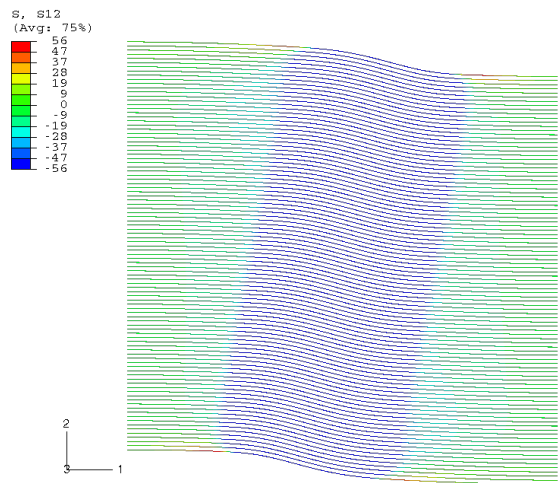
As the compression continues, the thin band under compression is loaded further more, reaching $\sigma_{22}^{first\ fibre\ failure} = -51\text{MPa}$; in addition, two larger bands under tension are formed right next to the central one, with tensile stresses around $\sigma_{22}^{first\ fibre\ failure} = 13\text{MPa}$.



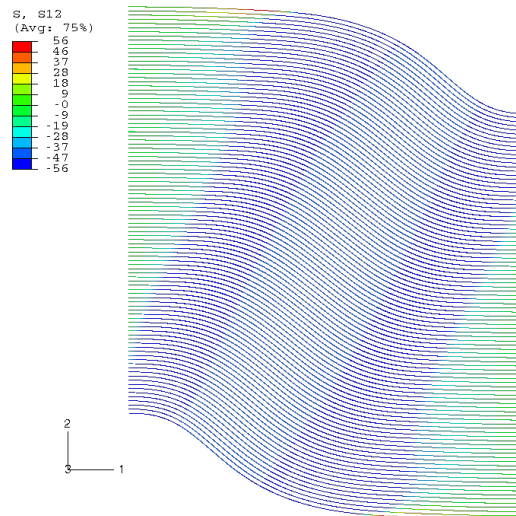
(a) Band formation ($P = 5.5\text{N/mm}$).



(b) Softening domain ($P = 3.5\text{N/mm}$).



(c) First fibre failure (edges).



(d) Central fibre failure.

Figure 4.16: Shear stresses in the matrix (τ_{12}^m) in the *softening* domain (*cohesive*).

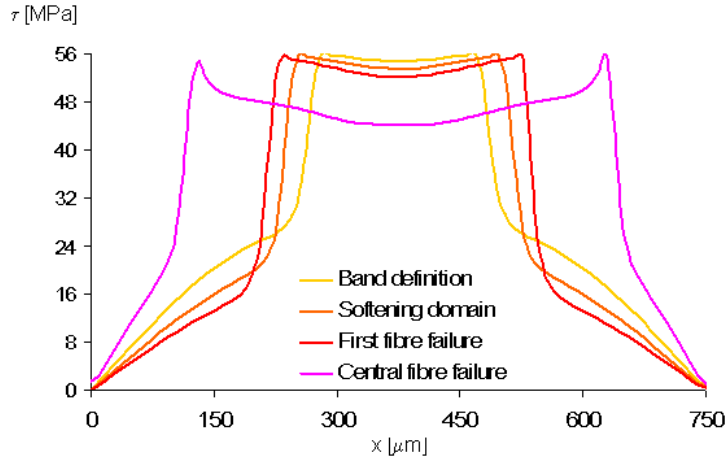


Figure 4.17: Shear stresses in the central layer of matrix (τ_{12}^m) in the *softening* domain (*cohesive*).

Splitting

This model stops being representative after central fibre failure; however, continuing the simulation (not represented in the load and displacement curves), 60 fibres split from the model by matrix failure (figure 4.23); after this, the axial stresses are significantly reduced in the central group of fibres.

Numerical variations

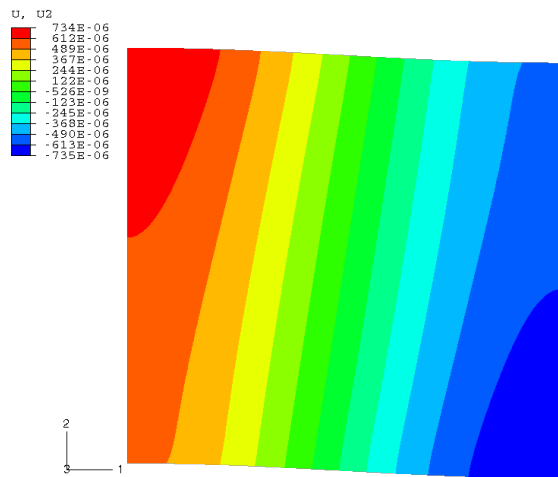
The model previously presented considered 100 fibres and made use of numerical stabilization; for comparison purposes, a short overview on the results of two similar models - *cohesive_0stab* (with no damping applied) and *cohesive_20fibres* (with only 20 fibres) - is given.

From the graphics in figure 4.24, one can confirm that material's response is approximately the same in these three models. However, a significant difference can be found in the initial stiffness of the model with reduced number of fibres; the peak load also decreases from the standard model (*cohesive*) to both the *cohesive_0stab* and *cohesive_20fibres* models; in addition, the model with no stabilization (*cohesive_0stab*) shows a more sudden softening right after the peak load.

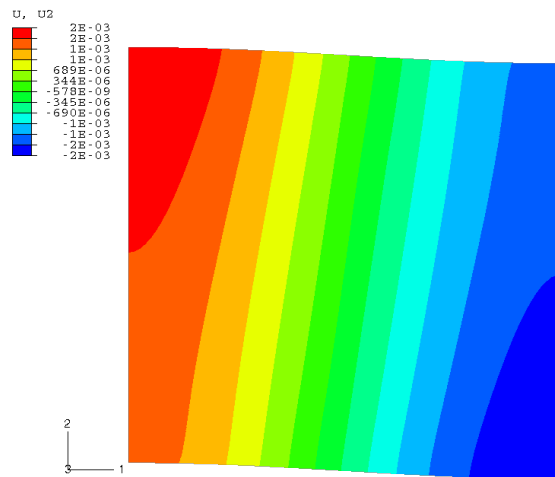
Notwithstanding the previously pointed differences, the overall behaviour in latter stages within the *softening* domain converges for the three models here analysed.

When it comes to stress fields, the model with no damping (*cohesive_0stab*) gives the same qualitative response as the standard model with stabilization (*cohesive*). Figure 4.25 shows the axial and shear stresses in fibres and matrix respectively, for a load $P = 3.5\text{N/mm}$ in the *softening* domain; in relation to the corresponding results for the standard (*cohesive*) model, the only difference noticed is the slightly higher axial stresses in the damped model.

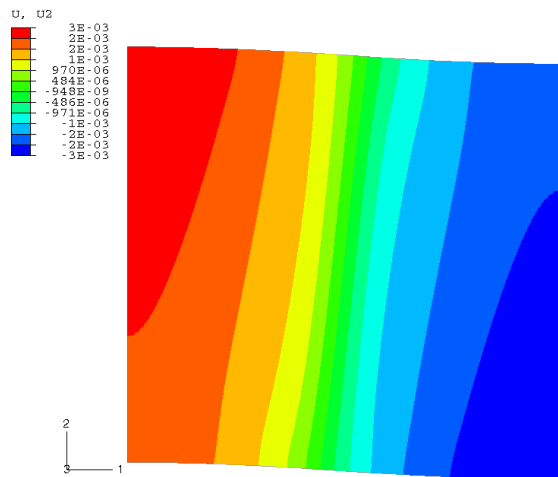
The model with reduced number of fibres (*cohesive_20fibres*) presents a different free-edge effect from the standard one (*cohesive*): a yield circle is seen instead of a band, extended almost all across model's height and at first matrix yielding (figure 4.26).



(a) Elastic domain ($P = 2.5\text{N/mm}$).



(b) First matrix yield.



(c) Peak load.

Figure 4.18: Deflection (v , global referential) in the *elastic* domain (*cohesive*).

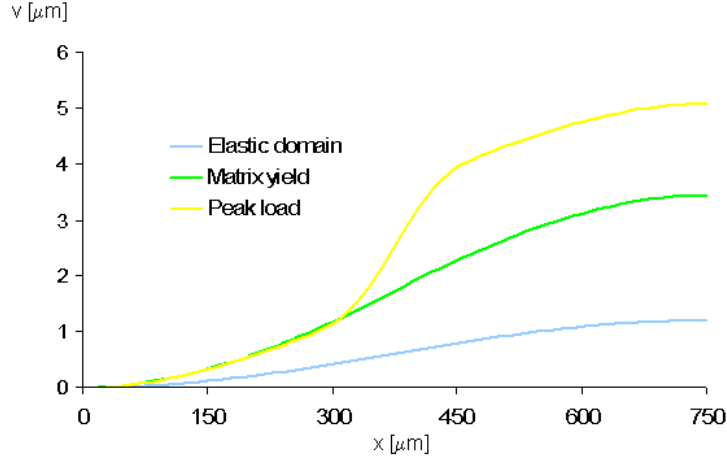


Figure 4.19: Deflection of the central fibre (v , global referential) in the *elastic* domain (*cohesive*).

4.3.4 Model with elastic-plastic matrix (*matrix*)

In this simulation, the interface between fibres was modelled with common plane strain elements, assuming a linear elastic - plastic with hardening - perfect plastic constitutive law for the matrix.

This model's behaviour is very similar to the one with cohesive elements, both qualitatively and quantitatively. The only significant difference is found in latter stages in the *softening* domain: in the *matrix* model, the two *maximum bending bands* defined after the peak load (figure 4.27 a) disappear as the *yield band* reaches the model's transverse boundaries, and deformation is confined to the upper right and lower left corners (figure 4.27 b).

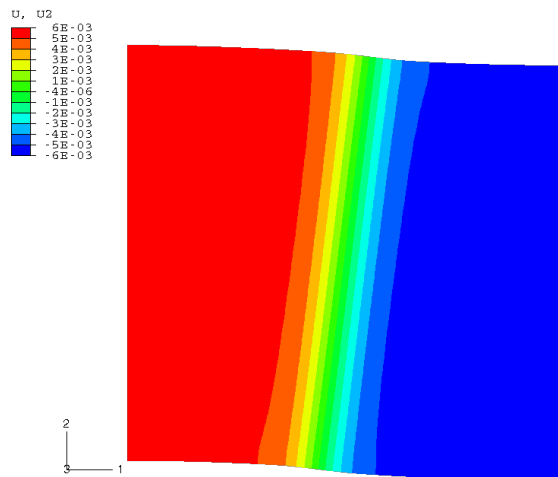
Following this change in the global deformed shape, the axial stresses in the model's central fibres decrease in latter stages; for the central fibre, the maximum compressive stress found during the analysis is $\sigma_{11,C}^f = 2228\text{MPa}$, so failure never initiates ($\sigma_{11,C}^f < X_C^f$).

4.3.5 Extended model with elastic-plastic matrix and failing fibres (*CDM_extended*)

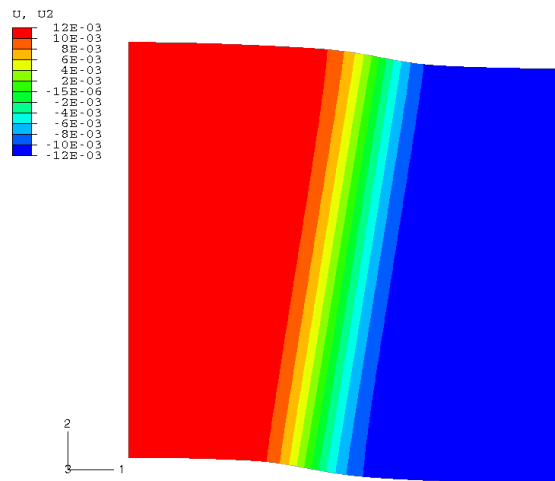
The *CDM_extended* model was analysed with the goal of studying the composite's response after first fibre failure; the model's geometry was extended with two straight ends (figure 4.29 a), and a CDM was implemented to allow fibre failure both under axial compression and tension. The fibres follow therefore a bi-linear material response, and the matrix a linear elastic - plastic with hardening - perfect plastic constitutive law.

The damage model used for the fibres is available in ABAQUS Standard library; it was specifically conceived for meso-scale modelling of composite materials, but by adjusting its several parameters it is possible to transform it into a maximum axial stress criterium; a plane stress state is required for the CDM to be used, and therefore both fibres and matrix were modelled with plane stress elements.

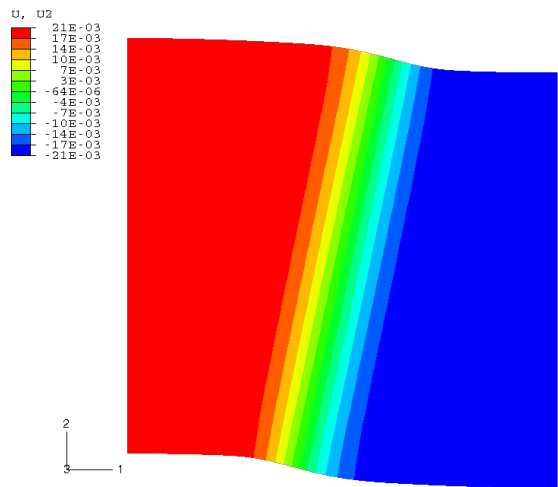
Figure 4.28 a shows the evolution of this model after first fibre failure, with the kink band (between the two *maximum bending bands*) becoming wider and more inclined as the compression continues; inside the band, fibre rotation increases too.



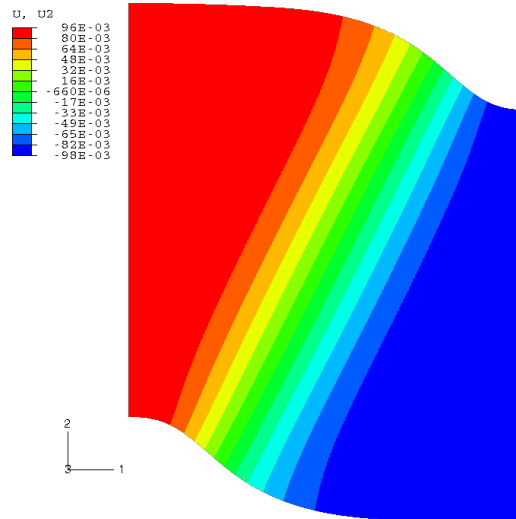
(a) Band formation ($P = 5.5\text{N/mm}$).



(b) Softening domain ($P = 3.5\text{N/mm}$).



(c) First fibre failure (edges).



(d) Central fibre failure.

Figure 4.20: Deflection (v , global referential) in the *softening* domain (*cohesive*).

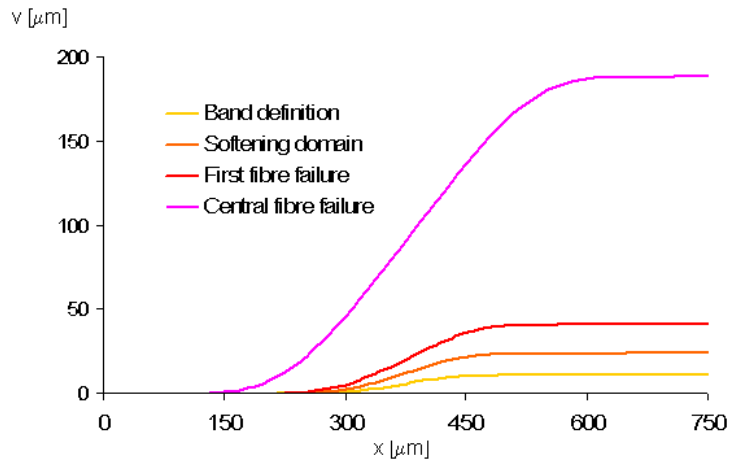
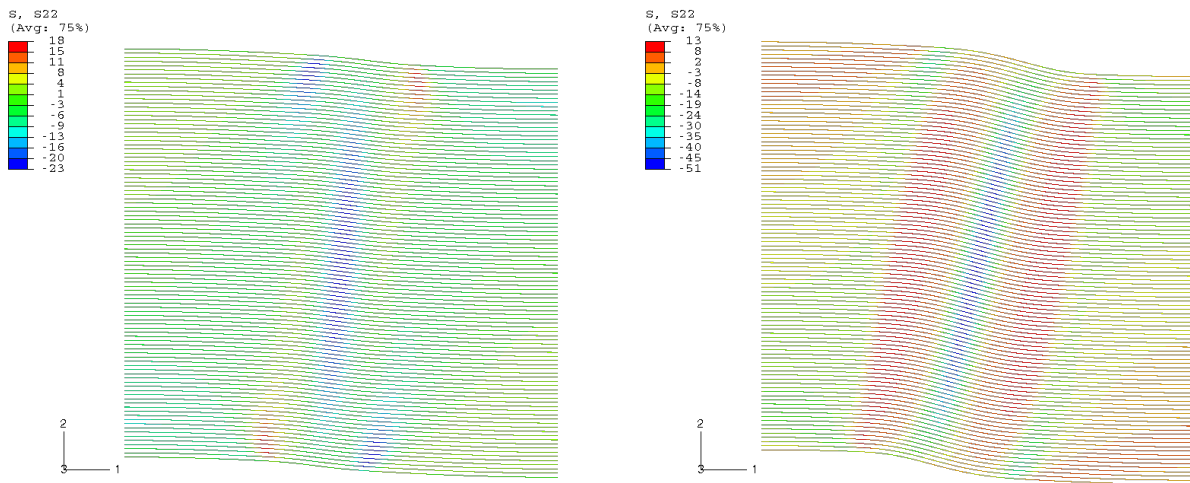


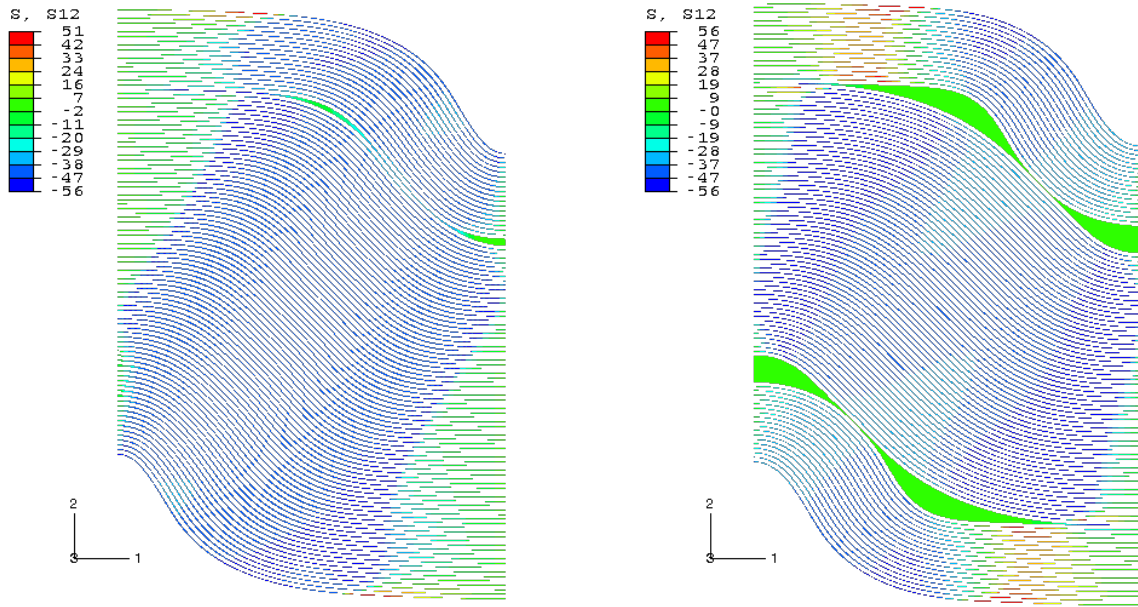
Figure 4.21: Deflection of the central fibre (v , global referential) in the *softening* domain (*cohesive*).



(a) At yield band's formation.

(b) At first fibre failure.

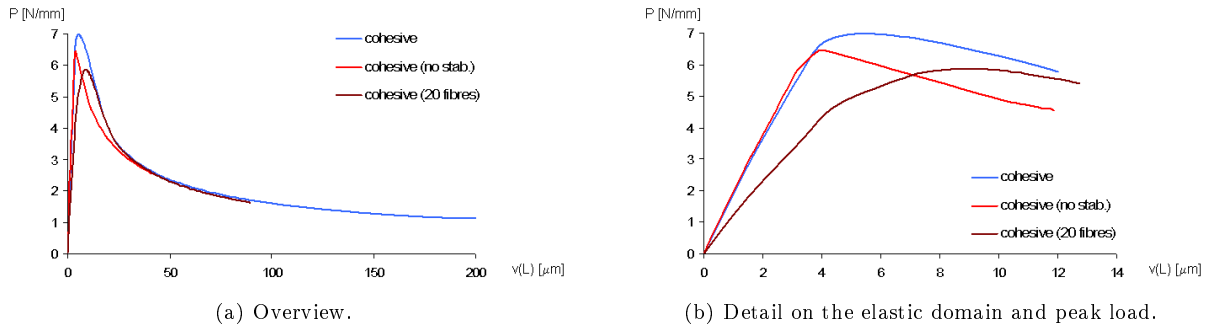
Figure 4.22: Transverse stresses in the matrix (σ_{22}^m , local referential) (*cohesive*).



(a) First splitting appears.

(b) Splitting fully developed.

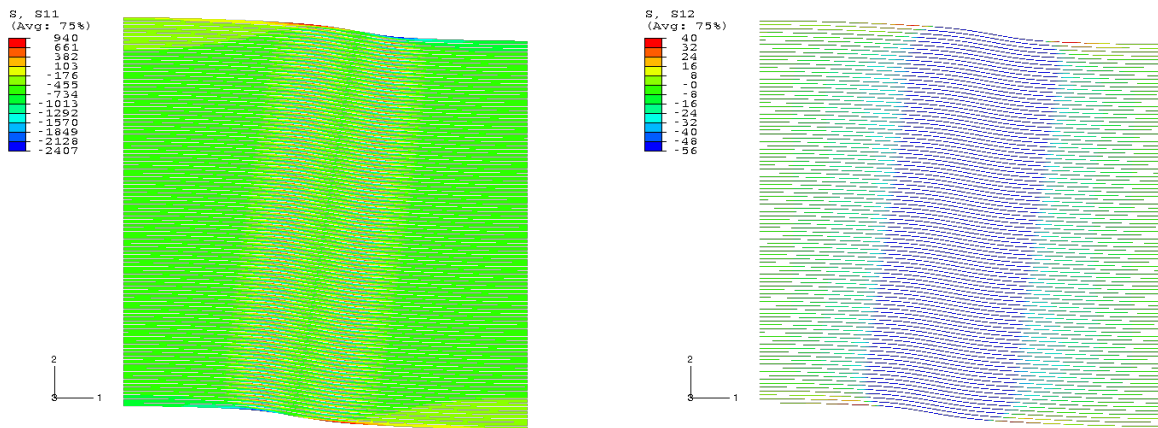
Figure 4.23: Split group of fibres, at the end of *cohesive* simulation.



(a) Overview.

(b) Detail on the elastic domain and peak load.

Figure 4.24: Load (P) versus deflection ($v(L)$) curves for the numerical variations of the *cohesive* model.



(a) Axial stresses in the fibres.

(b) Shear stresses in the matrix.

Figure 4.25: Stress fields for the model with no stabilization (*softening* domain, $P = 3.5\text{N/mm}$).

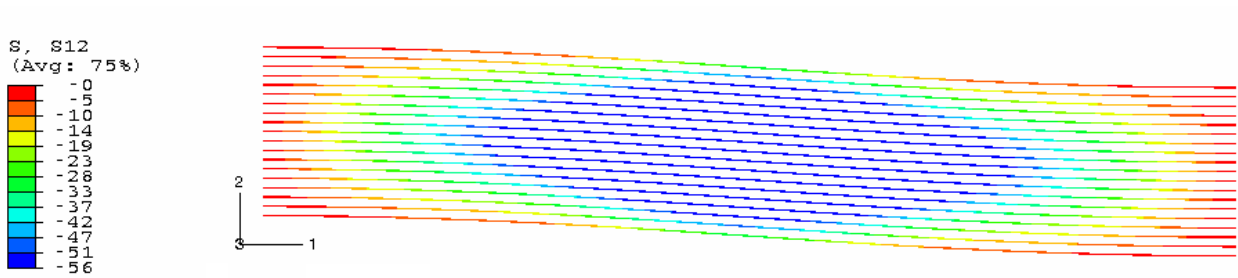
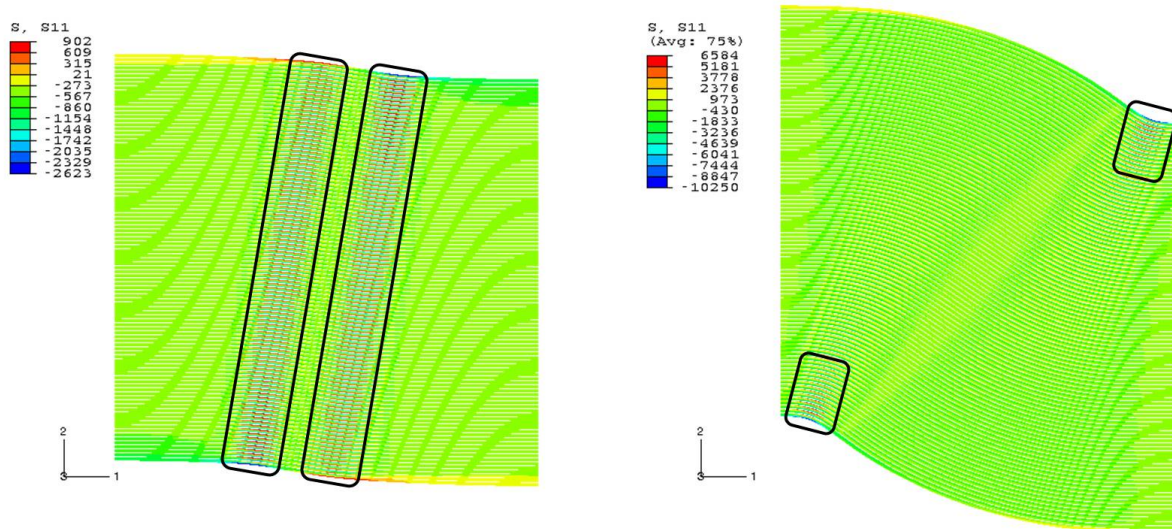


Figure 4.26: Shear stresses in the matrix for the model with *cohesive_20fibres* (at first matrix yielding).



(a) At $P = 3.5\text{N/mm}$.

(b) At shortening of *cohesive's* central fibre failure.

Figure 4.27: Axial stresses in fibres (σ_{11}^f) for the *matrix* model, in the *softening* domain, with overstressed areas highlighted.

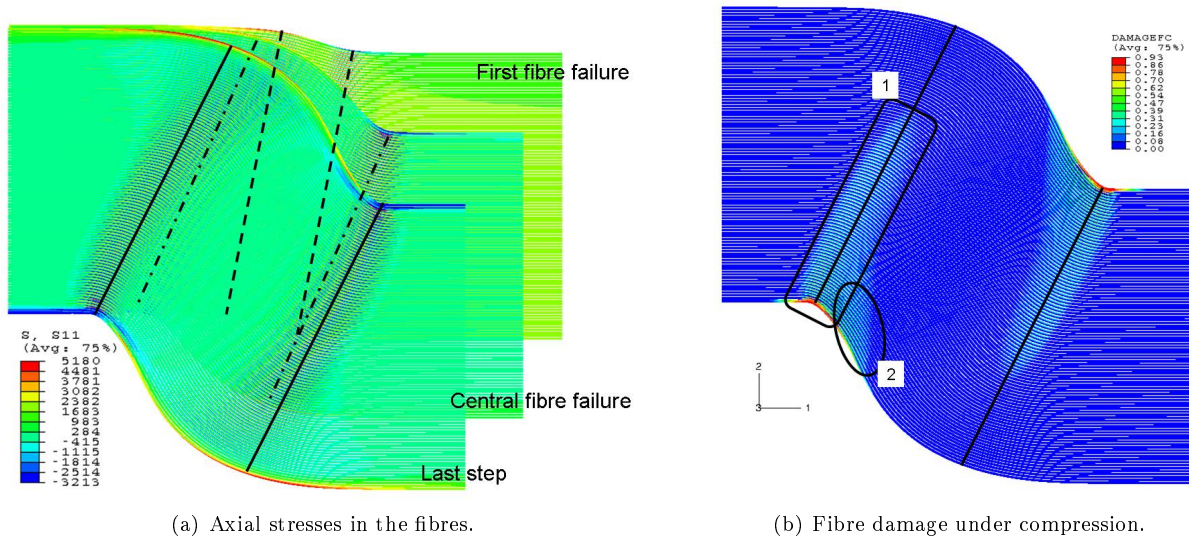


Figure 4.28: *CDM_extended* model: configuration during fibre failure process.

At the simulation's last step, none of the fibres is completely broken yet; damage under compression (figure 4.28 b) is seen not only along the maximum bending bands (feature 1) but also between them, near the upper and lower longitudinal edges (feature 2).

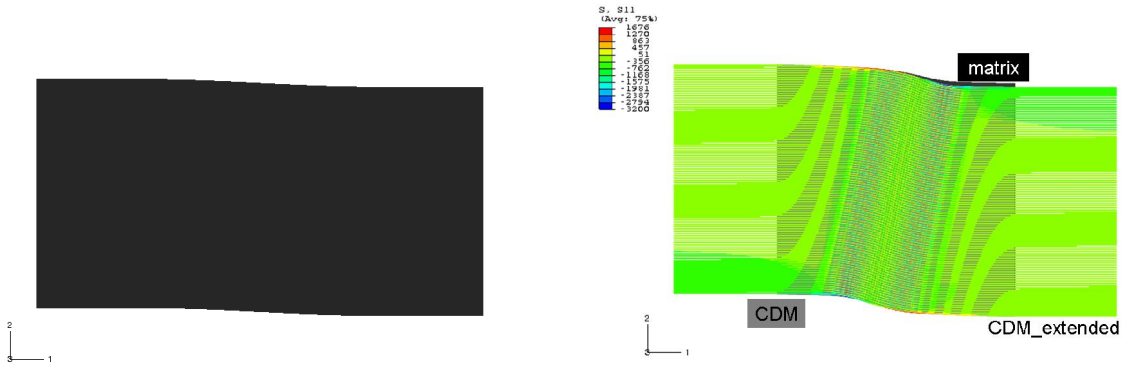
Figures 4.29 b to d show the axial stress fields for each configuration given in figure 4.28 a; it can be seen that failure starts under compression (b), and that tensile breakage begins only after the central fibre is already damaged.

A comparison between this model (*CDM_extended*) and the corresponding ones - without extended geometry (*CDM*) and without extended geometry and damage (*matrix*) - is also given in figures 4.29 b to d: at fibre failure (b), the three models are almost coincident; as the compression continues (c), the *matrix* model evolves into a more rounded deformed shape, with the areas of higher curvature confined at the model's corners; from the moment when the *yield band* reaches the transverse boundaries in the *CDM* model on, this model (*CDM*) starts diverging from the extended one (*CDM_extended*) too (d).

4.3.6 Results from model with kink band propagation (*propagation*)

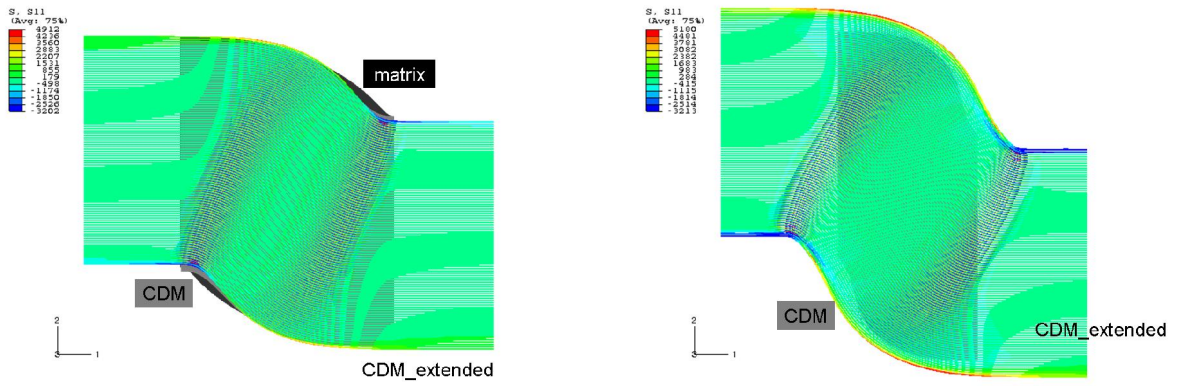
All models previously presented assumed an initial imperfection, which is reasonable when kink band initiation (triggered by some kind of defect) is studied; however, a composite does not present a global imperfection, so after initiation the kink band has to propagate through (almost) perfectly aligned fibres. For this reason, another numerical model - with 50 initially imperfect fibres (sinusoidal shape as previously used, with amplitude of misalignment constant along the first 25 fibres and decreasing linearly to straight fibres along the other 25 ones) and 150 straight fibres - was used to simulate kink band propagation (figure 4.30).

In the *propagation* model, the fibres are linear elastic. The matrix follows a bi-linear law (linear elastic + softening) in shear (decohesive constitutive law); however, the transverse stresses are governed by a simple linear elastic law.



(a) Initial geometry.

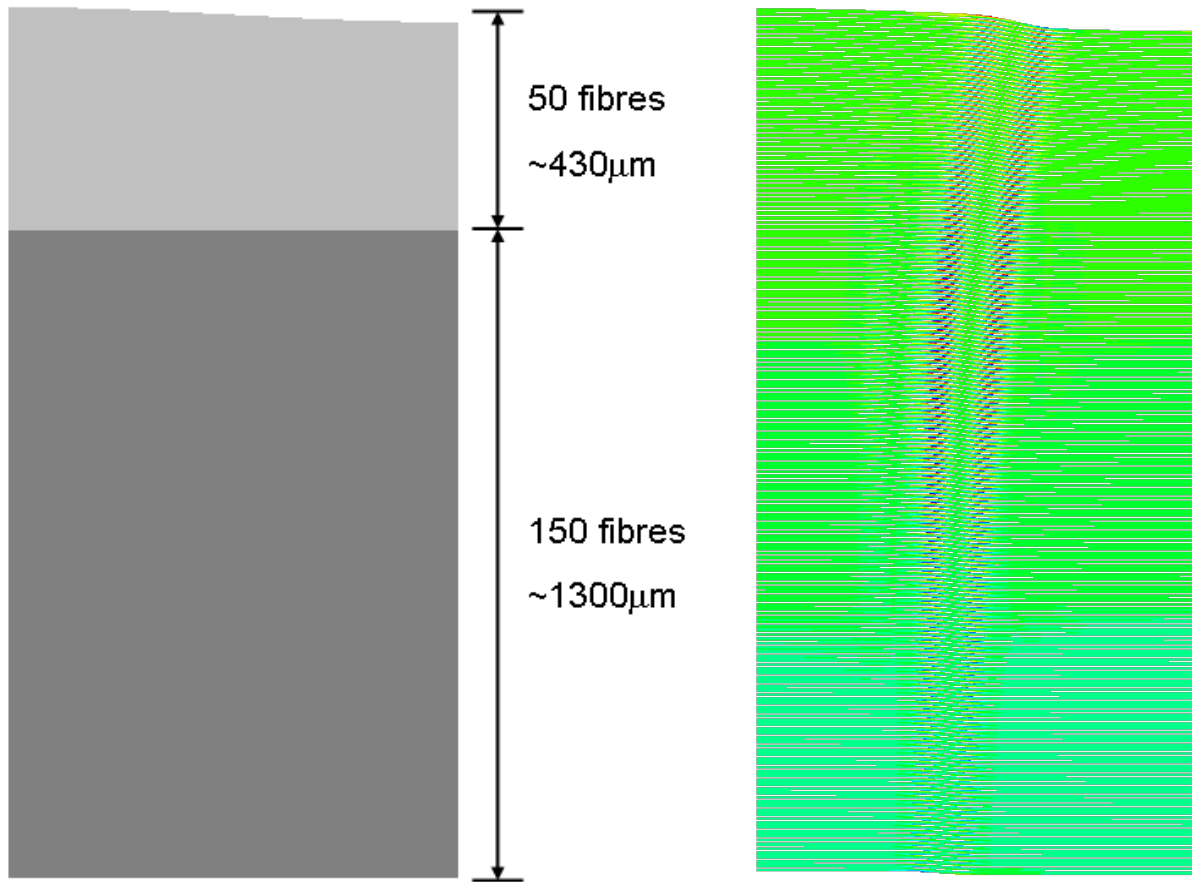
(b) At first fibre failure.



(c) At central fibre failure.

(d) At the last step.

Figure 4.29: *CDM_extended* model: geometry, axial stresses and comparison with *matrix* and *CDM* deformed shapes.



(a) Initial geometry.

(b) Kink band propagation.

Figure 4.30: Model for kink band *propagation*.

Kink band propagation

Figure 4.31 presents the sequence of events in the model for kink band propagation:

1. A wide *yield band* is formed in the matrix surrounding the imperfect fibres;
2. A narrow kink band starts forming in the imperfect fibres; the *yield band* narrows and propagates towards the initially straight fibres;
3. The kink band crosses the entire imperfect region towards the perfect fibres, and fibre failure starts at the model's upper fibres; the *yield band* is propagating across the perfect fibres;
4. The kink band propagates across the straight fibres, which become sufficiently stressed to start failing in compression; the tip of the *yield band* reaches the model's bottom boundary;
5. The kink band is fully propagated, both in terms of fibres and matrix; its inclination is still reduced from the top to the model's bottom;
6. The band broadens and rotates, so its geometry - w , β and α - is constant across the entire model at the end; stresses are considerably released.

Figure 4.32 shows the stress fields σ_{11}^f and τ_{12}^m for kink band propagation in straight fibres; the band is almost vertical ($\beta = 2^\circ$) and narrow ($w = 75\mu\text{m} \approx 10 \cdot \phi_f$), and the propagation length (estimated by the distance from the tip of the *yield band* (*matrix yielding*) to the tip of the overstressed fibres (*fibre failure*) is $L_{prop} \approx 550\mu\text{m} \approx 78 \cdot \phi_f \approx 7.3 \cdot w$. In addition, it is unquestionable that matrix yielding precedes fibre failure.

Transverse stresses in the matrix

Figure 4.33 presents the field of transverse stresses in the matrix (σ_{22}^m) in the *propagation* model, during propagation across straight fibres (subfigure a, corresponding to figure 4.32) and after full band propagation (subfigure c, corresponding to figure 4.31 e).

As one can see, when the kink band is propagating (between the tip of the yield band and the last overstressed fibre), the material outside the band is under transverse compression on the right and transverse tension on the left, and inside the band almost no transverse stresses are found (figures 4.33 a and b). After the kink band is fully propagated across the model's transverse direction (figures 4.33 c and d), the band's centre is under compression and its boundaries under tension.

Variations of the model

As it was stated, the previous *propagation* model has an interface (matrix) able to fail in shear but not in tension; two variations - *propagation_failure* and *propagation_constrained* - of this model, with tensile failure allowed, were analysed as well.

The difference between *propagation_failure* and *propagation* models is just matrix's constitutive law in the transverse direction (changing from linear elastic in *propagation* to bi-linear in *propagation_constrained*). These two models' responses are the same until matrix tensile stresses reach its tensile strength; however, afterwards, the *propagation_failure* model starts opening splits between fibres: the first splitting (feature 1 in figure 4.34)

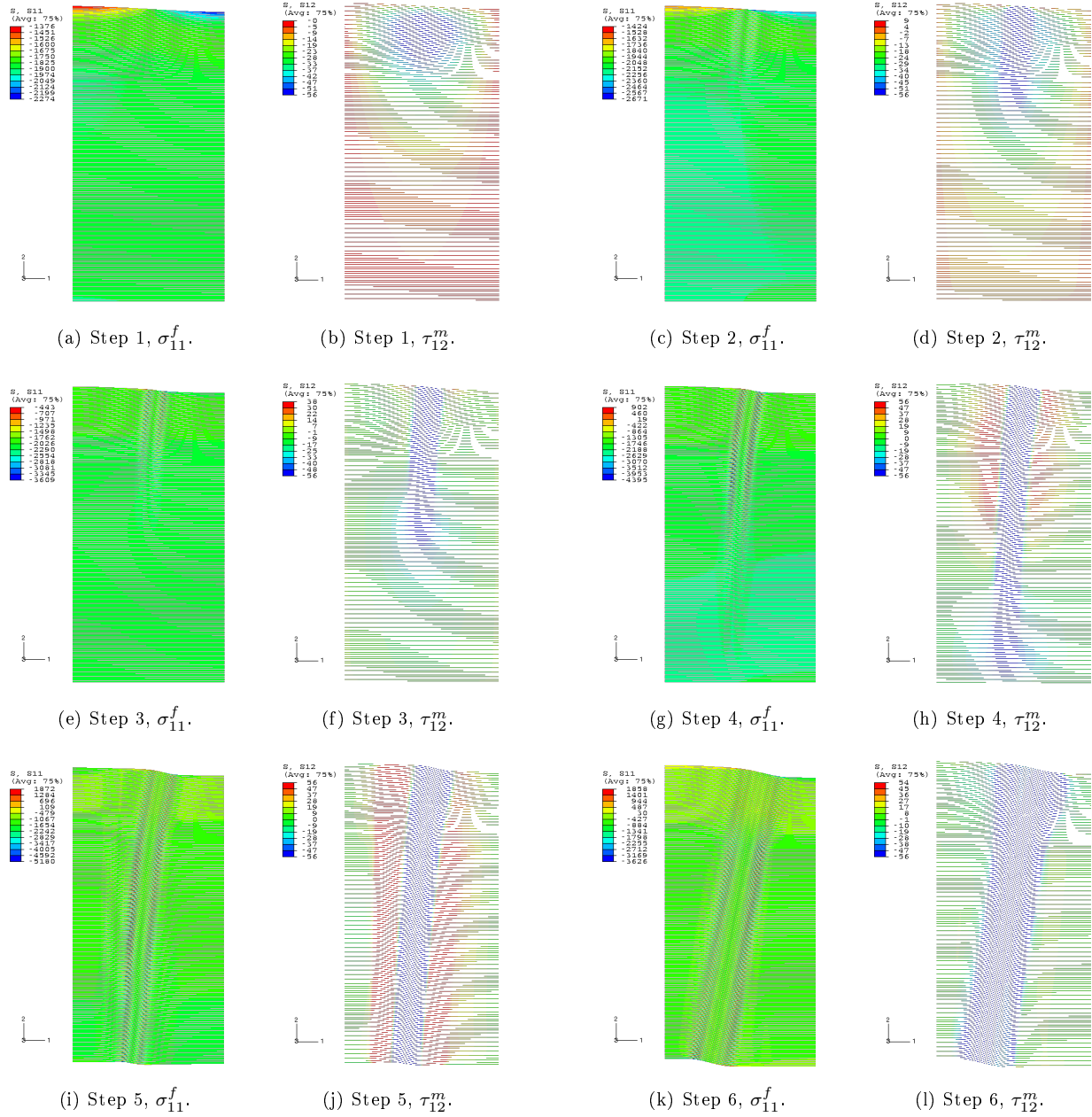


Figure 4.31: Kink band *propagation* (full model): sequence of events.

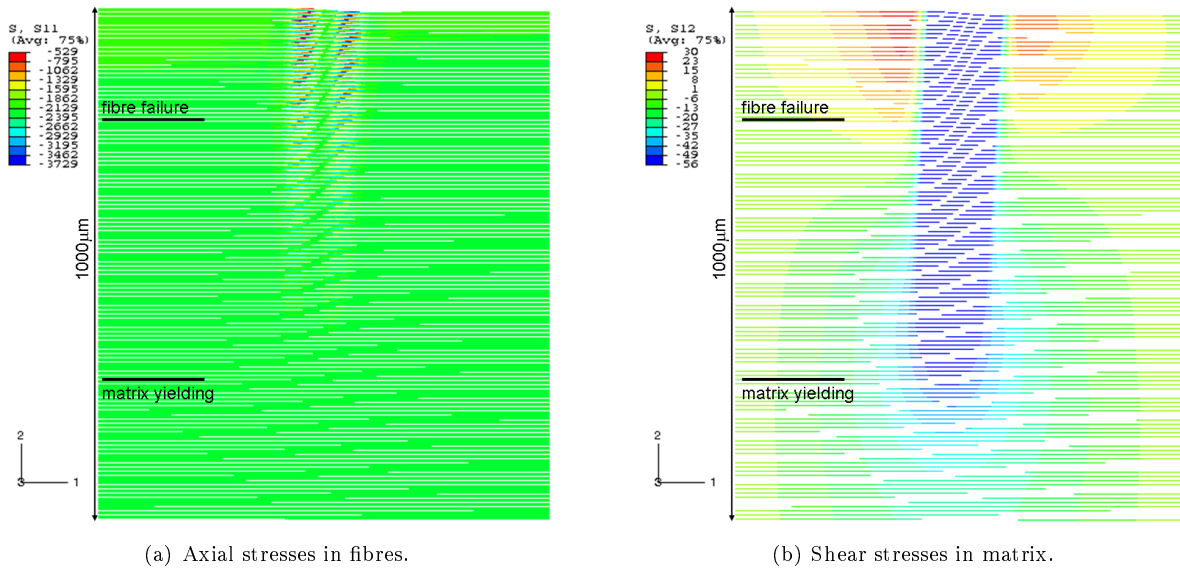


Figure 4.32: Kink band *propagation* in straight fibres.

occurs for a group of three fibres, where the imperfection ends, and the second splitting (feature 2) opens 40 fibres below the first one, leading to the formation of a V-shape (feature 3) within the fibres between splittings.

Propagation_constrained model differs from the original (*propagation*) one also in the transverse constitutive law for matrix (which is now bi-linear); in addition, the kink band is propagated with the upper fibre fixed, after its first failure.

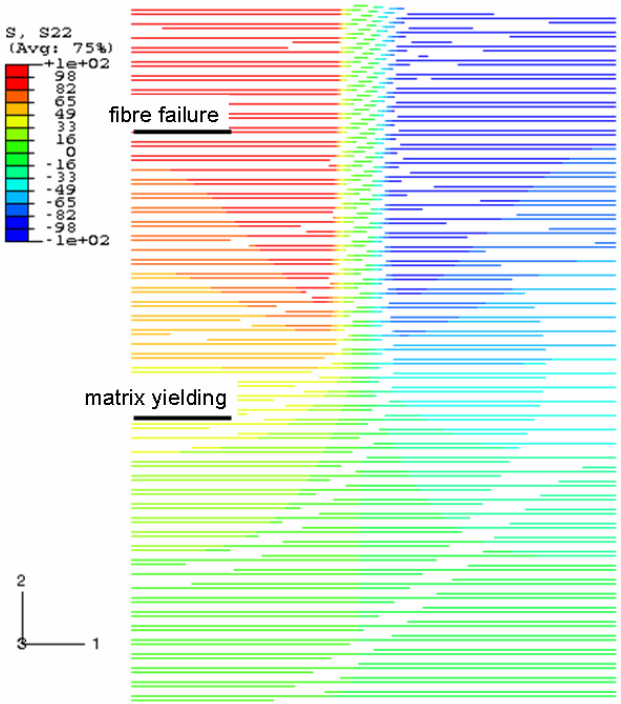
As the fibres are further compressed, they split from the top (fixed) fibre as seen in figure 4.35a (feature 1); the split fibres deform in a V-shape (as highlighted by features a and b), leading to the formation of a complementary yield band (figure 4.35 b, feature 2). At the same time, transverse stresses (figure 4.35c) show compression in the matrix on the left side and tension on the right one, triggering the formation of a splitting in the initially straight fibres (feature 3).

Compression continues (figure 4.35 d to f), and the splitting below the constrained fibre (feature 1) propagates to the right until it opens completely; at that moment, all the fibres in the model progressively deform to the typical kink shape (feature c), and one fully developed kink band crosses finally the entire model.

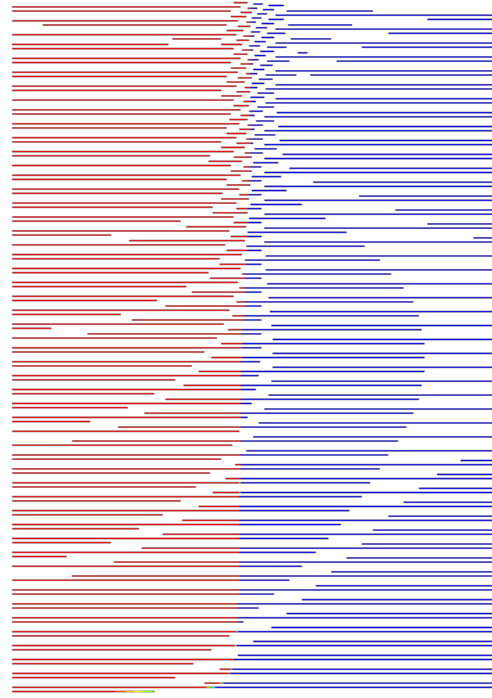
4.3.7 Results from model with complementary kink band (*CDM_complementary*)

The model presenting a complementary kink band (*CDM_complementary*) is very similar to the extended model with failing fibres (*CDM_extended*); the only difference is that, in the present case, the top left node was clamped (restraining rigid body movement) and higher damping was used.

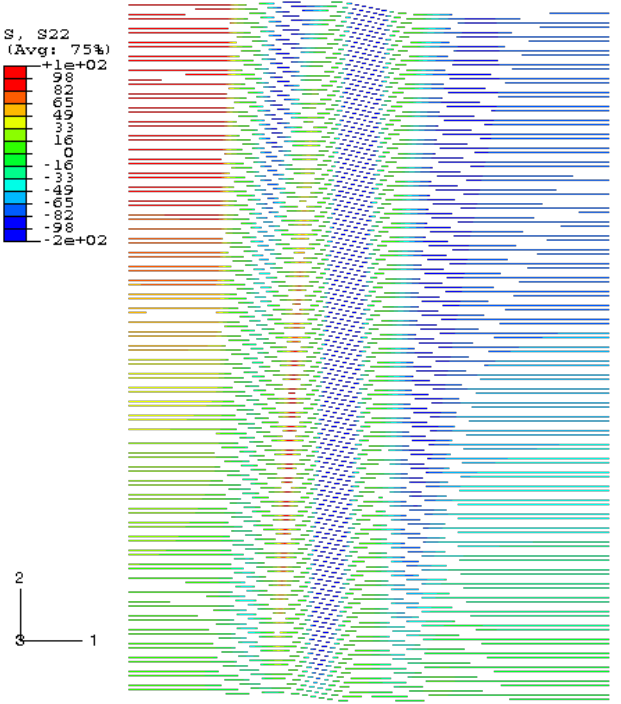
The composite's configuration at the simulation's last step is shown in figure 4.36; the first kink band was developed at the centre, followed by the complementary one on its left. Fibre failure (subfigure a) started from the boundaries under global compression (concave sides) and progressed transversely towards the opposite (convex) edges, with each fibre failing both in compression and tension. Inside the bands defined by fibre overstressing (damage model active), the matrix yielded completely (subfigure b).



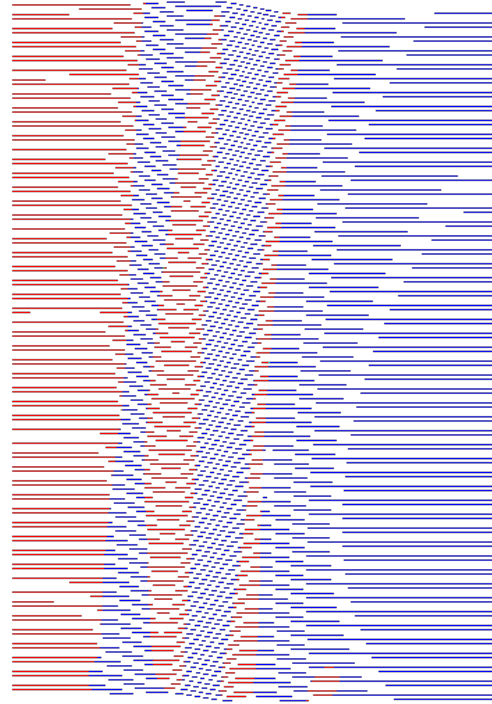
(a) Stress field for kink band propagation.



(b) Tension (red) vs compression (blue) for kink band propagation.



(c) Stress field after kink band propagation.



(d) Tension (red) vs compression (blue) after kink band propagation.

Figure 4.33: Transverse stresses in the matrix (σ_{22}^m) during kink band *propagation*, in initially perfect fibres.

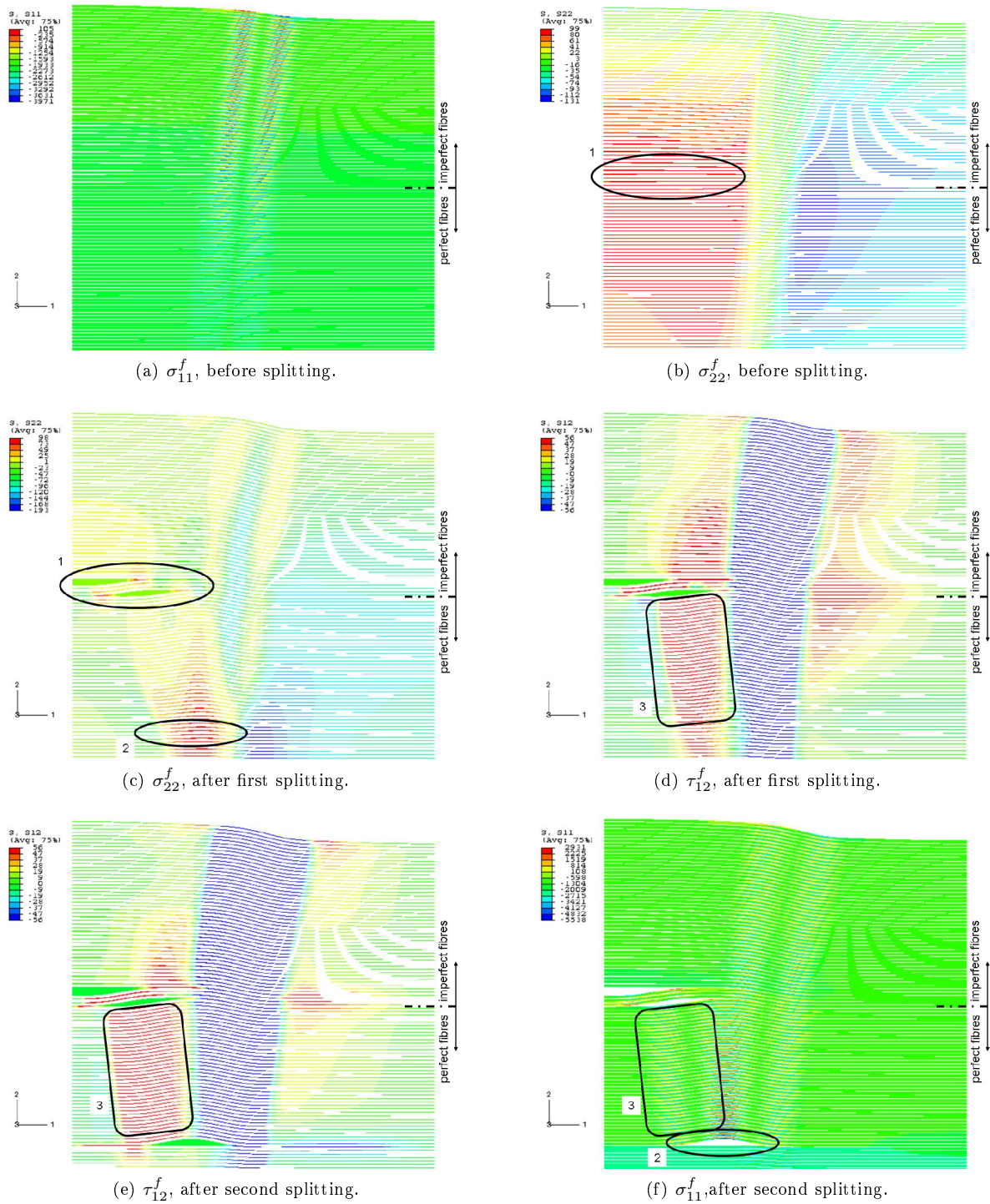
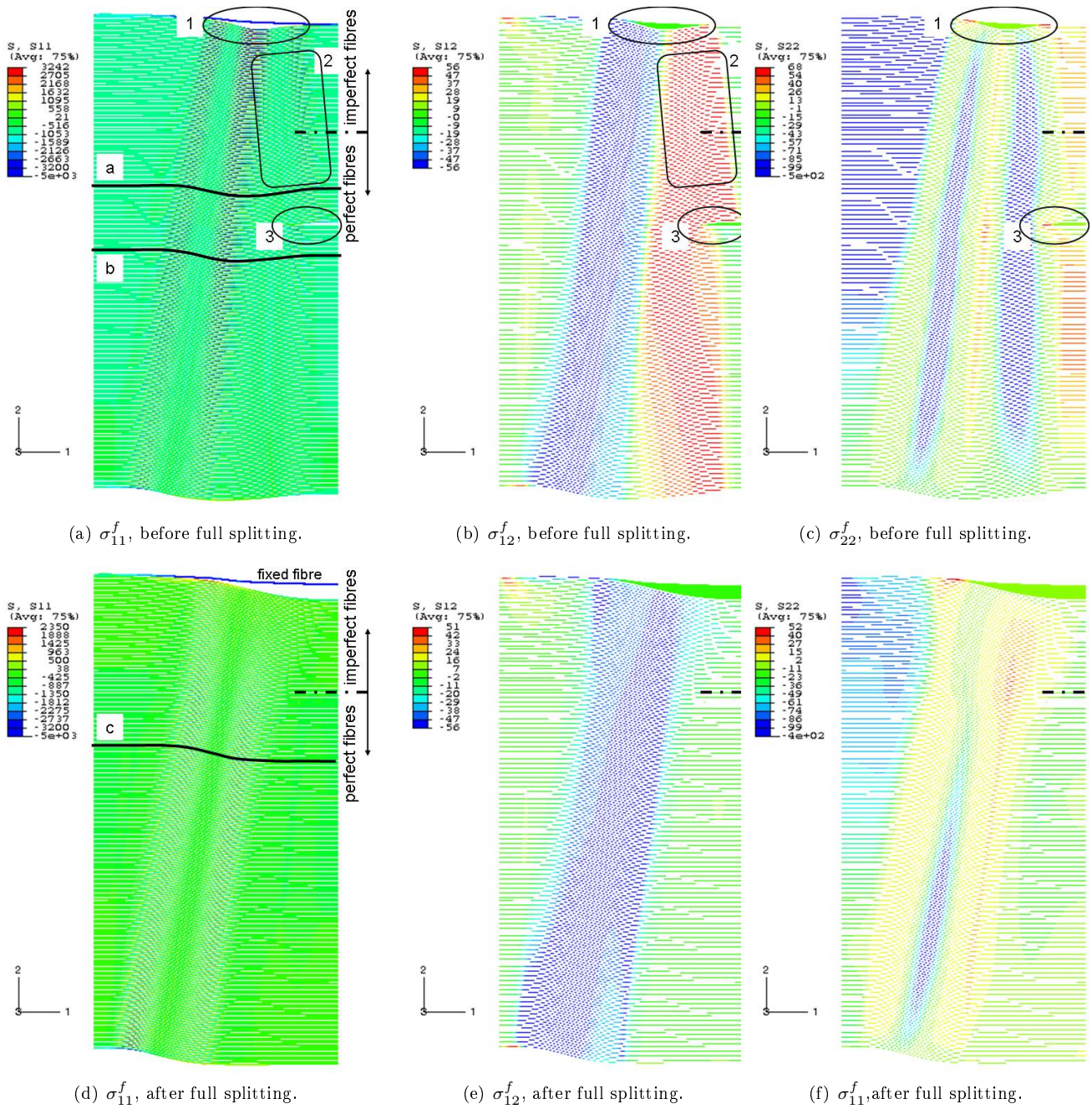


Figure 4.34: *Propagation* with transverse failure: splittings.



Key:

- | | |
|---|---------------------------------------|
| 1: first splitting - upper fibre (fixed after first failure); | a) V-shape between splittings; |
| 2: complementary yield band; | b) V-shape after second splitting; |
| 3: second splitting - between perfect fibres. | c) kinked shape after full splitting. |

Figure 4.35: *Propagation* with top fibre constrained.

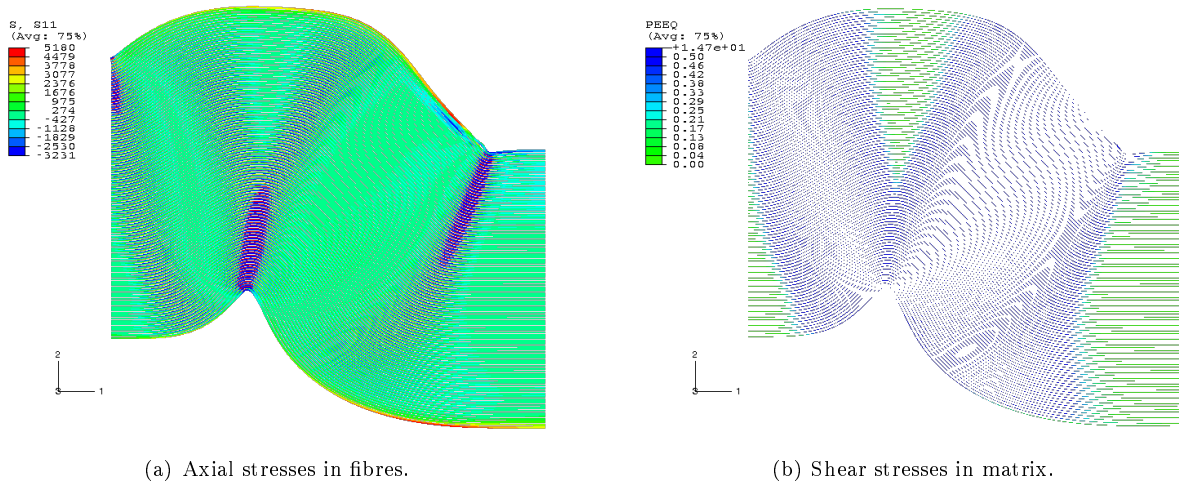


Figure 4.36: Complementary kink band in the *CDM_complementary* model.

Figure 4.37 shows the stages in the development of the complementary kink band. The first band was formed like in the other models, but a small curvature on the left side (near the clamped node) could be already noticed at that stage (a, b); right after this, the complementary band started developing (all across model's height), both in terms of matrix yielding and fibre overstressing (c, d). The two *yield bands* broadened then symmetrically until they met each other (e, f), and afterwards broadening continued unilaterally.

Looking onto shear stresses in the matrix (figure 4.38) when the first band (in blue) was initiated, two almost symmetric bands with high shear are also shown (in red). These bands were formed at the location where the initial misalignment ended, and the asymmetry between them is found near the clamped node.

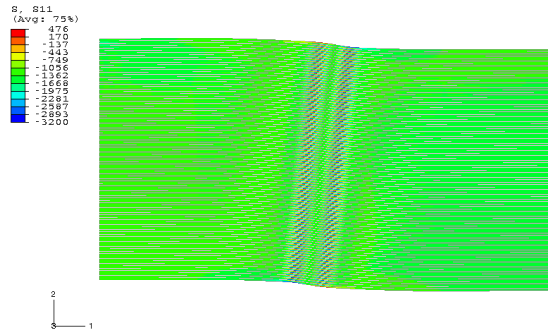
4.4 Discussion

4.4.1 Model representativeness

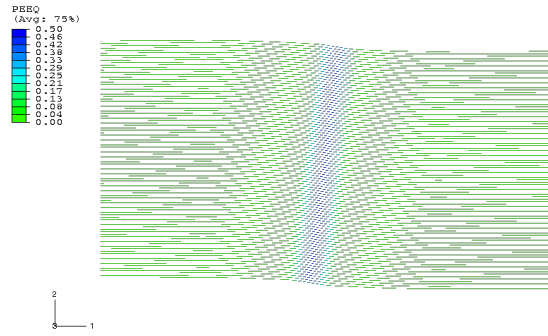
As it was discussed when the modelling strategy was presented, using numerical models to assess the mechanical behaviour of a complex material can result into non physical models; for this reason, the modelling features most likely to induce qualitative errors or inaccuracies in the models - use of numerical damping, shape of constitutive laws for matrix and fibres (especially for yielding / softening domains), initial imperfection - were applied in a controlled way.

Besides, the decision on what can be considered a numerical kink band depends on the idealisation of what a kink band actually is, which was a question with no clear answer a priori; nevertheless, all the models here discussed do present a kinked shape (fibres rotated in a sharper way than in a sinusoidal deflection), localized deformation in a band (with the models' boundaries almost in a stress-free state) inclined in relation to the transverse direction ($\beta \neq 0$), and a load history and stress / displacement fields in agreement with experimental results.

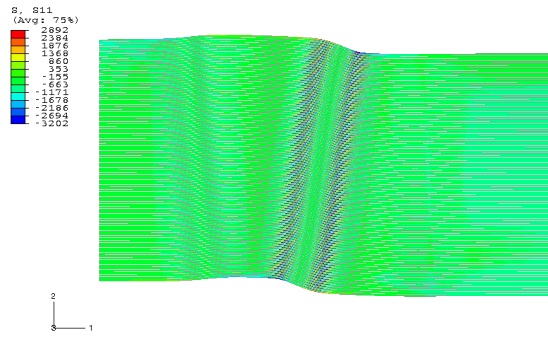
Finally, in addition to kink band initiation, other reported features - propagation, complementary bands, splittings - were actually reproduced in the numerical simulations; although this was sometimes achieved through non physical mechanisms, a correspondence between numerical and experimental results was always observed.



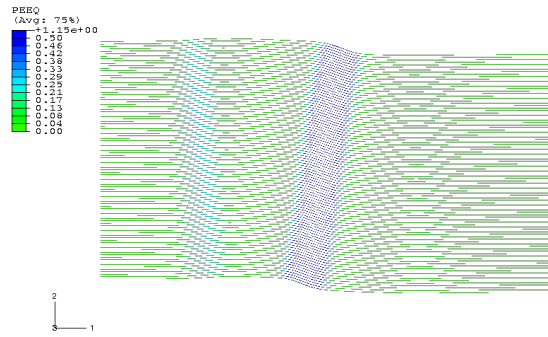
(a) Axial stresses in fibres, at first band formation.



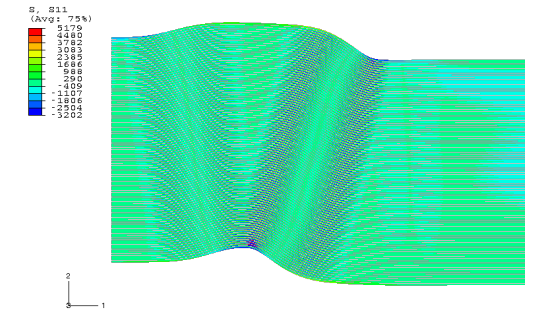
(b) Plastic deformation in matrix, at first band formation.



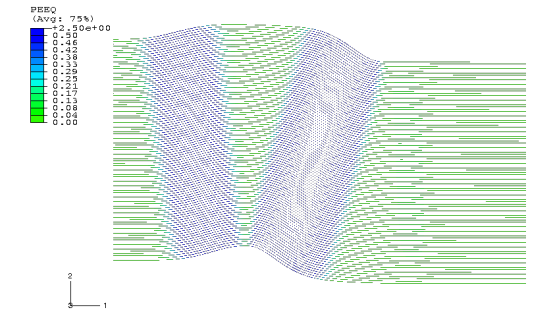
(c) Axial stresses in fibres, at complementary band formation.



(d) Plastic deformation in matrix, at complementary band formation.



(e) Axial stresses in fibres, with two bands developed.



(f) Plastic deformation in matrix, with two bands developed.

Figure 4.37: Formation of a complementary kink band (*CDM_complementary*).

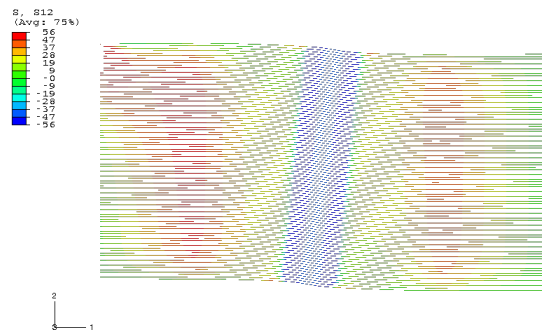


Figure 4.38: Shear stresses in the matrix (τ_{12}^f) in model with complementary kink band, after first band formation (*CDM_complementary*).

The current modelling strategy is not only capable of capturing the basic phenomena involved in kink band formation, but it is also representative of some of its detailed physics.

4.4.2 Load versus displacement curves for kink band initiation

The four $P(u)$ and $v(u)$ curves presented for the initiation models - *cohesive*, *matrix*, *CDM* and *CDM_extended* - evidence the same mechanical response; one can therefore conclude that the different features experimented - different matrix constitutive laws, different fibre response after failure, different types of geometry - do not represent critical features for kink band initiation. Kinking is then possible regardless initial matrix non-linearity, matrix softening for large strains, fibre failure and damage propagation.

In the *elastic* domain (before the peak load is reached), both matrix and fibres follow (almost) linear elastic constitutive laws; the effect of the initial imperfection in the compression is negligible, resulting into the almost linear behaviour found in $P(u)$ and in a small deflection $v(u)$. The peak load is reached when the matrix yields by shear, so the stresses cannot increase in the matrix within a band at the model's centre; this promotes a sudden change in the deformed shape, with a kinked area that corresponds approximately to the *yield band*, and consequently to an abrupt stiffness reduction and unstable deflection. Afterwards the material continues softening, as the *yield band* is extended towards model's boundaries.

The small differences found between the four models are easily justified. The different slope found for the extended model (*CDM_extended*) is due to its different geometry, as the shortening for first matrix yielding needs to be larger (the lateral extensions have to be compressed as well); no significant change is seen in the peak load, as the required stress for matrix yielding does remain the same. Continuing with the peak load, the higher value found for the model with a failing constitutive law for the matrix (*cohesive*) can be explained by the higher stabilization used (to help model's convergence in further steps), which is also a likely reason for the deflection v to be slightly smaller than in the other models, in the *softening* domain; when it comes to the evolution found for the load P , this model differs from the others by the lack of axial stiffness of the cohesive elements, resulting into slightly lower loads P for a similar compression u .

Just before the end of the analysis, both the models without fibre failure (*cohesive* and *matrix*) show a bizarre behaviour, with the load P increasing for further compression u . This phenomenon is justified by the boundary effect: as compression increases, the *yield band* is further extended towards the model's vertical edges, which cannot rotate due to the boundary conditions; for this reason, the response stiffens. The effect is delayed in the model with the same geometry but failing fibres (*CDM*), because as soon as first fibre failure takes place the fibres start softening and the *yield band's* expansion towards the boundaries is hindered. Finally, the model with extended geometry (*CDM_extended*) is almost not sensitive to the boundary effect, as the kink band is kept within a confined region far away from the transverse edges.

It is also worth to be noticed that, despite the different geometry with extended straight ends, the transverse displacement $v(L)$ in the *CDM_extended* model is not much larger than in the *CDM* one, in the *softening* domain; this suggests that the deflection, when a kink band is formed, is kept mainly within the length of the initial imperfection, with no significant effect in the straight extensions (which correspond to perfect segments of fibre).

4.4.3 Numerical features

Two numerical parameters were analysed: the use of stabilization and the number of fibres represented.

Stabilization is a numerical form of damping, so it delays and smooths sudden changes in the model by adding a residual viscous force (acting like an inertial force). Consequently, the model ran without any stabilization (*cohesive_0stab*) presents a lower peak load, being that effect spread to the early stage of the *softening* domain; away from the peak load, the two (with - *cohesive* - and without - *cohesive_0stab* - stabilization) responses are coincident. Looking now into the stress fields, one must notice at first that, although the same load ($P = 3.5\text{N/mm}$) is given for the two sets of plots (figures 4.16 b and 4.25 b), in the load versus displacement graphic (figure 4.24) the model with stabilization (*cohesive*) is more deflected; for that reason, slightly higher stresses are found in that model, but qualitatively the fields are exactly the same. The use of stabilization was always controlled by the ratio damping-to-strain energy (kept under 5%, except in the model *CDM_complementary*), so the models' response is not over affected.

The number of fibres included in the models can influence the results both by the overall model's stiffness and the extension of free-edges effect. Comparing the load versus deflection $P(v)$ curves from the models with 20 (*cohesive_20fibres*) and 100 (*cohesive*) fibres, the lower initial modulus in the model with less fibres suggests that, in this domain, the response is global, so the smaller number of fibres allows the model to deflect in a much easier way; in the *softening* domain, however, the deflection occurs fibre by fibre, so the effect of their number is vanished (this agrees with the σ_{11}^f stress fields in both the *elastic* and *softening* domains). In addition, having fewer fibres makes the yield circle (figure 4.26) to cross the *cohesive_0stab* model quicker; this, together with the lower stiffness in the *elastic* domain, lowers the peak load when compared to the models with 100 fibres.

4.4.4 Role of the matrix in kink band initiation

The results provided by the model for kink band initiation with failing interface (*cohesive*) evidence the important role played by the matrix in the initiation of fibre kinking.

It had already been pointed by some researchers (Chapter 2) that matrix yielding was a critical feature for kink band formation; considering the numerical simulations and also some experimental results, one can reasonably assume that matrix yielding is actually what defines the process of kink band formation.

Matrix acts as an interface between fibres; the dominant stresses in the matrix are the shear τ_{12}^m ones (figure 4.39), especially in early kinking stages; matrix's direct contribution to the axial stiffness is negligible due to its small Young's modulus (when compared to the fibre's modulus), and the transverse stresses have a zero-resultant force in the fibres and do not affect yielding significantly (for kink band initiation). The role of the matrix is therefore to provide support to the fibres by transferring shear stresses to their surface.

Matrix yielding in shear defines (apart from model's free-edges effect) the peak load and, for that reason, the composite's strength X_C ; in addition, first matrix yielding coincides with the development of the kinked deformed shape that is found in the *softening* domain and, consequently, with the change in the distribution of axial stresses in fibres. The formation of a *yield band* is the only feature that can justify the differences in the composite's mechanical response between the *elastic* - when no kinking occurs - and *softening* - when a kink band is formed - domains.

Considering all this, and recalling the experimental conclusion about fibre failure being a simple consequence of kinking, it can be stated that matrix yielding is actually the event that triggers kink band initiation, being the development of a *yield band* the most important feature in its formation.

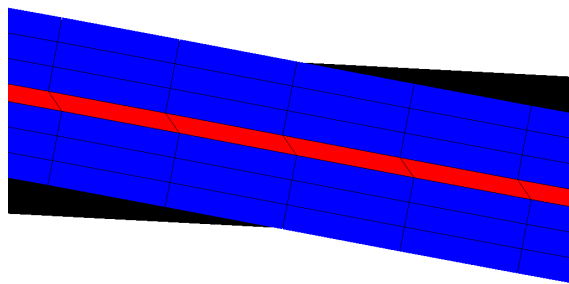


Figure 4.39: Detail of deformed shape (over initial shape) in *cohesive* model (*softening* domain): two fibres (blue) and one layer of matrix (red).

4.4.5 Shear stresses and deformation in the matrix

As it was just discussed, shear stresses govern matrix's response during kinking, so their evolution both in terms of load history and axial position is of the highest relevance.

Before the peak load and for the *cohesive* model, matrix's behaviour in shear is linear-elastic; the evolution of shear stresses in a layer of matrix (figure 4.15) suggests a cosinusoidal law. In the *softening* domain, shear in the matrix inside the *yield band* is approximately constant along the fibre (figure 4.17); although the last curve shows a significant decrease in the shear stress (due to element degradation), this is considered to be a free-edge effect (the *yield band* reaches model's transverse boundaries when degradation starts to be more relevant). The damage in the cohesive elements within the *yield band* is high, but the high value of shear toughness allows the stresses to remain almost constant; this behaviour was verified to be independent from numerical damping. At the same time, outside the *yield band* the matrix is still in the *elastic* domain; however, shear stresses do not follow a cosinusoidal law anymore.

Shear stresses are influenced at first by the matrix's constitutive law; in the simulations run, two laws - linear elastic - plastic with hardening - perfect plastic and linear elastic - linear softening - were used; qualitatively, the only difference is found at latter stages of formation, making it difficult to subtract boundary effects in the comparison. The model with failing interface (*cohesive*) shows, at the end of the simulation, the band's boundaries well defined, which leads to a similar curvature for all fibres (figure 4.40 a); the model with yielding interface (*matrix*), on the other hand, presents at the last increment a non uniform deformed shape across the transverse direction, with fibres' curvature increasing along the model (figure 4.40 b). Looking onto shear stresses in the matrix on both models, it is found that the two models start diverging when shear stresses in the *cohesive* model start decreasing (due to damage propagation); in the *matrix* model, shear stresses inside the *yield band* are constant. At the last increments, the *yield bands* are extended along the entire models; for this reason, the *matrix* model has constant shear stresses across both its axial and transverse directions, so a central band cannot be defined and deflection becomes global.

4.4.6 Role of fibres in kink band initiation

The previous discussion about the importance of the matrix in kinking leaves the fibres with a simpler role in the process, as their failure may not contribute actively to the composite's failure in this specific mode.

All the numerical models (and particularly the *cohesive* one, analysed in detail) show that the major stress component in the fibres during kink band formation is the axial one, which agrees with the common response of

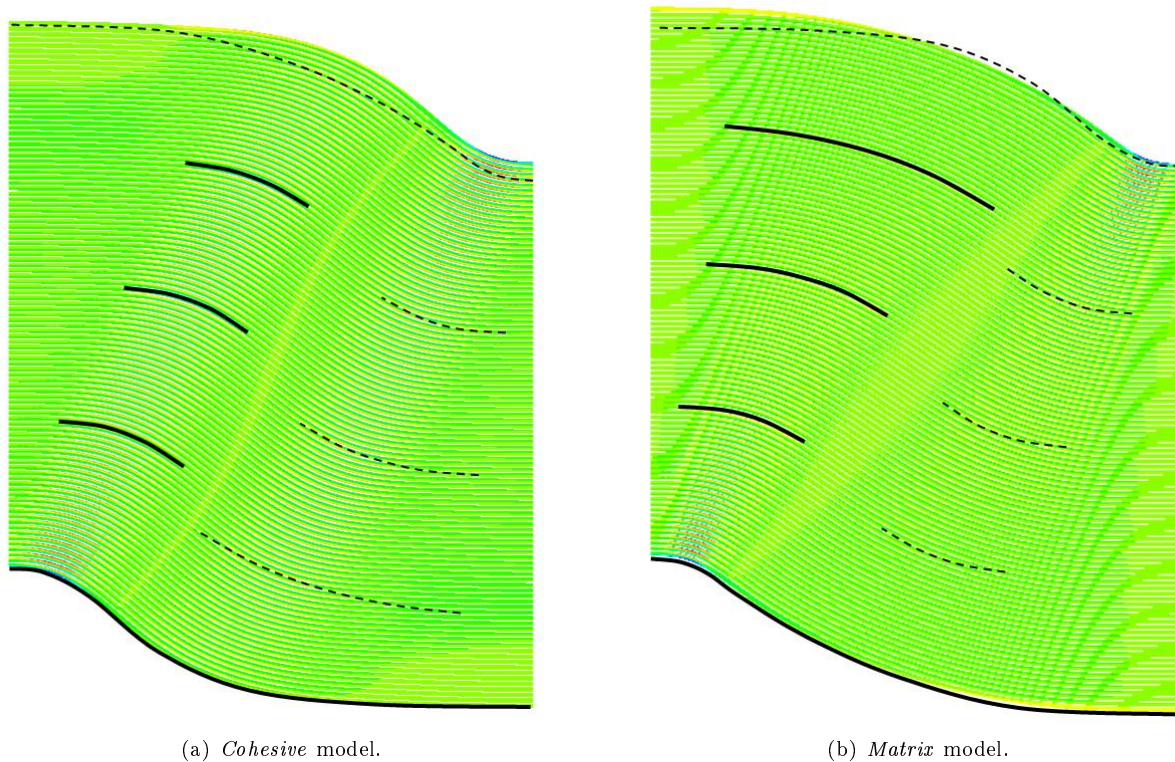


Figure 4.40: Comparison between final deflection in *cohesive* and *matrix* models (other model's deflection in dashed line).

a FRP. The σ_{11}^f fields, during both the *elastic* and *softening* domains, suggest loading due to compression and bending, as there is an almost constant component along the fibre's cross section (compression) superimposed with a symmetrical one (bending), having the latter the maxima located at the areas of highest curvature.

At the beginning of analysis (figure 4.10), the constant component (along the fibre's length) of the axial stresses is considerable, so the response is dominated by compression; as the matrix yields, that component is still the most important one, but bending starts being perceived at the central region. After full formation of a *yield band* (figure 4.12), the overall compressive strain in the model (due to compression) is progressively reduced, followed by a significant increase in the bending component; this suggests that, in this domain, the shortening is caused mainly by fibre deflection and less by pure compression, which agrees with the experimental conclusions suggested by the type of fibre failure seen in some micrographs (Chapter 3).

As the compression continues, bending moments increase and the fibre's axial strength (in compression, in the present case) is reached; fibre failure starts at this point. The material's behaviour after this event was not fully tracked, and a discussion is given in section 4.4.7; nevertheless, it can be suggested that kink band's final width (w) and angle (β) are roughly defined at first fibre failure, without the influence of free-edge effects.

4.4.7 Response after first fibre failure

The *CDM_extended* model provides information on fibre behaviour after first failure (of the fibres at the edges). Figure 4.28 a shows that the kink band's geometry cannot be defined by first fibre failure in the model, as in the last step the band is considerably wider and more inclined; this is confirmed by figure 4.28 b, in which one can see that damage occurs first nearer fibre's centre, moving then outwards along the axis of the fibres at the

horizontal edges (feature 2). However, it is also suggested by the same image that that is a free-edge effect, as after crossing the outer fibres the damage starts propagating transversely within a band (feature 1); looking back onto figure 4.28 a, it is confirmed that the band's width and inclination stabilizes after central fibre first failure, which agrees with the previous hypothesis.

Figure 4.29 can be used to assess the relevance of modelling damage propagation during fibre failure. The two shorter models (*CDM* and *matrix*) diverge from the extended one (*CDM_extended*) for latter stages in compression, but that effect is mainly due to the transverse boundaries: in subfigure c, one can see that the two *maximum bending bands* are reaching the free transverse edges of the shorter models, and in subfigure d they are significantly over them, even for the central fibres. Also in subfigure c, the model without CDM (*matrix*) shows a different curvature at the horizontal boundaries; although the overall deflection (v) is very similar to the deflection in the models with the CDM implemented, the central fibre does not present a similar shape in the three models, as it never reaches fibre's compressive strength in the *matrix* model.

Fibre failure plays a role in the definition of kink band's geometry; however, for the analysed models it is not clear how to distinguish between the effects of model's boundaries and damage propagation, so this issue is still open to discussion.

4.4.8 Transverse stresses in the matrix

As it was mentioned, damage propagation and final failure in the matrix are not modelled accurately (both due to the linear shape of the softening law and the values of toughness); for this reason, once under in-plane shear or transverse tension, it is possible that the matrix in the real composite presents a faster or slower degradation, so splittings can actually appear after or before they are predicted in the numerical models. Unfortunately, having a splitting open under transverse tension is not qualitatively similar from having a partially damaged matrix, as the former will not be able to transfer shear stresses and the latter will; taking this into account, it is important to know if the models predict transverse tension or transverse compression between the fibres inside the kink band, as completely different behaviours (in terms of shear stresses transferred to the fibres) will occur in each case.

Looking onto σ_{22}^m in the *cohesive* model for kink band initiation in misaligned fibres (figure 4.22), a central band under considerable transverse compression is found; there, and even if full splittings develop in shear, the matrix will always be able to support the fibres, as any crack will be closed and shear stresses can be transferred as friction. When the kink band is at a latter stage of formation, however, in its boundaries the stress state is a tensile one, so if the matrix fails completely then no stresses can be transmitted and the fibres will be totally unsupported in those regions.

When it comes to kink band formation in initially perfect fibres (*propagation* model and its variations), a different behaviour is found: during propagation, the model is under transverse compression in one side, and under transverse tension in the other, being that behaviour noticed inside the kink band as well (figure 4.33); these global transverse stresses are discussed in section 4.4.12. After full propagation across all fibres in the model, the transverse stress state changes to a similar one as found in the models for initiation: a band under compression forms inside the kink band, and two bands under tension at its boundaries (figures 4.33 c and d, 4.34 c and f, 4.35 c), both for the areas with initially misaligned and perfect fibres. This reveals that, once the kink band is fully formed and the effects of propagation are reduced, the fibres are compressed transversely in kink band's centre and tensioned at its edges; therefore, stresses from matrix to fibre are effectively transferred inside the band, but at its boundaries cracks can be open so continuity is not guaranteed.

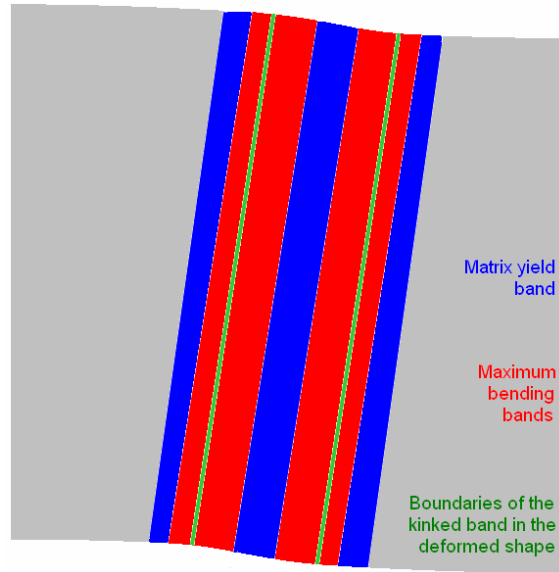


Figure 4.41: Bands formed during kinking (*softening* domain, $P = 3.5\text{N/mm}$).

Notwithstanding this conclusion, it should be noticed that fibre failure is not modelled in the simulations with failing interface (*cohesive* and propagation models); it is then possible that, when fibres start breaking, the deformed shape changes in a way that promotes transverse tensile stresses, with the already discussed implications.

4.4.9 Bands formed in kinking

During fibre kinking, three different bands - each one taking into account a stress or displacement field - are developed (figure 4.41).

The first and wider one is the *yield band*, defined by matrix yielding in shear (τ_{12}^m); it is the only band in which the material's constitutive law changes from the *elastic* domain to the *softening* one, so it is suggested that this is the primary band in fibre kinking, being all the others its consequences.

The second band is actually defined by two parallel bands itself, where the axial stresses in the fibres (σ_{11}^f) are maxima (*maximum bending bands*); outside these band the fibres are almost straight, so bending is reduced and axial stresses are almost uniform (and mainly due to the pure compression component).

In the *yield band*'s centre is the band defined in terms of deflection (v), with the fibres actually rotated from their initial configuration; the location of the maximum bending bands suggests that they were formed because of this band.

Summarizing, the dominant band formed in fibre kinking is the matrix *yield band*, leading to the formation of a secondary band with fibres strongly kinked inside it; the centre of maximum bending bands (if fibre failure occurs) will dictate the kink band's final width.

4.4.10 Sequence of events for kink band initiation

Considering the results already presented from the model with failing interface (*cohesive*), it is possible to define the sequence of events leading to kink band formation.

At first, the composite deforms in a nearly linear mode, merely magnifying its initial imperfection, with both constituents - fibres and matrix - following linear (in this case) constitutive laws; the fibres are mostly under compression (superimposed with a very low bending component) and the matrix responds mainly in shear and approximately in-phase.

As the material is compressed further more, the shear stresses in the matrix continue to increase, until the matrix shear strength is reached and the material starts yielding. A *yield band* is then defined across the fibres, and the peak load is reached when it crosses completely the material in the transverse direction. The composite's strength under axial compression is reached and failure is imminent under load control.

After matrix yields and the peak load is reached, the *yield band* broadens along the axial direction; as it happens, the fibres start deforming in a kinked shape instead of a sinusoidal one; the axial stress field changes consequently, with a response that is due to pure compression only in a small amount and has the major component due to bending, both with tensile and compressive stresses.

As the compression continues, the *yield band* enlarges and so does the kinked area; fibre rotation increases inside it, and near the band's boundaries the fibres bend more and more. The bending stresses increase to a level that cannot be supported, and fibres finally start breaking under compression where stress concentrations exist (at free-edges).

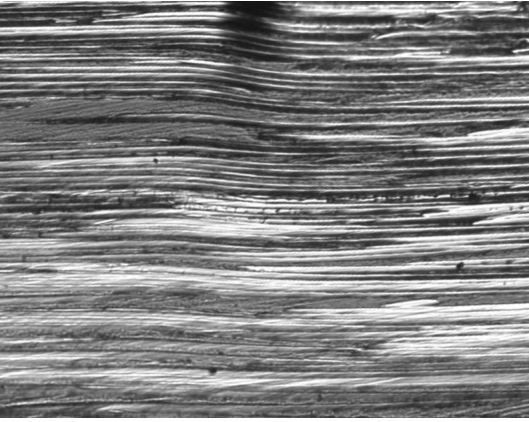
After this point, the model with failing fibres (*CDM_extended*) has to be used; the behaviour after first fibre failure is not as well studied as the previous stages, but some hypothesis can be raised. The boundary fibres are slowly damaged but the *yield band* widens quickly, changing continuously their deformed shape; due to this and for the values of fibre toughness used, damage propagates diagonally (towards model's centre along the transverse direction and towards model's boundaries along the longitudinal direction), so the fibres at boundaries are partially damaged in a large pathway. As compression continues, the inner fibres starts being damaged too, in areas free of edge-effects; from this moment on, damage propagation occurs transversely, and the kink band's width w and angle β are defined.

As fibre curvature increases, the tensile strength is reached as well; damage propagates across the composite both in compression and tension, along the path previously defined by β and w ; the fibres continue to rotate (α increases), until the point when final failure occurs in all of them.

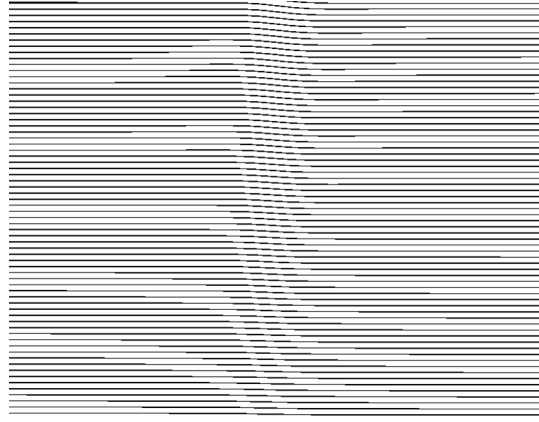
4.4.11 Kink band propagation

Kink bands were propagated through fibres with no initial imperfection in models *propagation*, *propagation_failure* and *propagation_constrained*. It is shown that the already discussed mechanisms found for kink band initiation - formation of a *yield band* with bounded shear stresses and consequent reduction on support provided to the fibres, followed by fibre bending and further failure - participate in propagation as well. These mechanisms are put in evidence in figure 4.32, where it is unquestionable that matrix yielding in shear occurs for very small deflection and, therefore, much before fibre failure.

Kinking starts at the misaligned fibres (figure 4.31); their deflection induces (through matrix deformation) the initially perfect fibres to rotate as well, and the band's angle (β) is reduced significantly as the band moves into the straight area (figure 4.30 b). If no matrix transverse final failure occurs, the band continues to propagate across the composite - first in terms of matrix yielding and then in fibre failure -, until it reaches the last fibre in the model; at this moment, the band is very narrow and still presents a change in its orientation where the



(a) Experimental result (specimen r-UD_2d2, loaded).



(b) Numerical result (*propagation*).

Figure 4.42: Kink band propagation: comparison between experimental and numerical results (same scale).

imperfection ends. However, after full propagation across all the fibres, the band starts widening, and it quickly becomes into a single oriented wider band, with no geometric difference between the imperfect and perfect areas. Comparing these results with the sequence commonly described in the literature for fibre kinking (Chapter 2), the agreement is notorious: the band *initiates* at an imperfection (or near stress concentrations), it *propagates* transversely across all the fibres until it reaches a free edge, and then it *broadens* axially.

When the band broadens to its final configuration, it does so asymmetrically (in figure 4.31 from i to k, the band broadens towards right near the top and towards left at the bottom); this behaviour (uneven broadening) was actually noticed in the experiments (Chapter 3), although it is not known if it had occurred there for the same reason.

Between the already kinked fibres and the aligned ones, the material is tensioned in the transverse direction in one side and compressed in the other; for this reason, splittings open in the tensile side and can be followed by fibre deflection in a V-shape (figures 4.34 and 4.35); this behaviour is further analysed in section 4.4.12.

Figure 4.42 shows a kink band propagating both in a real micrograph (specimen r-UD_2d2, loaded configuration) and in a numerical model (*propagation*), using the same scale; the similarity between them is notable. The propagation length is very difficult to define accurately both numerically (as the fibres cannot fail completely) and experimentally (as the deflection is progressively reduced), but with the methods used the agreement is very good as well ($L_{prop}^{r-UD-2d2} \approx 600\mu\text{m}$, $L_{prop}^{r-UD-aux} \approx 550\mu\text{m}$, $L_{prop}^{r-UD-2d2} \approx 550\mu\text{m}$).

4.4.12 Splittings in kink band formation and propagation

Splittings were found both in models for kink band formation and propagation when a failing matrix was used.

The standard model for kink band formation (*cohesive*) does not present matrix failure for the steps in which it is representative (i.e. controlled boundary effects and before central fibre first failure); nevertheless, after kinking begins, the matrix soon starts developing tensile transverse stresses at band's boundaries (figure 4.22). As it was already discussed in section 4.4.8, failure is not accurately represented in the numerical models, so the fact that failure is not seen may not be representative.

In the experimental results (Chapter 3), splitting was also analysed; despite being inconclusive (when loaded),

some micrographs did suggest open splittings at band's boundaries. This supports qualitatively the numerical results, as the transverse tensile stress states are found precisely at that location. Besides, the last increments in the *cohesive* model show a central group of fibres splitting; this results is not fully representative (as it is mainly due to the finite model's length), but it is interesting that matrix failure had occurred at the right place and not in the first layers of matrix.

Models for propagation with failing matrix in the transverse direction - *propagation_failure* and *propagation_constrained* - do present splitting as well. As it was also discussed for the experimental results (Chapter 3), kink band propagation promotes transverse tension in the material on one side of the kink band and compression on the other, which is confirmed in all models for propagation (figure 4.33); splittings are then naturally open in the tensile side, if matrix failure is allowed (figure 4.34).

In addition, in these numerical models splitting is always followed by the formation of a V-shape (figures 4.34 and 4.35); this might be similar to the formation of the second band in the specimen CC_6d (Chapter 3), which would then support the hypothesis of V-shaped deformed configuration there discussed. Besides, splittings were formed in groups with different numbers of fibres, which agrees with the experimental results as well.

Finally, no splittings were found at the kink band's centre.

4.4.13 Formation of a complementary kink band

The complementary kink band was created in a model with no rigid body movement allowed and high damping applied; although not being physically representative, these features constrain the movement of the model along the transverse direction, in similar way as when a confining pressure is applied experimentally; at this situation, the composite cannot move freely to accommodate the rotation of the fibres within the band, so a complementary band with the fibres rotated in the opposite direction is formed.

The damping energy was not monitored in this model; the stabilization factor was considerably higher than in the corresponding *CDM_extended* model, which suggests that model's response is likely to be overaffected by numerical damping; nevertheless, the effect of this non-physical feature has a physical meaning, so it is considered that the model here presented is representative of complementary kink band formation.

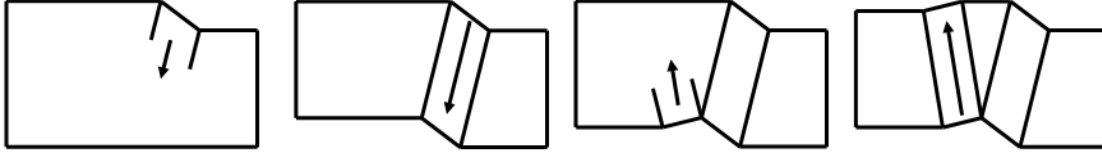
Real complementary kink bands usually form as shown in 4.43 a; in the numerical models, the formation of a single kink band starts (in terms of matrix yielding) from the centre of the model (subfigure b), and so does the complementary one.

The formation of the complementary kink band follows the same process as the single one: shear stresses in the matrix increase within a band (figure 4.38), yielding occurs (figure 4.37 d) and is followed by fibre rotation inside the *yield band*; fibres become highly curved at band's boundaries (figure 4.37 c), and eventually start failing first under compression at the horizontal boundaries (triggered by free-edge effect), and then damage propagates fibre by fibre, both in compression and tension.

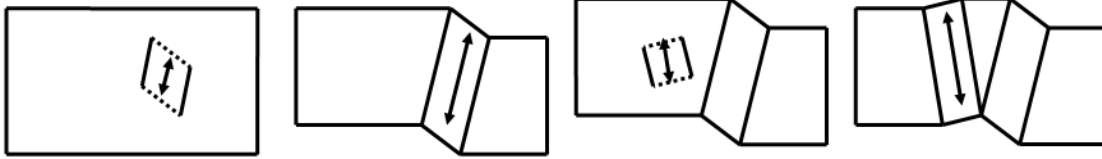
4.5 Conclusions

Load domains in kink band formation

Two load domains - *elastic* and *softening* - are found in the global load versus displacement curves for composites under axial compression.



(a) Experimental complementary kink band.



(b) Numerical complementary kink band.

Figure 4.43: Formation of a complementary kink band.

In the *elastic* domain, the load response $P(v)$ is stiff, nearly linear and fibre deflection is small. In the *softening* domain, the material softens and the load is reduced for further compression, with a tendency to stabilize for large deformations; the deflection v follows the same tendency, but it stabilizes in a slower way than the load P .

Between the two domains, an instability occurs due to a change in the deformed shape of each fibre; the compressive load drops abruptly and the deflection increases suddenly as well, with the overall strain energy being reduced instantaneously too. Matrix yielding is the event setting these two domains apart.

Fields in the *elastic* and *softening* domains

The three most important fields during fibre kinking are the shear stresses in the matrix τ_{12}^m , axial stresses in the fibres σ_{11}^f and transverse displacement / deflection v ; their configuration changes considerably when moving from the *elastic* to the *softening* domain.

In the *elastic* domain, those three fields follow, for each fibre, an evolution that is sinusoidal (or its derivative), with a law that fits the entire fibre length.

In the *softening* domain, however, a central band - *yield band* - is defined for each field, with well distinguished evolutions inside and outside it. Inside the *yield band*, shear stresses in matrix are bounded by matrix shear strength, axial stresses in fibres increase quickly to a maximum value, and the deflection assumes a kinked shape; outside the bands, however, both fibres and matrix are less stressed than when in the *elastic* domain.

Mechanical response of the constituents

During kink band formation, fibres respond in compression (compressive load P) and bending (due to the offset between the two fibre's boundaries v).

Matrix acts as an interface between fibres, being its deformed shape imposed by fibre rotation due to bending; matrix's behaviour is governed by shear, which has a non-zero resultant force acting at its interface with the fibres. Along each fibre's length, the shear stresses transferred by the matrix $\tau_{12}^m(x)$ induce an in-plane torque

in the opposite direction to the bending moment $P \cdot v$; as continuity is guaranteed by a compressive transverse state stress, the matrix does support the fibres by shear.

Sequence of events for kink band formation

The formation of a kink band under axial compression starts with an *elastic* phase, in which all the components respond elastically and in a global way. The initial fibre misalignment promotes bending moments, which result into further deflection and therefore increase bending moments in a positive feedback process.

Fibres' deflection shears significantly the matrix between them, so considerable shear stresses are developed in the matrix. A peak load is reached when matrix shear yielding occurs; at this point, the support in shear given by the matrix to the fibres cannot increase furthermore, so fibres suddenly kink and the load drops abruptly; an incipient kink band (defined in terms of matrix yielding) is formed.

As compression proceeds, the material continues to soften but now in a stabler fashion; the *yield band* widens and fibre rotation inside it increases. Bending is controlled fibre by fibre now, and the maxima axial stresses are found inside the *yield band* (near its boundaries); outside it, the fibres do straight and relax as compression increases.

For further compression, fibre bending increases near the *yield band*'s boundaries, and eventually failure begins under compression in a fibre with stress concentrations (as at a free-edge); failure propagates fibre by fibre in the composite, and reaches an area free of stress concentration effects. At this point, the bands stop broadening (β and w stabilize) but fibre rotation (α) continues to increase; failure in fibres continues to propagate, until they break one by one.

Relevant features in kink band initiation and propagation

The most important feature for the development of a kink band is matrix yielding in shear, as it is the event that defines kink band formation in terms of the constitutive laws, deflected shape and formation of maximum bending bands.

Apart from matrix response in shear with bounded stresses and fibre's axial stiffness, no other feature plays a crucial role in fibre kinking. Specifically, fibre orthotropy, matrix plastic hardening for small strains and matrix softening are not relevant; in addition, fibre breakage is effectively not required for kink band formation, although fibre failure (if actually taking place) does affect kink band's final geometry.

Transverse stresses and splittings

The transverse stresses in the matrix σ_{22}^m during kink band formation were found to be compressive inside the kink band and tensile at its boundaries at latter stages of compression; only the effect of kink band propagation lead to the development of considerable tensile stresses and representative splittings (outside the band) in the numerical models.

As transverse stresses inside the band are compressive, one can conclude that shear stresses are effectively transferred, no matter the real toughness values; at the band's boundaries, this is true only if matrix toughness in mode I is considerable high (of the same order as it usually is), as otherwise cracks are likely to open.

Kink band as final deformed shape

A kink band proved to be the most favourable final deformed shape for a composite under axial compression; some models (for propagation) show intermediate buckled (or V) shapes of some fibres, but once the material is further compressed the fibres deform in such a way that a kink band is found at the end.

Kink band propagation

Kink band propagation through perfect fibres was modelled as well, both allowing and preventing splittings in the transverse direction.

The incipient kink band starts forming in a misaligned area, following the same sequence of events as previously defined; as compression proceeds, it propagates across model's transverse direction until it reaches the fibres with no initial imperfection.

Propagation in initially perfect fibres is triggered by the deflection of the fibres above band's tip, both by transverse compression in one side and transverse tension in the other; due to this transverse tensile stress state, cracks can open during propagation. Apart from this detail, propagation in perfect fibres occurs by similar mechanisms to the ones seen for initiation, with a *yield band* propagating and leading to the formation of a kinked shape and, afterwards, to fibre failure in the two *maximum bending bands*.

During propagation, the tip of the *yield band* is ahead of failing fibres: in initially straight fibres and during propagation, matrix yielding precedes fibre further deflection and failure as well.

Role of the initial imperfection

An initial imperfection was found necessary to initiate a kink band, but propagation is possible without it; imperfections are required to trigger fibre kinking, but once initiated the process is self-sustaining.

It was also found that, when a partially imperfect fibre (so with straight extensions) is considered, no significant differences are seen in its response to kinking.

Complementary kink bands

The simulation of a complementary kink band was also achieved by constraining the model in the transverse direction. The formation of a complementary kink band follows the same principles - matrix yielding, fibre kinking and fibre failure - as a single one, and reduces considerably the gap between fibre's ends.

Representativeness

The strategy developed to model composites under fibre kinking proved to be efficient and representative of reality. Besides kink band initiation, propagation, broadening, formation of complementary bands and splittings were also reproduced in the numerical models, and similarities to experimental results were always found.

Chapter 5

Analytical model

The development of a physically based analytical model on kink band formation, tracking and explaining the micromechanics of the process and capable of predicting the composite's axial compressive strength and the kink band's geometry, was the main goal of the work presented in this report.

5.1 Strategy

5.1.1 Inputs from experimental and numerical work

The experiments (Chapter 3) and numerical simulations (Chapter 4) already discussed had the aim to provide guidelines for an analytical model. For this reason, before developing the model into deep detail, it is convenient to summarize all the inputs potentially useful to formulate hypotheses and outline theories.

Both experimental and numerical results show two distinct domains in the overall behaviour of the composite while in compression: at the beginning, the response is stiff and close to linear (*elastic domain*), until a peak load is reached; at that point, the composite softens suddenly and a kink band starts to be formed (*softening domain*).

From the stress fields obtained from numerical simulations, it was concluded that the relevant stresses on the fibres during kinking are the axial ones (σ_{11}^f), due to bending and compression; transverse and shear stresses within the fibres are not relevant. On the other hand, the matrix undergoes mainly shear (τ_{12}^m) as the fibres deform, being its contribution to the composite's axial stiffness negligible. When it comes to constitutive laws and material anisotropy, it was found that both constituents can be considered linear elastic - perfect plastic and isotropic.

The role of shear stresses and matrix yielding was enforced experimentally, as very similar specimens failed either by kinking or by splitting, which confirms that similar stress states are found in both. In addition, in the numerical models it was found that, around the peak load, the matrix yields within a band - *yield band* - that progressively extends along the axial direction; inside this *yield band*, the shear stresses in the matrix are kept approximately constant at matrix's shear strength, even for large deformations and for a failing interface.

The existence of fibre imperfections was confirmed in experiments, as well as the sinusoidal shape as its reasonable approximation. Besides, from micrographs of loaded material, it was concluded that kink band formation

begins with the fibres deforming in a sine-like shape near the kinking zone, but remaining nearly straight after a relatively short distance (transversely). The deformation of the fibres was also tracked numerically and considering both perfect and imperfect initial geometries; it was found that, during the *elastic domain*, the fibres deform approximately in-phase by amplifying the sine-shaped waviness. However, at the peak load, that shape suddenly changes to a different one, with the points of maximum bending moving into the incipient kink band; a clear angle $\beta \neq 0$ is defined by the *yield band*'s boundaries and by the *maximum bending bands* in fibres, being the *yield band*'s boundaries and the *maximum bending bands* close. Outside that band, the deformation seems to be kept in-phase.

Experimental and numerical results also give a consistent sequence of events leading to fibre kinking: at first, a misaligned shape is developed in the material, inducing in-plane shear stresses that magnify the misalignment in a positive feedback process; then, the bounded matrix strength is responsible for localization and fibres are progressively bent, until final failure.

5.1.2 Model outline

Although a quantitative validation (against experimental data) of the numerical results was not performed, the overall behaviour of the FE models captured accurately the physics and micromechanics of kink band formation. For this reason, and notwithstanding the fact that numerical models are approximations of reality, the model hereafter described aims to be an analytical version of the FE models for kink band formation that were previously discussed (Chapter 4).

In global terms, the model considers the formation of a kink band as a process developed in two time domains:

1. *Elastic domain*: at the beginning, both constituents follow linear elastic material laws; the deformation of fibres is perfectly in-phase and dominates the solution, defining the deformation (in shear) that the matrix - perfectly bonded to the fibres - undergoes. This stage ends when the shear stresses in the matrix equal its shear strength, being the peak load defined at this moment too;
2. *Softening domain*: after the peak load is reached, a central area (incipient kink band or *yield band*) where the matrix yields and the shear stresses are bounded coexists with two lateral areas (*elastic regions*) where the deformation develops under the laws verified in the *elastic domain*. As the compression progresses, the *yield band* grows axially, followed by an increase on fibre bending that leads to failure.

Due to the major differences on their elastic and strength properties, the two constituents have different responses to the compression: fibre's behaviour is dominated by bending, while the matrix deforms mainly in shear. It is considered that, although the matrix's shear strength is reached, there is no final failure of the interface, being therefore the fibres always supported by the matrix.

An initial (unloaded) geometric imperfection is considered in the model, in order to avoid failure by pure buckling. Finally, the model predicts the kink band's geometry based on the fibre's deformed configuration when first fibre failure occurs as a result of the bending moments and compressive load applied.

5.1.3 Assumptions and applicability

The main and non-trivial hypotheses and the applicability of this analytical model are now discussed.

Fibres deform in bending and compression, matrix deforms in shear with limited strength.

According to this, the analytical model can be used not only with composites, but it is applicable to every pair of *material + interface*, given that the *interface* (matrix in FRPs) is thin and much softer than the *material* (fibres in FRPs).

With the required modifications, the model can also be applied for layered materials with frictional interface; a typical application would be the formation of a kink band in rocks. Rocks have usually a layered structure and are under multidirectional compression; between layers, and due to the transverse compression, there is a frictional stress τ_μ that is bounded by the frictional coefficient μ and the confining pressure p , as $\tau_\mu^{max} \leq \mu \cdot p$. Considering this, the frictional interface between layered rocks and the matrix in composites have similar mechanical behaviours (although the physics are different), so it is possible to adjust this analytical model to represent properly that case too.

Fibres are fully supported in shear by the matrix.

The model considers that, during all the stages of kink band formation, the matrix is able to transfer shear stresses to the fibre's surface, being its value limited by matrix's shear strength; actually, the entire process of kink band formation is governed by the action of these shear stresses.

For this to be possible, the continuity between fibres and matrix has to be ensured, which can happen by three ways. One option is that, after yielding, the matrix behaves as a perfect plastic material, without softening mechanisms to degrade its response; in this case, continuity is ensured by the constitutive law itself. Another possibility is that, after failure initiation, a change in the deformed shape occurs and stresses are redistributed in such a way that strains in the matrix are nearly constant; the continuity is now guaranteed by the global mechanical response. Finally, if degradation is considered and final failure of the matrix occurs, shear stresses can still be transmitted as friction to the fibres if the cracks are closed by a compressive state.

Considering that the matrix undergoes significant deformation before the kink band is completely formed, the first hypothesis is not likely to happen: in fact, and even if it is sensible to approximate its shear behaviour for large deformations by a perfect plastic law, the fracture toughness for matrix tension is relatively low, so in the presence of completely yielded material cracks would open even for small tensile stresses. However, in Chapter 4 it was proved that, for a large range of deformation, if an imperfection is considered then the second option is found to happen. In another hypothetical situation where *interface* failing actually occurs, if the material is sufficiently constrained in the transverse direction (e.g. when hydrostatic pressure is applied) then the contact between previously formed cracks is ensured, so friction exists (third possibility). These are common situations, so this hypothesis is acceptable for a wide range of applications.

The rotation of the fibres is small.

Considering small rotations avoids the use of high order relations between trigonometric functions and the rotation angle itself, simplifying the problem considerably. However, such approximations are valid for angles up to 20° ; as fibre angles in kink band are reported to reach $\alpha = 40^\circ$ in the literature (Chapter 2), this hypothesis has to be reviewed for those cases when such high values appear in the solution.

An equivalent and systematic 2D model of the real 3D composite is meaningful.

The real composite is a tridimensional structure in which fibres and matrix are arranged in a non-systematic pattern; besides that, fibres are not perfectly straight (or sine-shaped) neither have a perfectly circular section.

However, modelling the mechanical behaviour of a structure cannot take into account physical randomness unless statistical parameters are included; as that is far beyond the scope of this project, assuming a 3D regular pattern for the fibres within the composite is mandatory. Among the possibilities, the hexagonal arrangement provides the best distribution of matrix between fibres, being for this reason the assumption for the model; having this 3D pattern defined, a 2D approximation considering one of its principal planes is reasonable.

Moreover, there is experimental evidence that the formation of a kink band is a tridimensional phenomenon (affected by a 3D stress state); for this reason, the applicability of a fully 2D model (considering in-plane initial imperfection, in-plane loading and in-plane displacement) is not guaranteed a priori. Nevertheless, a 2D model must be seen as an approximate formulation of the micromechanics governing kink band formation, as if it captures correctly the physics of the process then a 3D extension is attainable.

The fibre has an unloaded initial imperfection with the anti-symmetric shape of half a sine wave.

This hypothesis is partially supported by experimental evidence: kink band initiation is found to be linked to fibre waviness, either by the nearness to stress concentrations (as notches and splittings) or by imperfections developed during lay-up or curing. However, the assumption of a totally stress-free imperfection is not completely true, being that state more likely to be found when the fibres are straight; nevertheless, during the curing the matrix releases much of the stresses added during manufacturing, so the fibres would be allowed to recover to an “almost” stress-free imperfect configuration.

Above all the possible justifications, the assumption of an initial imperfection is mandatory (unless a pure buckling failure is considered) and was used by several other researchers, so if the imperfection is kept within small limits it should be seen as a reasonable hypothesis.

In addition, the model considers the bending theory for thin and straight fibres; despite being trivial not to consider shear stresses on fibre’s cross section, the fibres do have an initial curvature, so the accuracy of the results provided by this model decreases for large imperfection amplitudes.

The fibre, outside the imperfect length, is always straight and aligned with the loading direction.

This assumption is required to define simple boundary conditions for the model, but is not supported by experimental evidence: in micrographs of kink bands under development (Chapter 2), the fibres are rotated or even bent within a considerable distance (axial direction) from the actual kink band.

In this topic, every assumption will be an approximation, so the best compromise between accuracy and simplicity should be aimed; one can consider that the imperfection is long enough to accommodate the length of fibre that is affected by the formation of the kink band. As each fibre is highly constrained by the surrounded composite and the failure process requires localization, then it is reasonable to assume that kink band formation is confined to an area not one order of magnitude larger than the actual kink band width ($200\mu\text{m}$), which is within the common values for imperfection length (2mm).

5.2 Development of the model

This model considers one portion (with length L along the longitudinal global axis) of a single fibre, embedded in a composite with a fibre volume fraction V_f . The fibre’s diameter is ϕ_f (area A_f , second order moment of inertia I_f), its Young’s modulus is E_f and its compressive and tensile strengths are respectively X_C^f and X_T^f , being S_m the shear strength of the matrix and G_m its initial shear modulus.

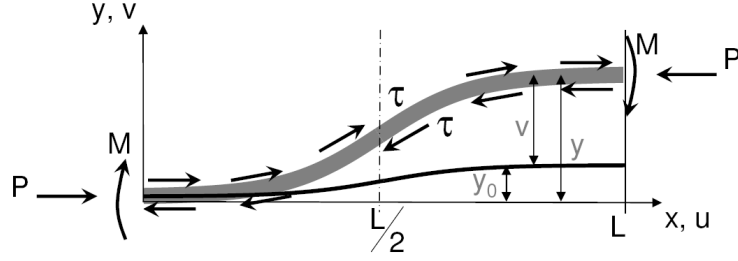


Figure 5.1: Schematics of the fibre considered in the model: geometry and loads.

5.2.1 2D equivalent model

Although a great part of this model is applicable in more general terms, the definition of a 2D equivalent geometry (with unit thickness in the normal direction, $A_f = \phi_f$ and $I_f = 1/12 \cdot \phi_f^3$ per unit thickness) is helpful to some developments related to the shear stresses acting on the fibres; for this reason, let one consider a layered material as already defined in the numerical models (Chapter 4). Assuming that, in the 3D composite, the cylindrical fibres are in a hexagonal arrangement, then along this pattern's principal plane there is a 2D layered material in which the fibre's thickness corresponds to its diameter ϕ_f , and matrix's thickness t_m is such as the overall fibre volume fraction corresponds to the specified value:

$$t_m = \phi_f \left(\sqrt{\frac{\pi}{2 \cdot \sqrt{3} \cdot V_f}} - 1 \right) \quad (5.1)$$

At this point, it must be stressed that this 2D equivalent is adopted just for the sake of simplicity; other 2D simplified models could be used as well, and a 3D geometry would be computable, but the benefit on the accuracy at this early stage would not balance the additional complexity. In addition, it should be referred that the 3D pattern is not relevant for the results, as the thickness of the matrix layer would always be computed as proportional (by a factor defined by the 3D pattern's geometry) to the fibre diameter.

5.2.2 Equilibrium of the fibre

Let one consider that the fibre has an initial waviness (y_0 , slope θ_0) represented by the sine shape

$$y_0(x) = \bar{y}_0 \left(1 - \cos \left(\frac{x}{L} \pi \right) \right) \quad (5.2)$$

The fibre deforms along the transverse axis, with a displacement $v(x)$, as it is loaded by the compressive load P , by two bending moments M at its extremities (with the same magnitude, as the deflection is anti-symmetric) and by the distributed shear force $\tau(x)$ at its interface with the matrix. The fibre's final position is given by $y(x) = y_0(x) + v(x)$, being $\theta_f(x)$ and $\theta(x)$ the slopes of the final position $y(x)$ and displacement $v(x)$, respectively (figure 5.1).

The equilibrium of the fibre is deduced considering an infinitesimal part of its length (all the load components P , τ and M defined per unit length in the normal direction, figure 5.2). Imposing the equilibrium of moments, then it comes:

$$\delta M + P \cdot \delta y - \tau \cdot \phi_f \cdot \delta s = 0 \quad (5.3)$$

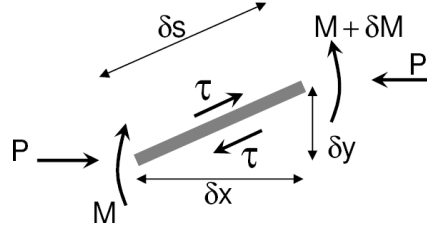


Figure 5.2: Equilibrium of an infinitesimal part of the fibre.

The development of each one of these three terms, considering P and $v(x)$ as the unknowns of the problem, is presented next.

5.2.3 Loads applied to the fibre

Bending moment This term is given by the bending theory for thin and straight fibres under small deflections:

$$M = E_f \cdot I_f \cdot \frac{\delta^2 v}{\delta x^2} \quad (5.4)$$

considering both E_f and I_f constant along x .

Compressive load The moment due to this term has to include both the initial imperfection and the deflection, and therefore it comes as:

$$P \cdot \delta y = P \cdot \delta y_0(x) + P \cdot \delta v(x) \quad (5.5)$$

Shear stress As it was mentioned, the shear stresses at the fibre's surface τ^f are due to its interface with the matrix, and therefore not possible to be computed considering just one fibre.

However, by assuming a very thin matrix layer, the shear stresses $\tau_{12}^m(x)$ are only dependent on the axial position, and the approximation $\tau^f(x) = \tau_{12}^m(x)$ is valid, so this term can be defined by the geometry of the matrix under deformation and its constitutive law.

For small deformations and considering a linear behaviour of the matrix, the shear stress $\tau_{12}^m(x)$ is related to the shear deformation $\gamma_{12}^m(x)$ by $\tau_{12}^m(x) = G_m \cdot \gamma_{12}^m(x)$; yet for small deformations, the fibres deform in-phase, being the matrix perfectly bonded to them. Then, considering the 2D equivalent model and for a given in-phase rotation $\theta(x)$ of the fibres, the shear deformation of the matrix can be deduced from figure 5.3.

$$\gamma_{12}^m = \frac{\delta v^m}{\delta x} + \frac{\delta u^m}{\delta y}, \text{ where } \begin{cases} \delta v^m = \delta x \cdot \tan \theta \\ \delta u^m = \phi_f \cdot \tan \theta \end{cases} \text{ so } \gamma_{12}^m = \frac{\delta x \cdot \tan \theta}{\delta x} + \frac{\phi_f \cdot \tan \theta}{\delta y} \quad (5.6)$$

Then, for small and in-phase rotation of the fibres, and considering $\tau_{12}^m(x)$ to be constant through the thickness t_m and also the shear deformation γ_{12}^m small enough for the material's response to be linear, the shear stresses on the matrix are given by

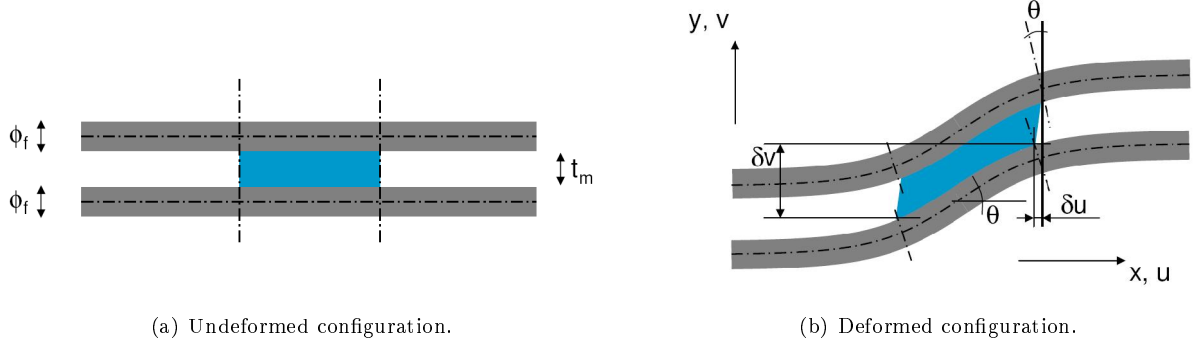


Figure 5.3: Matrix in-phase deformation.

$$\tau_{12}^m(x) = G_m \left(1 + \frac{\phi_f}{t_m} \right) \tan(\theta(x)) \quad (5.7)$$

However, the formation of a kink band requires large rotations of the fibres and therefore large deformation of the matrix, so a full constitutive law (and not only its linear elastic domain) has to be used. In this case, and taking into account the outputs from the numerical analyses, a simple linear elastic - perfect plastic law will be adopted, and therefore:

$$\tau_{12}^m(x) = \begin{cases} G_m \cdot \gamma_{12}^m(x) & , \text{ if } \gamma_{12}^m(x) \leq \frac{S_m}{G_m} \\ S_m & , \text{ if } \gamma_{12}^m(x) > \frac{S_m}{G_m} \end{cases} \quad (5.8)$$

Finally, the shear distributed force $\tau^f(x) = \tau_{12}^m(x)$ acting on the fibre is given by:

$$\tau^f(x) = \begin{cases} G_m \left(1 + \frac{\phi_f}{t_m} \right) \tan(\theta(x)) & , \text{ if } \tan(\theta(x)) \leq \frac{S_m}{G_m \cdot \left(1 + \frac{\phi_f}{t_m} \right)} \\ S_m & , \text{ if } \tan(\theta(x)) > \frac{S_m}{G_m \cdot \left(1 + \frac{\phi_f}{t_m} \right)} \end{cases} \quad (5.9)$$

One comment shall be made on the law just defined: considering that, for any 3D arrangement of the constituents within the composite, the 2D equivalent matrix layer has a thickness $t_m = 1/k \cdot \phi_f$ (k constant), then for the *elastic domain* it comes $\tau^f(x) = G_m(1+k) \cdot \tan(\theta(x))$. Considering a 2D fibre volume fraction defined as

$$V_f^{2D} = \frac{\phi_f}{\phi_f + t_m} ,$$

then a 2D equivalent shear modulus for this model is given as

$$G_m^{2D} = G_m \cdot (1+k) = \frac{G_m}{1-V_f} \quad (5.10)$$

which is exactly the simplified formula for (general) composite's shear modulus.

The shear stresses acting in fibre's surface can be directly related to their rotation by

$$\tau^f(x) = \begin{cases} G_m^{2D} \cdot \tan(\theta(x)) & , \text{ if } \tan(\theta(x)) \leq \frac{S_m}{G_m^{2D}} \\ S_m & , \text{ if } \tan(\theta(x)) > \frac{S_m}{G_m^{2D}} \end{cases} \quad (5.11)$$

5.2.4 Governing differential equations

According to the previous two sections, the formation of a kink band is governed by the following differential equations:

$$\begin{aligned} & \delta M + P \cdot \delta y - \tau \cdot \phi_f \cdot \delta s = 0 \Leftrightarrow \\ \Leftrightarrow & \begin{cases} \left[E_f \cdot I_f \cdot \frac{\delta^3 v(x)}{\delta x^3} \right] + [P \cdot \delta y_0(x) + P \cdot \delta v(x)] - [G_m^{2D} \cdot \tan(\theta(x)) \cdot \phi_f \cdot \delta s] = 0 & , \text{ if } \tan(\theta(x)) \leq \frac{S_m}{G_m^{2D}} \\ \left[E_f \cdot I_f \cdot \frac{\delta^3 v(x)}{\delta x^3} \right] + [P \cdot \delta y_0(x) + P \cdot \delta v(x)] - [S_m \cdot \phi_f \cdot \delta s] = 0 & , \text{ if } \tan(\theta(x)) > \frac{S_m}{G_m^{2D}} \end{cases} \end{aligned} \quad (5.12)$$

Considering (again) that, for small rotation angles ($\theta < 20^\circ$), the trigonometric functions can be approximate as

$$\begin{cases} \sin \theta \approx \tan \theta \approx \theta & , \text{ so } \theta \approx \frac{dv}{dx} \\ \cos \theta \approx 1 & , \text{ so } \delta x \approx \delta s \end{cases}$$

and being

$$\tan(\theta(x)) = \omega(x) = \frac{dv(x)}{dx} \quad (5.13)$$

then the equations become:

- Without matrix yielding (*pre-yielding*)

$$E_f \cdot I_f \cdot \frac{d^2 \omega^{pre}(x)}{dx^2} - [G_m^{2D} \cdot \phi_f - P] \cdot \omega^{pre}(x) = -P \cdot \frac{dy_0(x)}{dx} , \text{ if } \omega^{pre}(x) = \omega(x) \leq \frac{S_m}{G_m^{2D}} \quad (5.14)$$

- With matrix yielding (*post-yielding*)

$$E_f \cdot I_f \cdot \frac{d^2 \omega^{post}(x)}{dx^2} + P \cdot \omega^{post}(x) = -P \cdot \frac{dy_0(x)}{dx} + \phi_f \cdot S_m , \text{ if } \omega^{post}(x) = \omega(x) > \frac{S_m}{G_m^{2D}} \quad (5.15)$$

5.2.5 Continuity and Boundary Conditions

Equations 5.14 and 5.15, together with equation 5.13, define the fibre's deformed shape at a given compressive load P . Initially, for a very low compression, the material deforms in the linear *elastic domain*, and therefore equation 5.14 applies for the whole fibre; however, as the shear stresses in the matrix reach its shear strength, the deformed shape of the fibre has to be computed using both equations 5.14 and 5.15 (figure 5.4).

The boundary conditions and the continuity of the deformed shape through its length and loading history are discussed next. Before that, it is convenient to notice that the deformed shape of one fibre within the kink band (in formation or developed) is anti-symmetric with respect to $x = L/2$, as this will simplify significantly the definition of continuity and boundary conditions.

5.2.5.1 Deformed shape before matrix yielding

Prior to any matrix yielding, only equation 5.14 is required to compute fibre's deformed shape. Therefore, in the *elastic domain*, only the rotation of the boundaries and any rigid body movement have to be restrained, resulting into the following boundary conditions:

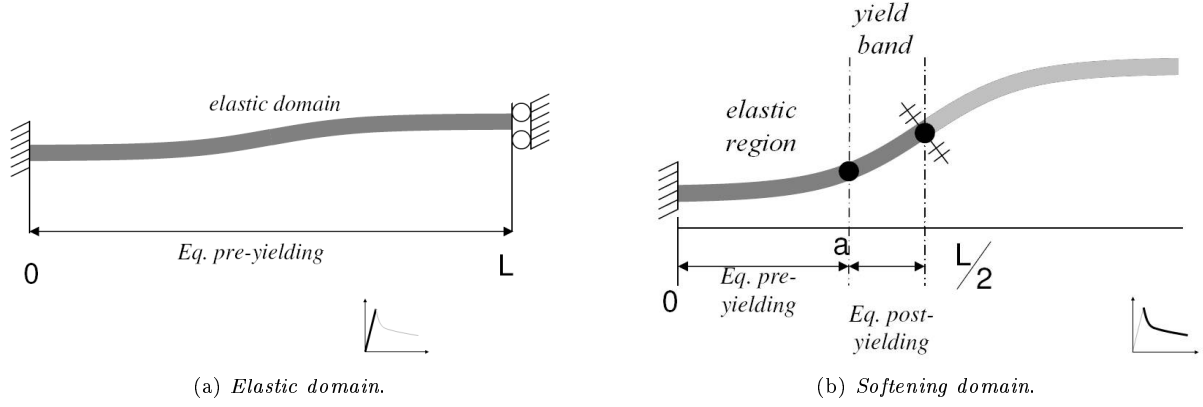


Figure 5.4: Continuity and boundary conditions.

- $\omega^{pre}(0) = \omega^{pre}(L) = 0$, to avoid rotation at the boundaries;
- $v^{pre}(0) = 0$, to avoid rigid body movement.

Within this domain, only one differential function is required to establish the equilibrium of the fibre; for this reason, and as all the functions in 5.14 have C^∞ continuity, the given deformed shape and its derivatives are also continuous.

5.2.5.2 Deformed shape after matrix yielding

After the beginning of matrix yielding (in the *softening domain*), two differential equations are required: equation 5.14 applies to the fibre's boundaries (*elastic regions*), and equation 5.15 applies to the central part of the fibre (*yield band*). For this reason, besides avoiding the rotation of fibre's edges and rigid body movements, it is also necessary to impose continuity between the three domains (left *elastic region*, *yield band*, right *elastic region*) of the fibre.

Considering the anti-symmetry previously mentioned for the deformed shape of one single fibre during kink band formation, the following boundary conditions apply:

- $\omega^{pre}(0) = 0$, to avoid rotation at the left boundary;
- $v^{pre}(0) = 0$, to avoid rigid body movement;
- $\omega^{post'}(L/2) = 0$, to impose the anti-symmetric shape on the deflection.

In order to ensure the continuity of fibre's deformed shape, it is necessary to define the location where equation 5.14 stops being applicable and equation 5.15 becomes the governing one; if one defines that point in the fibre by $x = a$ (with $a < L/2$), then the following conditions arise:

- $v^{pre}(a) = v^{post}(a)$, to ensure continuity on the deflection;
- $\omega^{pre}(a) = \omega^{post}(a) = \frac{S_m}{G_m^2 B}$, for continuity on the slope and on shear stresses in the matrix;
- $\omega^{pre}'(a) = \omega^{post}'(a)$, for continuity on the bending moment (equation 5.4) along the fibre.

Equations 5.14 and 5.15 are differential equations in the third order on the displacement $v(x)$, so six boundary conditions are enough to define the deflection. However, seven conditions were just defined, being the first six absolutely necessary to ensure a sensible deformed configuration; the remaining condition (continuity on the bending moments) is used to define the beginning $x = a$ of the *yield band*.

5.2.6 Definition of composite's compressive strength

As it was suggested by the numerical analyses, the moment when the matrix starts yielding defines the peak load for compression under displacement control.

Before matrix yielding, the equation 5.14 for the elastic domain gives as slope

$$\omega^{pre}(x) = \frac{\frac{\bar{y}_0 \cdot P \cdot \pi}{L}}{G_m^{2D} \cdot \phi_f + \frac{\pi^2}{L^2} \cdot E_f \cdot I_f - P} \cdot \sin\left(\frac{x}{L}\pi\right) \quad (5.16)$$

being therefore the maximum rotation found in the middle of the fibre:

$$\omega^{pre,max} = \omega(L/2) = \frac{\frac{\bar{y}_0 \cdot P \cdot \pi}{L}}{G_m^{2D} \cdot \phi_f + \frac{\pi^2}{L^2} \cdot E_f \cdot I_f - P} \quad (5.17)$$

Fibre rotation is related to the shear stresses found in the matrix by equation 5.7; combining these two equations, then the peak load P^{peak} can be defined by the condition

$$P^{peak} : \tau_{12}^m(L/2) = S_m \Leftrightarrow \omega^{pre,max} (@P^{peak}) = \frac{S_m}{G_m^{2D}}$$

which gives the composite's compressive strength as being:

$$P^{peak} = S_m \cdot \frac{G_m^{2D} \cdot \phi_f + \frac{\pi^2}{L^2} \cdot E_f \cdot I_f}{S_m + \frac{\bar{y}_0}{L} \cdot \pi \cdot G_m^{2D}} \quad (5.18)$$

5.2.7 First fibre failure

In this model, it is considered that the fibre starts breaking (fibre failure, ff) at a certain location $x = b$ (with $b < L/2$) when the axial stress at a point in the fibre's cross section, resultant from the combined action of the compressive load (P , σ_{11}^P) and bending moment (M , σ_{11}^M), reaches the fibre's strength:

$$\begin{cases} \sigma_{11}^f(b^{ff}) = \sigma_{11}^{f,P}(b^{ff}) + \sigma_{11}^{f,M}(b^{ff}) = X_C^f & , \text{ failure under compression} \\ \sigma_{11}^f(b^{ff}) = -\sigma_{11}^{f,P}(b^{ff}) + \sigma_{11}^{f,M}(b^{ff}) = X_T^f & , \text{ failure under tension} \end{cases} \quad (5.19)$$

Let one assume that the composite's strength under compression is not much higher than under tension; as the axial stresses due to bending are symmetric and the compressive load is superposed, then the failure is likely to happen in compression first¹. Considering this hypothesis, the stresses due to each load component are deduced (in the local axes) below.

¹For this reason and from now on, by default σ_{11}^f will be taken under compression ($\sigma_{11}^f > 0$ corresponds to compression) and on the fibre's top surface.

The axial stresses due to the compressive load are computed assuming an uniform stress distribution on the cross section A_f ; then, remembering the assumption of small slopes on the deformed shape, it comes:

$$\sigma_{11}^{f,P}(x) = \frac{P^n}{A_f}, \quad (5.20)$$

where $\begin{cases} P^n \text{ is the compressive load projected along fibre's axis, } P^n = P \cdot \cos(\theta_0 + \theta) \approx P; \\ A_f \text{ is the fibre's cross sectional area, assumed to be constant.} \end{cases}$

For the compressive stresses induced by the bending moments, according to beam theory (being e the distance of the considered point to the neutral axis within the cross section) they come as:

$$\sigma_{11}^{f,M}(x, \bar{y}) = \frac{M(x)}{I_f} \cdot e$$

So, as $e^{max} = \phi_f/2$ and considering equation 5.4, the maximum compressive stress due to bending within a cross section is given by:

$$\sigma_{11}^{f,M}(x) = \frac{\phi_f \cdot E_f}{2} \cdot \frac{d^2v}{dx^2}(x) \quad (5.21)$$

Finally, the equation for first fibre failure is defined at (P^{ff}, b^{ff}) as:

$$\begin{aligned} \frac{P^{ff}}{A_f} + \frac{\phi_f \cdot E_f}{2} \cdot \frac{d^2v}{dx^2}(b^{ff}) &= X_C^f, \text{ and as } \omega = \frac{dv}{dx}, \\ \frac{d\omega}{dx}(b^{ff}) &= 2 \cdot \frac{X_C^f - \frac{P^{ff}}{A_f}}{\phi_f \cdot E_f} \end{aligned} \quad (5.22)$$

In this equation, the compressive failure load P^{ff} and the maximizer b^{ff} of the first derivative of the slope must be either known a priori or explicit functions of ω . Whenever this is not feasible (due to too complex expression for the slope ω), the problem has to be solved numerically, so a closed formulation may not be possible.

5.3 Results

A numerical application of the model previously presented is now provided. The parameters were chosen in order to reproduce the FE model with failing interface (*cohesive*):

$$\begin{aligned} L &= 750\mu\text{m}, \bar{y}_0 = 15\mu\text{m} \\ \phi_f &= 7\mu\text{m}, E_f = 276\text{GPa}, X_C^f = 3200\text{MPa} \\ t_m &= 1.6\text{mm}, G_m = 1478\text{MPa}, S^m = 56\text{MPa} \end{aligned}$$

For better evaluation of the results provided by the analytical model, results from the numerical simulations (Chapter 4) will be provided as well; as this analytical model considers a fibre embedded in the composite, all the numerical results to be presented will be taken from the model's central fibre and matrix layer.

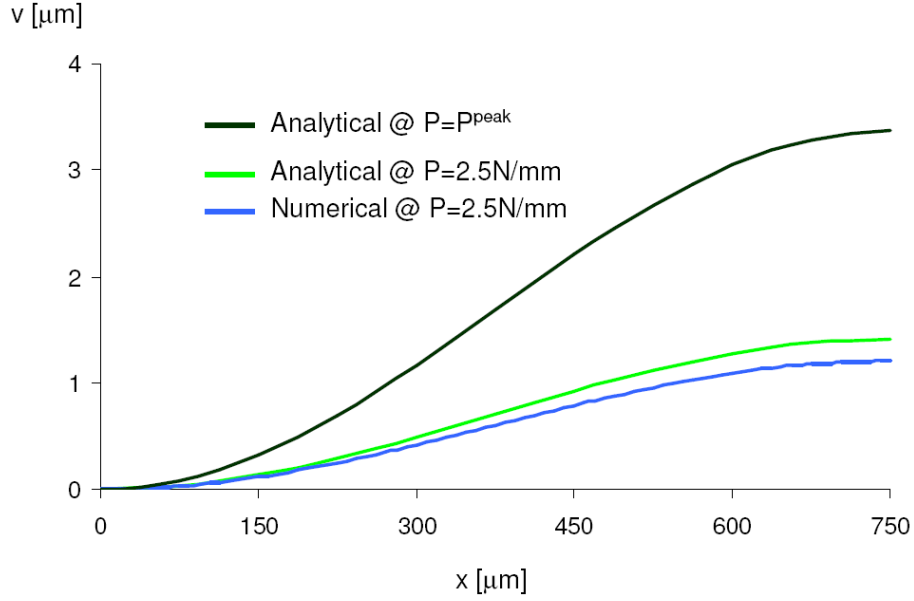


Figure 5.5: Fibre's deflection in the *elastic domain*.

5.3.1 Response in the *elastic domain*

Prior to first matrix yielding, the model predicts the composite's behaviour as quasi-linear with respect to the load P , as the only source of non-linearity is the continuous update of its application point.

During this phase, fibre's deflection can be defined for any position and for a compressive load P by:

$$v^{pre}(x, P) = \frac{\bar{y}_0 \cdot P}{G_m^{2D} \cdot \phi_f + \frac{\pi^2}{L^2} \cdot E_f \cdot I_f - P} \cdot \left(1 - \cos\left(\frac{x}{L}\pi\right)\right) \quad (5.23)$$

This gives a sinusoidal shape for the deflection, which means that the fibre will, while in the *elastic domain*, simply amplify its original shape given by y_0 (figure 5.5).

Considering the maximum deflection of a fibre (at $x = L$), the load versus displacement curve ($P(v)$) is shown in figure 5.6; as it can be seen, until the peak load is reached, load and deflection increase in a quasi proportional way.

Having such a simple expression for the transverse displacement, it is possible to compute analytically the stress fields σ_{11}^f (at the top of the fibre, under compression) and τ_{12}^m (shear, on the interface with the matrix). As it can be confirmed by expressions 5.24 and 5.25, this fields are sinusoidal as well; the maximum shear stress is located at the middle of the fibre ($x = L/2$), while the maximum compressive stress is found at the boundaries ($x = 0$ and $x = L$).

$$\tau_{12}^m(x, P) = G_m^{2D} \cdot \frac{\bar{y}_0 \cdot P \cdot \frac{\pi}{L}}{G_m^{2D} \cdot \phi_f + \frac{\pi^2}{L^2} \cdot E_f \cdot I_f - P} \cdot \sin\left(\frac{x}{L}\pi\right) \quad (5.24)$$

$$\sigma_{11}^f(x, P) = \frac{P}{A_f} + G_m^{2D} \cdot \frac{\phi_f \cdot E_f}{2} \cdot \frac{\bar{y}_0 \cdot P \cdot \left(\frac{\pi}{L}\right)^2}{G_m^{2D} \cdot \phi_f + \frac{\pi^2}{L^2} \cdot E_f \cdot I_f - P} \cdot \cos\left(\frac{x}{L}\pi\right) \quad (5.25)$$

For two given loads within the *elastic domain* - $P = 2.5\text{N/mm}$ and P^{peak} -, these two stress fields are plotted in figures 5.7 and 5.8; as it can be noticed in the last one, the compressive component in equation 5.19 dominates

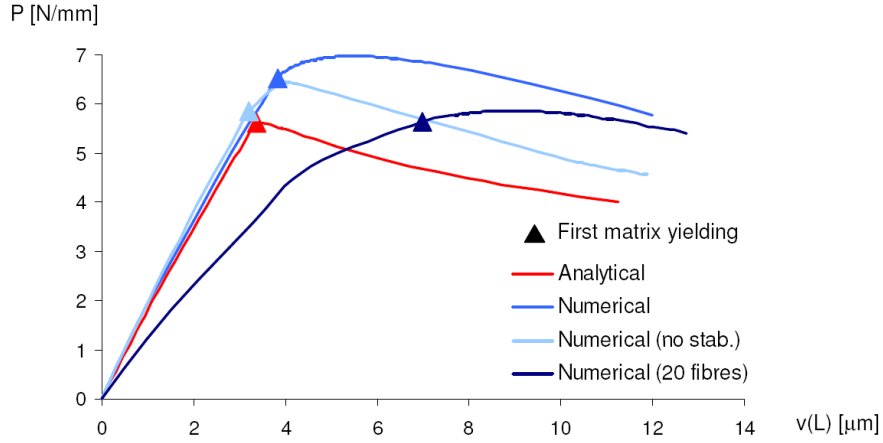


Figure 5.6: Load versus maximum displacement curve for the *elastic domain* and peak load.

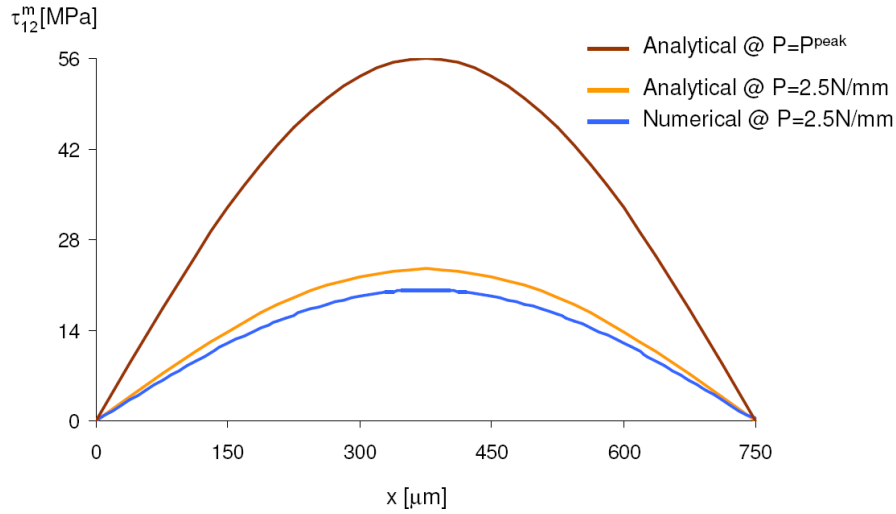


Figure 5.7: Shear stresses along x in the *elastic domain*.

the response, as the axial stress is almost constant along the fibre and increases with the load.

The *elastic domain* ends when the maximum shear stress on the matrix reaches its yield strength ($\tau_{12}^m(L/2) = S_m$), after which the material's response begins to soften; the peak load here defined can be equationed in terms of S_m as in equation 5.18, and its quasi-linear dependence for this application is shown in figure 5.9. At this very same moment, the deformed shape is also fully defined from material's properties and can be computed by the combination of the expressions 5.23 and 5.18:

$$v(x, P^{peak}) = \frac{L \cdot S_m}{\pi \cdot G_m^{2D}} \cdot \left(1 - \cos\left(\frac{x}{L}\pi\right)\right) \quad (5.26)$$

As one realizes, the maximum deflection at the peak load $v(L, P^{peak})$ is totally dominated by the geometry and by the matrix, following a perfectly linear relation with shear strength S_m .

For this specific numerical application, peak load and its correspondent maximum deflection are $P^{peak} = 5.62\text{N/mm}$ and $v^{peak}(L) = 3.37\mu\text{m}$; as these values correspond to the moment when the material starts to

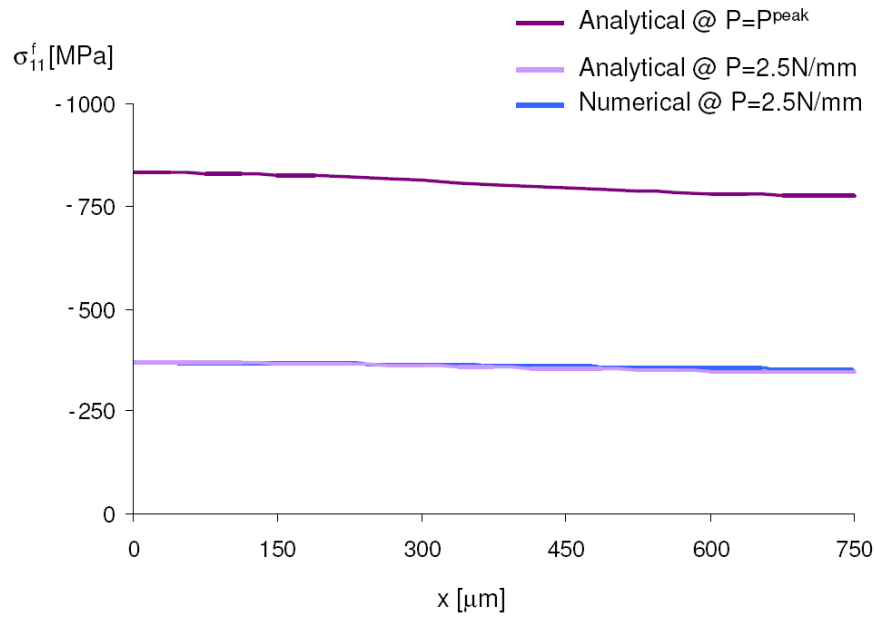


Figure 5.8: Axial stresses on the top of the fibre, along x and in the *elastic domain*.

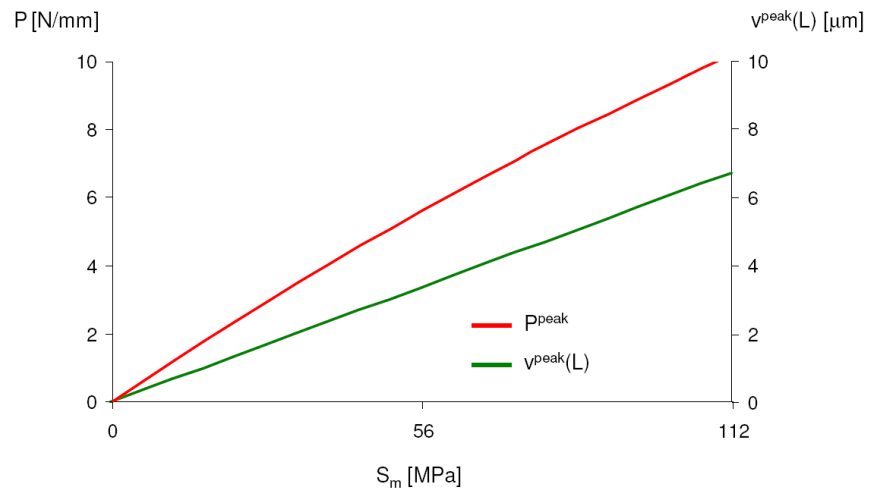


Figure 5.9: Peak load and maximum deflection for different interface's strength.

soften (begin for that reason unable to support any further loading action), then they can be used to compute the composite's strength. Considering the already mentioned input values for fibre compressive strength and initial imperfection, then the composite's compressive strength and fibre's yielding angle are given as:

$$X_C^C = 803\text{MPa} = 25\% \cdot X_C^f$$

$$y^{C,peak} = 33.37\mu\text{m} \Rightarrow \theta_f^{composite} = 2.51^\circ$$

5.3.2 Response in the *softening domain*

After the peak load, model's behaviour is governed by two different differential equations (5.14 and 5.15); solving these with the boundary conditions described in section 5.2.5, the slope $\omega(x)$ comes as:

Elastic region:

$$\omega^{pre}(x) = C^{pre} \cdot \left(e^{\sqrt{\frac{G_m^{2D} \cdot \phi_f - P}{E_f \cdot I_f}} \cdot x} - e^{-\sqrt{\frac{G_m^{2D} \cdot \phi_f - P}{E_f \cdot I_f}} \cdot x} \right) + \frac{P}{G_m^{2D} \cdot \phi_f + \frac{\pi^2}{L^2} \cdot E_f \cdot I_f - P} \cdot \frac{\bar{y}_0 \cdot \pi}{L} \cdot \sin\left(\frac{x}{L}\pi\right), \quad x \leq a \quad (5.27)$$

$$\text{being } C^{pre} = \frac{1}{e^{\sqrt{\frac{G_m^{2D} \cdot \phi_f - P}{E_f \cdot I_f}} \cdot a} - e^{-\sqrt{\frac{G_m^{2D} \cdot \phi_f - P}{E_f \cdot I_f}} \cdot a}} \cdot \left(\frac{S_m}{G_m^{2D}} - \frac{P}{(G_m^{2D} \cdot \phi_f + \frac{\pi^2}{L^2} \cdot E_f \cdot I_f - P)} \cdot \frac{\bar{y}_0 \cdot \pi}{L} \cdot \sin\left(\frac{a}{L}\pi\right) \right)$$

Yield band:

$$\omega^{post}(x) = C_1^{post} \cdot \sin\left(\sqrt{\frac{P}{E_f \cdot I_f}} \cdot x\right) + C_2^{post} \cdot \cos\left(\sqrt{\frac{P}{E_f \cdot I_f}} \cdot x\right) + \frac{S_m \cdot \phi_f}{P} - \frac{P}{P - \frac{\pi^2}{L^2} \cdot E_f \cdot I_f} \cdot \frac{\bar{y}_0 \cdot \pi}{L} \cdot \sin\left(\frac{x}{L}\pi\right), \quad a < x \leq \frac{L}{2} \quad (5.28)$$

$$\text{being } \begin{cases} C_1^{post} = \frac{1}{\cot\left(\sqrt{\frac{P}{E_f \cdot I_f}} \cdot \frac{L}{2}\right) \cdot \cos\left(\sqrt{\frac{P}{E_f \cdot I_f}} \cdot a\right) + \sin\left(\sqrt{\frac{P}{E_f \cdot I_f}} \cdot a\right)} \cdot \left(\frac{P \cdot \frac{\bar{y}_0 \cdot \pi}{L} \cdot \sin\left(\frac{a}{L}\pi\right)}{P - \frac{\pi^2}{L^2} \cdot E_f \cdot I_f} - S_m \cdot \left(\frac{\phi_f}{P} + \frac{1}{G_m}\right) \right) \\ C_2^{post} = \frac{1}{\cos\left(\sqrt{\frac{P}{E_f \cdot I_f}} \cdot a\right) + \tan\left(\sqrt{\frac{P}{E_f \cdot I_f}} \cdot \frac{L}{2}\right) \cdot \sin\left(\sqrt{\frac{P}{E_f \cdot I_f}} \cdot a\right)} \cdot \left(\frac{P \cdot \frac{\bar{y}_0 \cdot \pi}{L} \cdot \sin\left(\frac{a}{L}\pi\right)}{P - \frac{\pi^2}{L^2} \cdot E_f \cdot I_f} - S_m \cdot \left(\frac{\phi_f}{P} + \frac{1}{G_m}\right) \right) \end{cases}$$

The definition of the transition point between the two regions ($x = a$) is done imposing continuity on the deflection's curvature, $\omega^{pre'}(a) = \omega^{post'}(a)$; as one can deduce from the expressions for $\omega(x)$ just presented, an analytical solution for this last equation is not possible to be computed, being an iterative process used instead.

Once a and both $\omega^{pre}(x)$ and $\omega^{post}(x)$ are found, the expressions for the deflection $v(x)$, bending moments $M(x)$, shear stresses on the matrix $\tau_{12}^m(x)$ and axial compressive stresses on the fibres $\sigma_{11}^f(x)$ can be computed using equations 5.4, 5.9, 5.13 and 5.19. As the algebraic expressions are not possible to be written, numerical applications for three loads within the *softening domain* - $P = 5.5\text{N/mm}$, $P = 3.5\text{N/mm}$ and $P = P^{ff} = 1.35\text{N/mm}$ - are shown in the graphics 5.10, 5.11 and 5.12.

In the *softening domain*, fibre's transverse displacement does not follow a sinusoidal function anymore, being replaced by a shape with almost flat ends and a nearly straight central region, linked by two highly curved branches (figure 5.10). As the load decreases the maximum deflection increases, but not in an uniform way: while the central part becomes more and more inclined (therefore magnifying the displacement), the ends of the fibre become flatter (and the relative displacement is reduced). The central misoriented region progressively

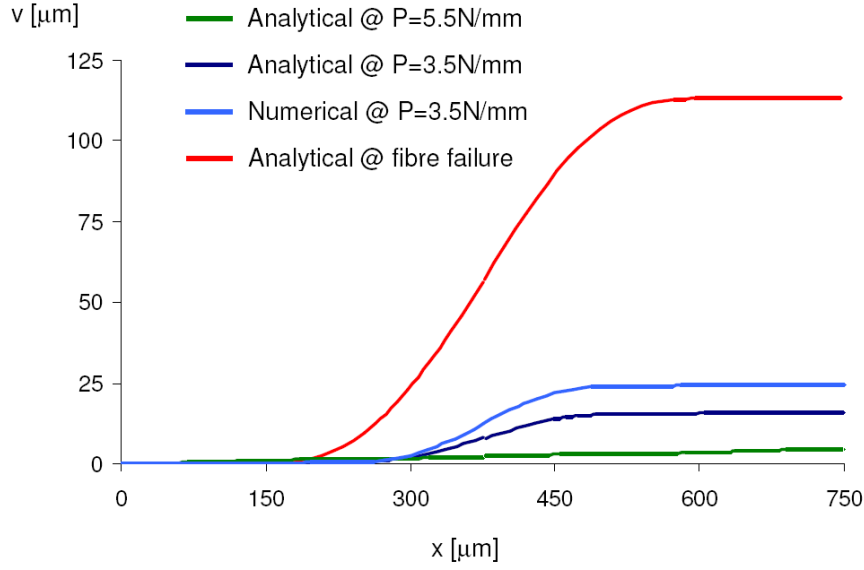


Figure 5.10: Fibre's deflection in the *softening domain*.

extends in direction to fibre's boundaries and rotates further and further, increasing the offset between the two ends and consequently the moment generated by P ; the global stiffness of the fibre decreases, and the compression continues with a decaying load, as the central rotation ($\omega(L/2)$) and distance between straight ends ($v(L)$) increase.

A change on global shape affects the shear stresses on the matrix as well (figure 5.11). Once the peak load is reached ($P^{peak} = 5.62\text{N/mm}$), a *yield band* (defined between $x = a$ and $x = L - a$) forms almost instantaneously (for a load close to that value ($P = 5.5\text{N/mm}$), the band's width is already considerable), with constant shear stresses within it; as the overall stiffness decreases - and therefore the compressive load does so as well -, this band extends towards fibre's boundaries. Outside the band, τ_{12}^m still follows fibre rotation (equation 5.7), going from $\tau_{12}^m = 0$ to $\tau_{12}^m = S_m$ between $x = 0$ and $x = a$ in a way that varies with the load: when near the peak load, the shear stresses increase smoothly (with increasing x) along the *elastic domain*, but as the load comes down the transition is sharpened and the stresses change abruptly within a very short distance.

The axial stresses found on the fibres (σ_{11}^f) also undergo a dramatic change when the *yield band* starts being defined, going from a sinusoidal shape with maximum value at the fibre's boundary (where the boundary conditions are applied) to a completely different shape (figure 5.12). Apparently, this new stress distribution is divided in two regions: in the *elastic regions*, the axial stresses are nearly constant, so the response is dominated by the compressive component in equation 5.19; inside the *yield band*, the stresses follow an approximately sinusoidal law with wavelength equals to the band's width. As the load decreases, the compressive component obviously follow that tendency, being the axial stresses reduced near the fibre's boundaries; however, the amplitude of the sine-like distribution inside the *yield band* increases significantly, dominating the response on that region and reaching quickly the fibre strength at the compressive side.

During the formation of the kink band, the load versus maximum transverse displacement is given in figure 5.13. In the overall, and after the already discussed initial *elastic domain*, the existence of a *yield band* induces softening in the composite's response, being therefore the load reduced as deflection increases; the lost of stiffness is somehow abrupt just after the peak load, as the curve seems to have the tendency to stabilize for very large displacements.

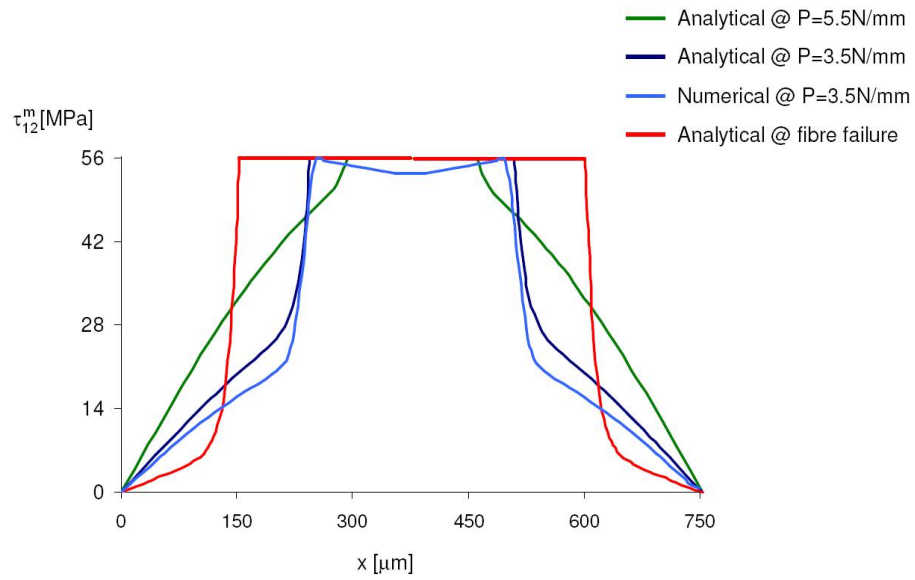


Figure 5.11: Shear stresses along x in the *softening domain*.

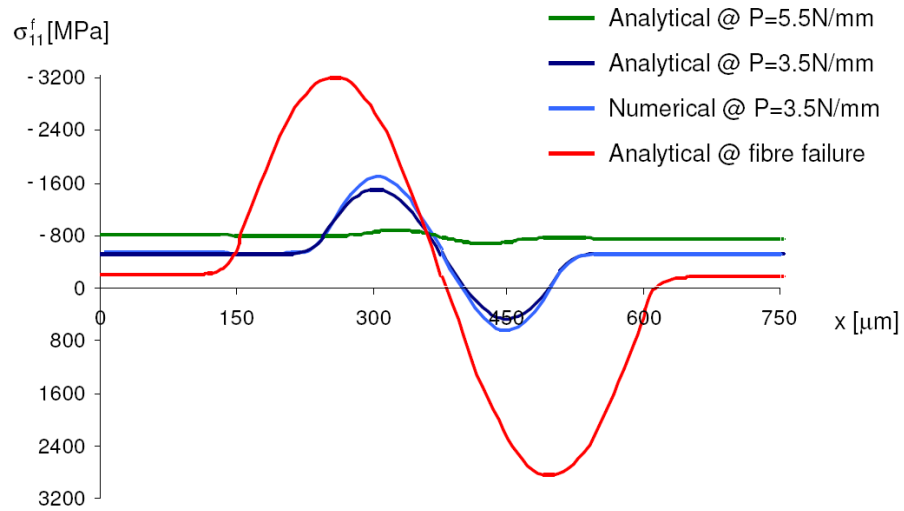


Figure 5.12: Axial stresses at the top of the fibre, along x and in the *softening domain*.

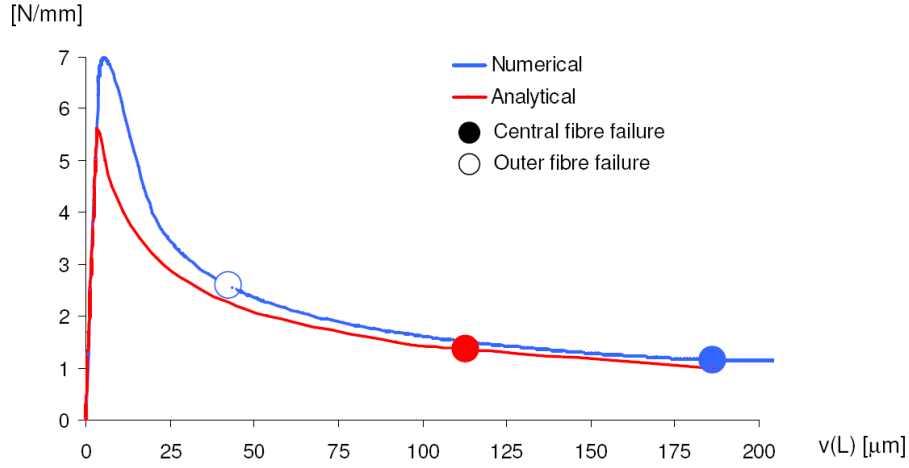


Figure 5.13: Load versus maximum displacement global curve.

During this stage, the limits of the *yield band* ($x = a$) and the location of the maximal bending moments ($x = b$) vary with the load. Figure 5.14 shows the evolution of these two points with the maximum axial stress; as it can be noticed, as soon as the peak load is surpassed, the formation of the *yield band* is almost instantaneous (the matrix yields at a practically constant load), being afterwards smoothly extended as the bending increases. The two points of maximum axial stress are located, during the *softening domain*, inside the *yield band*, following the same tendency of moving apart towards the fibre's boundaries as the compression progresses.

At fibre failure, the compressive axial stress on the top of the critical section is $\sigma_{11}^f(b^{ff}, P^{ff}) = X_C^f$; as the curve $\sigma_{11}^f(x)$ can be determined for each value of P , it is possible to define iteratively the location of the critical section b^{ff} and the load P^{ff} for which first fibre failure occurs. For the case here, considered, it comes:

$$b^{ff} = 260\mu\text{m}$$

$$P^{ff} = 1.35\text{N/mm}$$

$$v^{ff}(L) = 112.8\mu\text{m}$$

Considering the kink band's width to be defined at this moment as being equal to fibre's length between the two points of maximum axial stress ($b^{ff}, y(b^{ff})$) and ($L - b^{ff}, y(L - b^{ff})$), then:

$$w = 249\mu\text{m}.$$

The angle defined by the fibre ($\theta_f^{ff} = \theta_0 + \theta^{ff}$), at this moment and at the central cross section, is

$$\theta_f^{ff}(L/2) = 16.3^\circ.$$

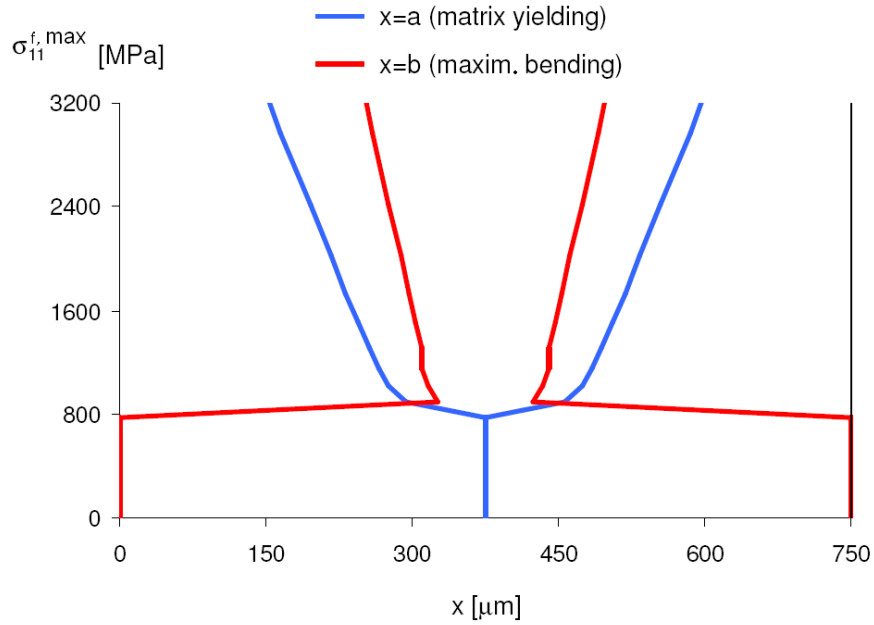


Figure 5.14: Boundaries of the *yield band* and location of maximum bending moments.

5.4 Discussion

5.4.1 Load versus displacement response

From a load versus displacement point of view, the analytical model predicts an evolution that is, qualitatively, the one shown in experiments: the composite follows an almost linear-elastic law at the beginning, going through an abrupt reduction of stiffness after the peak load and continuing with a softened response.

Quantitatively, and comparing with the FE results, one can see that the initial modulus in the *elastic domain* is accurately predicted, as it can be seen in figure 5.6. The only exception comes from the FE model with 20 fibres (*cohesive_20fibres*), which is much more sensitive to the geometric non-linearity; this is due to its smaller transverse dimension: as 10% of the fibres (2 out of 20, against 2 out of 100 - 2% - in the other models) are not supported from one side, the edge effect easily propagates through the entire model and affects its general behaviour.

The accuracy of peak load estimation is more complex to evaluate: in the analytical model, first yielding and peak load are seen as the same event, but in the numerical simulations more fibres are considered and a gap is found between the moment when the central layer of matrix yields and the moment when a *yield band* actually crosses the whole model. The issue here is the propagation of the *yield band* along the transverse direction, which depends obviously on the number of fibres (and matrix layers) present in the model; as it can be deduced from figure 5.6 (*cohesive* model with 100 fibres and *cohesive_20fibres* model with 20 fibres), the gap between yielding and peak load is smaller when less fibres are taken into account. Another parameter that has an influence on the peak load determination in the numerical models is the use of stabilization; this numerical form of damping adds a resistance to the deformation in the model, leading for that reason to a more stable solution but increasing the load applied as well. Therefore, the FE model using stabilization (*cohesive*) gives a peak load above the load given by the model without stabilization (*cohesive_0stab / no stab.*), which is closer to the analytical solution.

5.4.2 Stress and displacement fields

Besides a good agreement in the general response, the stress and displacement fields are also well captured by the analytical model, especially qualitatively. Although no conditions were imposed to the functions and fields in the model, all the features found in the numerical simulations - a different deflection shape in the *elastic* and *softening* domains, the points of maximum axial stresses moving inwards the *yield band*, the abrupt reduction in the shear stresses at the *yield band*'s boundaries - are well captured by the analytical model.

Quantitatively, the model here presented is not far away from the numerical one; the major difference is found in the deflection, especially for later stages of kink band formation. Two features can justify this fact: the linear relations for the mathematical treatment of trigonometric functions and the law for the interface. As for the first, the accuracy of the approximations $\sin \theta \approx \tan \theta \approx \theta$ and $\cos \theta \approx 1$ is also highly degraded for large angles; as the kink band is developed, the angles used in the equations reach $\theta = 16.3^\circ$, which can lead to a significant difference when several approximations are used in chain. When it comes to the shear stresses in the matrix, the constitutive law is assumed to be linear elastic - perfectly plastic in the analytical model, so the shear stresses inside the *yield band* are constant; that is not exactly true when one looks on the shear stress field from the numerical (*cohesive*) model, especially at latter stages in the *softening domain*, when there is a reduction in the shear stresses due to material softening inside the *yield band*.

In addition, the use of stabilization in numerical simulations can also lead to a small difference in the stress fields obtained; however, that difference was found not to be much relevant when the numerical results were discussed (Chapter 4), so it is not likely that stabilization is in the root of this problem.

If an iterative process is used to solve the governing equations of the analytical model, better approximations for both the trigonometric functions and the shear stresses within the matrix yield band can be used; however, increasing the accuracy will increase the complexity as well, which is not desirable at all when a closed formulation is aimed.

5.4.3 First fibre failure

The analytical model here presented ends at the moment when first fibre failure occurs; in this version of the model, fibre failure is initiated in compression, but it can easily be changed for initial failure in tension.

Fibre failure does not take into account the effect of the surrounding material or stress concentrations; this is not accurate, as both the effect of free-surfaces or already broken fibres will surely affect the stresses acting in the fibre and, therefore, the moment when it will start breaking.

As it was seen both in experimental and numerical results, in a composite with several fibres failure will occur first at the ones on a free-surface (notch in experiments or top/bottom boundaries in numerics); in this situation, the fibre is supported only on one side, which reduces material's stiffness locally. The analytical model considers that the fibre fails embedded within the composite, totally surrounded by matrix and under the effect of shear stresses transmitted across their interface and which, as it is discussed in the following section, improve the composite's performance. One option to include free-edge effect in the analytical model would be to consider only half of the shear contribution to the equations; this would, however, affect the fibre's deformed shape as well, which is not desirable as the deflection is dominated by the overall response (the effect of the free-boundaries is almost negligible in the overall deformed shape, due to continuity among fibres).

On the other hand, it was also shown (both in experiments and numerical simulations) that a kink band propagates through a chain effect, being each fibre deformed to follow the deflection of the previous one. When kink band initiation is analysed, the fibres near the free-surface will start breaking first, reducing the overall stiffness of the composite; transverse stresses, induced by the new broken shape, will probably increase to a relevant level and then transmitted from fibre to fibre by the matrix, affecting the deflection suffered even by intact fibres. Considering this, it is excluded any hypothesis to use the analytical model as it is here described to predict kink band propagation.

Taking all this into account, it is understandable that the analytical model could not predict accurately (in relation to the numerical models) the moment when fibre failure occurs, as shown in figure 5.13. Nevertheless, the analytical load for first failure is actually very close to the numerical load for first failure in the central fibre, being the difference found in the deflection due to other problems that not related directly to fibre failure. Concluding, and notwithstanding the already discussed limitations of the analytical model in this field, the agreement on first fibre failure is promising as well.

5.4.4 Terms in the slope equations

The expressions found for the slope $\omega(x)$ (and, consequently, displacement and stress fields) have some terms that are physically representative of the phenomena involved in kink band formation; a short analysis is given hereafter.

Elastic domain

All the expressions for the slope for *elastic regions* - both in the *elastic* and *softening* domains - share a common term:

$$\omega^{elastic}(x) = \left[\frac{P}{G_m^{2D} \cdot \phi_f + \frac{\pi^2}{L^2} \cdot E_f \cdot I_f - P} \right] \cdot \left[\frac{\bar{y}_0 \cdot \pi}{L} \sin\left(\frac{x}{L}\pi\right) \right]. \quad (5.29)$$

This term leads to the magnification of the initial misalignment, as the initial slope is precisely the second term (function of x) in the equation. It corresponds to the *elastic domain* in the load versus displacement curve, as it increases as the compressive load P increases too, and the slope follows a sinusoidal shape with the initial imperfection's wavelength.

The denominator in the previous expression is $G_m^{2D} \cdot \phi_f + \frac{\pi^2}{L^2} \cdot E_f \cdot I_f - P$; the term $G_m^{2D} \cdot \phi_f$ reflects the support given by the matrix, and $\frac{\pi^2}{L^2} \cdot E_f \cdot I_f$ the fibre's stiffness. If the term $G_m^{2D} \cdot \phi_f$ could be neglected, the expression $\omega^{elastic}(x)$ would correspond precisely to the slope obtained in the typical buckling analysis of a beam; however, computing each term with the values used for the numerical application of the model, it comes

$$G_m^{2D} \cdot \phi_f = 55.6\text{N/mm} \text{ and } \frac{\pi^2}{L^2} \cdot E_f \cdot I_f = 0.14\text{N/mm};$$

these values make it evident that the contribution of $G_m^{2D} \cdot \phi_f$ is dominant for the stiffness in $\omega^{elastic}(x)$ and, therefore, for the response in the *elastic domain*. If one term is to be neglected, then it should be the one corresponding to fibre's stiffness. This result is not surprising, as for the elastic domain/region an in-phase fibre deformation was imposed; physically, this constrain is given by the shear stiffness of the matrix, and it is precisely what avoids the instability of a thin and unsupported long fibre.

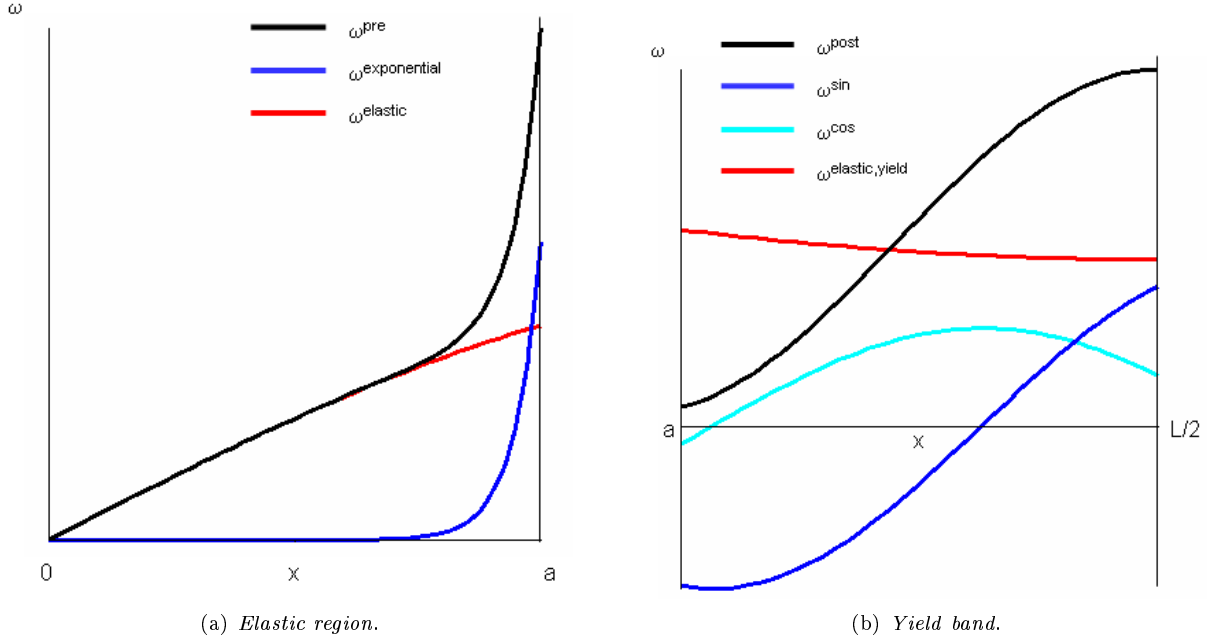


Figure 5.15: Slope components, in the *softening domain*.

In addition, it should be noticed that the load $P^{inst} = 55.7\text{N/mm}$ for which buckling instability (corresponding to zero in the denominator) occurs is much higher than the peak load $P^{peak} = 5.62\text{N/mm}$ found for the composite; this is the final proof (according to this model) that fibre kinking is not an instability problem, as it occurs much before any instability load can be reached. On the contrary, was the fibre considered unsupported and an instability would occur for a very low load (0.14N/mm).

Elastic region

In the *softening domain*, the slope in the *elastic region* is governed by the expression:

$$\omega^{pre}(x) = \omega^{exponential}(x) + \omega^{elastic}(x), \text{ with } \omega^{exponential}(x) = C^{pre} \cdot \left(e^{\sqrt{\frac{G^2 D_m \cdot \phi_f - P}{E_f \cdot I_f}} \cdot x} - e^{-\sqrt{\frac{G^2 D_m \cdot \phi_f - P}{E_f \cdot I_f}} \cdot x} \right), \quad x \leq a. \quad (5.30)$$

The second component in the expression, $\omega^{elastic}(x)$, is dominant at the boundaries (figure 5.15 a); near the *elastic region* limit ($x \rightarrow a$), the first component - $\omega^{exponential}(x)$ - increases significantly, promoting an abrupt change in the slope evolution; this is the direct responsible for the correct behaviour captured in shear, as in this region $\tau_{12}^m(x) \propto \omega(x)$.

As it can be concluded by observing the figure 5.15 a, none of the two terms is negligible.

Yield band

Inside the *yield band*, the slope is given by:

$$\omega^{post}(x) = \omega^{sin}(x) + \omega^{cos}(x) + \omega^{elastic,yield}(x), \quad a < x \leq \frac{L}{2}, \text{ with}$$

$$\omega(x) = C^{post} \cdot \sin\left(\sqrt{\frac{P}{E_f \cdot I_f}} \cdot x\right), \quad \omega^{cos}(x) = C_2^{post} \cdot \cos\left(\sqrt{\frac{P}{E_f \cdot I_f}} \cdot x\right), \quad (5.31)$$

$$\text{and } \omega^{elastic,yield}(x) = \frac{S_m \cdot \phi_f}{P} + \frac{P}{\frac{\pi^2}{L^2} \cdot E_f \cdot I_f - P} \cdot \frac{\bar{y}_0 \cdot \pi}{L} \cdot \sin\left(\frac{x}{L} \pi\right). \quad (5.32)$$

Analysing the previous equation, all the three components are sinusoidal functions; the last one - $\omega^{elastic,yield}(x)$ - corresponds to the magnification of the initial imperfection, keeping its wavelength. Contrarily to what happened for the *elastic region*, this term is not exactly the same as in the *elastic domain*, as the shear contribution for the stiffness has changed; in the present case, it is found as an independent (in relation to x) term, because it is no more implied with the deformed shape.

The other two components - $\omega^{sin}(x)$ and $\omega^{cos}(x)$ - correspond to sinusoidal functions with variable half wavelength $L^{yield} = \pi/2 \cdot \sqrt{E_f \cdot I_f / P}$: as the load decreases (in the *softening domain*, so due to further compression) the wavelength increases, leading to the *yield band*'s expansion towards fibre's boundaries.

It should be noted that the final response $\omega^{post}(x)$ has (almost) exactly half wavelength within the region $x \in [a, L/2]$ (figure 5.15 b); this justifies the location of maximum bending stresses at $x = b \approx L/4 + a/2$ (which is therefore maximizer of the curvature).

All the three terms are important for the overall response, so none can be neglected.

5.4.5 Attempt of a simplified model

As it was mentioned in the previous section, this model may not lead to a closed solution if the expressions found for the displacement are not simple ones; for this reason, a simplified version of the model was aimed, and one attempt tried is now presented.

From the numerical models, one did conclude that the boundaries of the *yield band* (here defined by $x = a$) are located close to the critical cross section of the fibre (here defined by $x = b$). At fibre failure, it comes:

$$\begin{cases} E_f \cdot I_f \cdot \frac{d^2 \omega^{post}(b^{ff})}{dx^2} + P^{ff} \cdot \omega(b^{ff}) = -P^{ff} \cdot \frac{dy_0(b^{ff})}{dx} + \phi_f \cdot S^m \\ \frac{d\omega}{dx}(b^{ff}) = 2 \cdot \frac{X_C^f - P_{A_f}^{ff}}{\phi_f \cdot E_f} \end{cases} \quad (5.33)$$

So, considering $a^{ff} \equiv b^{ff}$, and remembering the definition of a and b^{ff} , it comes:

$$\begin{cases} \frac{d^2 \omega^{post}(b^{ff})}{dx^2} = \max \Rightarrow \frac{d^2 \omega^{post}(b^{ff})}{dx^2} = 0 \\ \omega(b^{ff}) = \omega(a^{ff}) = \frac{S^m}{G_m \cdot \left(1 + \frac{\phi_f}{i_m}\right)} \end{cases} \quad (5.34)$$

which, together with the previous equation, would lead to:

$$\begin{cases} P^{ff} \cdot \frac{S^m}{G_m \cdot \left(1 + \frac{\phi_f}{i_m}\right)} = -P^{ff} \cdot \frac{dy_0(a^{ff})}{dx} + \phi_f \cdot S^m \\ \frac{d\omega}{dx}(a^{ff}) = 2 \cdot \frac{X_C^f - P_{A_f}^{ff}}{\phi_f \cdot E_f} \end{cases} \quad (5.35)$$

This simplification removes one unknown, b^{ff} , and turns the first equation in 5.35 into a algebraic (instead of differential) one; from that equation, the failure load P^{ff} is related to the location of first of fibre failure and

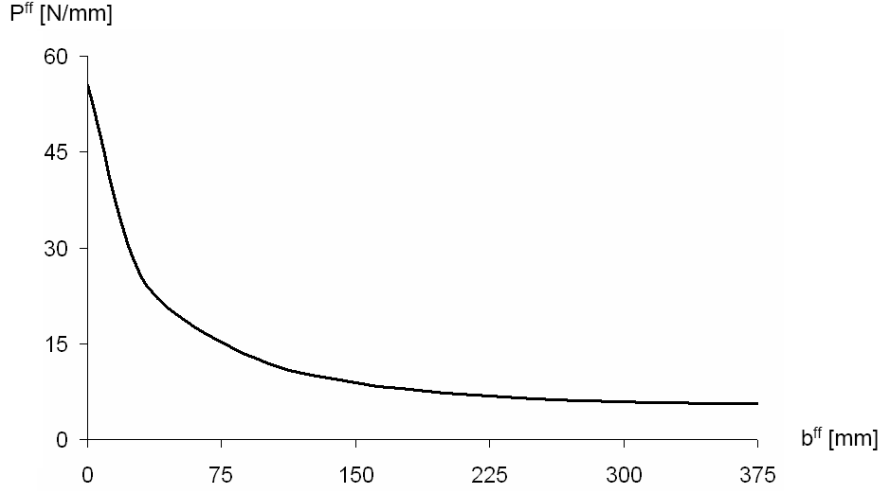


Figure 5.16: Fibre failure load versus failure position, in a simplified model.

first matrix yielding ($a^{ff} = b^{ff}$) by

$$P^{ff} = \frac{\phi_f \cdot S^m}{\frac{S^m}{G_m \cdot \left(1 + \frac{\phi_f}{\epsilon_m}\right)} + \bar{y}_0 \cdot \frac{\pi}{L} \cdot \sin\left(b^{ff} \frac{\pi}{L}\right)}, \quad (5.36)$$

plotted in figure 5.16.

From this graphic, P^{ff} decreases by positive values as the *yield band* and the segment between broken cross-sections are reduced (b^{ff} increases); the minimum failure load obtainable (for a zero-width kink band) is $P^{ff} = 5.6\text{N/mm}$, much higher than the load found in the non-simplified model. Analysing expression 5.35, the term corresponding to the slope at $x = b^{ff}$ is approximated by the slope at the boundary of matrix yielding $\omega(a)$, an underestimation of its real value (ω continuously increases for $x \in [0, L/2]$), which makes the result P to increase significantly and to unacceptable values.

Besides, and analysing the axial stresses in the fibre (figure 5.12), one can realize that the point of maximum bending (b^{ff}) is approximately at the same distance from the *yield band*'s boundary (a) as from the fibre's centre ($L/2$), being the evolution of the axial stresses between this two points almost symmetrical with respect to b^{ff} . For this reason, approximating $a^{ff} \equiv b^{ff}$ would change completely the shape defined by this field, leading to erroneous results.

5.4.6 Model outputs

The main purpose defined for this work was to develop an analytical model capable of predicting the geometry - α , β and w - of a kink band formed under a compression.

The model developed uses, as inputs, standard properties of the composite (volume fraction), fibres (diameter, Young's modulus, compressive strength) and matrix (shear strength, shear modulus); in addition, two parameters to characterize the initial imperfection - wavelength and amplitude - are required as well. No fracture toughness values are needed; this is an advantage as these properties are sometimes not available a priori and usually less straight forward to obtain, but a disadvantage as the matrix shear strength is required on the other hand.

As it was previously mentioned, this model reproduces accurately the composite's overall response during kink band formation, with a load versus displacement curve that is computable until fibre first failure. It is able to predict, in a closed form, the peak load supported by each fibre during this failure mode, which can be converted into the composite's strength under compression X_C^C . In addition, the model predicts the fibre's load and deflection for first fibre failure; if one considers that fibre breakage is catastrophic, then final fibre failure will follow immediately, being the ultimate compressive strain computable (by the combined effect of the compressive global stress outside the kink band and the shortening in bending inside the band).

As for the final kink band's geometry, this model predicts only its width w , using an iterative process and assuming fibre failure to be sudden (so first failure defines the cross sections at which final failure will occur) as well. When it comes to the band's angle, the model leaves that parameter partially free, as inside the *yield band* there is no assumption of an in-phase deformed shape.

The angle of fibre rotation at first fibre failure (θ_f^{ff}) can be related to the angles β and α . Assuming the orientation of the kink band β to be defined analytically at first fibre failure (between first fibre failure and central fibre failure in the numerical simulations), and imposing both rigid rotation of fibre's cross section and a very thin matrix, then it would come $\beta = \theta_f^{ff} (L/2)$. For α , the common assumption of volumetric conservation within the band ($\alpha = 2 \cdot \beta$) would result into $\alpha = 2 \cdot \theta_f^{ff} (L/2)$. Using the previous numerical application of the analytical model, then $\alpha \approx 33^\circ$ and $\beta \approx 17^\circ$, which are reasonable values for real kink bands; however, when looking into the FE simulations it is found that $\beta > \theta_f^{ff} (L/2)$ (at first fibre failure $\beta \approx 11^\circ$ and $\theta_f^{ff} (L/2) \approx 15^\circ$, and at central fibre failure $\beta \approx 23^\circ$ and $\theta_f^{ff} (L/2) \approx 40^\circ$), so a more accurate approach should be developed.

Chapter 6

Conclusions

6.1 Experimental

An experimental program was carried in this project (Chapter 3), with the goal to provide useful inputs for the development of the analytical model.

In this scope, several testing set-ups for FRP axial compression were tried; it was found that, using reduced and thick UD specimens, with in-plane shear induced by a fibre global misalignment and / or by the loading scheme, and compressing them under a small clamp or rig, it is possible to generate kink bands observable at the microscale, loaded and with a high magnification, under the optical microscope or SEM.

Some conclusions arose from the experimental results. A sequence of events for kink band initiation (with main emphasis in the relation between fibre failure and deformation within the band) was defined. The observation of a kink band without fibre failure lead to the hypothesis of being matrix yielding the main feature for its formation. Fibre breakage, when occurring, was found to agree with a failure by bending and to be consistently asymmetric. The deformed shape was confirmed to follow approximately a sinusoidal shape, both with in- and out-of-plane components and also including elastic and plastic deformation. Splittings were found locally at band's boundaries and inside fully-developed (with broken fibres) kink bands (in post-mortem specimens); besides, several specimens failed also by development of macro splittings.

Notwithstanding all these conclusions (some of them open to discussion, as it can be read in Chapter 3), the experimental program rose more questions than it answered; several complex features were observed and are still somehow unexplained, even considering the developments achieved in terms of numerical and analytical models. Nevertheless, there are now solid bases for further analysis using the specifically conceived rig for observation of loaded kink bands under the SEM.

6.2 Numerical

An extended analysis of kink band formation was done using FE simulations (Chapter 4).

Several 2D numerical models for initiation and propagation of kink bands were developed; the models include initial fibre waviness, a refined representation of fibres and matrix and different types of constitutive laws for both constituents (with plastic and damage formulations) and were run in static analysis.

For kink band initiation, the main result is the definition of its sequence of events, which emphasizes the role of matrix yielding in shear; in fact, this is the feature that leads to composite's softening after its compressive shear strength X_C^C is reached. During kink band formation, the fibres were confirmed to deflect due to the combined action of bending moments and compression, being supported by the matrix through shear stresses transferred at their (fibre-to-matrix) interface. Matrix's response was found to take place mainly in shear, developing stresses proportional to the rotation of the adjacent fibres until the shear strength was reached; from that moment on, a *yield band* developed in the composite, followed by a reduction in the support provided to the fibres. The support given by the matrix as shear is effective, as no cracks are predicted to open; this would be verified even if a very low value for mode I toughness was used, as the material is under transverse compression in the band's centre.

This *yield band* presents some interesting particularities: it crosses the material (along the transverse direction) following a misaligned orientation, with an approximately constant width between fibres (for each analysis increment), and with increasing inclination and width as the compression proceeds (for each matrix layer); these features make it actually very similar to a kink band in a real composite. Outside this band, the composite relaxes, but inside it the stresses increase furthermore until the moment when the fibres under the free-edge effect get overstressed in compression by the action of bending moments; after first fibre failure (at the model's longitudinal boundaries), damage propagates towards the other fibres.

Besides this global behaviour, the numerical models predict as well reasonable stress fields for both matrix and fibres during fibre kinking; it was found that the fields' shape changes abruptly (in time) as one moves from the initial *elastic* domain to the *softening* one, and also (within the fibre) when one moves from the *elastic regions* (matrix in the elastic domain) to the *yield band*. The two *maximum bending bands* move from the model's transverse boundaries inwards the *yield band*, adopting its orientation as well; the shear stresses in the matrix are kept almost constant within the *yield band*. This change in material's behaviour is considered to be a direct result of matrix constitutive law.

In addition to these developments for kink band initiation, other experimental features were also reproduced numerically: kink bands were propagated in straight fibres, through the same mechanisms found for initially misaligned ones; complementary kink bands were developed in models with transverse displacement constrained; splittings occurred under representative conditions in models for propagation.

In the overall, the numerical analyses proved to be representative of the real phenomenon of kink band formation, and provided valuable inputs for the development of the analytical model.

6.3 Analytical

Model overview

An analytical model for kink band formation was developed in Chapter 5.

The model is based on a 2D layered media equivalent of the 3D composite, and considers both the contributions of fibres and matrix.

Equations are derived from the bending equilibrium of a single imperfect fibre under the action of a compressive load (applied to its ends), of two bending moments (applied at its left and right boundaries as well) and distributed shear stresses (representing matrix's action on fibres, applied on its upper and lower surfaces). The

fibre is considered to develop internal bending moments and internal compressive stresses only, so only its axial stresses and stiffness are computed in the analysis.

Matrix respond in shear, with a linear elastic - perfect plastic behaviour; shear stresses in the *elastic* domain are related to shear strains, and these are governed by fibre rotation considering in-phase deformation. After the shear strength is reached, matrix presents a length (*yield band*) with constant shear stresses, and no in-phase constrain is imposed there. Due to the existence of two different domains for matrix's constitutive law, two governing equations are deduced for the fibre.

The fibre's equilibrium equation (whatever the domain is) is solved in order to the slope, using boundary conditions that constrain end rotation and impose C^1 (bending moments) continuity; all the relevant fields - axial stresses in fibres, shear stresses in matrix, transverse deflection - can be derived afterwards, depending on the position within the fibre and on the compressive load. The model intends to represent accurately the composite's behaviour from the beginning of compression until first fibre failure.

For the resolution of the governing differential equations, an iterative process has to be used in the *softening* domain; in the overall, small deflections, small rotations and small strains are assumed.

Applicability

The model is applicable to the pure compression of a strong and stiff *material* interposed with a soft *interface*, under the condition of continuity between both constituents in terms of shear stresses. For this reason, the model is applicable to FRP composites and also to layered materials; it can be adapted to consider a frictional *interface* instead of a material (matrix) one. This model is not useful, however, if open splittings are found in the middle of the kink band, as in this case no shear stresses can be transmitted to the fibres.

The model assumes an initial imperfection; for this reason, it should not be used for kink band propagation across straight fibres. In addition, as it considers shear stresses acting on fibre's surface, it cannot be used when splittings are open during fibre kinking; however, that feature makes the model suitable (after performing the required changes) for composites under hydrostatic pressure, as in that situation shear is always transferred to fibres (no matter how degraded the matrix is, as continuity is ensured either by the matrix itself or by friction).

Model's capabilities

The analytical model is able to compute, in a closed formulation, the composite's strength X_C^C ; besides, if an iterative process is used, it calculates the kink band width w as well.

In addition, the main fields and the load versus displacement curve can be determined too, analytically for the *elastic* domain and iteratively for the *softening* one.

Agreement with experimental results

The qualitative agreement between the analytical and the experimental results was not deeply studied; however, the general shape of the load versus deflection curves, the fibre's deformed shape and the fibre's axial stresses given by the analytical model are supported experimentally in an effective way.

Agreement with numerical models

The analytical results were validated against numerical results, both when it comes to load versus deflection curves and to stress and displacement fields. Qualitatively, the results are very good, as all the features found in the numerical model are reproduced by the analytical one. Quantitatively, the results are good, especially when it comes to stress fields; however, for large rotations the deflection computed analytically is considerably smaller than the numerical one.

Fields' shape

The displacement and stress fields computed with the analytical model do reproduce (qualitatively) the numerical ones.

In the *elastic domain*, all the fields - axial stresses, shear stresses, deflection - do follow sinusoidal expressions; for each field, an unique expression is able to describe the response of the entire fibre length; the deflection is an anti-symmetric sinusoid, the shear stresses follow a symmetric sinusoid, and the axial stresses are practically constant along fibre length, with a very small sinusoidal component superimposed (due to bending).

In the *softening domain*, however, the shape of these three fields changes completely. The shear stresses are bounded by the matrix shear strength inside the *yield band*, and as one moves to the *elastic regions* τ_{12}^m decays quickly near the band's boundaries. When it comes to the axial stresses σ_{11}^f , the compressive component is reduced and the bending one becomes dominant, and significant stresses are found only inside the *yield band*, where two peaks are defined. The deflection v presents a kinked shape, with almost no deflection outside the *yield band* but with considerable fibre rotation within it. It has to be noted that the different shapes, in this domain, obtained for the *elastic region* and *yield band* result from nothing else than the change in the matrix's constitutive law.

Closed and iterative formulations

While in the *elastic domain*, the model can be dealt with analytically; however, as soon as the fibre goes into the *softening* domain, an iterative solution is required if any output is aimed. For this reason, no closed formulation is available for the moment when fibre failure is predicted.

No constrains in fibre's final shape

On the contrary to what happens in many analytical models, the one just developed does not impose any type of shape for the deflection; the only features constraining fibre's deformed shape are material's properties and constitutive laws, the equilibrium equations and an in-phase condition for small (*elastic domain* and *regions*) strains.

In addition, no in-phase constrains are imposed to fibres' deformed shape for large strains, so the kink band angle β is free to vary.

Limitations of the model

The model cannot calculate the fibre angle inside the kink band (α) neither the band angle (β) when the kink band is formed; besides, it is not suitable for use after first fibre failure as well.

In addition, after first matrix yield occurs and the peak load is reached, the composite's response has to be predicted through an iterative process.

The model is also limited to the response under pure compression as well, and no 3D extension is available at the moment.

Possibilities for further developments

The analytical model can be easily developed with the goal of simplifying its fields for the *softening domain*, by imposing known and simple functions as model's outputs and solving therefore the governing equations in a simplified way; a closed formulation is likely to be possible.

In addition, simply by adding those components to the equilibrium equations, it is possible to include in the model the effect of global in-plane shear and / or transverse loading; the model would, in that case, be able to deal with any in-plane load case. Besides, if shear or transverse stresses are considered, the requirement for an initial imperfection vanishes.

Developing a full 3D version requires deeper changes to the present model, as the relation between shear stresses and fibre rotation would be much more difficult to define; in addition, this 2D version considers kinking to occur in a specific (symmetry) plane, so it has to be used carefully (t_m recalculated) in any semi-3D approach.

Chapter 7

Future work

7.1 Experiments

Experimentation under the SEM

The SEM proved to be the most efficient equipment to use for kink band observation. Using a rig especially-conceived for loading r-UD specimens inside the SEM allows the composite to be observed loaded, with high magnification and resolution and with no influence of out-of-plane movements, which will hopefully help answering the question still open to discussion.

Kink band formation and propagation

The formation and propagation of a kink band was not observed with a sufficient detail to provide effective inputs for analytical models, so there is still much work to be done. Propagation would be followed under the same load scheme, with the compression increasing in a systematic way (constant shortening increments), and the same areas of the composite should be observed at each load step; this would allow the effects of material randomness to be identified and discarded from the general behaviour during kink band formation.

Analysis of splitting

The presence of splitting and open cracks is an important issue which can only be closed by effective experimental observation. Splittings should be looked for inside the kink band and at its boundaries, both before and after fibre failure; important parameters (if splittings actually appear) would be their position (in relation to the kink band), location (matrix / interface between matrix and fibres), the stage in which they are formed and the number of fibres between splittings.

Fibre failure

Fibre failure mechanisms are still unknown, as it is both numerically and experimentally a process difficult to track and simulate accurately. It is suggested that fibres fail mainly in bending and that that fact can be observed experimentally by looking into the fibres' surface after final failure; however, a systematic analysis was

not done, and it could provide an important support to the analytical model. In addition, following the failure process and damage propagation would reveal if it is reasonable or not to approximate the kink band's final width to the fibre's length between the two sections where first failure occurs.

In-plane kinking

A considerable out-of-plane component was report in the experimental results; this is not a problem when the kink band at the specimen's surface is representative of the one developed in its inner layers, but it must be avoided when affecting material's behaviour so much that single fibre failure or local V-shapes are found. To do so, a support should be added to the specimen's surface during the experiments; this, however, needs to be transparent so it can be kept during observation, tough enough to withstand the composite's deformation during loading, and well lubricated so it has a minimal effect in in-plane kinking.

Kink band formation without fibre failure

The formation of kink bands is usually followed by fibre failure at its boundaries; however, when fibre failure occurs, the composite's response is usually unstable, so some features (as formation of splittings) are more difficult to analyse when fibre breakage occurs. For this reason, it would be interesting to observe loaded kink bands fully developed without fibre failure. This was achieved in this experimental program by coincidence, but it is suggested that inducing large initial misalignments can result into kink bands with no fibre failure; another hypothesis to trigger this is to use materials with different matrix-to-fibre strengths.

7.2 Numerical

Investigation on the latter stages in the *softening* domain

In the analysis run, the composite's response for latter stages in the *softening* domain was not studied as deeply as the response around the peak load. A new model with failing matrix and extended geometry (so boundary effects are avoided) should be run and analysed, to confirm whether the same matrix behaviour assumed for the analytical model ($\tau_{12}^m = \text{constant}$ inside the *yield band*) is reasonable or not when fibre rotation increases further more.

Behaviour after first fibre failure

The material's behaviour as first fibre failure occurs needs a deeper study as well. Ideally, the best would be to run a model until final failure of all fibres takes place and further rotation is locked-up, so to analyse properly the band's final geometry; however, if this is not possible to achieve (convergence problems are likely to appear for such late stages), there is still work to do until the band's width w and angle β for which fibres start failing can be accurately defined; for this, the model with extended geometry and damage propagation in the fibres can be run further. New models, with more fibres and a longer geometry, could be analysed as well to check whether propagation of fibre failure really stabilizes along parallel lines as soon as the free-edge effect disappears.

In addition, the effect of fibre's fracture toughness should be analysed as well, as it is likely that, if it is reduced, fibre propagation will occur much quicker; it should be checked, within its reasonable range of values, how the composite's response does vary due to this parameter.

Combined matrix and fibre failure / damage propagation

The overall composite's behaviour for latter stages in kink band propagation should also be studied when damage propagation and failure are possible both for fibres and matrix (so by using cohesive elements to model the matrix and using a CDM implemented to the fibres); a numerical model like this would probably be difficult to make converge, but its representativeness would make it worthwhile even if only the initial stage after first fibre failure was reached. An extended geometry is likely to be necessary for such a model.

Effect of shear constitutive law

The matrix behaviour in shear is the most relevant feature for kink band initiation; unfortunately, this constitutive law is not fully understood yet, so an accurate modelling is (by now) not possible at all. The standard analyses here presented should, for that reason, be re-run (using an extended geometry) with representative qualitative variations of matrix response in shear; a more pronounced plastic behaviour for small strains, a continuous plastic hardening (with no perfectly-plastic region), a plastic hardening with stiffening for large strains and a bi-linear law (failing) with reduced toughness could be tried.

Shear loading

Besides pure compression, loading the composite in shear will affect the composite's behaviour when kinking; for this reason, numerical models with direct in-plane shear loading could be run as well.

The modelling strategy used for pure compression could be used with shear, but the initial imperfection would not be required anymore for initiation. Besides, following the conclusions from the analytical model, pure in-plane shear will lead to kink band formation as well; therefore, applying a transverse displacement to one model's vertical edge should be a suitable approach to start.

Propagation

In kink band propagation, the effect of fibre failure should be checked as well; adding a CDM to an already problematic model might make convergence impossible using the implicit solver, so the hypothesis of using an explicit code should be revisited.

In addition, it should be checked whether a kink band is actually propagated along the model's entire transverse direction model when splittings are allowed; the model for propagation with transverse failure could be used for this purpose.

Modelling fibre-to-matrix interface

In the models presented in Chapter 4, the *interface* was considered to be the matrix (fibre-to-fibre interface). Although, at the beginning of the numerical work, models with fibres, matrix and fibre-to-matrix interface were developed, they were soon abandoned as no additional information as obtained.

Nevertheless, now that modelling with decohesive elements is controlled, it could be interesting to model fibre-to-matrix interface, with variable interface parameters (namely $S_{interface}$ and $\mathcal{G}_{C, interface}$), to predict numerically for which range of material properties interface failure starts before matrix failure.

Role of boundary conditions and model's dimensions

The effects of model's transverse and horizontal edges are reported in all the analysis; to be able to subtract them to the results asks for similar models (with different extended lengths, different imperfection parameters and different numbers of fibres) to be analysed, so a parametric study could be done.

7.3 Analytical

Simplified models from known curves

An analytical model was proposed, but no closed formulation can be found for the *softening* domain without imposing a priori simpler laws for the deflection, both in the *elastic region* and *yield band*. Now that the fields from the original model are known, simplified functions for deflection, shear and axial stresses could be tried, to define the location of first fibre failure - and, therefore, band's width - in a closed form.

A suggestion is to impose a sinusoidal law for the axial stresses in the fibres inside the *yield band*, and constant stresses outside it, deriving the deflection and slope from the curvature. Another option is to use a sigmoid (S-shape or logistic) function to represent the deflection within the whole *softening domain*, and to derive the axial stresses through the curvature of such geometry.

Continuous shear constitutive law

Another option that might simplify considerably the model is to use a continuous constitutive law for the matrix, as the use of two different governing equations for the *yield band* and *elastic region* is actually one of the causes for the impossibility to find a pure analytical solution. Suggestions given are to adopt the sigmoid function or the hyperbolic tangent, as they approximate well the elastic-perfect plastic behaviour.

Kink band geometry

The only parameter that can be estimated from the analytical model developed is the band's width w ; the objective of this project was to develop a model able to define the three geometric parameters (band's width, band's angle and fibres' angle), so the model needs to be developed to achieve those results.

From the model, fibre's angle at fibre failure can be defined as well; some relations between fibre (α) and band (β) angles were already proposed by other researchers, but the numerical models might be able to provide information as well.

Model extension

The analytical model considers, at the moment, planar (2D) fibre kinking under axial compression ($[\sigma^\infty]$ has only one non-zero component, σ_{11}^∞). Further developments must include at least the effect of in-plane shear (τ_{12}^∞), as if existing it results into a torque that affects the governing equations for fibres in both domains; transverse stresses (σ_{22}^∞) are not likely to play a major role in the fibre's equilibrium equation, but they might affect matrix yielding significantly so they should also be accounted for.

In addition, a extended formulation suitable for 3D composites should be aimed as well.

Inclusion of matrix damage

In the analytical model, matrix behaviour is linear elastic - perfectly plastic; however, the role of matrix softening for large strains is still open to discussion. If it is proved to be important, then the analytical model should be changed to accommodate non-constant shear stresses; this can be done by replacing, in the governing equation for the *yield band*, the constant term in shear by a term depending on the strain and with the proper constitutive law. It should be noticed, however, that the relation defined between shear strain and fibre's slope inside the *yield band* should not add any in-phase restriction.

Bibliography

- [1] C.R. Schultheisz, A.M. Waas. Compressive failure of composites, part I: testing and micromechanical theories, *Progress Aerospace Science*, Vol. 32 (1996).
- [2] S.T. Pinho. Modelling failure of laminated composites using physically-based failure models (PhD report). Imperial College London (2005).
- [3] A. Law. Comparison of the failure mechanisms for a range of different high-performance carbon-epoxy systems (MEng report). Imperial College London (2007).
- [4] A.M. Waas, C.R. Schultheisz. Compressive failure of composites, part II: experimental studies. *Progress Aerospace Science*, Vol. 32 (1996).
- [5] S. Kyriakides, R. Arseculeratne, E.J. Perry, K.M. Liechti. On the compressive failure of fiber reinforced composites. *International Journal of Solids and Structures*, Vol. 32 (1995).
- [6] P.M. Moran, X.H. Liu, C.F. Shih. Kink band formation and band broadening in fiber composites under compressive loading. *Acta Metallurgica et Materialia*, Vol. 43 (1995).
- [7] T.J. Vogler, S. Kyriakides. On the axial propagation of kink bands in fiber composites: Part I experiments. *International Journal of Solids and Structures* 36 (1999).
- [8] T.J. Vogler, S. Kyriakides. On the initiation and growth of kink bands in fiber composites. Part I: experiments. *International Journal of Solids and Structures* 38 (2001).
- [9] A.B. Morais. Modelling Lamina Longitudinal Compression Strength of Carbon Fibre Composite Laminates. *Journal of Composite Materials*, Vol. 30 (1996).
- [10] T.J. Vogler, S.Y. Hsu, S. Kyriakides. On the initiation and growth of kink bands in fiber composites. Part II: analysis. *International Journal of Solids and Structures* 38 (2001).
- [11] V.W. Rosen. Mechanics of composite strengthening, *Fibre Composite Materials*, American Society of Materials, Metals Park, Ohio (1965).
- [12] A.S. Argon, *Fracture of composites*, Treatise on Materials Science and Technology, Academy Press, New York (1972).
- [13] C.R. Chaplin. Compressive fracture in unidirectional glass reinforced plastics. *Journal of Materials Science*, Vol.12 (1977).
- [14] B. Budiansky. Micromechanics. *Computers and Structures*, Vol. 16 (1983).

- [15] H.T. Hahn, J.G. Williams. Compression Failure Mechanisms in Unidirectional Composites. Composite Materials: Testing and Design (Seventh Conference), American Society for Testing and Materials, Philadelphia (1986).
- [16] P.S. Steif. A model for kinking in fiber composites - I. Fiber breakage via micro-buckling. International Journal of Solids and Structures, Vol. 26 (1990).
- [17] A.B. Morais, A.T. Marques. A Micromechanical Model for the Prediction of the Lamina Longitudinal Compression Strength of Composite Laminates. Journal of Composite Materials, Vol. 31 (1997).
- [18] C.G. Dávila, P.P. Camanho, C.A. Rose, Failure Criteria for FRP Laminates. Journal of Composite Materials, Vol. 39 (2005).
- [19] ABAQUS, Inc. ABAQUS version 6.6 Documentation. Dassault Systèmes / SIMULIA (2006).